Exploring Exosomes and Circulating Tumor Cells as Biomarkers for Head and Neck Cancer

Dissertation

zur Erlangung des akademischen Grades

Doktorin der Naturwissenschaften

(Dr. rer. nat.)

am Fachbereich Biologie der

JOHANNES GUTENBERG UNIVERSITÄT MAINZ

Vorgelegt von

Madita Wandrey

geboren am 21.03.1994 in Hannover

Mainz, 2024

Die vorliegende, kumulativ gestaltete Arbeit wurde im Zeitraum von April 2019 bis Juli 2024 in der Forschungsgruppe *Molekulare und Zelluläre Onkologie* der Universitätsmedizin der Johannes Gutenberg Universität Mainz angefertigt. Die erzielten Ergebnisse wurden in Teilen in der Fachliteratur veröffentlicht, und werden im Folgenden zusammenfassend diskutiert.

Dekan: Prof. Dr. Eckhard Thines

Tag der mündlichen Prüfung: 02.12.2024

Ganz gleich, was du auch ausrichtest, es wird nie mehr sein
als ein einzelner Tropfen in einem unendlichen Ozean.
Aber was ist ein Ozean, wenn nicht eine Vielzahl von Tropfen?

- David Mitchell, Der Wolkenatlas

I ZUSAMMENFASSUNG

Kopf-Hals-Tumore (HNC) gehören zu den weltweit häufigsten bösartigen Tumorerkrankungen. Trotz umfangreicher Bemühungen die Behandlung zu optimieren, bleibt die Patientensterblichkeit hoch. Einer der Gründe für das Behandlungsversagen und die niedrige Überlebensrate ist die Entwicklung von Chemotherapie-Resistenzen, was die Notwendigkeit zur Identifizierung neuer prädiktiver Biomarker unterstreicht. Ein vielversprechender Ansatz in diesem Zusammenhang ist die Verwendung von Flüssigbiopsien, einer Methode, die auf der Analyse von Biomarkern aus Körperflüssigkeiten, meist Blut, basiert. Im Rahmen dieser Arbeit wurde das Potential von zirkulierenden Tumorzellen (CTCs) und kleinsten extrazellulären Vesikeln, sogenannten Exosomen, als Biomarker für Flüssigbiopsien bei HNC-Patienten untersucht. Zusätzlich sollte eine potentielle Rolle von Exosomen bei der Entstehung und Übertragung von Chemotherapie-Resistenzen charakterisiert werden.

Der erste Schritt zur Etablierung neuer Biomarker ist die Entwicklung solider Detektionsverfahren. Hierzu wurde eine geeignete Modell-Zelllinie identifiziert und auf die Expression relevanter CTC-Marker untersucht. Protokolle zur manuellen CTC-Isolation wurden mit verschiedenen *Bead*-basierten Methoden getestet. Um die klinische Implementierung zu erleichtern, wurde die Automatisierung des Isolationsprozesses mit Hilfe der *CTCelect* Plattform angestrebt. Eine erste Machbarkeitsstudie mit Patientenproben erzielte vielversprechende Ergebnisse. Zur Nutzung von Exosomen als Biomarker wurden zunächst Protokolle zur Isolation und Charakterisierung erstellt und die generierten Ergebnisse gemäß etablierter Richtlinien validiert.

Um eine potentielle Rolle von Exosomen bei der Übertragung von Chemotherapie-Resistenz zu untersuchen, wurden geeignete HNC Zellmodelle etabliert, welche Cisplatin-resistente und -sensitive Tumore *in vitro* abbilden. Die transkriptomische Charakterisierung der Exosomen aus diesen Zellen ergab signifikante Unterschiede in der Genexpression im Allgemeinen, sowie im Speziellen bezüglich der Expression von Genen, welche für Cisplatin-Resistenz, epithelial-mesenchymale Transition und Krebsstammzellen relevant sind. Zusätzlich führte die Korrelation der transkriptomischen Daten mit klinischen Parametern zur Identifikation potentieller exosomaler Biomarker, wie zum Beispiel TPT1 und ZNF706, die Rückschlüsse auf Behandlungserfolg und 5-Jahres-Überleben von HNC Patienten zulassen. Aus den transkriptomischen Daten resultierte zudem die Hypothese, dass Exosomen eine duale Rolle für die Cisplatin-Resistenz spielen könnten, indem sie durch spezifischen Transport von mRNAs zur Regulation der Genexpression beitragen. Einerseits stellt die Regulation der Verpackung spezifischer mRNAs in Exosomen eine Möglichkeit dar um die intrazelluläre mRNA- und

entsprechende Proteinmenge zu modulieren, was im Fall von reduzierter exosomaler Verpackung von Resistenz-relevanten mRNAs, wie CDK8 und HDGFRP3, die Cisplatin-Resistenz der Donorzelle erhöhen könnte. Andererseits könnte die exosomale Übertragung von mRNAs, welche eine Resistenz induzieren, benachbarte Zellen und die Tumormikroumgebung modulieren, was wiederum zur Cisplatin-Resistenz insgesamt beiträgt.

Um die anhand der Expressionsdaten aufgestellte Hypothese funktionell zu überprüfen, wurden Übertragungs-Experimente mit den etablierten Zellmodellen durchgeführt. So konnte gezeigt werden, dass Exosomen aus Cisplatin-resistenten Donorzellen das Migrationspotenzial von sensitiven Empfängerzellen erhöhen und ihre Morphologie in 3D-Zellkulturen beeinflussen. Ein messbarer Effekt von Exosomen auf die Cisplatin-Toleranz der Empfängerzellen basierend auf deren Viabilität konnte mittels der gewählten Modellsysteme nicht mit ausreichender Sicherheit nachgewiesen werden.

Zusammenfassend liefert die vorliegende Arbeit wichtige grundlagenwissenschaftliche Erkenntnisse, sowie anwendungsorientierte Protokolle zum Einsatz von zirkulierenden Tumorzellen und Exosomen als prädiktive Biomarker bei (Chemotherapie-resistenten) Kopf-Hals-Tumoren. Eine Translation der erzielten Ergebnisse in den klinischen Alltag kann somit in Zukunft zu einem verbesserten klinischen Management von HNC-Patienten beitragen.

II ABSTRACT

Head and Neck cancer (HNC) is among the most prevalent malignancies worldwide, and though extensive efforts were made to improve its treatment, morbidity remains high. Among the prevalent causes for treatment failure is chemotherapy resistance, highlighting the need for novel predictive biomarkers. Here, a promising approach is the use of liquid biopsies, a method relying on the analysis of biomarkers from bodily fluids, most commonly blood. Thus, this study explored circulating tumor cells (CTCs) and small extracellular vesicles, so-called exosomes, as biomarkers for liquid biopsy of HNC patients. Additionally, a potential role of exosomes in the development and transmission of chemotherapy resistance was explored.

The first step in introducing novel biomarkers is establishing a solid detection procedure. Therefore, a suitable model cell line was identified and tested for expression of relevant CTC markers. Different protocols for manual CTC isolation were evaluated using bead-based methods. To foster clinical implementation, automation of the isolation process using the *CTCelect* platform was sought. A first feasibility study with patient samples generated promising results. To exploit exosomes as biomarkers, isolation and characterization procedures were validated according to established guidelines. To investigate the potential transmission of chemotherapy resistance via exosomes, suitable HNC model cell lines were established, representing cisplatin-resistant and -sensitive tumors *in vitro*. Transcriptomic characterization of exosomes from these cell lines revealed significant differences in gene expression in general, and in particular concerning the expression of genes relevant to cisplatin resistance, epithelial-mesenchymal transition, and cancer stem cells. Correlation of transcriptomic data with clinical parameters lead to the identification of potential exosomal biomarkers for treatment success and 5-year survival, e.g. TPT1 and ZNF706. The transcriptomic analysis also resulted in the hypothesis that exosomes might have a dual role in cisplatin resistance, by regulating gene expression through the specific packaging and transport of mRNAs. On the one hand, exosomal packaging of specific mRNAs poses a mechanism to regulate intracellular mRNA and thus protein levels, which in the case of resistance-relevant mRNAs, such as CDK8 and HDGFRP3, might contribute to the donor cells' cisplatin resistance. On the other hand, exosomal transmission of mRNAs that contribute to cisplatin resistance could modulate neighbouring cells and the tumor microenvironment, generally contributing to cisplatin resistance.

In conclusion, this study provides important scientific insights as well as application-oriented protocols for the use of CTCs and exosomes as predictive biomarkers in (chemotherapy-resistant) HNC. Translating the generated results into clinical practice could thus contribute to the improvement of clinical management of HNC patients in the future.

III Graphical Abstract

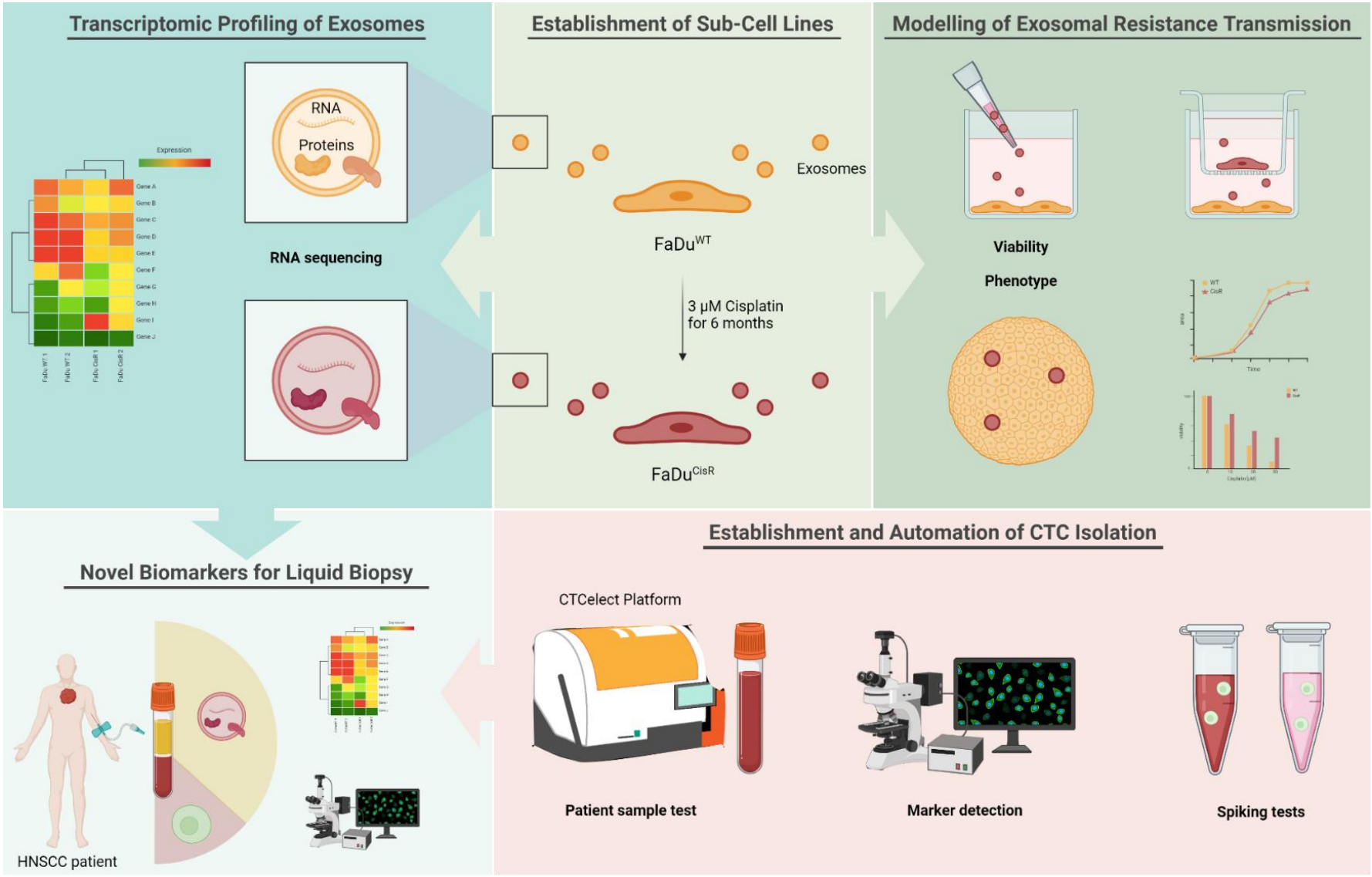

Graphical abstract: Exploring exosomes and circulating tumor cells (CTCs) as biomarkers for head and neck cancer

TABLE OF CONTENTS

1 INTRODUCTION

1.1 CANCER OF THE HEAD AND NECK

Head and neck cancer (HNC) is one of the most common malignancies worldwide, ranking as the sixth most common cancer type (Johnson et al. 2020). Despite modern advances in treatment options, the 5-year survival rate remains low at about 50 % (Shang et al. 2021). HNC survivors also have the second highest suicide rate among all cancer survivors, likely caused by the continual compromised quality of life (Osazuwa-Peters et al. 2018). With about 90 %, most HNCs are classified as squamous cell carcinomas (HNSCC), which originate from the mucosal epithelium lining the oral cavity, larynx, and pharynx (Forastiere et al. 2001). Figure 1 gives an overview of the anatomical sites affected by HNSCC (Cramer et al. 2019). Typically, HNSCC patients present at an advanced stage of disease progression. This is attributed to patients waiting until the onset of symptoms before seeking medical attention. Unfortunately, symptoms like pain, difficulty swallowing, and shortness of breath often occur at advanced stages, worsening the prognosis (Sharkey Ochoa et al. 2022). In general, men are more likely to develop HNSCC with a two- to four-fold higher risk than women (Windon et al. 2018). Among the known risk factors for HNSCC are tobacco and alcohol consumption, as well as infections with the Human Papilloma Virus (HPV) (Johnson et al. 2020). Notably, HPV-positive tumors mostly occur in the oropharynx, and have a more favorable prognosis compared to HPV-negative tumors (Prigge et al. 2017). While the overall number of SCC cases is declining, HPV-associated oropharyngeal tumors are on the rise in the western world (Sung et al. 2021).

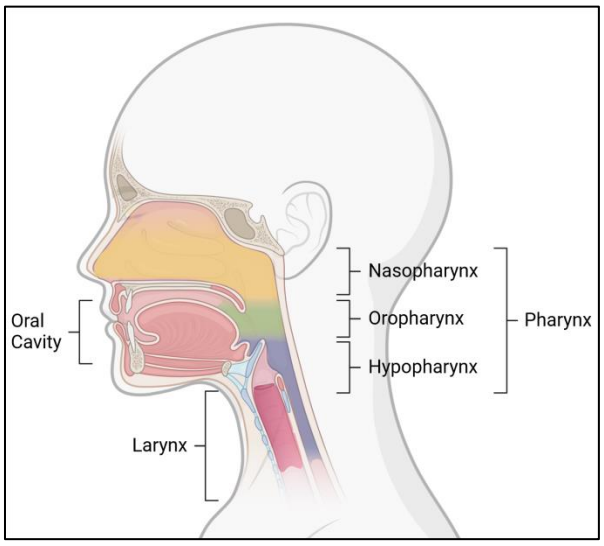

Figure 1. Anatomical sites affected by HNSCC

Treatment options for HNSCC include surgical resection, radiotherapy, and systemic therapy, which are often applied in combination. Treatment decisions are made based on tumor, node, and metastasis stage (TNM-stage), as well as HPV status in the case of oropharyngeal tumors (Huang and O'Sullivan 2017, Beltz et al. 2019). Generally, surgery is the most common first-line treatment for oral cavity cancers, while radiation is more commonly elected for pharyngeal and laryngeal cancers (Bledsoe et al. 2017). Systemic treatment options include chemotherapy and immunotherapy. Chemotherapy is mostly platinum-based, with cisplatin being the most common agent (Alsahafi et al. 2019, Oosting and Haddad 2019). Immunotherapy is mostly applied in patients with recurrent or metastatic HNSCC. Cetuximab, a monoclonal antibody inhibiting the epithelial growth factor receptor (EGFR), is approved by the FDA for combination treatment with radiotherapy and chemotherapy, or as a single agent after platinum-based therapy (Muraro et al. 2021). The check-point inhibitor Pembrolizumab, a monoclonal antibody targeting programmed death 1 (PD-1), was established as first- and second-line treatment in recurrent and metastatic HNSCC (Burtness et al. 2019).

Despite all treatment efforts, the 5-year survival rate of HNSCC patients remains low at less than 20 %. Regardless of aggressive first-line treatment regimens, over 50 % of HNSCC patients develop invasion and metastasis (Ferlito et al. 2001, Jemal et al. 2008). Moreover, therapy resistance leads to near and distant relapses, resulting in high morbidity and a median survival of only 10 months (Jou and Hess 2017).

1.1.1 Platinum-Based Chemotherapy

The primary goal of chemotherapy is to inhibit tumor cell proliferation, and subsequently to prevent invasion and metastasis. Applied drugs typically interfere with DNA, RNA, or protein synthesis. Chemotherapeutic agents can be classified based on their mode of action into alkylating agents, antimetabolites, anti-microtubular agents, and antibiotics (Amjad et al. 2022). The platinum (Pt-) based drugs cisplatin, carboplatin, and oxaliplatin belong to the class of alkylating agents and are the first choice for malignant tumor treatment. The first generation Pt-based drug cisplatin was discovered in the late 1960s and has been approved for cancer treatment since 1976. Today, about 50 % of all cancer patients are treated with cisplatin (Ghosh 2019). After intravenous administration cisplatin circulates with the blood stream. Because of the high chloride concentration within the blood serum, aquation of cisplatin is low and it remains largely inactive (Figure 2). Upon cellular uptake cisplatin undergoes activation through chloroligand replacement by water molecules, as the intracellular chloride concentration is much lower. These aquo-cisplatin species are highly reactive and contain unstable alkyl groups, which

bind to nucleophilic DNA sites and lead to crosslinks that alter the DNA structure. These structural changes are referred to as DNA adducts and prevent DNA damage repair, eventually leading to apoptosis induction (Dasari and Tchounwou 2014, Zhang et al. 2022). Cisplatin also binds to nucleophilic non-DNA targets like phospholipids, glutathione (GSH), and other thiol-containing molecules. In fact, only 1 % of intracellular cisplatin is believed to interact with DNA. This non-specific binding to other biomolecules likely contributes to cisplatin's cytotoxic effects, but can also decrease the amount of active drug within the cell, increasing its cisplatin tolerance (Fuertes et al. 2003, Galluzzi et al. 2012). Unfortunately, the non-specific cellular uptake of cisplatin also causes systemic toxicity. Among the common side effects are mucositis, nausea, vomiting, hepatotoxicity, nephrotoxicity, and neurotoxicity. Recently, chemical modifications of Pt-based drugs like nanomaterial drug carriers have emerged as promising tools to increase biosafety (Siemer et al. 2021, Zhang et al. 2022). In addition to its high systemic toxicity, many patients also develop resistance to cisplatin during the course of their treatment. To circumvent this, the next-generation Pt-agents carboplatin and oxaliplatin were introduced, but with little success. They do not reach the same efficacy as cisplatin, and cross-resistance and multi-drug resistance (MDR) still pose a major challenge in chemotherapy treatment (Galluzzi et al. 2012). In fact, 90 % of deaths in patients with metastatic tumors can be attributed to chemotherapy resistance (Hayatudin et al. 2021).

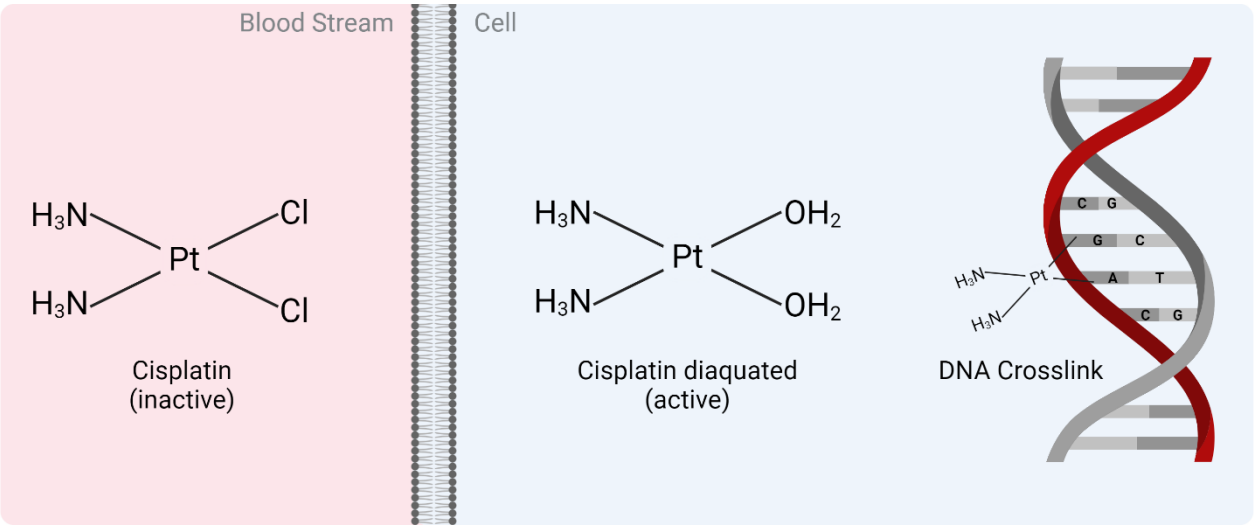

Figure 2. Intracellular cisplatin activation and interaction with DNA
While circulating with the blood stream cisplatin remains largely inactive due to the high chloride concentration. Within the cell, cisplatin is activated by mono- or diaquation and binds to purines within the DNA, leading to intra- and inter-strand crosslinks.

1.1.2 Chemotherapy Resistance

There are two common scenarios that can lead to chemotherapy resistance in cancer patients: a general MDR or the resistance against a specific agent (Stavrovskaya 2000). Figure 3 summarizes the most common molecular mechanisms involved in chemoresistance. Drug uptake may be reduced by changes in the plasma membrane constitution or in the expression of transporters responsible for drug import, resulting in decreased intracellular drug concentrations. Upregulation of drug export mechanisms can also counteract intracellular drug accumulation. Drugs can also be detoxified inside the cell, mostly by enzymatic processes. On the DNA level, pro-survival gene expression can be upregulated, leading to the evasion of apoptosis. Additionally, DNA repair mechanisms can be increased to counteract the drug's DNA damaging effects (Zhu et al. 2016).

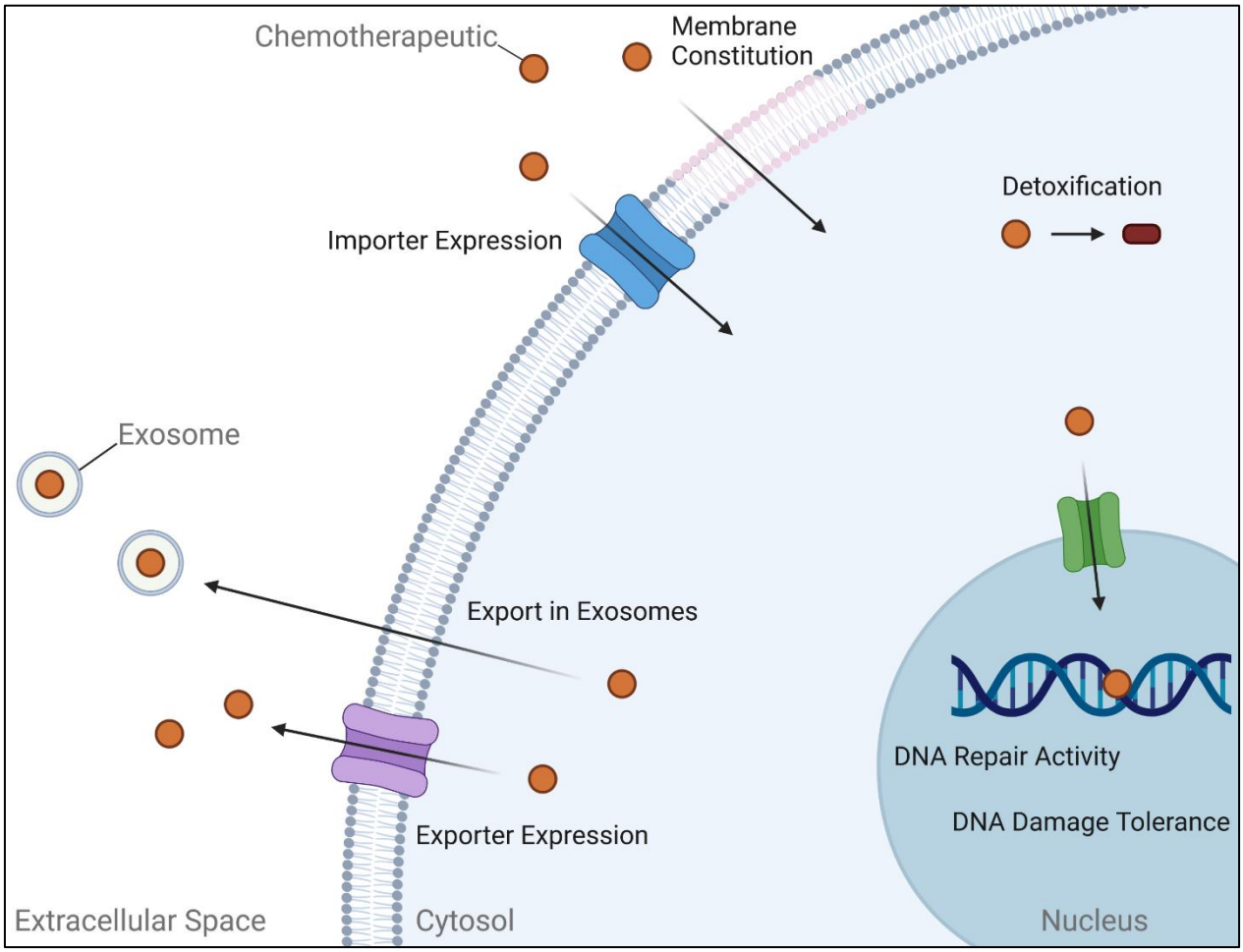

Figure 3. Molecular mechanisms of chemotherapy resistance
Drug uptake can be mediated by active import or passive diffusion, which can be influenced by decreased importer expression and altered membrane constitution in resistant cells. Once inside the cell, drugs can be detoxified or actively exported to decrease the intracellular active drug concentration. On the DNA level, repair mechanisms and pro-survival gene expression can be enhanced in resistant cells.

Cisplatin is a widely used agent in chemotherapy for various entities, including HNSCC. Unfortunately, cisplatin treatment often results in therapy resistance. On the cellular level, resistance to Pt-based agents is typically achieved by reduction of intracellular active drug concentration and increased DNA damage response (Rottenberg et al. 2021). In the broader context, epigenetic factors and the tumor microenvironment, including immune cells and cancer stem cells, also play a role in resistance acquisition (Lord and Ashworth 2012).

Cisplatin's main mode of action is DNA damage by crosslinking of purine bases, resulting in DNA adduct formation. This adduct formation prevents DNA repair, leading to DNA damage and subsequent induction of apoptosis. Cisplatin-resistant cells show an enhanced DNA repair activity or a higher tolerance to unrepaired DNA damage (Galluzzi et al. 2012, Zhu et al. 2016). There are multiple known DNA repair pathways, with the most important ones for cisplatin resistance being nucleotide excision repair (NER) and mismatch repair (MMR). NER is a highly conserved pathway targeting changes in the helical structure of the DNA. One of the over 20 proteins involved in NER is excision repair cross-complementation group 1 (ERCC1), an endonuclease that specifically cleaves at the 5' side of junctions between double-stranded and single-stranded DNA, as occurring in cisplatin-induced DNA adducts. ERCC1 is upregulated in cisplatin-resistant cells, reducing their responsiveness to therapy (Martin et al. 2008, Torii et al. 2014). MMR corrects DNA mismatches that occurred during replication and escaped proofreading. Deficient MMR leads to increased DNA damage tolerance and cisplatin resistance. Two major players in MMR, MutS homolog 2 (MSH2) and Post-meiotic segregation 2 (PMS2), have been shown to be downregulated in cisplatin-resistant cells, while overexpression of PMS2 leads to increased cisplatin-induced apoptosis in HeLa cells (Lanzi et al. 1998, Zhang et al. 2010).

Cisplatin-induced apoptosis is essential for its anti-cancer effect and can be triggered through the extrinsic death receptor pathway or the intrinsic mitochondrial pathway. Multiple proteins (e.g. p53, Caspases, Bcl-2 family) and signaling pathways (e.g. MAPK, NF-κB) involved in apoptosis induction are dysfunctional in cisplatin-resistant cells (Zhu et al. 2016). One study could show that cisplatin therapy is more beneficial to patients with wildtype p53 expression compared to those with mutated p53 in cervical cancer (Garzetti et al. 1996). Additionally, proteins of the inhibitor of apoptosis (IAP) family like survivin are often upregulated in cancer cells, which leads to further interference with apoptotic pathways (Santarelli et al. 2018).

Cisplatin is believed to be taken up by passive diffusion, as well as active transport. During malignant transformation, cells acquire alterations to their plasma membrane's lipid profile and biophysical properties (Choromanska et al. 2021). Binding assays using a large unilamellar vesicle (LUV) model have revealed that cisplatin interacts with all negatively charged

phospholipids. Binding of cisplatin to anionic phospholipids can reduce its cellular uptake and thereby facilitate resistance. It has also been shown that tumor cell membranes have an increased ratio of sphingomyelin to phosphatidylethanolamine, leading to inactivation of the MAPK pathway (Alves et al. 2016). Active cisplatin uptake can be achieved by different ion channels including copper transporter receptor 1 (CTR1), which has been found to be downregulated in different cisplatin-resistant cell lines (Zisowsky et al. 2007). Other cisplatin importers are volume-regulated anion channel (VRAC), organic cation transporters (OCT1/OCT2/OCT3), and organic cation/carnitine transporters (OCTN1/OCTN2) (Harrach and Ciarimboli 2015). Knockout of VRAC has been shown to increase cisplatin tolerance *in vitro*, and low VRAC expression in HNSCC patients could be correlated with residual disease after chemoradiation (Siemer et al. 2021). Cisplatin efflux is mediated by ATP-binding cassette (ABC) transporters like multi-drug resistance proteins (MDRPs) and P-glycoprotein (P-gp), which are upregulated in resistant cells (Zhu et al. 2016). Recently, the export of cisplatin in exosomes has been proposed as an additional mechanism to actively remove the drug from the cell (Safaei et al. 2005, Sharma 2017). Another mechanism to reduce the concentration of active cisplatin within the cell is its detoxification. Upon binding to thiol-containing nucleophilic species like GSH, methionine, and metallothionines, or thiol-containing proteins cisplatin's cytotoxicity is reduced. It has been shown that overexpression of enzymes involved in GSH synthesis and conjugation can facilitate cisplatin resistance (Galluzzi et al. 2012).

1.1.3 Cell Culture Models for Cancer Research

Cell culture models are a helpful tool to approach research questions *in vitro*, as they can be observed under controlled conditions. In cancer research, primary cells as well as immortalized cell lines are routinely used. Primary cells are extracted from tissue and transferred to cell culture, where they can proliferate for a finite amount of time until they reach senescence. In immortalized cell lines, cell cycle checkpoint pathways are disabled, leading to a loss of senescence and subsequent uncontrolled proliferation. This immortality can be artificially induced or already be present due to mutations in cancer cells (Maqsood et al. 2013). Traditionally, cells are cultured as adherent monolayers on flat surfaces (2D) since the early 1900s (Figure 4A). To achieve a better representation of the conditions *in vivo*, synthetic extracellular matrix (ECM) matrices can be integrated into 2D cell culture. Using transwell cell culture inserts is advisable for co-culturing different cell types without allowing for direct cell-cell contacts (Figure 4B). This is especially interesting for the study of cell-cell communication via extracellular messengers like exosomes (Guo et al. 2016, Zhu et al. 2019).

In vivo, tumor cells grow in three-dimensional (3D) structures, and are in constant cross-talk with other cells and components of the tumor microenvironment (TME). This 3D architecture leads to differences in the supply of oxygen, nutrients, and other extracellular components like drugs or exosomes, depending on the cell's localization within the tumor. Growing cells in 3D spheroids can help to mimic this situation *in vitro* (Figure 4C). Due to the surrounding cell-cell contacts within spheroids, cells can also develop a polarity. Overall, the morphological and cellular characteristics of tumor spheroids are more in agreement with *in vivo* tumors when compared to conventional monolayer models (Kim 2005, Ma et al. 2012, Ravi et al. 2015). Spheroids can be generated from different sources, including cell lines and *ex vivo* (tumor-) tissue. When using patient material, spheres will not only contain tumor cells but also immune cells, endothelial cells, and fibroblasts, giving an even better representation of tumor heterogeneity. Such spherical cultures are often referred to as organoids or tumoroids (Weiswald et al. 2015).

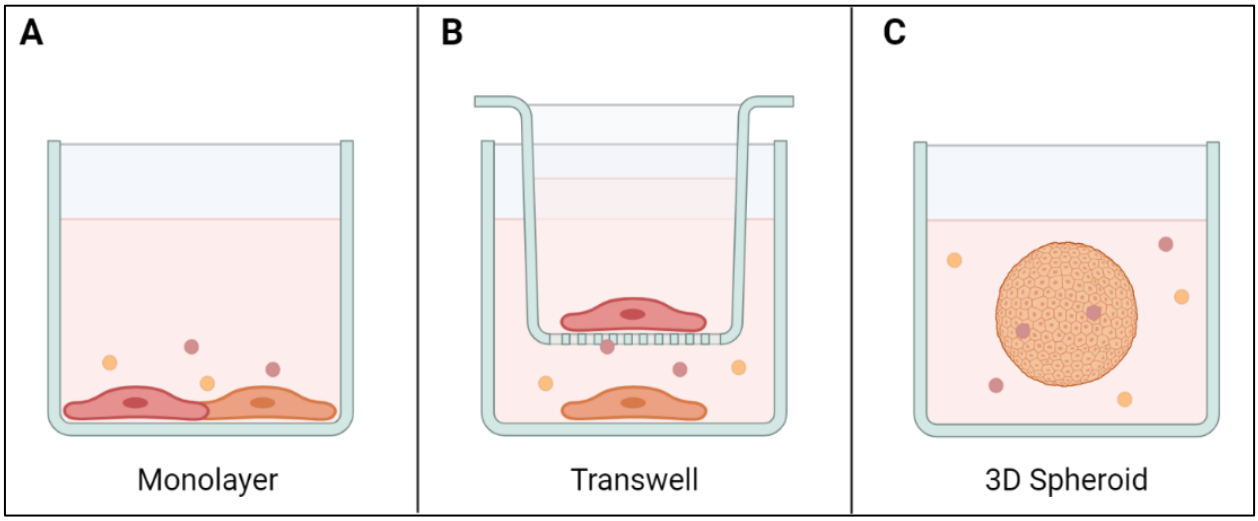

Figure 4. Schematic illustration of different cell culture models for cancer research
A) Cells are grown in adherent monolayers on a flat surface and can freely communicate via direct contact or extracellular messengers. **B)** Cells are co-cultured using a transwell insert. Depending on the pore size of the transwell membrane, cells can communicate via various extracellular messengers. **C)** Cells are grown in low adhesion plates, resulting in the formation of 3D spheroids. Availability of extracellular components to the cells depends on their respective localization within the spheroid.

1.1.4 LIQUID BIOPSY

For tumor screening and therapy surveillance, it is standard procedure to take tissue biopsies from cancer patients. For this procedure tissue is extracted and analyzed for pathological markers. Besides causing stress to the patient, it is not always possible to take such biopsies due to complicated anatomical locations as often encountered in HNSCC. Additionally, the results only reflect a snapshot of the heterogeneous tumor mass. Therefore liquid biopsies have become increasingly popular in recent years, as they represent a minimal-invasive alternative that can complement standard cancer detection and monitoring (Figure 5). Compared to tissue biopsies they are lower in costs and easily performed, making multiple samplings throughout a patient's treatment possible (Vaidyanathan et al. 2018). Liquid biopsy relies on the analysis of biomarkers mostly in blood, but also other bodily fluids like urine or saliva. Among the examined biomarkers are circulating tumor cells (CTCs), cell-free DNA (cfDNA), circulating RNA, and extracellular vesicles (EVs), including exosomes (Xiao et al. 2019, Mishra et al. 2022).

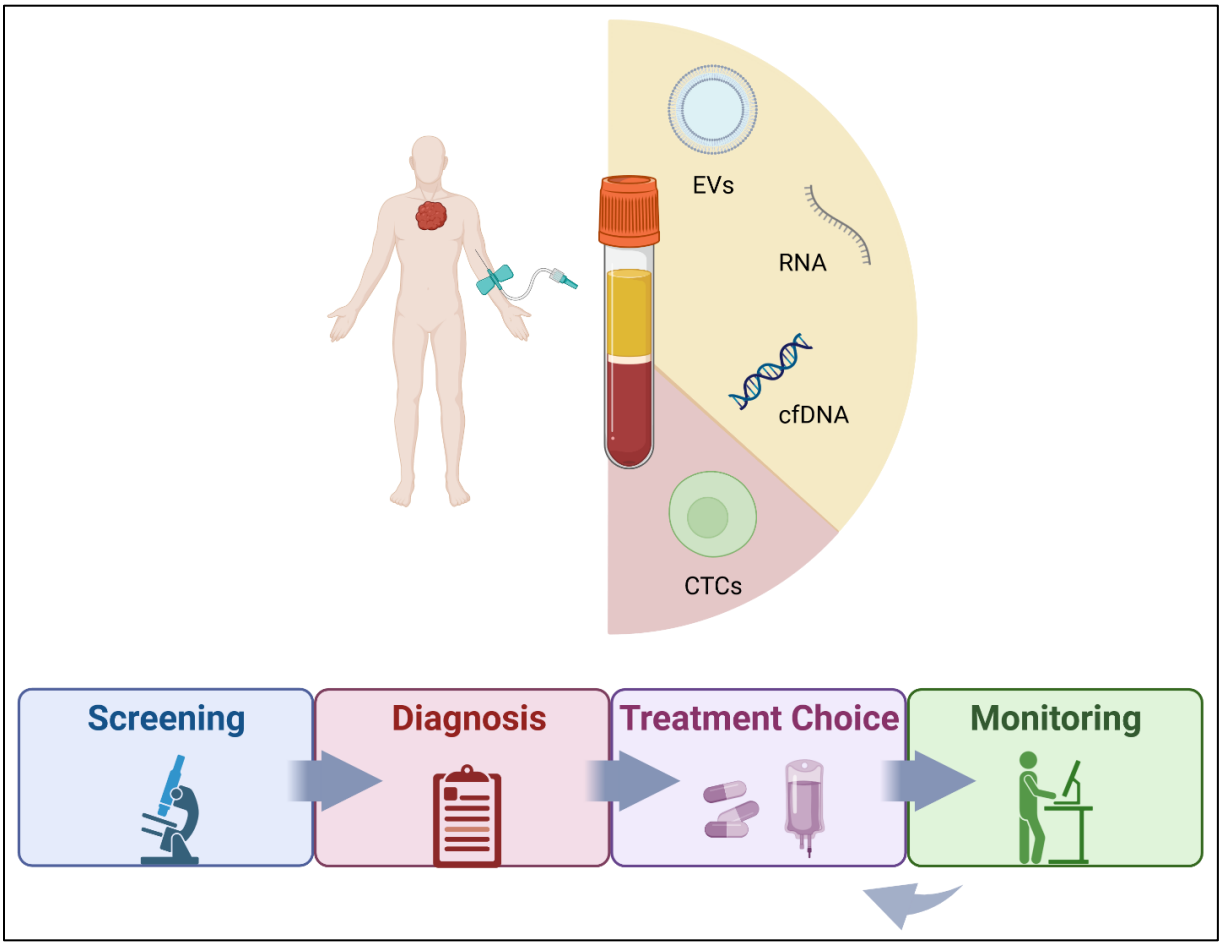

Figure 5. Liquid biopsy for cancer patients
Periodic sampling and analysis of blood-borne markers like extracellular vesicles (EVs), circulating RNA, cell-free DNA (cfDNA), and circulating tumor cells (CTCs) facilitates easy screening, diagnosis, treatment decisions, and therapy monitoring for cancer patients.

1.2 EXOSOMES

In 1983, Pan and Johnstone, as well as Harding et al. first described nano-sized extracellular vesicles (EVs) originating from exocytosis of multivesicular endosomes. These specific EVs were termed exosomes shortly after. All kinds of eukaryotes, including humans, animals, plants, and fungi, as well as prokaryotes, have been proven to produce exosomes (Gurung et al. 2021). Within the human body, almost all cell types shed exosomes, so they can be found in various bodily fluids (e.g. blood, urine, saliva) as well as in medium from human cell culture (Zhang et al. 2019, Elzanowska et al. 2021). While exosomes share many common features with other classes of EVs, they are distinct in their size, content, and biogenesis (Figure 6). Over the past decades, more and more biological functions of these membranous vesicles have emerged, sparking a wide research interest.

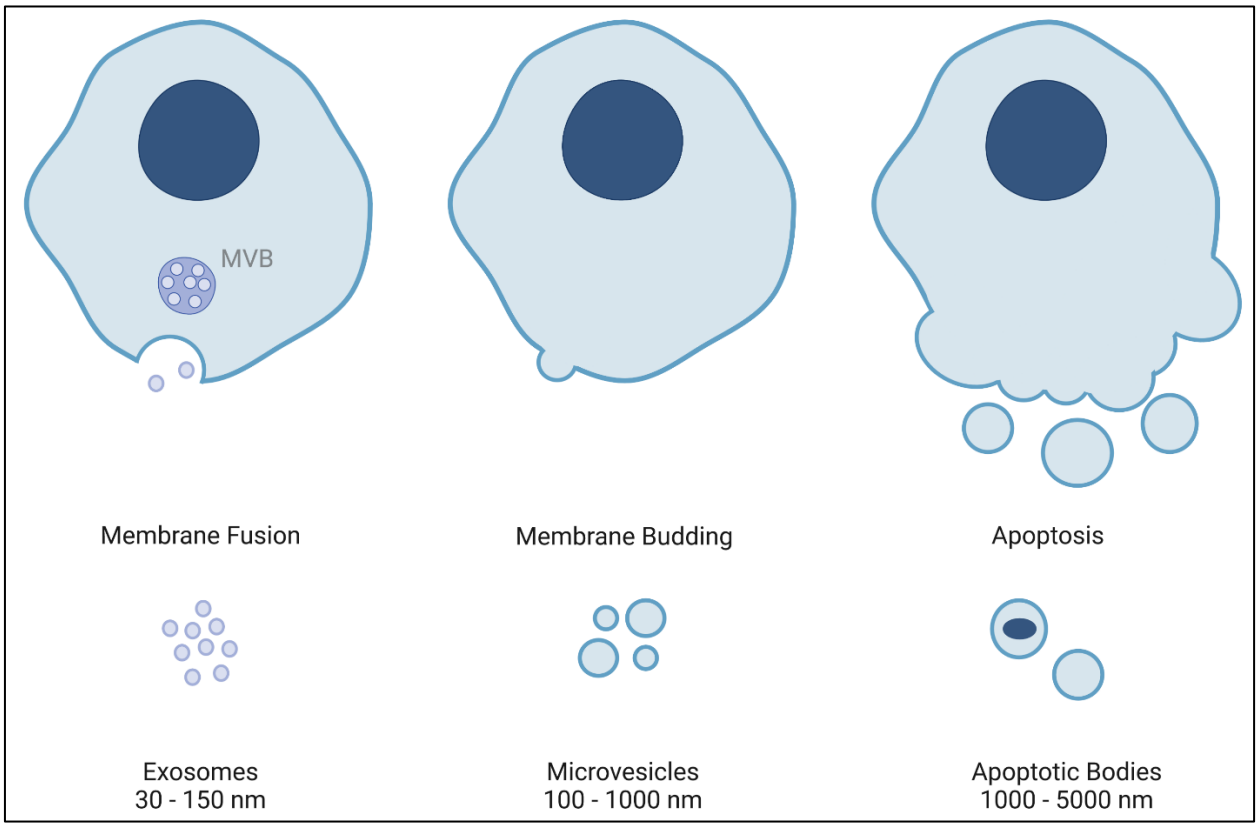

Figure 6. Different types of extracellular vesicles
Exosomes are released by membrane fusion of the multivesicular body (MVB) with the plasma membrane. Microvesicles bud directly from the plasma membrane, while apoptotic bodies are the result of cell death associated membrane blebbing.

1.2.1 Biogenesis and Cargo Sorting

Exosomes originate from intraluminal vesicles (ILVs) formed in late endosomes. The endosomal pathway typically begins with the (receptor-mediated) endocytosis of extracellular materials by plasma membrane invagination, and the endocytosed components are directed to the early endosomes. From here, they can either be transported back to the plasma membrane for recycling or move further along the endosomal pathway (Doherty and McMahon 2009, Hu et al. 2015). Through acidification, the early endosomes mature into late endosomes, which can receive additional cargo from the Trans-Golgi network (Huotari and Helenius 2011). Upon interaction of the endosomal sorting complex required for transport (ESCRT) with exosome-targeted proteins, the endosomal membrane buds inwards, resulting in the formation of ILVs (Figure 7) (Henne et al. 2011, Minciacchi et al. 2015). These ILVs are the precursors of the later secreted exosomes. Alternatively, ILVs can also originate from ceramide- or tetraspanin-enriched microdomains of the endosomal membrane (Airola and Hannun 2013, Perez-Hernandez et al. 2013, Castro et al. 2014). The resulting multivesicular body (MVB) eventually fuses with the plasma membrane and releases the ILVs into the extracellular space as exosomes (Zhang et al. 2019). MVBs can also fuse with lysosomes, typically resulting in the degradation of their contents. However, there have also been reports of lysosomes fusing with the plasma membrane and subsequent exosome release (Buratta et al. 2020). There is also a limited number of studies reporting exosomes budding directly from endosome-like microdomains of the plasma membrane (Booth et al. 2006, Fang et al. 2007). Nevertheless, the prevailing definition of exosomes asserts that they originate from the endosomal pathway.

While exosomes were thought to be a cellular mechanism for waste disposal until the 1990s, research has since shown that they facilitate cell-cell communication by delivering complex cargos. Nowadays they are viewed as extracellular messengers delivering specific signals to their recipient cells. Exosomes contain different nucleic acids, metabolites, soluble and membrane proteins, as well as lipids (Valadi et al. 2007, Waldenstrom et al. 2012, Elzanowska et al. 2021, Harmati et al. 2021). Typical exosome marker proteins include tetraspanins (CD63, CD81, CD9), heat shock proteins (HSPs) (HSP70, HSP90), MVB formation associated proteins (TSG101, Alix), and proteins related to membrane transport and fusion (GTPases) (Vlassov et al. 2012). The most common RNA species contained in exosomes are non-coding RNAs (ncRNAs), including micro RNAs (miRNAs), circular RNAs (circRNAs), and long ncRNAs (lncRNAs). Upon uptake, ncRNAs can alter the protein expression of the recipient cell. miRNAs bind to target messenger RNAs (mRNAs), resulting in post-translational silencing. lncRNAs and circRNAs are sponging miRNAs by competitively binding to them, resulting in increased

expression of the respective miRNA's target mRNA. They can also directly interact with proteins (Xu et al. 2022). The DNA species found in exosomes include genomic DNA (gDNA) and mitochondrial DNA (mtDNA). Exosomal packaging of DNA is a cellular mechanism to maintain homeostasis, but its uptake can also lead to alterations in the recipient cell by incorporation of the DNA into its genome (Elzanowska et al. 2021). Exosomes also contain metabolites like amino acids and their derivates, carbohydrates, carbonic acids, and folates (Harmati et al. 2021). When it comes to their membrane composition, exosomes are generally enriched in cholesterol, ceramides, sphingomyelin, and phosphatidylserine. They can also contain lipolytic enzymes, enabling the autonomous production of units of bioactive lipids (Zhang et al. 2019, Wei et al. 2021).

Protein sorting into ILVs, and subsequently exosomes, is largely dependent on post-translational modifications (PTMs). The most relevant PTM in this context is ubiquitination. The ESCRT subunits ESCRT-0, ESCRT-I, and ESCRT-II all interact with ubiquitinated proteins and recruit them to the endosomal membrane (Moreno-Gonzalo et al. 2014). A known signal for MVB sorting is the PPYX motif, which is recognized and ubiquitinated by the Nedd4 family of ubiquitin ligases (Boase and Kumar 2015, Goel et al. 2015). Other frequently detected PTMs of exosomal proteins are SUMOylation, phosphorylation, and glycosylation (Anand et al. 2019). As mentioned before, ILV formation also occurs at specific microdomains within the endosomal membrane. Activity of neutral sphingomyelinase (nSMase) leads to ceramide-enriched regions, which curve spontaneously and thereby facilitate ILV formation. nSMase is therefore also frequently found in exosomes (Li et al. 2018, Anand et al. 2019). Another poorly understood sorting mechanism is cargo-clustering. It involves proteins targeted to tetraspanin-enriched microdomains to be actively incorporated into ILVs (Leidal and Debnath 2020).

The sorting mechanisms for nucleic acids remain largely unknown. RNA packaging is thought to be dependent on specific EXOmotifs, which have been identified in numerous exosome-associated miRNAs. These facilitate the interaction with RNA-binding proteins, for example the SUMOylated hnRNPA1, and thus facilitate sorting into exosomes (Villarroya-Beltri et al. 2013).

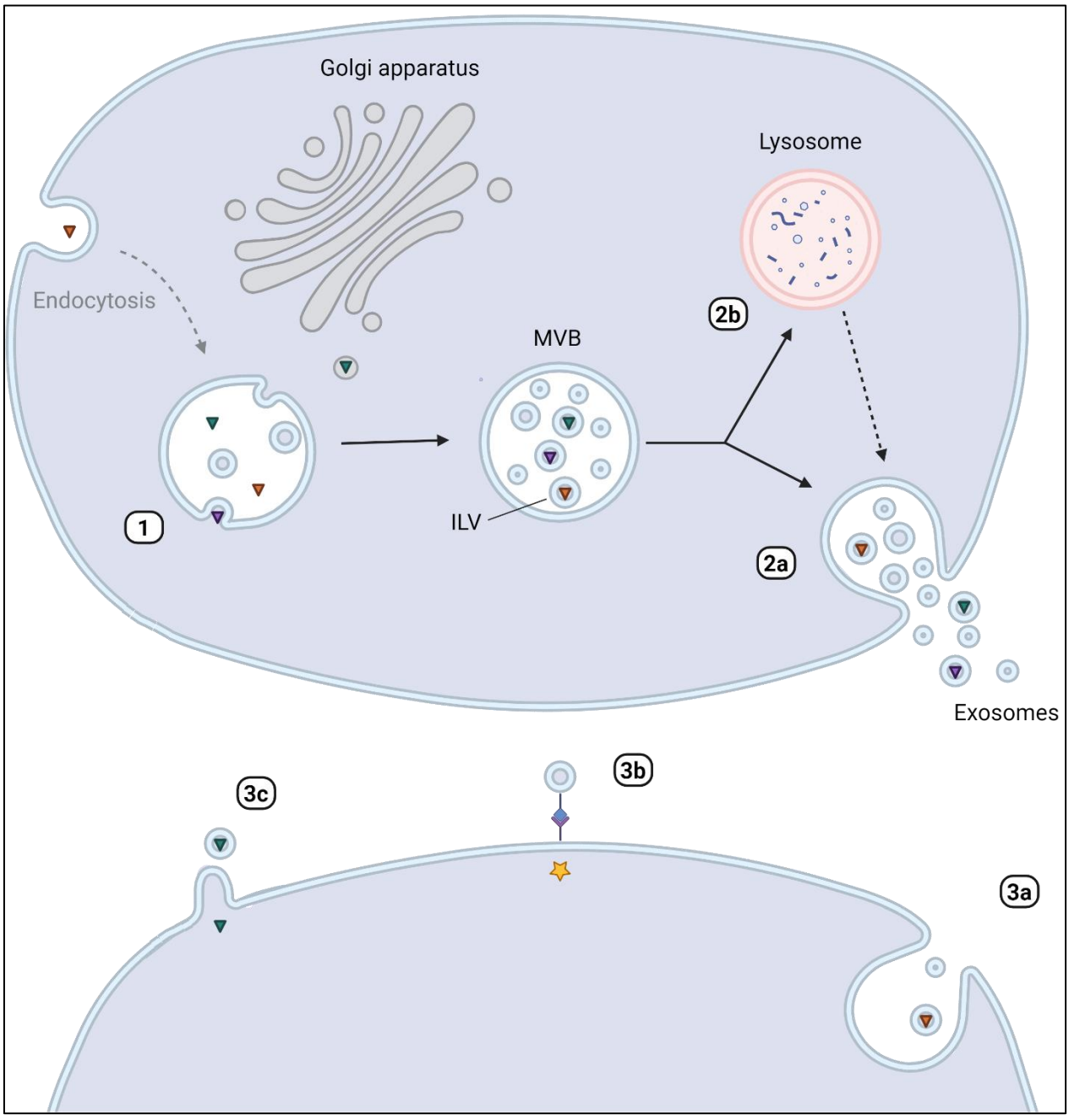

Figure 7. Exosome biogenesis and -activity
After maturation from early to late endosomes, ILVs are formed, resulting in the formation of the MVB (1). Cargo can originate from the cytosol, other organelles like the golgi apparatus, and endocytosis. Upon fusion of the MVB with the plasma membrane (2a) ILVs are released into the extracellular space as exosomes. Alternatively, MVBs can fuse with lysosomes, where contents are either recycled or exosomes are released by fusion of the lysosome with the plasma membrane (2b). Upon reaching the recipient cell, exosomes can be internalized by endocytosis or phagocytosis (3a), elicit signaling through receptor-ligand interaction (3b), or directly release their contents by membrane fusion (3c). MVB = Multivesicular body; ILV = Intraluminal vesicle

1.2.2 BIODISTRIBUTION AND -ACTIVITY

As almost all cell types shed exosomes, they are distributed throughout the whole body, locally and systemically. If taken up by endocytosis, exosomes can go through multiple cycles of uptake and release, allowing for deep tissue penetration. There are multiple factors influencing the specific tropism of exosomes, including the cell of origin, the membrane constitution, and the physiological state of the organism (Gurung et al. 2021). Unfortunately, most studies concerning exosome biodistribution come from a pharmacokinetic background, meaning they use heterologous or engineered exosomes. In this case, dose and route of administration also play a crucial role for the exosomes' fate. Knowledge about the biodistribution of autologous exosomes is scarce, but their presence in various bodily fluids suggests that they can travel throughout the entire body (Choi et al. 2021).

Upon reaching the recipient cell, exosomal cargo can facilitate a variety of biological functions. Depending on the type of recipient cell, there are three known modes of exosome bioactivity, namely internalization, receptor-ligand signaling, and membrane fusion (Figure 7) (Abels and Breakefield 2016). Membrane fusion allows for a direct release of the exosomal cargo into the recipient cell's cytoplasm (Prada and Meldolesi 2016). Alternatively, exosomal ligands can interact with cellular receptors, thus inducing downstream signaling cascades. However, the main route of exosome bioactivity is internalization, either by endocytosis or phagocytosis. The ladder is specific to immune cells like macrophages and dendritic cells. After engulfing the extracellular exosomes, they are contained in the phagosome (Gordon 2016). Endocytosis can be receptor-mediated or occur at lipid rafts, which are enriched in cholesterol, sphingolipids, and GPI-anchored proteins (Doherty and McMahon 2009). Both ways of internalization ultimately direct the exosomes to the endosomal pathway. After internalization, the exosomes can be guided to different destinations along the endosomal pathway. Endosomes can fuse back with the plasma membrane, which would result in a re-release of the exosomes into the extracellular space (Doherty and McMahon 2009, Hu et al. 2015). Late endosomes can also interact with the nucleoplasmatic reticulum (NR), a compartment that penetrates the nucleoplasm. This could allow exosomal cargo to enter the nucleus (Santos et al. 2018). Another possibility is retrograde trafficking to the Golgi Aparatus. The typical endpoint however is the lysosome, where contents are usually degraded. To escape lysosomal degradation, cargo can diffuse out of the endosome or be released into the cytoplasm, either by exosomal-endosomal membrane fusion or by rupture of the endosome or lysosome (Tian et al. 2010, Gurung et al. 2021).

1.2.3 Isolation and Analysis

Isolating exosomes can be challenging, as they are small and low in density. However, these properties, along with the presence of specific exosomal biomarkers, can also facilitate their isolation. There are various approaches available, and the choice of a suitable method highly depends on the specific research goals and sample types. The most common approaches are ultracentrifugation, size exclusion chromatography (SEC), ultrafiltration (UF), polymer precipitation, and immunoaffinity capture. The advantages and disadvantages of these methods are summarized in Table 1. Figure 8 gives a schematic overview of how these different methods achieve exosome isolation.

Table 1. Common exosome isolation methods

Method	Underlying exosome property	Advantages	Disadvantages	Sources
Ultracentrifugation	Size, density	Well established, all sample types and volumes	Time consuming, cost intensive, high force, low yield	[1-5]
Size exclusion chromatography	Size	Easy, low force	Low purity	[6-7]
Ultrafiltration	Size	Easy	Low purity, low recovery rates	[4] [8]
Polymer precipitation	Biophysical properties	Easy, quick, low force	Low purity, reagent contamination	[5] [9]
Immunoaffinity capture	Biomarkers	Easy, high purity	Time consuming, high cost, variance based on antigen, low yield	[10-12]

Sources: [1] Livshits et al. 2015, [2] Thery et al. 2006, [3] Chen et al. 2021, [4] Yang et al. 2020, [5] Zhang et al. 2020, [6] Batrakova and Kim 2015, [7] Boing et al. 2014, [8] Vergauwen et al. 2017, [9] Oh et al. 1988, [10] Ruivo et al. 2017, [11] Zhang et al. 2018, [12] Chen et al. 2021

Analyzing exosomes is not only important to uncover their biological functions, but also to verify successful isolation. Therefore the *The International Society for Extracellular Vesicles* encourages researchers to follow the *Minimal Information for Studies of Extracellular Vesicles* (MISEV) guidelines. The MISEV guidelines recommend showing three positive and one negative marker for the respective EV type on protein level. Suitable methods therefor include western blot, flow cytometry, or mass spectrometry. Furthermore, two different but complementary techniques are to be applied to characterize EVs on single particle level. This shall include

image-based methods (electron microscopy) and single particle analysis (DLS, NTA, TRPS). Since the 2018 update it is also encouraged to describe EVs quantitatively by particle count, total protein content, or total lipid content (Thery et al. 2018, Welsh et al. 2024). A more in depth review of exosome isolation and analysis methods can be found in our review (Wandrey et al. 2023) (see also section 2.2.5).

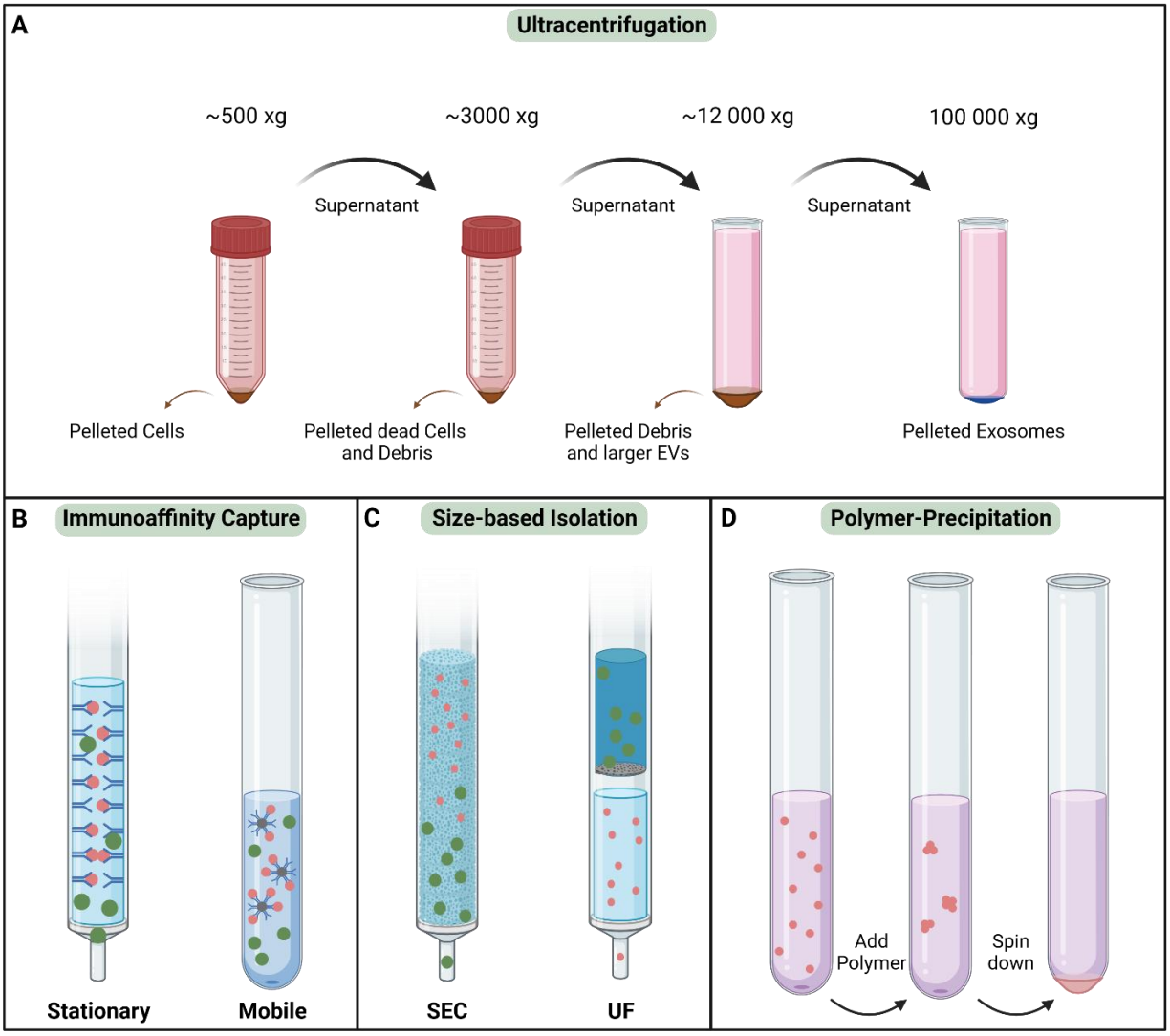

Figure 8. Overview of common exosome isolation methods
A) Ultracentrifugation relies on a series of lower-speed centrifugations to clear the sample of any cells, debris, and larger EVs. Afterwards, exosomes are precipitated by high-speed centrifugation. **B)** Immunoaffinity capture relies on the interaction between antigens on the exosomal surface and specific antibodies. These antibodies can be stationary, i.e. immobilized to a column (left), retaining the exosomes (red) while other particles (green) pass through. Alternatively, they can be fixed to mobile beads (right). Bead-bound exosomes are precipitated by centrifugation or magnetism, while other particles remain in the supernatant. **C)** Size-based isolation methods include SEC and UF. SEC is based on exosomes (red) getting trapped in a porous matrix, while larger particles (green) elute faster. UF relies on filter membranes with different molecular weight cut-offs, resulting in the separation from larger particles. **D)** The addition of polymers reduces the solubility of exosomes, leading to their aggregation, and subsequently allowing their precipitation at relatively low centrifugation speeds.

1.2.4 Exosomes in Chemotherapy Resistance

As discussed in section 1.1.2 there are multiple cellular mechanisms contributing to chemotherapy resistance. Exosomes have been implicated in the transmission of chemoresistance by shaping the TME and altering the recipient cells' phenotype by delivering functional proteins and RNAs (Sharma 2017).

In general, chemotherapy leads to an increase in exosome biogenesis (Kong et al. 2015). One proposed explanation is the exploitation of chemotherapeutic drug export via exosomes as a chemoresistance mechanism. For example, exosomes from cisplatin-resistant ovarian cancer cells incorporate two-fold more cisplatin than those from sensitive cells (Safaei et al. 2005).

Exosomes also contribute to the horizontal transfer of drug exporters like P-gp, MDRPs, and ABC transporters ABCA-3 and ABCG-2 (Sharma 2017). In a breast cancer model, exosomal delivery of P-gp was shown to facilitate the transfer of a chemoresistant phenotype, with P-gp functionality detectable only 2h after exosomal transfer (Bebawy et al. 2009, Lv et al. 2014, Wang et al. 2016). Similarly, exosomes could confer a chemoresistant phenotype in leukemia cells, by delivering functional MRP-1 and ABCA-3 (Chapuy et al. 2008, Lu et al. 2013). Exosomes have also been shown to carry pro-survival proteins like HSPs and the IAP survivin. Exosomal export of HSPs 60, 70, and 90 is increased by treatment with cisplatin or carboplatin in hepatocellular carcinoma cells (Lv et al. 2012). In prostate cancer patients, high exosomal levels of survivin could be associated with relapse after chemotherapy (Khan et al. 2012). Exosomes can also transfer resistance by delivering miRNAs. In breast cancer cells, tamoxifen resistance could be transferred to sensitive cells via exosomal miR-221/222 delivery (Wei et al. 2014). In another breast cancer model exosomal miR-100, miR-222, miR-30a, miR-24, miR-26a, and miR-27a could be linked to resistance phenotype transfer (Chen et al. 2014). In oral SCC, exosomal miR-21 was indicated in cisplatin resistance transfer by targeting DNA damage signaling (Liu et al. 2017).

The evidence for a significant role of exosomes in chemoresistance transfer *in vitro* is manifold. However, the number of studies providing *in vivo* data is very limited. Since conditions in the TME differ significantly from those *in vitro*, the kinetics of exosomal resistance transfer could differ significantly *in vivo* (Sharma 2017).

A more detailed review of the role of exosomes in (chemo-) therapy resistance can be found in our publication (Wandrey et al. 2023) (see also section 2.2.5).

1.2.5 EXOSOMES AS BIOMARKER

Exosomes can be found in a variety of bodily fluids and they contain complex cargos that can serve as biomarkers. In breast cancer, a correlation between the total amount of exosomal miRNA with malignancy and prognosis could be established (Joyce et al. 2016). Elevated levels of exosomal miR-21 and miR-4257 were associated with disease recurrence in non-small-cell lung cancer (Dejima et al. 2017). In HNSCC, exosome levels are nearly doubling with disease progression and can be correlated with the stage of disease (Muller et al. 2014, Ludwig et al. 2017). High expression of mesenchymal markers N-cadherin and TGF-β1 on plasma-derived exosomes of HNSCC patients could be associated with increased tumor proliferation, migration, and invasion, while photodynamic therapy leads to a shift towards epithelial markers (Theodoraki et al. 2018). After treating HNSCC patients with a combination of cetuximab, ipilimumab, and radiation, patients with recurrent disease showed increased levels of total exosome proteins, total exosome ratio, total CD3+, CD3(−)PD-L1+, and CD3+15s+ exosomes as opposed to patients who remained disease free (Theodoraki et al. 2019). 80 % of HNSCCs show overexpression of EGFR, which is also reflected in exosomes (Xiao et al. 2019). Reduction of exosomal EGFR and phospho-EGFR in HNSCC patients after cetuximab treatment could be correlated with treatment success. Serum-exosomal miR-21 and homeobox transcript antisense RNA (HOTAIR) could be associated with disease progression in laryngeal SCC, as patients with lymph node metastasis showed increased levels of both (Wang et al. 2014). The molecular profiles of exosomes in HNSCC are also reflective of the tumor's HPV status. Exosomal HPV-16-E7, SIRPA, and MUC16 have been proposed as potential biomarkers for HPV-16 associated oropharyngeal cancer. Additionally, exosomes from HPV-positive cancers only carry low levels of p53 (Kannan et al. 2017, Ludwig et al. 2018).

Exosomes pose a promising diagnostic and prognostic tool for different cancer entities including HNSCC, but so far the lack of standardized isolation and analysis methods is hindering the integration of exosomal biomarkers into the clinical routine (Ebnoether and Muller 2020).

1.3 Circulating Tumor Cells (CTCs)

Circulating tumor cells (CTCs) were first reported by Ashworth in 1869, as cells found in the blood of a cancer patient similar to those of the tumor. In 2004, Cristofanilli et al. were the first to indicate CTCs as biomarkers for progression-free survival in metastatic breast cancer. Since then, CTCs were recommended as tumor markers by the *American Society of Clinical Oncology* in 2007 and even integrated into the TNM staging of breast cancer in 2017 (Rossi and Fabbri 2019).

CTCs are cells originating from a primary or metastatic tumor mass that have entered the blood stream (Figure 9). Single CTCs can already be detected in patients with premalignant disease, highlighting their role in tumorigenesis early on (Pereira-Veiga et al. 2022). The shedding mechanism is not completely understood, but possible routes include direct shedding through leaky vasculature or active migration. While direct shedding likely occurs by chance, the acquisition of migratory potential involves partial or total epithelial-mesenchymal transition (EMT) (Lin et al. 2021).

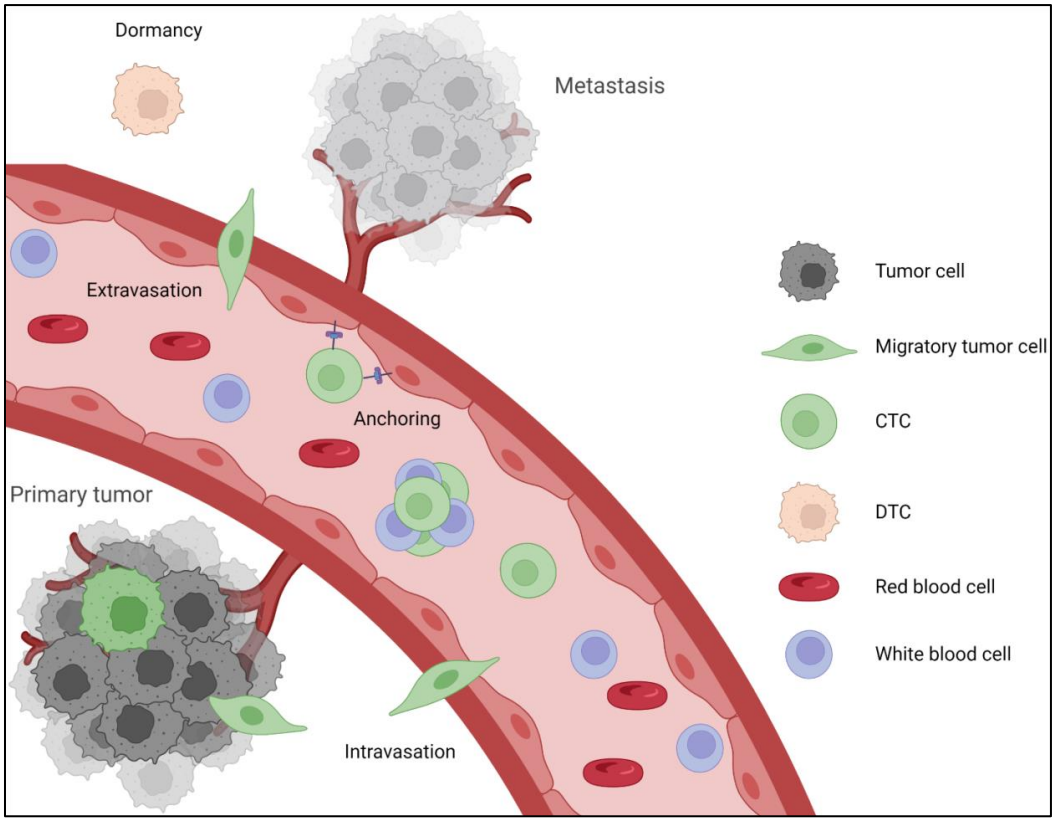

Figure 9. Circulating tumor cells (CTCs) and their role in metastasis
Cells of the primary tumor mass enter the bloodstream through leaky vasculature or gain migratory potential through epithelial-mesenchymal transition (EMT). CTCs are distributed with the circulation and potentially form circulating tumor microemboli with white blood cells. At distant sites they anchor at the luminal surface of endothelial cells through interaction of adhesions receptors. After extravasation CTCs can go into a dormant state (DTCs) or directly give rise to metastasis.

EMT is a cellular process, which leads to a loss of epithelial and gain of mesenchymal characteristics. It is reversible by the opposed process of mesenchymal-epithelial transition (MET). During EMT cells lose their apical-basal polarity, as well as cell-cell and cell-extracellular matrix adhesions, resulting in increased motility (Bakir et al. 2020, Amack 2021). There are multiple known signaling pathways that can induce EMT through EMT-promoting transcription factors (EMT-TFs). Prominent examples of EMT-TFs are the Snail, Slug, Twist, and ZEB families of transcription factors. Upon activation, they downregulate epithelial gene expression and activate mesenchymal genes (Dongre and Weinberg 2019). Classic epithelial marker proteins that are downregulated during EMT are involved in adherence junctions (E-cadherin, EpCAM) and tight junctions (ZO-1, Occludin). Mesenchymal marker proteins include N-cadherin, vimentin, and fibronectin. Some of these markers are also targeted for CTC isolation and analysis. Both EMT and MET are dynamic processes with intermediate states, leading to the appearance of cells carrying markers of both phenotypes (Bierie et al. 2017, Amack 2021). Besides its role in CTC biogenesis, EMT has also been associated with increased therapy resistance and a self-renewing cancer stem cell (CSC) phenotype in different entities (Guo et al. 2012, Lim et al. 2013, Quail and Joyce 2013).

After intravasation CTCs have to survive the high shear forces within the circulation and potential encounters with cells of the immune system. This leads to a rather short half-life of CTCs, which is estimated to be ≤ 24h (Dong et al. 2013, Payne et al. 2019). Increased half-life and metastatic potential have been attributed to CTCs occurring in clusters with white blood cells (WBCs), so called circulating tumor microemboli (Aceto et al. 2014). Those cells that survive the harsh conditions in the blood stream can reach distant sites, where they extravasate. The extravasation process involves anchoring of the CTCs to the luminal surface of the endothelial cells (ECs), which is thought to be mediated by interaction of adhesion receptors on CTCs and ECs (Lou et al. 2015). After extravasation the cells can enter a dormant state and persist in distant tissues for multiple years. These cells are referred to as disseminated tumor cells (DTCs) (Dasgupta et al. 2017). Both DTCs and CTCs can give rise to metastasis.

1.3.1 Isolation and Analysis

Isolating CTCs is rather challenging, as they are extremely rare compared to other cell types within the blood. CTC yields vary based on cancer entity, disease progression, and isolation method, but in one milliliter of blood roughly 1-100 CTCs can be found. That translates to one CTC in a billion circulating cells (Gribko et al. 2019, Kunzel et al. 2019). Isolation methods can be divided into those based on physical properties like size or density, and those based on biological properties, i.e. the expression of specific marker proteins (Figure 10) (Sharma et al. 2018, Payne et al. 2019). With a size of 9-19 µm CTCs are larger than other cells contained in the blood. This property can be exploited to separate CTCs using microfilters or microfluidic devices (Hosokawa et al. 2010, Ferreira et al. 2016). The main challenge here is the proximity in size to leukocytes (7-9 µm) (Coumans et al. 2013). There have also been reports of smaller CTCs which would be lost using such methods (Allard et al. 2004). Using centrifugation, CTCs can be separated by their specific density. Size and density based isolation techniques are often applied in combination (Banko et al. 2019). Dielectrophoretic field-flow fractionation (DEP-FFF) can be used to isolate CTCs based on their size and polarizability (Gascoyne et al. 2009). In general, methods based on physical properties have high throughputs, but they lack specificity and purity, as CTCs are a rather heterogeneous cell population (Sharma et al. 2018).

Techniques based on biological properties exploit immunoaffinity capture of specific surface antigens. If surface antigens on the CTCs are targeted, the process is referred to as positive selection. The complementary process of negative selection is based on depleting the sample by targeting antigens that are not expressed on CTCs, but on other blood cells. Both rely on the functionalization of surfaces or beads with the respective antibodies (Banko et al. 2019). For positive selection the CTC marker epithelial cell adhesion molecule (EpCAM) is the most common antigen. It is also employed by the FDA-approved CTC isolation platform CellSearch. Since EpCAM is only suitable for epithelial tumors and its expression can get lost during EMT, alternative antigens like epidermal growth factor receptor (EGFR) and cell-surface vimentin (CSV) have been used to isolate different CTC populations (Satelli et al. 2015, Sharma et al. 2018). Negative selection is mostly based on CD45, a WBC marker, and often combined with other depletion methods like red blood cell (RBC) lysis (Yang et al. 2009). When comparing the two immunoaffinity-based approaches, negative selection yields lower purity than positive selection. However CTCs isolated by positive selection are labeled, which can interfere with downstream applications. In addition, they most likely only represent a subpopulation based on the antigen chosen for CTC capture (Banko et al. 2019).

The choice of a suitable CTC isolation method largely depends on the downstream application. If CTCs are supposed to be cultured, label-free cells are favorable. For simple enumeration this might not be necessary. In general, it should be kept in mind that likely only a certain subpopulation of CTCs will be enriched based on the respective properties chosen for isolation. One of the main challenges of future CTC research will be to automate the isolation process, which is a crucial step towards integrating CTC analysis into clinical practice. While the approval of CellSearch was an important achievement in this regard, the system still comes with numerous limitations, is very laborious, and requires highly trained personnel. Therefore ongoing research is focusing on more flexible, reproducible, and user-friendly solutions (Andree et al. 2016).

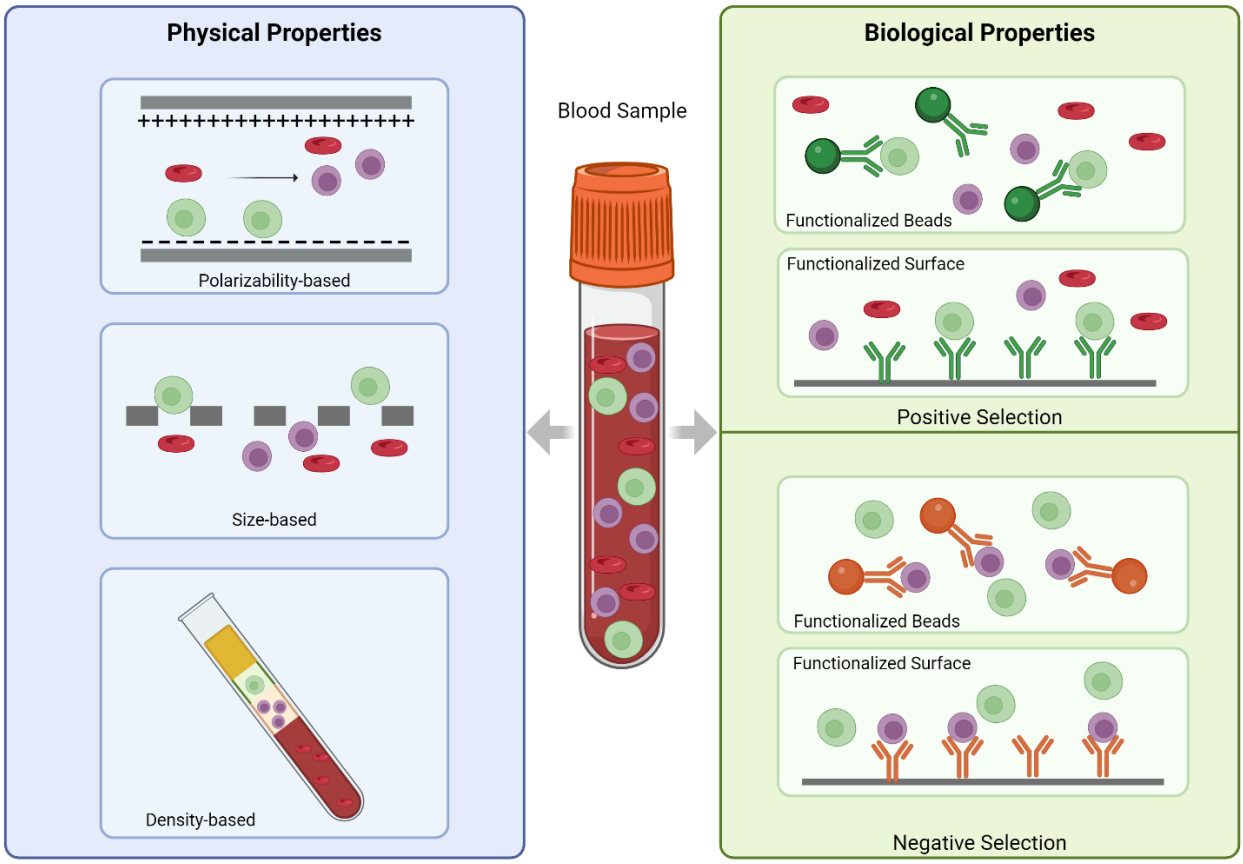

Figure 10. Isolation methods for circulating tumor cells (CTCs)
In a patient's blood sample CTCs (green) occur in a mixture with white blood cells (purple) and red blood cells (red). To achieve separation by physical properties, CTC polarizability, size, or density can be exploited. For isolation based on biological properties, either CTC markers (positive selection) or white blood cell markers (negative selection) can be targeted by functionalized beads or surfaces. The latter is often combined with red blood cell lysis or other additional depletion techniques. Size and quantitative ratio of cells were optimized for visualization purposes and do not reflect the *in vivo* situation.

Analysis of CTCs can be broadly divided into proteomic and transcriptomic approaches. Proteomic approaches focus on specific marker proteins expressed by CTCs. Labelling these proteins with specific antibodies allows for their visualization and quantification using optical systems. Typically, applied CTC markers include epithelial proteins like EpCAM, cytokeratins (CKs), and E-cadherin, mesenchymal proteins like N-cadherin and CSV, and stem-cell marker CD133. Additionally, CTCs have to be positive for a nuclear dye (e.g. DAPI) and negative for the leukocyte marker CD45. Other entity specific markers, for example prostate-specific antigen (PSA), can also be applied (Yap et al. 2014, Sharma et al. 2018). For transcriptomic analysis, DNA or RNA are targeted. Whole genome amplification allows for genotyping of CTCs on single cell level (Krebs et al. 2014). RNA can be analyzed by quantitative PCR (qPCR), digital PCR (dPCR), or fluorescence in-situ hybridization (FISH). While these methods are highly sensitive, they also require high purity samples. Additionally, they do not provide the option to enumerate CTCs (Sharma et al. 2018). Another approach to CTC research is culturing CTCs *ex vivo* or in xenografts to exploit them as models for drug development and personalized therapy. This requires high purity, label-free CTCs, and has only been successful in a small number of studies (Praharaj et al. 2018).

1.3.2 CTCs in Chemotherapy Resistance

Typically, the number of detectable CTCs goes down after successful treatment. A study with breast cancer patients found that in non-responders the number of CTCs expressing CSC marker ALDH1 and EMT marker TWIST1 was significantly increased after chemotherapy compared to responders (Papadaki et al. 2019). Similarly, another study found a correlation between the expression of ALDH and MDR proteins on CTCs with chemoresistance in breast cancer patients (Gradilone et al. 2011). Studies with immunodeficient mice have shown that in fact only those CTCs expressing mesenchymal and stemness markers are able to form metastasis after xenotransplantation (D'Alterio et al. 2020). There has also been evidence that exposure to shear stress leads to changes in morphology and increased expression of mesenchymal markers, again suggesting an involvement of EMT and in turn increased tolerance to chemotherapy (Xin et al. 2019). In general, chemotherapy leads to a selective pressure within the primary tumor that favors EMT and thereby gives rise to more migratory tumor cells that potentially become CTCs. In summary, it can be postulated that the process of EMT allowing for CTC intravasation and the selective pressure within the blood stream lead to molecular changes in the CTCs' constitution that also cause increased tolerance to chemotherapeutic drugs. Metastasis originating from such CTCs likely inherit these traits (D'Alterio et al. 2020).

1.3.3 CTCs as Biomarker

The easiest way to use CTCs as biomarker is to simply count how many CTCs are present in the circulation. For HNSCC patients, it has been shown in several studies that CTC counts significantly decrease after treatment, allowing for post-treatment monitoring (Buglione et al. 2012, Payne et al. 2019, Wang et al. 2019). A comparative study demonstrated that oropharyngeal and oral cavity cancers have increased CTC counts compared to other anatomical sites of HNSCC. The same study also revealed a correlation between CTC count and nodal stage, but not T status (Hristozova et al. 2011). On the contrary, a similar study found a correlation between disease progression and T status with increased CTC counts (Kawada et al. 2017). Both studies were carried out with HNSCC patients, but using different CTC isolation methods, flow cytometry and microfilters respectively. When looking at survival outcomes, one study found that increased CTC counts correlated with decreased disease-free survival (DFS) in HNSCC patients in a follow-up period of 19 months, using negative selection (Jatana et al. 2010). Another study using qPCR of EGFR for CTC detection found that increased CTC counts correlated with decreased DFS and overall survival (OS) in non-oropharyngeal cancers in a follow-up period of 34 months. For oropharyngeal cancers the same study found high CTC counts to be a sign of improved DFS and OS (Tinhofer et al. 2014). These ambiguous results highlight the importance of the applied CTC isolation method.

A lot of current research is focused on the genetic and proteomic characterization on single CTC level. For HNSCC, it could be shown that around a third of CTCs are negative for epithelial markers but express mesenchymal markers, showcasing the presence of different CTC populations (Balasubramanian et al. 2012). Another study found CTCs expressing both epithelial (cytokeratin) and mesenchymal markers (N-cadherin), with some even expressing additional stem cell markers (CD133). The presence of mesenchymal CTCs after resection was associated with decreased OS (Weller et al. 2014). A different study found that patients with > 20 % Podoplanin-positive epithelial CTCs had a decreased OS in a median follow-up period of 10,5 months (Hsieh et al. 2015). For recurrent/metastatic HNSCC the overexpression of exosomal PD-L1 after treatment was associated with decreased progression-free survival and OS (Strati et al. 2017).

One of the main questions in CTC research will be how to deal with their heterogeneity when it comes to isolation and subsequent interpretation of the results. To this end further single cell analysis and standardized clinical studies will be necessary to advance the integration of CTCs as biomarkers into clinical practice.

1.4 AIM OF THE STUDY

Early detection and consistent monitoring are pivotal for the successful treatment of numerous cancerous diseases, including HNSCC. Exploring novel biomarkers for liquid biopsy is a promising approach in this regard. Additionally, the establishment of novel biomarkers can also help to understand and thus overcome chemotherapy resistance, which remains a major cause of death in cancer patients. Understanding the molecular mechanisms underlying its emergence and transmission could further aid early detection and informed treatment decisions. Thus, this study set out to explore the role of exosomes in chemotherapy resistance, and discover possibilities to exploit exosomes and CTCs as biomarkers for liquid biopsy. To achieve this, the following work packages were defined:

1. Establishment and validation of exosome- and (automated) CTC isolation

2. Transcriptomic profiling of exosomal markers relevant to chemotherapy resistance *in vitro*

3. Establishment of different cell culture models to evaluate the role of exosomes in chemotherapy resistance transmission in HNSCC

4. Evaluation of different cell culture models in reaction to chemotherapy and exosomal communication

Taken together, the generated results will provide new insights into the role of exosomes as chemoresistance transmission vehicles in HNSCC. Furthermore, the identified exosomal resistance biomarker candidates and established (automated) CTC isolation can be exploited for liquid biopsies in the future, potentially improving clinical management of patients with (chemoresistant) tumors.

2 RESULTS AND DISCUSSION

This section contains the three peer-reviewed publications of the cumulative dissertation, reprinted with permission from the respective publishers. The copyright of the original publications is held by the authors. Table 2 summarizes the contributions to the individual publications, as confirmed by the primary supervisor's and PhD candidate's signatures.

Table 2. PhD candidate's contributions to the publications of the cumulative dissertation

Title	Authors	Journal/Book (Year)	Contributions	Status
Exosomes in Cancer Progression and Therapy Resistance: Molecular Insights and Therapeutic Opportunities	**Madita Wandrey**, Jadwiga Jablonska, Roland H. Stauber, Désirée Gül	Life (2023)	**90 %** (First Authorship) Conceptualization, Literature Review, Manuscript Preparation, Visualization, Review, Editing	Published
A Head and Neck Cancer Spheroid Model for Phenotypic High-Content Screening of Chemoresistance	**Madita Wandrey**, Aya Khamis Hassan, Roland H. Stauber, Désirée Gül	Methods in Molecular Biology (2024)	**90 %** (First Authorship) Conceptualization, Experimental Work, Data Analysis, Manuscript Preparation, Visualization, Review, Editing	Accepted
Characterization of a novel microfluidic platform for the isolation of rare single cells to enable CTC analysis from head and neck squamous cell carcinoma patients	Janis Stiefel, Christian Freese, Ashwin Sriram, Sabine Alebrand, Nalini Srinivas, Christoph Sproll, **Madita Wandrey** et al.	Engineering in Life Sciences (2022)	**10 %** (Co-Authorship) Conceptualization, Methodology and Validation, Immunostaining of HNSCC patient sample (Figure 6), Data Analysis, Visualization	Published

2.1 CTCs AS BIOMARKER FOR HNSCC

Liquid biopsies represent a minimal-invasive alternative to standard tissue biopsies, and pose a promising tool to complement cancer detection and monitoring. Among the potential biomarkers in liquid biopsies are CTCs. Efficient and reproducible isolation of CTCs is of utmost importance for their application as biomarker. Since they are extremely rare compared to other cell types within the blood stream, sensitive and easy-to-use isolation and analysis methods are still lacking, hindering their integration into clinical use. In the following sections, a suitable model for CTC isolation validation is introduced and different methods for manual and automated CTC isolation are tested and compared.

2.1.1 ESTABLISHMENT OF A SUITABLE MODEL FOR VALIDATION

When validating CTC enrichment, a popular first approach is the isolation of cells of a relevant cancer cell line spiked into cell culture medium. This allows for quick and easy access to samples and the possibility of controlling the recovery rate (Sharma et al. 2018).

To find a suitable cell line for the validation process, two established HNSCC cell lines were analyzed for their marker expression. HNSCCUM-02T cells were originally isolated from a male patient's primary lesion at the base of the tongue, while HNSCCUM-03T cells originate from a male patient's primary lesion of the pyriform sinus (Welkoborsky et al. 2003).

For the evaluation of marker expression, cells were seeded in microscopy dishes and stained for epithelial markers ZO-1 and EpCAM and mesenchymal marker CSV. HNSCCUM-02T cells show expression of all three evaluated markers. In HNSCCUM-03T there was no EpCAM expression detectable by microscopy, while ZO-1 and CSV were readily stained (Figure 11A). To validate the results, protein expression was additionally analyzed by western blot. Here, HNSCCUM-02T show a more epithelial cell type based on the expression of EpCAM and ZO-1. CSV was not detectable. HSNCCUM-03T show high expression of mesenchymal marker CSV, while there were no clear bands for ZO-1 and EpCAM detectable (Figure 11B).

Since the enrichment methods to be tested were based on positive selection for epithelial marker EpCAM, the validation process was continued with HNSCCUM-02T cells. They were additionally fixed and stained for epithelial marker E-cadherin and mesenchymal marker Pan-Cytokeratin (Pan-CK), and staining of ZO-1 and Pan-CK was further tested in HNSCCUM-02T isolated from whole blood (Supplementary Figure 1). Both markers were readily stained, even after the isolation process, while remaining blood cells remained stain-free. Thus, HNSCCUM-02T cells were considered a suitable model for the validation process.

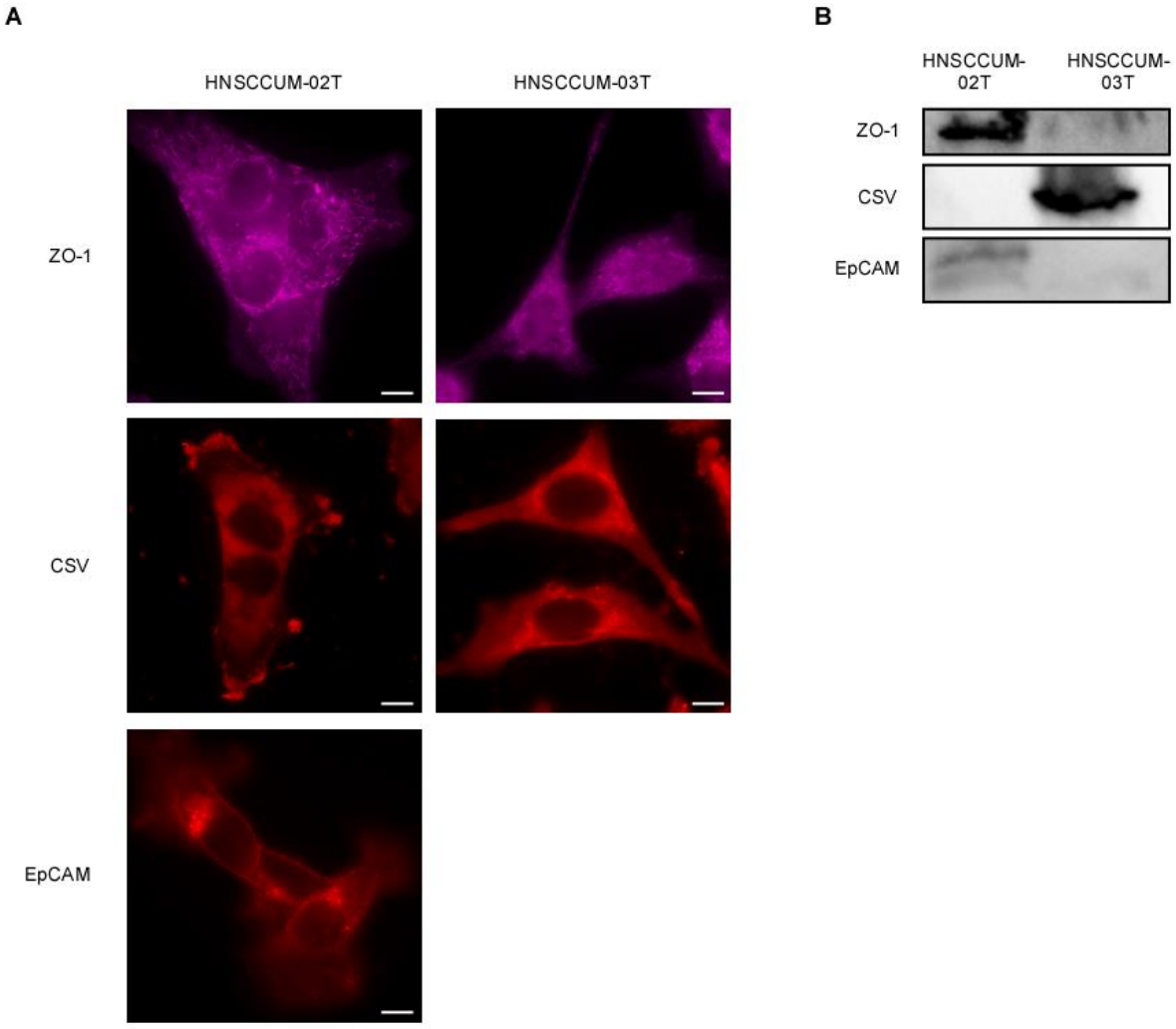

Figure 11. Expression of selected marker proteins on HNSCC cell lines
A) Representative fluorescence microscopy images. Cells were grown in microscopy dishes for 24h and then fixed and stained with fluorophore-labelled antibodies. Scale bars 10 µM. **B)** Western Blot analysis of marker protein expression. Lysates were prepared from confluent 10 cm dishes and the maximum possible amount of protein was loaded.

2.1.2 Evaluation of Different Positive-Selection Protocols

To obtain high purity CTCs, two positive selection methods were chosen for testing (Figure 12). The Dynabeads FlowComp Flexi Kit (Thermo Fisher Scientific, Dreieich) is based on biotinylated antibodies and streptavidin-functionalized magnetic beads. Any antibody can be DSB-X biotinylated and added to the sample. Antibodies will bind to the cells expressing the respective marker protein. When adding the streptavidin-functionalized beads, they will bind to the biotinylated antibodies. The bead-antibody-cell complex can be isolated using a magnet. Afterwards cells are released from the beads by addition of a release buffer containing excess biotin or desthiobiotin. The pluriBeads system (pluriSelect, Leipzig) is based on antibody-coated polystyrene beads. PluriBeads can be coupled to any desired antibody or be purchased readily coupled. The coupling mechanism is based on disulfide bonds, which can be resolved using a reducing agent. Cells expressing the respective marker protein will bind to the antibodies on the beads and will be held back on a specific sieve because of the large size of the beads. Afterwards the cells are released from the beads, allowing them to pass through the sieve, while the beads stay held back. Both methods yield bead-free, antibody-labelled CTCs.

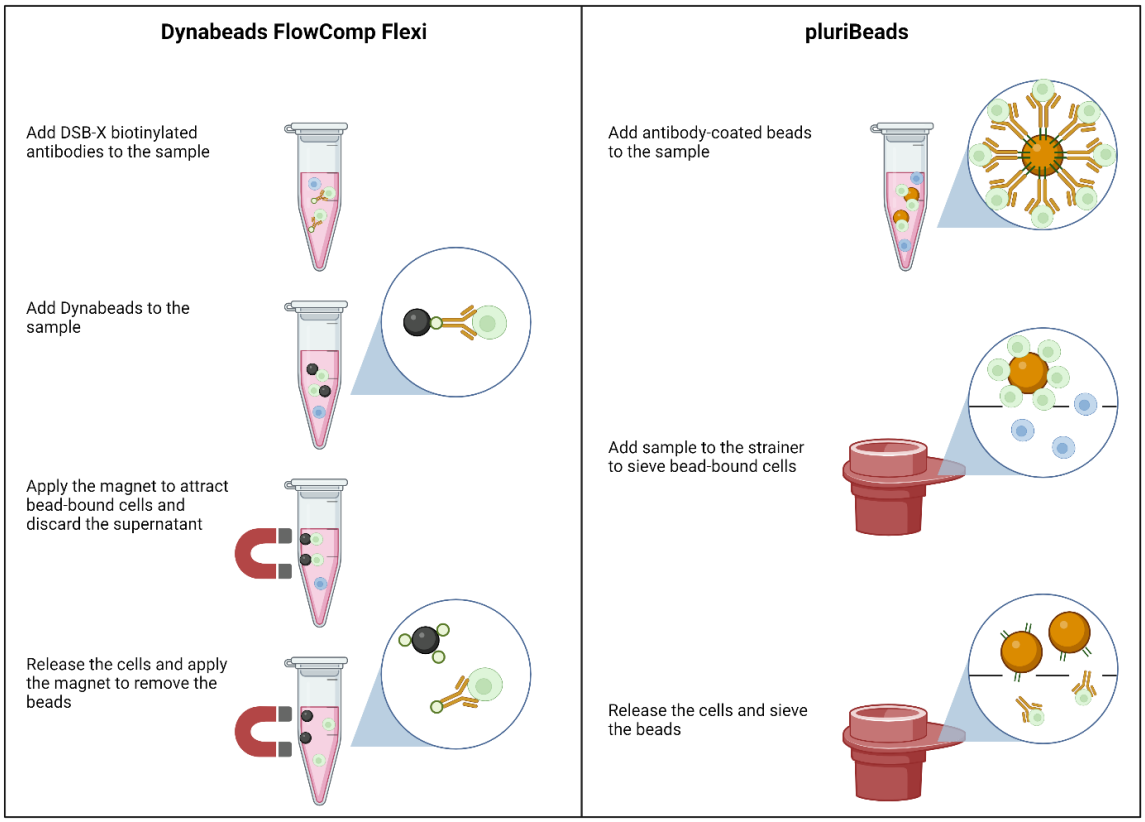

Figure 12. Schematic illustration of CTC isolation by Dynabeads FlowComp Flexi and pluriBeads
Target CTCs are shown in green, non-target blood cells in blue. Size and quantitative ratio of cells and beads were optimized for visualization purposes and do not reflect the *in vivo* situation.

For the validation process HNSCCUM-02T cells were detached and stained with Carboxyfluoresceinsuccinimidylester (CFSE) to allow for easy detection after the isolation procedure. 30-40 cells were spiked into 7,5 mL cell culture medium. Different protocol variations were tested for both methods. Initial tests were carried out according to manufacturer's instructions. To avoid potential loss of cell surface marker expression during trypsination of HNSCCUM-02T cells, accutase was introduced as an alternative detachment agent. For the Dynabeads a protocol using weaker magnets was tested, as some cells appeared to be squashed during the magnet attraction. Additionally, an automated enrichment protocol using the *IsoMAG* platform was tested (Gribko et al. 2021). Here the magnetic separation and washing steps were performed by the automated isolation unit. Subsequent evaluation and enumeration of isolated cells was performed manually. The pluriBeads were tested according to manufacturer's instructions using commercial and self-coupled anti-EpCAM beads. Figure 13 summarizes the results, while Table 3 contains detailed information on the applied protocol variations. With 62,5 % the highest recovery rate was achieved using commercial pluriBeads in combination with accutase-detached cells, followed by self-coupled pluriBeads with 47,5 %. Dynabeads reached recovery rates of only 20-30 %, regardless of manual or automated application. The use of weaker magnets lead to a further reduction of the recovery rate to 16,7 %, though it has to be considered that weak magnets and automated isolation were tested with EpCAM only, while the other Dynabeads protocols were tested targeting EpCAM and CSV, potentially increasing the yield. Nevertheless, Gribko et al. 2021 reported a recovery rate of 86,9 % using the *IsoMAG* platform, while reaching 88,9 % recovery in the same model system when performing manual isolation. These much higher recovery rates could be explained by the use of different cell lines. In the same study, Gribko et al. 2021 used the *IsoMAG* platform to isolate HNSCCUM-02T from blood, reaching a mean recovery rate of 95 ± 15 %. However, recovery rates of >100 % were reported and contributed to the mean value calculation, potentially leading to an overestimated recovery rate. Unfortunately, there are no further studies on the performance of the *IsoMAG* platform available. It also has to be kept in mind that the different isolation methods were only tested once or twice here, leaving the reproducibility and accuracy of the data up for debate.

The waste, which refers to any discarded medium, was also analyzed for target cells. Using Dynabeads 47,8 ± 21,4 % of the cells were found in the waste, while only 20,8 ± 11,2 % cells were found in the pluriBeads waste. A high amount of target cells in the waste is a sign for a low binding rate between beads and cells. Another potential reason for target cell loss is incomplete release from the beads. Unfortunately, enumeration of these cells was not possible, because the

Dynabeads seemingly destroyed any cells that remained bound during magnet attraction and pluriBeads elicit autofluorescence, making microscopic detection of target cells unfeasible.
Based on these initial tests, pluriBeads were elected for further evaluation for manual isolation based on higher recovery rates and lower target cell loss in the waste. Dynabeads were considered for further automation approaches.

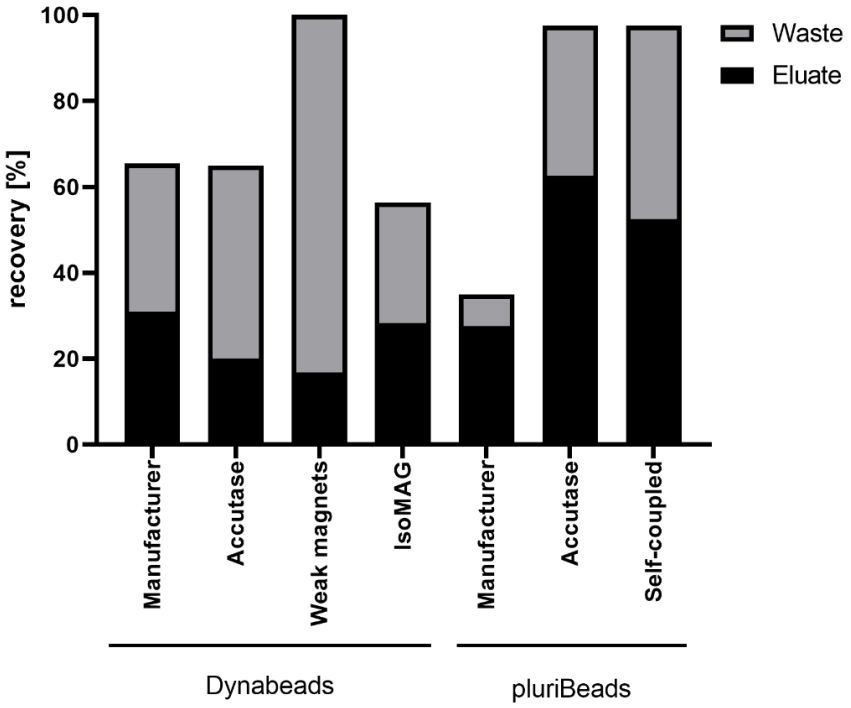

Figure 13. Testing CTC Isolation using different positive selection protocols
HNSCCUM-T02 cells were detached and stained with CFSE. Using a fluorescence microscope, 30-40 cells were counted and spiked into 7,5 mL cell culture medium. After isolation according to the described protocol variation (for details see Table 3), eluate and waste were analyzed for target cells by fluorescence microscopy and recovered cells were counted.

Table 3. Detailed information on tested CTC isolation protocols

Method	Protocol	Antigens	Details
Dynabeads	Manufacturer	EpCAM, CSV	-
	Accutase	EpCAM, CSV	Alternative to trypsin for cell detachment
	Weak magnets	EpCAM	Minimized force
	IsoMAG	EpCAM	Automated enrichment and washing
pluriBeads	Manufacturer	EpCAM	-
	Accutase	EpCAM	Alternative to trypsin for cell detachment
	Self-coupled	EpCAM	-

2.1.3 MANUAL CTC ISOLATION

For further evaluation of manual isolation using the pluriBeads system, commercial and self-coupled anti-EpCAM pluriBeads were compared (Figure 14A). CFSE stained HNSCCUM-02T cells (35 cells) were spiked into 5 mL of cell culture medium and isolated according to manufacturer's instructions. Commercial pluriBeads yielded a recovery of 56,4 ± 18,3 % and self-coupled pluriBeads achieved 49,5 ± 15,7 % recovery. Figure 14B shows a representative image of a pluriBead-bound cell before release. Statistically, there was no significant difference between the two types of pluriBeads. Since the self-coupled beads had a lower standard deviation and they are more flexibly applicable, as they allow for coupling with different antibodies, they were chosen for further evaluation in whole blood. Therefore, 35 CFSE-stained HNSCCUM-02T cells were spiked into 5 mL of whole blood from healthy donors and isolated using the same protocol. The recovery rate was comparable to that from cell culture medium (Figure 14C), but microscopy revealed a significant contamination with non-target blood cells (Figure 14D, Supplementary Figure 1B). One possible explanation for such contaminations would be the aggregation of non-target cells, leading to a size increase above 20 µM. This could lead to clogging of the sieve, which is additionally enhanced by the large beads. Even though the beads are thoroughly washed, they are much heavier than the cells and likely sediment much quicker onto the sieve, potentially blocking the passage of non-target cells.

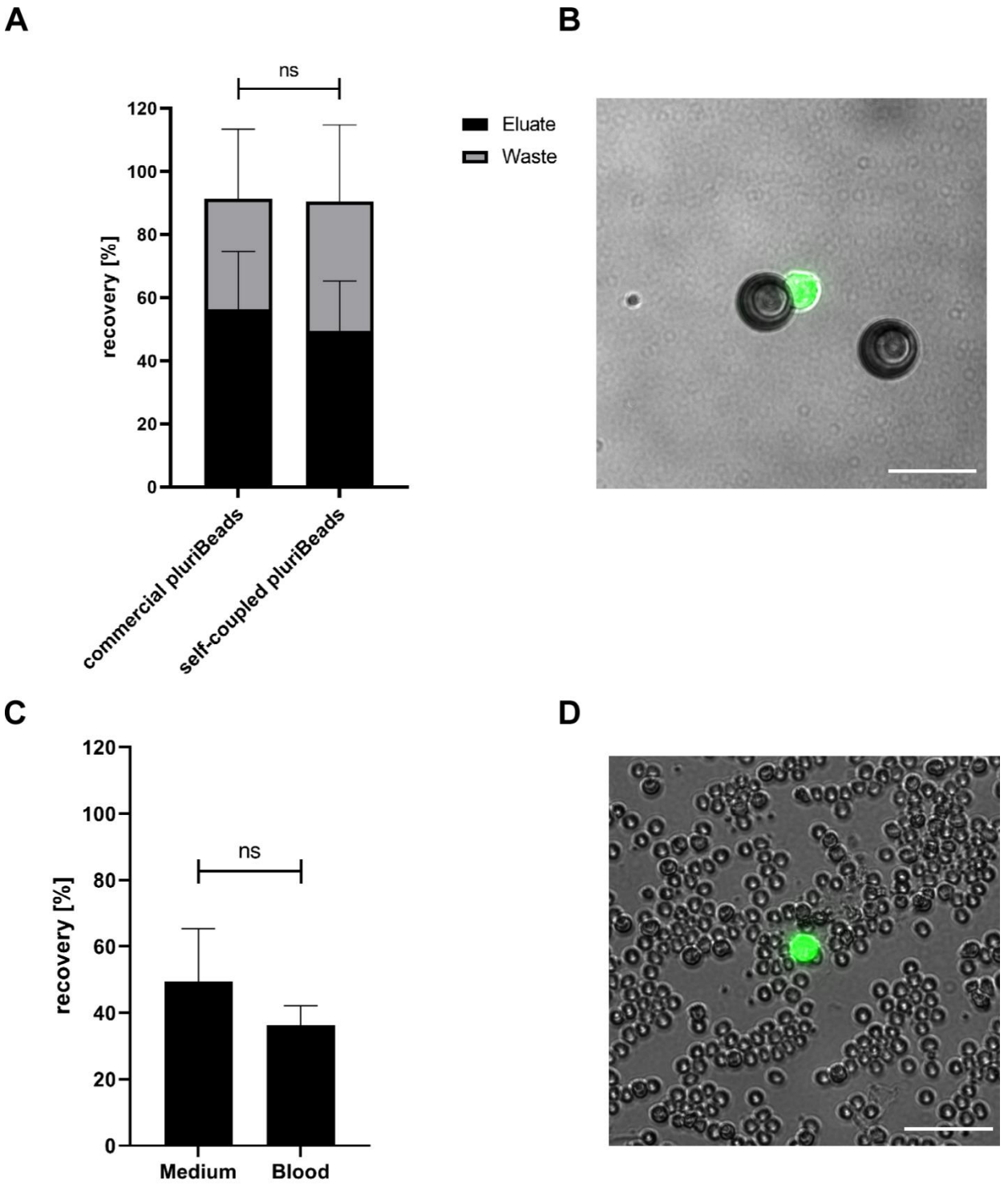

Figure 14. Validation of manual CTC isolation by pluriBeads
35 CFSE stained HNSCCUM-02T cells were spiked into 5 mL cell culture medium or whole blood and isolated using pluriBeads according to manufacturer's instructions. **A)** Comparison of isolation from cell culture medium using commercial (n=4) and self-coupled (n=3) anti-EpCAM pluriBeads. **B)** Representative microscopic image of a bead-bound target cell (green) before release. **C)** Comparison of isolation from cell culture medium and whole blood using self-coupled anti-EpCAM pluriBeads (n=3) **D)** Representative microscopic image of eluted target cell (green) among co-eluted blood cells. Scale bars 50 µM. Statistical analysis by unpaired student´s t-test. ns, $p \geq 0,05$

2.1.4 AUTOMATED CTC ISOLATION

As introduced, the standardization of CTC isolation and analysis is a major concern for the successful integration of CTC-related biomarkers into clinical use. Automating these processes would be a valuable step in this direction, and numerous attempts have already been made in this regard. One of those, the *IsoMAG* platform, was already tested in this thesis (sections 2.2.1.2 and 6.5). Even though Dynabeads achieved inferior recovery rates in manual tests compared to PluriBeads, they pose the better starting point for automation, as a prototype platform (*IsoMAG*) was already at hand. This platform was further developed by our collaborators, resulting in the *CTCelect* platform. The immunomagnetic enrichment unit of the *IsoMAG* was integrated into the *CTCelect* platform. Additionally, the successor platform applies microfluidic, fluorescence-activated cell sorting using fluorophore-labelled anti-EpCAM antibodies, allowing for the dispension of single cells. Detailed results on the isolation platform can be taken from our publication (Stiefel et al. 2022) (see also section 2.1.5).

In a pilot clinical test run, 7,5 mL whole blood were taken from a HNSCC patient and CTC isolation was performed at the Fraunhofer IMM using the *CTCelect* platform. Dispensed cells were pooled and stained for ZO-1 and CD45 using fluorophore-labelled antibodies, and for nuclei using Hoechst dye. Residual EpCAM staining from the isolation process was also probed, but remained undetectable in all cells (Stiefel et al. 2022, Figure 6). A total of 26 nucleated cells could be recovered. Cells were considered CTCs if they were $Hoechst^{+}/ZO\text{-}1^{+}/CD45^{-}$ in the staining. Accordingly, 18 CTCs could be identified in the patient sample, while 8 cells were non-CTCs (Figure 15). The most common contaminating cell type are white blood cells (WBCs). Based on the $CD45^{+}$ staining of all detected non-CTCs they can be considered WBCs. While this test was limited to only one patient, it shows that fully automated CTC isolation from whole blood is feasible. The fact that one third of the recovered cells are non-CTCs/WBCs highlights the importance of multiple marker analysis. Solely based on EpCAM expression, all of the 26 cells would have been considered CTCs. Using negative control markers like CD45 is crucial to prevent overestimation of CTC counts, which is of utmost importance when enumeration is the only evaluated parameter. Adding further markers like ZO-1 can increase the sensitivity and possibly even allow for the identification of different CTC subpopulations. However, a sophisticated staining procedure can interfere with other downstream applications like cell cultivation. Therefore, the isolation and characterization methods always need to be adjusted to the downstream applications.

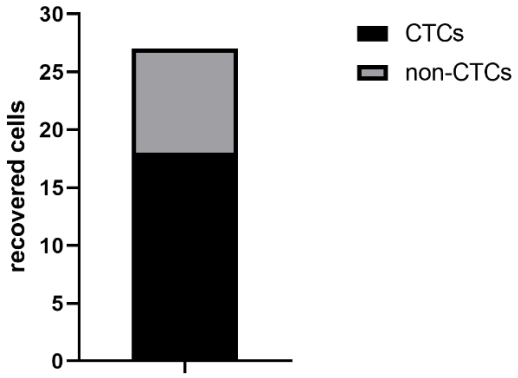

Figure 15. Cells recovered from patient blood using the *CTCelect* platform by population
CTCs were isolated from 7,5 mL whole blood of a HNSCC patient using the *CTCelect* unit. Dispensed cells were pooled and stained for cell nuclei, epithelial marker ZO-1, and WBC marker CD45. Cells were considered CTCs if nucleus^{+}/ZO-1^{+}/CD45^{-}. Full results from the same experimental run are included in the following section.

2.1.5 Characterization of a Novel Microfluidic Platform for the Isolation of Rare Single Cells to Enable CTC Analysis from Head and Neck Squamous Cell Carcinoma Patients (Research Article)

Janis Stiefel, Christian Freese, Ashwin Sriram, Sabine Alebrand, Nalini Srinivas, Christoph Sproll, **Madita Wandrey**, Désirée Gül, Jan Hagemann, Jürgen C. Becker, Michael Baßler

Abstract

Detailed examination of tumor components is leading-edge to establish personalized cancer therapy. Accompanying research on cell-free DNA, the cell count of circulating tumor cells (CTCs) in patient blood is seen as a crucial prognostic factor. The potential of CTC analysis is further not limited to the determination of the overall survival rate but sheds light on understanding inter- and intratumoral heterogeneity. In this regard, commercial CTC isolation devices combining an efficient enrichment of rare cells with a droplet deposition of single cells for downstream analysis are highly appreciated. The Liquid biopsy platform *CTCelect* was developed to realize a fully-automated enrichment and single cell dispensing of CTCs from whole blood without pre-processing. We characterized each process step with two different carcinoma cell lines demonstrating up to 87 % enrichment (n = 10) with EpCAM coupled immunomagnetic beads, 73 % optical detection and dispensing efficiency (n = 5). 40-56,7 % of cells were recovered after complete isolation from 7.5 mL untreated whole blood (n = 6). In this study, *CTCelect* enabled automated dispensing of single circulating tumor cells from HNSCC patient samples, qPCR-based confirmation of tumor-related biomarkers and immunostaining. Finally, the platform was compared to commercial CTC isolation technologies to highlight advantages and limitations of *CTCelect*. This system offers new possibilities for single cell screening in cancer diagnostics, individual therapy approaches and real-time monitoring.

Received: 14 October 2021 | Revised: 14 December 2021 | Accepted: 24 December 2021

DOI: 10.1002/elsc.202100133

Engineering in Life Sciences

RESEARCH ARTICLE

Characterization of a novel microfluidic platform for the isolation of rare single cells to enable CTC analysis from head and neck squamous cell carcinoma patients

Janis Stiefel[1] | **Christian Freese**[1] | **Ashwin Sriram**[2] | **Sabine Alebrand**[1] | **Nalini Srinivas**[2] | **Christoph Sproll**[3] | **Madita Wandrey**[4] | **Désirée Gül**[4] | **Jan Hagemann**[4] | **Jürgen C. Becker**[2] | **Michael Baßler**[1]

[1]Fraunhofer Institute for Microengineering and Microsystems IMM, Mainz, Germany

[2]Translational Skin Cancer Research, DKTK Partner Site Essen/Düsseldorf, West German Cancer Center, Dermatology, University Duisburg-Essen, Essen, Germany; German Cancer Research Center (DKFZ), Heidelberg, Germany

[3]Clinic for Oral and Maxilofacial Surgery, Düsseldorf University Hospital, Heinrich-Heine-University, Düsseldorf, Germany

[4]Department of Otorhinolaryngology/ENT, University Medical Center, Mainz, Germany

Correspondence
Mr. Janis Stiefel, Diagnostics, Fraunhofer Institute for Microengineering and Microsystems IMM, Carl-Zeiss-Straße 18–20, 55129 Mainz, Germany.
Email: janis.stiefel@imm.fraunhofer.de

Funding information This research was funded by the VIP+ program of the Federal Ministry of Education and Research (BMBF) Germany, grant number 03VP01061. J. Stiefel was financially supported by the Claudia von Schilling Foundation for Breast Cancer research.

Abstract

Detailed examination of tumor components is leading-edge to establish personalized cancer therapy. Accompanying research on cell-free DNA, the cell count of circulating tumor cells (CTCs) in patient blood is seen as a crucial prognostic factor. The potential of CTC analysis is further not limited to the determination of the overall survival rate but sheds light on understanding inter- and intratumoral heterogeneity. In this regard, commercial CTC isolation devices combining an efficient enrichment of rare cells with a droplet deposition of single cells for downstream analysis are highly appreciated. The Liquid biopsy platform *CTCelect* was developed to realize a fully-automated enrichment and single cell dispensing of CTCs from whole blood without pre-processing. We characterized each process step with two different carcinoma cell lines demonstrating up to 87 % enrichment (n = 10) with EpCAM coupled immunomagnetic beads, 73 % optical detection and dispensing efficiency (n = 5). 40 to 56.7 % of cells were recovered after complete isolation from 7.5 ml untreated whole blood (n = 6). In this study, *CTCelect* enabled automated dispensing of single circulating tumor

Abbreviations: μCS, microfluidic fluorescence-activated cell sorting; Ab, antibody; BSA, bovine serum albumin; CFSE, carboxyfluorescein succinimidyl ester; C_T, threshold cycle; CTC, circulating tumor cell; ctDNA, circulating tumor DNA; DTC, disseminated tumor cell; EDTA, ethylenediaminetetraacetic acid; EMT, epithelial-mesenchymal transition; EpCAM, epithelial cell adhesion molecule; FDA, Food and Drug Administration; HNSCC, head and neck squamous cell carcinoma; IMS, immunomagnetic separation; MCF-7, Michigan Cancer Foundation 7; PBMC, peripheral blood mononuclear cells; PE, phycoerythrin; pEMT, partial/post-EMT; pTNM staging, histopathologic tumor-nodes-metastasis staging; RT-qPCR, real time quantitative polymerase chain reaction; SCL-1, Squamous cancer line 1; WBC, white blood cell

cells from HNSCC patient samples, qPCR-based confirmation of tumor-related biomarkers and immunostaining. Finally, the platform was compared to commercial CTC isolation technologies to highlight advantages and limitations of *CTCelect*. This system offers new possibilities for single cell screening in cancer diagnostics, individual therapy approaches and real-time monitoring.

KEYWORDS
automation, liquid biopsy, microfluidics, precision medicine, tumor diagnostics

1 | INTRODUCTION

In the field of liquid biopsy, research on circulating tumor DNA (ctDNA) combined with the detection and analysis of circulating tumor cells (CTCs) has developed into an auspicious minimal invasive tool for the early detection in personalized medicine for tumor patients [1]. Due to the fact that CTCs play an important role in cancer metastasis as the main cause of tumor death, the number of CTCs in a blood sample is considered an independent prognostic factor for the overall survival [2]. In addition to the CTC count particularly on the hunt for the primary tumor in early stage cancer, CTC analysis refines the selection, adaptation and even development of therapies. Although the overall principle of complex metastasis, from the intravasation of CTCs into the circulatory system, arrest and extravasation through vascular walls into distant tissues to the final proliferation of cells to micrometastases, is understood, future intensive study on CTCs and their subtypes will result in much deeper knowledge of these multifaceted processes. Recent studies show that the characterization of CTCs and their subpopulations, that is, disseminated tumor cells (DTC), metastasis-initiating cells and even dual-positive cells ($CD45^+/EpCAM^+$) helps to understand the metastatic behavior of tumors and to deduce prognostic predictions and diagnostic statements [3, 4].

When developing isolation technologies for these cells, their rarity in a blood sample is the biggest hurdle to overcome. Besides billions of healthy blood cells, only one to hundreds tumor-associated cells can be found per ml blood [1]. Systems that are able to enrich CTCs from blood well-balanced between sensitivity and specificity, are therefore highly appreciated. In addition to the enrichment, such systems should exhibit a high capture efficiency, high isolation purity, and ideally the ability to handle a high sample volume in the shortest time possible [5].

Available techniques are based on two major principles: physical methods such as filtration and density dependent techniques or biochemical immuno-affinity dependent methods using ligand-surface interactions with bound antibodies or antibody-bound magnetic beads for the enrichment of CTCs.

The CellSearch system (Menarini Silicon Biosystems) uses magnetic beads that are biofunctionalized against epitopes of tumor-associated EpCAM (Epithelial cell adhesion molecule) to enrich CTCs from patient blood [6, 7]. It has been established to correlate the number of isolated $EpCAM^+$ cells in a blood sample with the overall survival prediction of breast cancer, metastatic colorectal cancer and prostate cancer patients [8–10]. Nevertheless, CTC research in other cancer entities like head and neck squamous cell carcinoma (HNSCC) remains comparably stagnant. With an annual incidence of almost a million new cases and 450,000 deaths worldwide, HNSCC ranks however the fifth most common cancer [11]. Besides carcinogenic polymorph dispositions, smoking, alcohol abuse, and an infection with human papillomavirus correlate with head and neck cancers [12]. In two third of HNSCC patients, initial diagnosis of the primary tumor goes hand in hand with the discovery of adjacent metastatic lymph nodes [13]. Increased mortality is associated with the abundant presence of micrometastases, whereas the 5-year survival rate of patients with distant metastatic sites sinks below 35 % [14]. HNSCC cells that undergo epithelial-mesenchymal transition (EMT) deregulate epithelial characteristics like cell adhesion and enhance invasive migration. EMT is a dynamic reversible process correlating with the development of stem cell properties and fostering metastasis. This fact stresses the importance of an in-depth understanding of metastatic metabolisms, including the heterogeneity of disease-driving CTCs, to pave the way for innovative therapeutics.

The aim of the present work was to characterize a fully-automated system in detail which is customizable for any tumor type with a reliable capture rate and CTC purity facilitating access to molecular diagnostics. The presented *CTCelect* system combines immunomagnetic enrichment from 7.5 ml whole blood, microfluidic fluorescence-activated cell sorting (μCS) and single cell dispensing through a microfluidic disposable cartridge independently of the tumor entity (Figure 1) in one

fully-automated benchtop device. This study aimed to evaluate the functionality and the diverse applicability of *CTCelect* by means of cutaneous squamous cell carcinoma and mamma carcinoma cell line models and to present data of dispensed single tumor cells from HNSCC patient blood.

PRACTICAL APPLICATION

Still today standardized therapeutic guidelines like relatively broadband chemotherapy are followed depending on the primary tumor entity neglecting the metastatic profile of systemic cancer. On the downside, disseminated and circulating tumor cells of many cancers show intratumoral heterogeneity and cause disease relapse years after surgery. Hence, easy-to-use platforms, like the show-cased CTCelect device, to isolate these rare cells in a completely automated way and analyze them on a single cell level will be of high significance as predictive measures for therapeutic success to accompany cancer treatment. The microfluidic chip-based cell sorting unit was implemented into a one-step device for user-friendly handling. Studies with the system could therefore directly provide new insights both in therapy monitoring as clinical application and in basic research of tumor biology to unravel metastatic processes.

2 | MATERIALS AND METHODS

If not otherwise indicated, reagents and supplements were purchased at Thermo Fisher Scientific, Darmstadt, DE.

2.1 | Cell lines

MCF-7 breast cancer cells were purchased from AdnaGen (Langenhagen, DE) and cultured in RPMI1640 medium with L-glutamine (Capricorn Scientific, Ebsdorfergrund, DE) supplemented with 10 % fetal calf serum (FCS; Merck, Darmstadt, DE). The SCL-1 squamous cell carcinoma line was kindly provided by Dr. Petra Boukamp (DKFZ, Heidelberg, DE) [15] and cultured in Gibco DMEM (low glucose, pyruvate) medium supplemented with 10 % FCS. Cell lines were split at subconfluence and incubated at 37°C in a humidified atmosphere in the presence of 5 % CO_2.

2.2 | Blood samples

Whole blood bags from healthy donors were obtained from the local Blood Transfusion Center (University Medical Center Mainz, DE) in 500 mL CompoFlex blood bags (Fresenius Kabi, Bad Homburg, DE) with CPD-1 anticoagulant and stored at room temperature for a maximum of three days. Patient samples were collected at the Tumor Center of Western Germany (University Hospital Essen, DE) from a HNSCC patient with increasing metastasis in adjacent lymph nodes (pTNM staging: pT2pN3b), at the Department of Otorhinolaryngology/ENT, (University Medical Center Mainz, DE; pTNM staging n.a.) and processed within 24 h after blood draw. Informed consent was obtained from the patients and approved by the ethical committee vote at the Medical Faculty of the Heinrich-Heine-University Düsseldorf (ref.no. 3090; 2016) and by the local ethics committee in Mainz (ref.no. 837.485.15 (10253); 2016).

2.3 | Immobilization of biotinylated antibodies on streptavidin coupled magnetic microbeads

The immunomagnetic separation (IMS) of CTCs from whole blood required tumor-specific coating of immunomagnetic beads with biotinylated monoclonal mouse anti-human EpCAM (CD326; 20 µg/mL) antibody 1B7. Various beads with different sizes ranging from 1 to 4.5 µm diameter and different surface properties (tosyl-activated, hydrophobic; carboxylic acid, hydrophilic) were tested with SCL-1 cells in our preliminary work and the herein used Invitrogen Dynabeads MyOne Streptavidin T1 (10 mg/ml) with a binding capacity of 400 pmol biotinylated peptides per mg beads enabled the best recovery rates in our setting. These microbeads indicate a low sedimentation rate and high binding capacity due to their small diameter and are hence ideal for automated enrichment. EpCAM antibody was immobilized on the bead surface with an extended incubation time of 1 hour. After immobilization, magnetic beads were added a saturated biotin/PBS solution for 30 min with gentle rotation of the tube to block free streptavidin binding sites and prevent clumping. After an additional washing step, anti-EpCAM magnetic beads (hereinafter abbreviated as EpCAM beads) were stored in PBS/0.1 % BSA at 4°C for several weeks.

2.4 | Determination of *CTCelect* recovery rates of cultured tumor cells

To evaluate the *CTCelect* enrichment efficacy, recovery rates of cultured tumor cells after automated IMS from

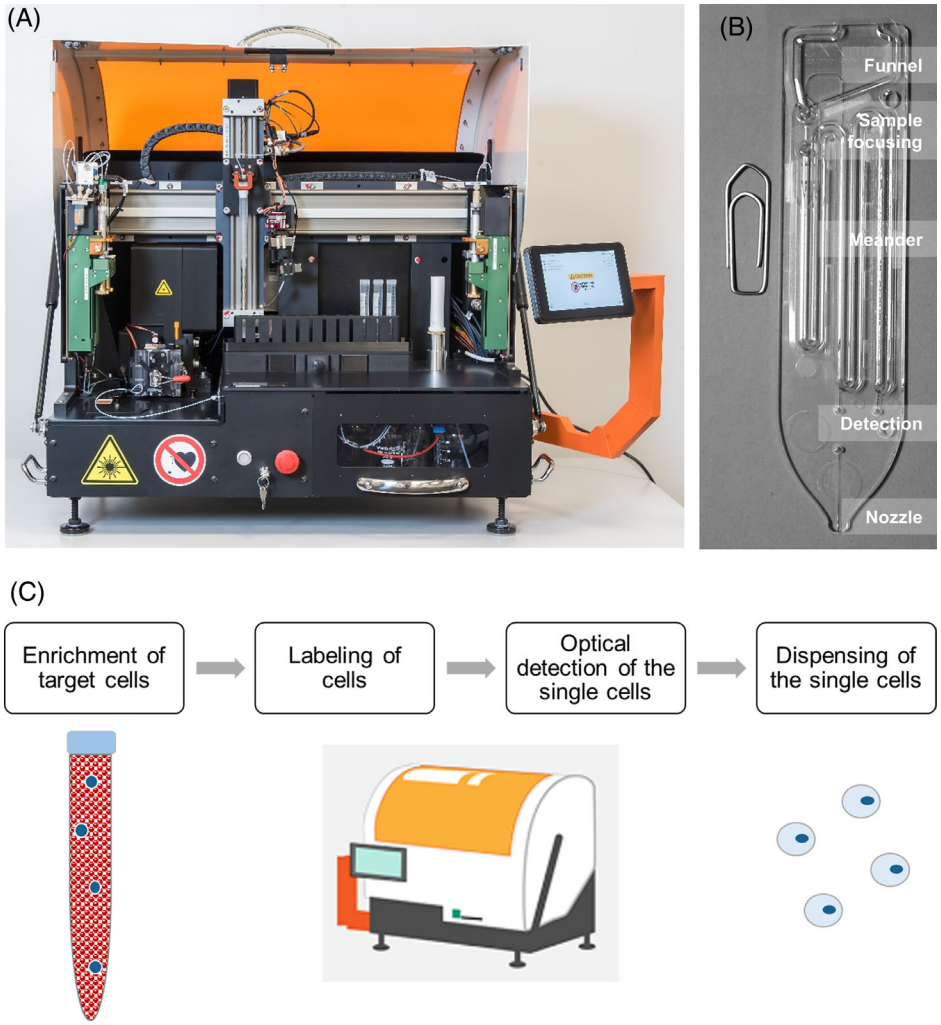

FIGURE 1 *CTCelect* system, microfluidic chip and process conception. (A) The benchtop device consists of an immunomagnetic enrichment module (right-sided) and a microfluidic fluorescence-activated cell sorting (μCS) subunit (left-sided). The fully-automated isolation process is user-controlled via touchscreen. Sample handling and transfer is managed by a pipetting robot. (B) The *CTCelect* chip is placed in the chip holder of the cell sorting subunit and disposed after isolation. The chip consists of a reservoir funnel for the cell suspension, a hydrodynamic focusing channel, a detection zone and a nozzle for cell dispensing. (C) *CTCelect* concept for single cell dispensing from 7.5 mL samples

medium and whole blood were determined. Robust cancer cell models were required and MCF-7 and SCL-1 cells are a suitable candidate for immunomagnetic enrichment to prevalidate the functionality of the platform. We tested both cell lines to have high EpCAM expression (see Supporting Information S1). Cells were stained using the CellTrace CFSE Cell Proliferation Kit (CFSE) according to the manufacturer instructions. 15 mL sized ROTILABO centrifuge tubes without rim (Carl Roth, Karlsruhe, DE) are most suitable for the tube holder of *CTCelect* and were used in all the experiments. Culture medium or whole blood from healthy donors was aliquoted in volumes of 7.55 mL medium or 7.5 mL blood and spiked with different numbers of stained tumor cells, respectively (tube I). 100 µl EpCAM beads (1 mg) were added to medium samples, blood samples contained 150 µl EpCAM beads (1.5 mg), both resulting in a total volume of 7.65 mL and a final beads concentration of 0.13 - 0.2 mg/ml. Subsequently, tubes II, III and IV were prepared with 5 mL buffer 1 (PBS/20 % FCS, 2 mM EDTA) and two tubes (V-VI) were filled with 0.5 mL buffer 2 (PBS/0.1 % BSA, 2 mM EDTA).

To start the automated enrichment, tubes I-VI and a 10 mL pipet tip were placed in the holders of the *CTCelect* device as described in Table 1 and the process was initiated on the touchscreen. Before moving on to the next tube, each washing step was alternated with magnetic capture of bead-bound tumor cells and residual beads in the pipet tip (see Supp. S2). The processed samples were

TABLE 1 Automation process of the complete *CTCelect* single cell isolation

Process	Location	Volume [mL]	Contents	Description (Duration)
IMS	Tube I	7.65	Spiked medium/whole blood; immuno-magnetic beads	Incubation (30 min) with gentle mixing
Washing	Tube II	5	Buffer 1	Wash off beads-cell complexes; leukocyte reduction
	Tube III	5		
	Tube IV	5		
Staining	Tube V	0.3	Buffer 2	Ab staining, volume reduction
Transfer	Tube VI	0.3	Transfer buffer	Transfer to *CTCelect* chip
Reservoir	Tube VII	0.5	Transfer buffer	Overlay on residual sample
µCS	*CTCelect* chip	0.25 max	Transfer buffer/PBS	Laser-based detection; Single cell dispensing

manually separated in a magnet separator for evaluation purposes. Supernatant buffer was discarded and the bead cell pellet was resuspended in 50 µl PBS. CTC counts were determined in a Neubauer counting chamber using fluorescence microscopy.

2.5 | Automated *CTCelect* single cell isolation of cultured tumor cells and CTCs from patient blood

Fully-automated *CTCelect* single cell isolation was evaluated with cultured tumor cells from medium and whole blood (2.5.a). The automated workflow is depicted in Figure 1C. Further, potential CTCs from HNSCC patient blood were isolated by means of the *CTCelect* single cell dispensing unit after manual pre-enrichment using detachable beads (2.5.b) and complete isolation (2.5.c). Experiments were performed at different sites in Germany which was easily manageable because both sites have their own CTCelect device to address time-sensitivity. In total, the team built three devices.

a. The functionality of the developed assay was confirmed with spike-in experiments using intracellular CFSE dye. 20 CFSE pre-stained tumor cells were added to 7.55 mL medium or 7.5 mL whole blood from healthy donors.
b. To confirm epithelial/pEMT origin of HNSCC cells from patient blood, single cell dispensing was investigated after manual pre-enrichment from peripheral blood using detachable Invitrogen™ CELLection™ Epithelial Enrich anti-CD326 and -CD51, -CD61, -CD106 immunomagnetic beads (Miltenyi Biotec, Bergisch Gladbach, DE) combined with phycoerythrin-coupled monoclonal CD326 and CD51 antibody (EpCAM-PE Ab/Integrin α-V-PE Ab; both Biolegend, Koblenz, DE). Pre-enrichment was performed manually to detach the beads from the cells. The respective research group has access to downstream NGS technologies that is, Nanostring, 10x Genomics that require bead-free cells after single cell dispensing.
c. Complete single cell isolation was verified with 7.5 mL actual patient blood with EpCAM-PE Ab 1B7 (1:30 in buffer 2). Single cell isolation was performed as described in Table 1 and outlined in Figure 2A.

The enriched and labeled sample was then transferred to the disposable *CTCelect* chip with a final volume of 300 µL in the chip reservoir. Similar to a conventional flow cytometer, the *CTCelect* cell detection is based on the principle of hydrodynamic focusing and optical fluorescence detection (Figure 2B). Microfluidic handling of the chip was managed with a system of two syringes directing sample and sheath flow. The sample flow consisted of a self-formulated transfer buffer, while sheath flow and dispenser were supplied with PBS. The maximum sample volume (250 µl) was loaded in the chip meander and µCS was initiated by the *CTCelect* software for the first measurement. Fluorescent cells were dispensed in the cavities of a 96-well plate if matching the given real-time peak analysis criteria of the fluorescence detection algorithm. Subsequently, 500 µL transfer buffer was pipetted from tube VII to the chip funnel to overlay the residual 50 µL sample and to avoid air bubble formation in the chip channels. The rest of the sample was then loaded in the chip for a second measurement cycle. Dispensed single cell droplets on the 96-well plate were evaluated using fluorescence microscopy (10x objective) in the FITC and TRITC channel or RT-qPCR.

2.6 | Characterization of blood cell contamination in CTC enriched samples

Especially on single cell level, white blood cell (WBC) contamination in tumor cell isolates complicates

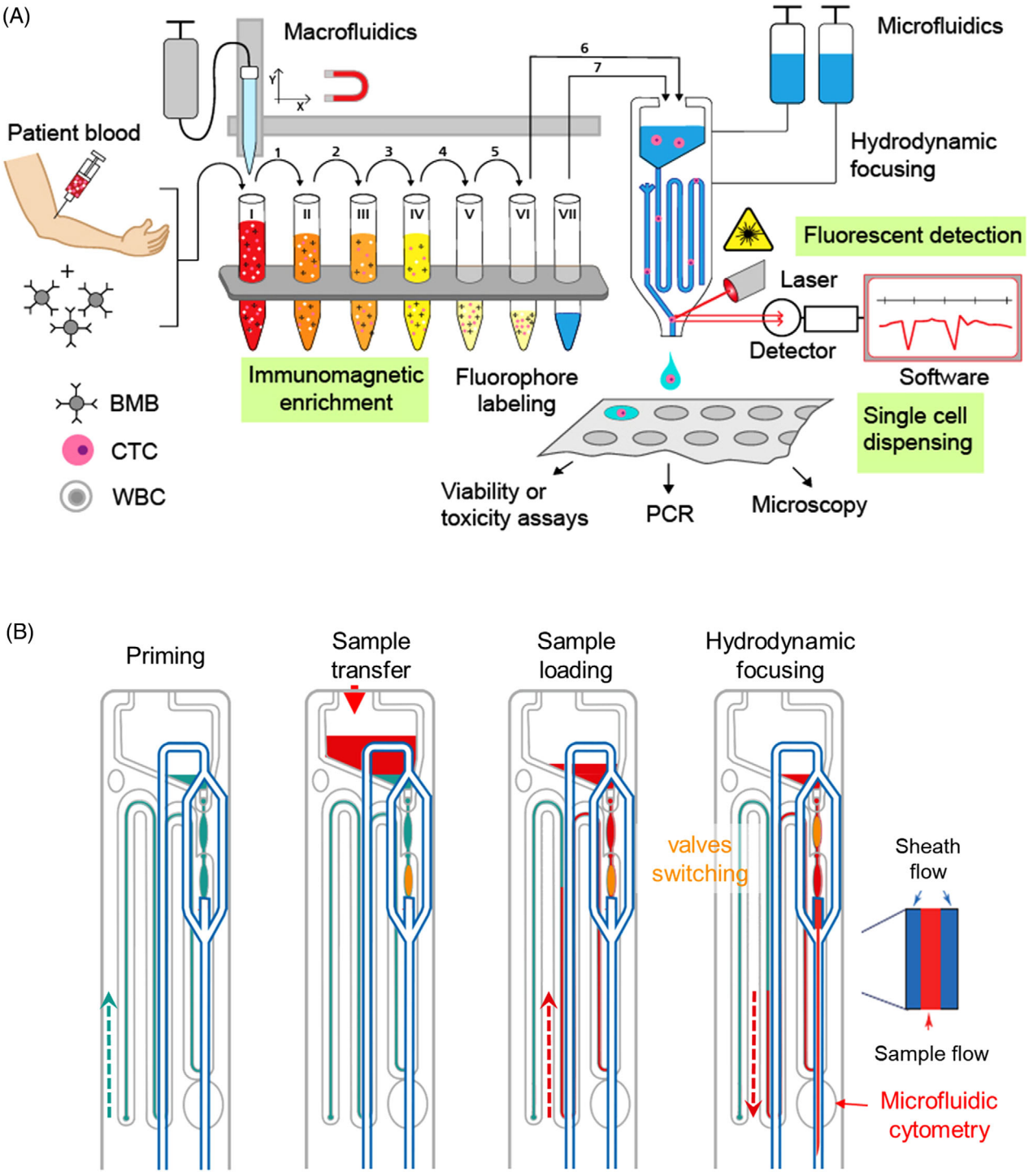

FIGURE 2 Automated workflow of *CTCelect* single cell isolation. (A) BMB: Biofunctionalized magnetic beads; CTC: Circulating tumor cell; WBC: White blood cell. 7.5 mL Patient blood sample is incubated with BMB to capture CTCs. Positive selection of tumor cells with subsequent depletion of WBCs and fluorophore-coupled labeling takes place in the enrichment module of the device. The enriched sample is then transferred to the cell sorting subunit into the microfluidic chip for cell sorting and single cell dispensing in microliter droplets. Singularized CTCs can be administered to transcriptomic and cytobiological downstream analyses. (B) Functioning principle of the microfluidic CTCelect chip. The chip meander is primed with sheath flow buffer. Subsequently, the enriched sample is transferred in the chip funnel and loaded in the meander. By switching the valve positions, the sample can then be pushed back in the detection channel and hydrodynamically focused for cytometry using two outer sheath flows

molecular downstream analyses. The number of CD45+ WBCs after IMS was determined by flow cytometry. Wash buffers were prepared and placed in the tube holder of the *CTCelect* device as described in Table 1 and 150 µL EpCAM beads were added to 7.5 mL whole blood before initiating automated IMS. The final sample was separated in a magnet separator. The supernatant was discarded and the bead cell pellet was stained with CD45-FITC Ab solution (diluted 1:5 in buffer 2; BD Biosciences, Franklin Lakes, USA). Flow cytometry was performed using the BD Accuri C6 flow cytometer. Gates were set with CD45-FITC stained beads as negative control and peripheral blood mononuclear cells (PBMCs) from a buffy coat as positive control (see Supp. S3). CD45+ cell counts after IMS were obtained from two samples of different healthy donors and the average WBC contamination with standard deviation (SD) was calculated.

2.7 | Single cell RT-qPCR of isolated CTCs

To confirm the CTC/DTC transcriptomic character in the single cell isolates from HNSCC patient blood, two-step real time quantitative PCR (RT-qPCR) of target RNAs for EpCAM, Integrin α-V and Stratifin was performed. β-actin (RPLP0) served as housekeeping RNA control. RNA was extracted from dispensed droplets immediately after *CTCelect* isolation using a single cell RNA purification kit (GenElute, Merck, DE) and reverse transcribed with the Invitrogen SuperScript double stranded cDNA synthesis kit. qPCR was conducted in triplicates (Invitrogen^{TM} SYBR Green PCR Master Mix) on a single cell cDNA per well in a 384 well cycler (BioRad CFX384 Touch Real-Time PCR Detection System, Feldkirchen, DE) and individual threshold cycle values (C_T) were obtained. Relative mRNA expression was calculated using the ΔC_T method. Primer sequences are available upon request.

2.8 | Immunostaining of isolated CTCs

CTCelect single cell isolates were pooled together to assess tumor origin of the isolated cells using immunostaining. The sample was stained with fluorescent CD45-FITC antibody (1:1000; BD Biosciences, Franklin Lakes, USA) to label leukocytes. Subsequently, the sample was resuspended in EndoPrime medium (Capricorn Scientific, Ebsdorfergrund, DE) and transferred to an ibidi 8-well slide to set overnight. Cells were centrifuged to the bottom of the slide by a CytoSpin device (300 x g, 10 min) and fixed by using 4% paraformaldehyde for 15 minutes. After further washing steps, cells were permeabilized (0.1% Triton X in PBS, 5 minutes) and stained with nuclear dye Hoechst33342 (1:1000) for 20 min. Alternated with several washing steps, unspecific binding was blocked for 30 min using 0.5% BSA in PBS and the sample was incubated with polyclonal anti-Zonula occludens-1 primary antibody 40–2200 (ZO-1; 1:200, 1 h) and anti-rabbit Alexa Fluor 633 secondary antibody (1:500, 1h).

2.9 | Statistical analyses

Each experiment was repeated at least three times. Data is depicted as means with SD and statistical analysis was done using GraphPad PRISM 8.2.0 for Windows (GraphPad Software, San Diego, California USA, www.graphpad.com). P values of two-tailed unpaired t-tests were reported as not significant (ns) when $P^{ns} > 0.05$ and as significant when $P^* \leq 0.05$.

3 | RESULTS

3.1 | *CTCelect* enrichment performance

The functionality of the *CTCelect* enrichment unit was investigated by spike-in experiments with different tumor cell lines in culture medium. 7.55 mL medium aliquots were spiked with 10, 25, and 50 CFSE-stained breast cancer cells (MCF-7) or squamous cell carcinoma cells (SCL-1). EpCAM beads were added and the samples were processed in the *CTCelect* enrichment unit with the above described protocol (Table 1). After evaluating the device functionality in culture medium, comparable experiments were performed in 7.5 mL whole blood from healthy donors. Following the protocol, all buffers were placed in the device and the enrichment assay was started. Samples were automatically enriched and washed from blood components, subsequently (Figure 3D).

Cell counts after *CTCelect* enrichment were determined visually using fluorescence microscopy. Intact cells were identified as round-shaped, green fluorescing objects with a bead-bound surface (Figure 3C). MCF-7 cells were automatically enriched with an 86.8 ± 9.7 % recovery rate from medium and with 72 ± 8.4 % from whole blood, hence the enrichment efficacy from blood was lower than from culture medium with only minor significance ($P^* = 0.0122$).

Further, 51.8 ± 18.9 % of SCL-1 cells were recaptured from medium and 38.8 ± 18.9 % from donor blood after automated IMS with EpCAM beads, meaning enrichment efficacy between blood and medium was not significantly different ($P^{ns} = 0.2437$). The mean recovery rates of all experiments are shown in dependency of the cell line, respectively (Figure 3A). Observed cell counts after *CTCelect* enrichment from medium were plotted against the

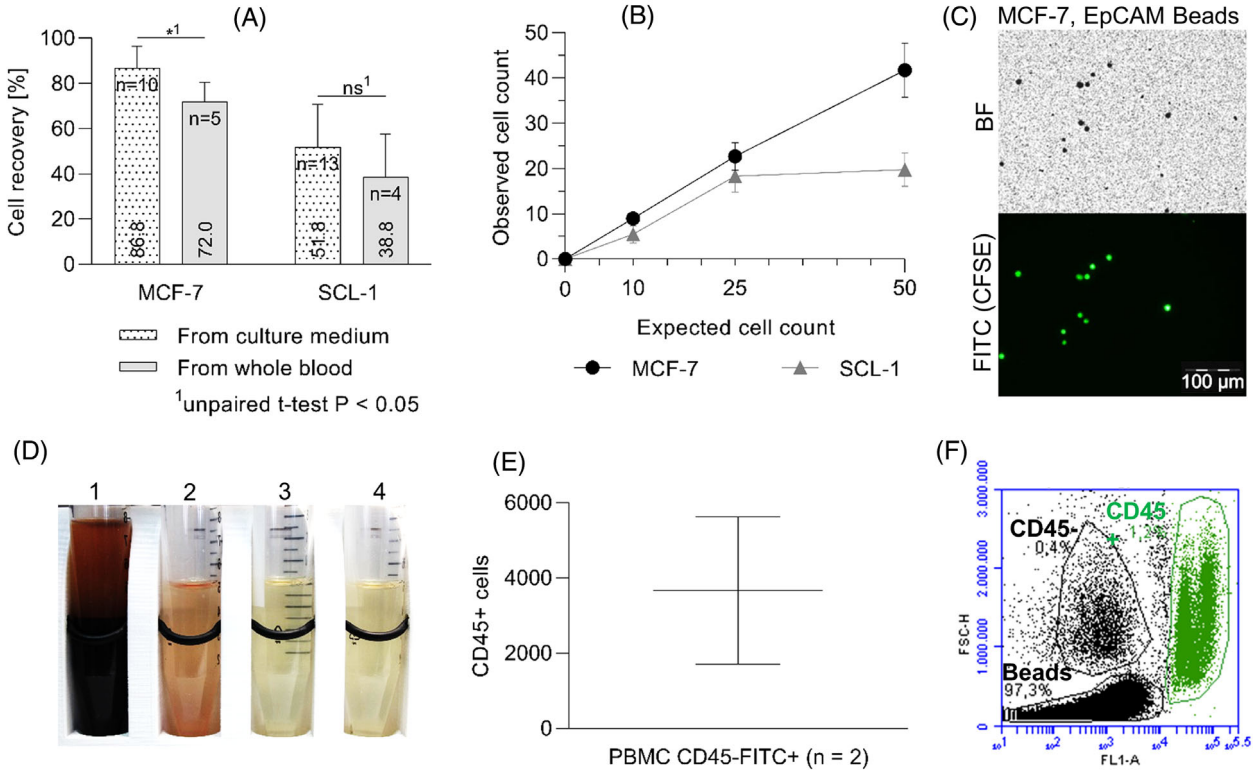

FIGURE 3 *CTCelect* enrichment performance. (A) Recovery rates of MCF-7 and SCL-1 cells after automated IMS from culture medium (black dotted) and whole blood (gray). 10 to 50 cells were spiked into the samples, respectively. Cells were stained with CFSE and enriched with 1 µm EpCAM Beads. Recovery rates of all experiments were averaged and are shown as means with SD and statistical analysis using a two-tailed unpaired t-test $P < 0.05$. (B) Observed MCF-7 (black circles) and SCL-1 (gray triangles) cell counts after *CTCelect* enrichment from medium were plotted as means with SD against the expected cell count ($n \geq 3$). (C) Bright field (BF) and fluorescence microscopy of CFSE stained and EpCAM bead-bound single MCF-7 cells (scale bar: 100 µm). (D) Blood residues (1) and wash buffers with blood component waste (2-4) of subsequent *CTCelect* enrichment process steps in a magnetic separator. In this case almost no loss of sample/beads occurred. Otherwise, beads would be visible as brown accumulations on the backside of the tube. (E) Cell count of $CD45^+$ blood cell contamination after *CTCelect* enrichment with EpCAM beads from 7.5 mL donor blood. Contamination was determined via flow cytometry with CD45-FITC Ab staining. (F) Flow cytometry data of a 7.5 mL blood sample after *CTCelect* enrichment. The scatter plot shows green fluorescence (FL1) on the x-axis against forward scatter (FSC) particle size on the y-axis. Populations of beads, $CD45^-$ and $CD45^+$ cells (green) are distinguished in circles

expected cell count of 10, 25 and 50 spiked cells and summarized in Figure 3B. Recovery rates of MCF-7 cells showed a nearly linear correlation, independently of the expected cell count between 10 to 50 cells. Up to 25 expected cells, automated recovery of SCL-1 cells followed a similar stable linearity but resulted in a flattened curve at an expected cell count above 25 cells input. Less than half of 50 spiked SCL-1 cells could be automatically enriched with EpCAM beads.

As blood cell contamination is a disruptive factor for CTC downstream molecular analyzes, the reduction of $CD45^+$ PBMCs in CTC enriched samples was determined additionally. Therefore, processed blood samples were stained with CD45-FITC Ab after automated *CTCelect* enrichment from 7.5 mL donor whole blood. On average, 3,665 counts of PBMCs were measured in a total volume of 300 µL via flow cytometry (Figure 3E-F; population indicated in green). Comparing to the $CD45^+$ cell count in blood sample #1 ($19*10^6$ $CD45^+$ cells; data not shown), the number of $CD45^+$ cells was significantly reduced using the *CTCelect* enrichment.

3.2 | Automated single cell isolation from culture medium and donor blood

Complete automated single cell isolation was evaluated by means of spike-in experiments of 20 MCF-7 and SCL-1 cells in culture medium and whole blood from healthy donors. *CTCelect* device functionality was confirmed using CFSE staining according to Table 1. Regarding the MCF-7 cell line model with CFSE dye, 58.3 ± 15.3 % of single cells

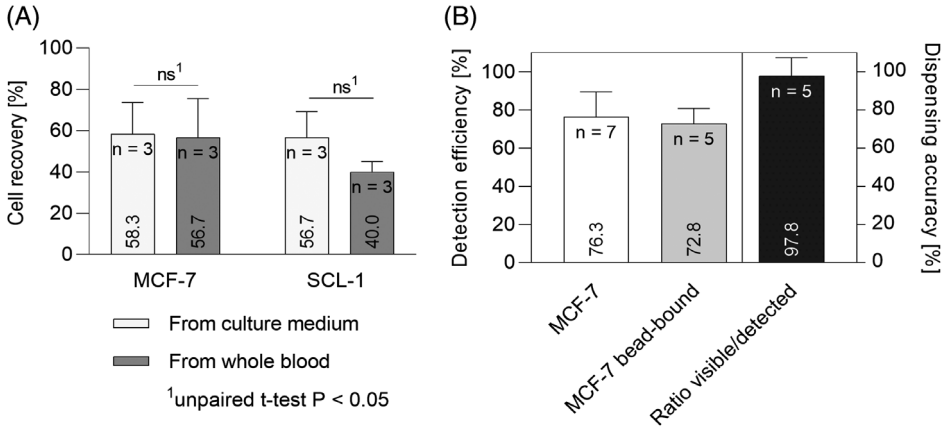

FIGURE 4 *CTCelect* single cell detection, dispensing and isolation from 7.5 mL samples. (A) Recovery rates of MCF-7 and SCL-1 cells after automated single cell isolation from culture medium (light gray) and whole blood (dark gray). 20 CFSE stained cells were spiked into 7.5 mL samples and incubated with 1 µm EpCAM beads. Pre-enriched cells were automatically singularized and dispensed in droplets after µCS in the *CTCelect* chip. Recovery rates of all experiments were determined with fluorescence microscopy of the droplets and are displayed as means ± SD (ns; two-tailed unpaired t-test $P < 0.05$). (B) Detection efficiency and dispensing accuracy of *CTCelect* µCS. 50 CFSE stained, unbound and bead-bound MCF-7 cells were directly spiked in the *CTCelect* chip for single cell isolation. Droplets were microscopically screened for single cells and detection efficiency was averaged by the observed cell count in dependency of the spiked cell number. Dispensing accuracy was calculated dividing the actual number of visible cells in the droplets by the number of events detected by the software

were counted after isolation from culture medium and 56.7 ± 19 % were detected after isolation from whole blood with comparable recovery efficiency. With the same experimental setup, SCL-1 cells were automatically isolated at rates of 56.7 ± 18.9 % (medium) and 40.0 ± 5.0 % (whole blood) recovery (Figure 4A). No significant differences in enrichment efficiencies between 'from medium' or 'from donor blood' is seen for both SCL-1 ($P^{ns} = 0.1807$) and MCF-7 cells ($P^{ns} = 0.8870$).

More specifically detailed, the detection efficiency and dispensing accuracy of the peak analysis software and microfluidic dispensing through the chip was investigated (Figure 4B), Direct processing of CFSE stained MCF-7 cells led to visible detection of 76.3 % unbound cells and 72.8 % bead-bound cells without significant difference. Furthermore, a very high dispensing accuracy of 97.8 % was determined as the ratio between visible bead-bound cells in the droplets and the detected events in the software, respectively. The microfluidic parameters and flow properties of single cells were intensively studied in our preliminary work to set the dispensing criteria (data not shown).

3.3 | Verification of epithelial/pEMT origin of HNSCC cells from patient blood

Tumor-specific single cell dispensing was investigated in peripheral blood of HNSCC patients. According to method 2.5 b), manual immunomagnetic enrichment was performed with EpCAM beads for pre-EMT CTCs and Integrin α-V, CD61, CD106 beads for partial/post-EMT CTCs. Pre-enriched samples were then detached from the beads and labeled with either EpCAM-PE or Integrin α-V-PE staining (Figure 5A). In this patient, 30 $EpCAM^+$ CTCs and 20 $CD51^+$ CTCs were detected in 7.5 mL blood with fluorescence microscopy, respectively. Pre-enriched and labeled samples were pipetted in the *CTCelect* chip and then automatically processed for single cell isolation in droplets (Figure 5B).

The successful single CTC isolation from patient blood by means of the microfluidic *CTCelect* unit was confirmed using RT-qPCR. 11 epithelial-like and 13 mesenchymal/pEMT-like CTCs were isolated and singly dispensed from the pre-enriched 7.5 mL blood samples of the same HNSCC patient (Figure 5B). RT-qPCR was performed to detect target RNAs encoding EpCAM, Integrin α-V, Stratifin and β-actin as positive control. C_T values for each well were determined and relative mRNA expression was normalized to β-actin (Figure 5C).

Samples with a $C_T < 40$ for β-actin were identified as "positive" (droplet contained a cell) and samples with a $C_T < 40$ for β-actin *and* at least one of the other three markers as "CTC-positive" (droplet contained a potential CTC). False-positive results were identified via melt curve analysis and excluded from the calculations. In this regard, 100 % of the dispensed droplets were CTC-positive, since all of the 11 epithelial-like and 13 mesenchymal-like *CTCelect* samples had a $C_T < 40$ for β-actin, EpCAM and

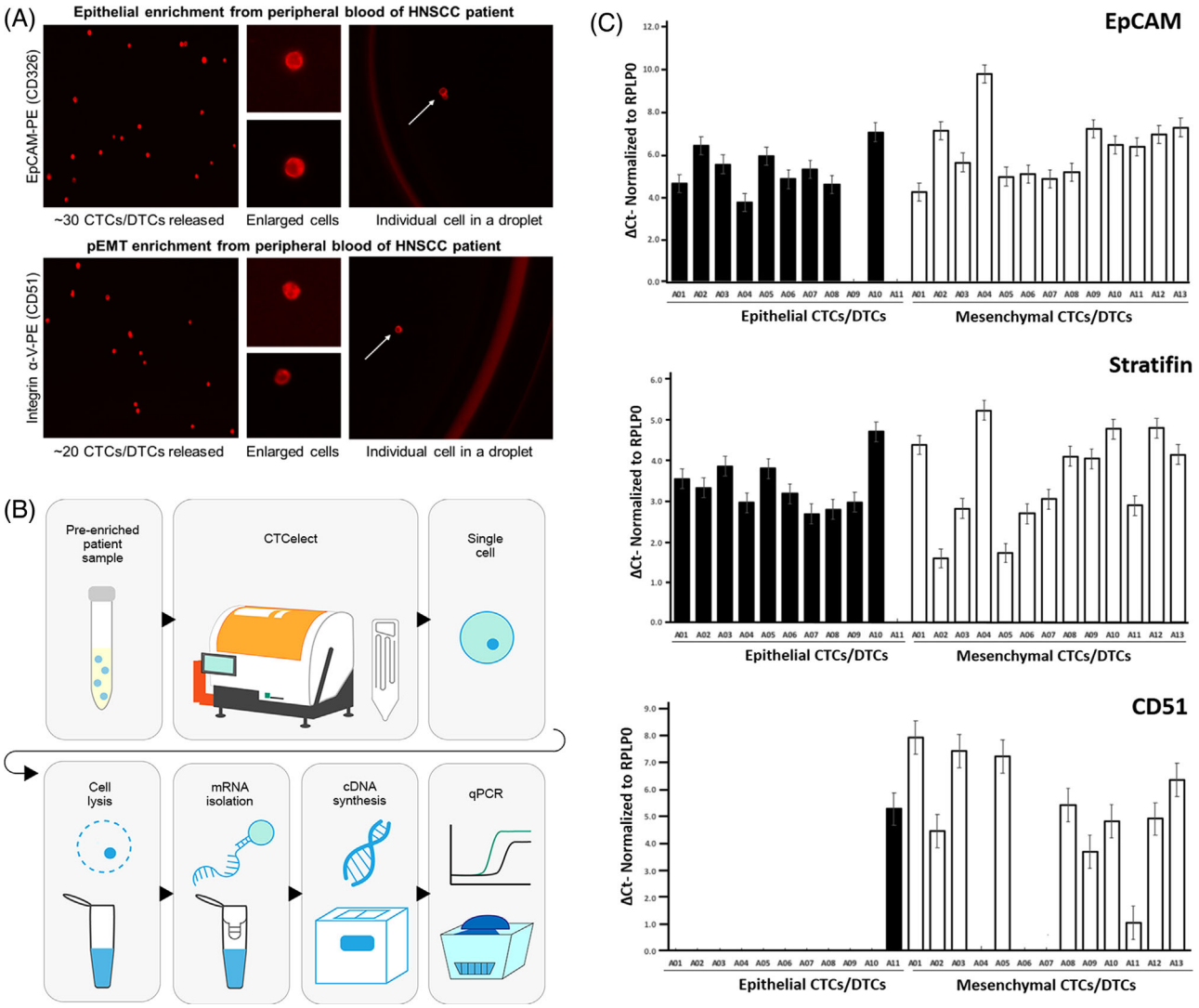

FIGURE 5 RT-qPCR of CTC isolates after *CTCelect* single cell dispensing from pre-enriched HNSCC patient blood. (A) Immunofluorescent staining of potential pre-enriched CTCs/DTCs from HNSCC patient blood. Pre-EMT CTCs were enriched with EpCAM beads and stained with EpCAM-PE Ab from a 7.5 mL blood sample (left top). Integrin α-V, CD61, CD106 beads and Integrin-PE staining was used for partial/post-EMT CTCs (left bottom). Cells were released from the beads by DNase I cleavage. The pre-enriched samples were pipetted in the microfluidic cartridge of *CTCelect* and beads-free CTCs were then single cell isolated in droplets by means of the *CTCelect* μCS subunit. The set of images on the right side shows potential single CTCs in droplets highlighted with white arrows and the droplet outlines. (B) Workflow of single cell RT-qPCR. (C) Relative mRNA expression encoding EpCAM, Stratifin and CD51 normalized to β-actin (RPLP0) by RT-qPCR in epithelial and mesenchymal CTCs. Single cell total RNA was extracted from dispensed droplets and reverse transcribed into cDNA. cDNA was aliquoted and qPCR was conducted with one cDNA aliquot per well amplifying target nucleic acids respectively for EpCAM, CD51, Stratifin and β-actin as positive control of epithelial-like CTCs (pre-EMT enrichment) and mesenchymal-like CTCs (pEMT enrichment). Relative expression was calculated from triplicates using the ΔC_T method and is displayed as means with SD

Stratifin RNA at comparable levels. Additionally, all of the mesenchymal-like CTCs were positive for CD51 RNA with sample A01 showing the highest an 8-fold level of CD51 compared to β-actin. In contrast, only 4 epithelial-like CTCs (A03, 04, 10, 11) contained detectable CD51-related nucleic acid and A11 even exhibited higher CD51 than EpCAM RNA. The 13 mesenchymal/pEMT-like CTCs also significantly contained EpCAM RNA of at least 4-fold greater than the housekeeping RNA.

Following method 2.5 c), completely automated CTC isolation from 7.5 mL HNSCC patient blood was performed. The dispensed droplets were pooled and stained using Hoechst33342 cell core staining, ZO-1 as epithelial marker for potential CTCs and CD45 as negative control

for contaminating WBCs. 18 potential isolated CTCs and 9 contaminating WBCs could be detected using fluorescence microscopy (Figure 6).

4 | DISCUSSION

From the patient's point of view, single CTC isolation from peripheral blood is the least invasive procedure to evaluate tumor heterogeneity based on epigenomic, genetic or transcriptional markers and is therefore more time effective and reproducible than assays drawn from primary tumor tissue. This study covered a profound biological validation of the design, biotechnological effort and engineering concept of the *CTCelect* platform for automated single cell isolation from whole blood. *CTCelect* helps to identify, enrich, isolate and analyze CTCs and their subpopulations. Many researchers suggested that the precise characterization of CTCs will facilitate estimating both metastization patterns and outcome, driving clinical decision-making and surveillance strategies [16].

For these purposes, the subunits of the system were separately tested and evaluated. Concerning cell enrichment, *CTCelect* provided recovery rates from medium of 68 - 100 % in breast cancer single cells and 28% to 88 % in cultured squamous cell carcinoma cells. Further, 65% to 85 % of MCF-7 cells and 20% to 55 % of SCL-1 cells could be enriched from 7.5 mL whole blood from healthy donors (Figure 3). In comparison, Chudziak and colleagues determined 69.5 % enrichment efficiency of spiked lung cancer cells in their marker-free CTC enrichment device Parsortix although it has to be mentioned that the sample input only ranged from 0.5 to 4 mL volume [17]. We extensively characterized the enrichment sub-unit in our previous study before it was implemented in the overall CTCelect platform [18]. Similar to manual enrichment, there was no significant loss of cells due to vibrational disruption or tube surface adhesion. The enriched cells were accurately detected using fluorescent microscopy. More detailed, decreased enrichment efficiency by 15 % (MCF-7) and 13 % (SCL-1) in donor blood compared to culture medium was noted. As it has previously been postulated that the magnetic susceptibility in blood is significantly less negative than in aqueous solutions like medium [19, 20], we consequently hypothesize a generally lower magnetic force attracting immunomagnetic beads in whole blood. In addition, a steric competition with the abundant blood cell background could possibly prevent a proportion of the target CTCs from binding beads and being magnetized. Another important aspect influencing cell recovery rates is that cell deformability, viscoelasticity, and stability (density of actin filaments etc.) could play a role for robustness against shear stress in automated pipetting and these characteristics will be different among various cell types. Comparing the two cell lines, MCF-7 cells were detected at higher rates than SCL-1 cells. The density of antigens blocking phagocytosis could be higher on the cell surface of MCF-7 cells and therefore be more favorable for spike-in experiments. Breast cancer-associated HER2 and lymphoma-related CD47 exhibit a "*please don't eat me*" signal to macrophages [21, 22]. Besides that, Figure 3B showed that when the number of spiked SCL-1 cells is higher than 25, there is an inconsistency between observed and expected cell count. This however does not suggest that the platform is not efficient in recovering larger numbers of CTCs as according to the results, the enrichment efficiency of MCF-7 cells followed a linear trend at higher expected cell counts. In our recently published work, we screened several melanoma and carcinoma cell lines (MV3, SCL-1, SCL-2, BLM, patient-derived HNC cells) and targets (MCSP, EpCAM, cell surface vimentin) to find a suitable candidate for the testing of microfluidic platforms. The enrichment fluctuation appeared frequently depending on the cell line and the sample volume also in manual enrichment. Further, we observed a similarly efficient cell line-dependent recovery rate at even higher cell counts of 1000 cells for that is, A431 cells using the same beads [18]. The practicability of spike-in experiments to test novel CTC platforms, in cell line models without evolutionary pressure in vitro combined with intracellular synthetic dyes, remains discussable and limits the study design. Nevertheless, these prevalidations are inevitable to investigate the proof-of-concept and invented design of the device. In this context, it has to be centered that the actual CTC count in a cancer patient has a multifactorial nature and therefore represents a dynamic measure with discrepancies.

For a successful singularization of the CTCs in the microfluidic cartridge and a high purity of the single cell dispensing it is also important to reduce the amount of WBC contamination during immunomagnetic enrichment. Thus, the automated enrichment process was characterized in terms of leukocyte by-catch. Enriched samples of 7.5 mL whole blood from healthy donors were labeled with WBC marker CD45-FITC and roughly 3.700 CD45 positive PBMC were detected via flow cytometry (Figure 3E). Healthy adults normally have a wide range of 3 - 10 million leukocytes per mL blood [23], which concludes a by-catch reduction of 1:10^5 by means of *CTCelect* enrichment. Other devices like marker-dependent CellSearch® or Isoflux™ and label-free ScreenCell™ or ClearCell showed similar contaminations of 10^2–10^4 blood cells while authors also discussed a patient-dependent discontinuity in leukocyte by-catch using Parsortix [17, 24].

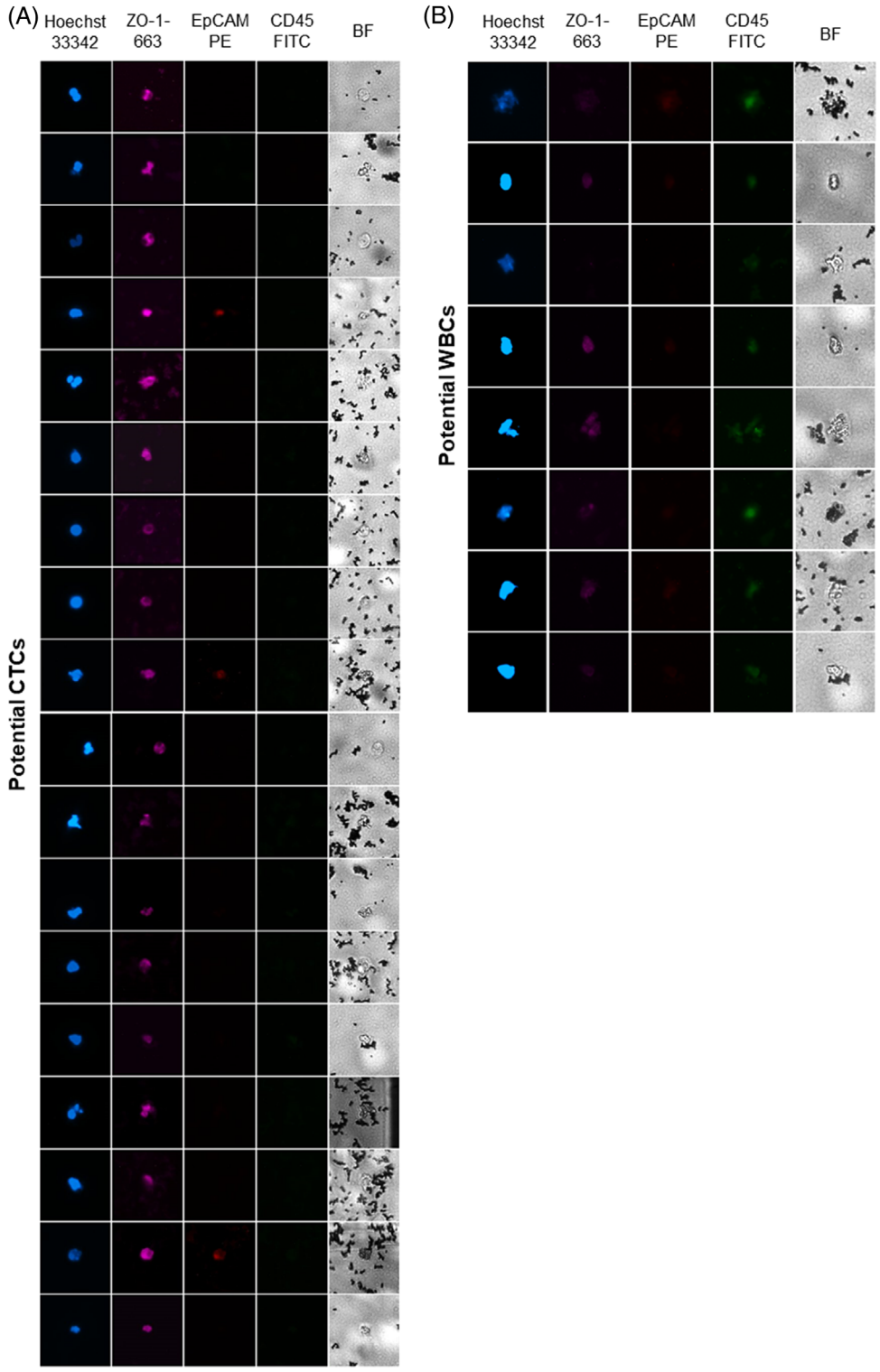

FIGURE 6 Immunostaining of potential CTCs and WBCs after CTCelect isolation. Dispensed cells were pooled together and subsequently stained with cell core dye Hoechst33342 (blue), ZO-1 as epithelial marker (magenta) and CD45 as WBC marker (green). Residual EpCAM staining from CTCelect isolation is displayed in red. Cells were identified as (A) potential CTCs if $Hoechst^{+}/ZO\text{-}1^{+}/CD45^{-}$ and (B) as WBCs if $Hoechst^{+}/CD45^{+}$

TABLE 2 Comparison between CTCelect and different CTC isolation technologies.[1]

	CTCelect	DEPArray	CellSearch	Sievewell	Parsortix
Sample type	Whole blood, cell suspension	Cell suspension	Whole blood, leucapheresis	Cell suspension	Whole blood, cell suspension
Automated isolation of viable cells	Yes	yes	no	manually	Yes
Automated optical counting	Yes	setup	Yes	Yes	No
Isolation method	Marker	Electrophoresis, marker	Marker	Marker, size	Size, compressibility
Single cell dispensing	yes	yes	No	CellCelector	No
Isolation efficiency	Enrichment 38.8% to 72 % Dispensing 72.8 % Isolation 40% to 56.7 %	99.7 %[a)]	93 %[c)] 81 %[d)]	n. a.	98 %[g)] > 80 % (7.5 mL blood)[h)] 30% to 70 % (1 mL blood)[h)] 37 %[i)]
Purity (WBC contamination)	66 - 90 %	100 %[a)]	800 WBCs/ sample[e)]	n. a.	97 %[g)] 29 %[h)]
Throughput	$4*10^{11}$ cells/chip[2]; 96 wells (3.3 mL/h)	10-10,000 cells/chip[b)]	n. a.	370,000 cells/chip[f)]	n. a.
Working volume	0.3–10 mL	n. a.	7.5 mL	0.5–2 mL/chip	10 mL
Cycle duration	2.25 h	2 - 3 h	n. a.	n. a.	n. a.

[1] *No claim to be exhaustive.*

[a)] Di Trapani et al. 2018. Cytometry. Part A, 93(12), 1260–1266.

[b)] http://www.siliconbiosystems.com/deparray-technology-faqs.

[c)] https://documents.cellsearchctc.com/pdf/e631600006/e631600006_EN.pdf.

[d)] Riethdorf et al. 2007. Clin Cancer Res 13(3), 920–928.

[e)] Sieuwerts et al. 2009. Breast Cancer Res Treat 118, 455.

[f)] https://www.sievewell.com/product-information.

[g)] Ciccioli et al. 2021. ANGLE plc AACR 2021 Virtual Meeting. https://angleplc.com/wp-content/uploads/EMT-assay-poster-AACR-2021-final.pdf [2021-09-10].

[h)] Chudziak et al. 2014. CRUK – Manchester, NCRI conference 2014. https://angleplc.com/wp-content/uploads/CRUK-Manchester-poster-1.pdf [2021-09-10].

[i)] Gorges et al. 2014. The University Medical Center Hamburg-Eppendorf (UKE), ACTC Conference. https://angleplc.com/wp-content/uploads/Angle_Hamburg_MC_poster_ebook-2.pdf [2021-09-10].

[2] *Not dispensable. Current limitation: 96-well plate; drive duration of object table: 500 ms.*

Their approaches often provide a final sample pooled with WBCs while subsequent marker-based single cell detection in *CTCelect* further purifies the CTC fraction for compatible molecular analysis.

Combined enrichment with single cell detection and dispensing in one assay resulted in only minor cell losses with recovery rates of almost 60 % for both MCF-7 and SCL-1 cells from culture medium in the model system. Even from 7.5 mL whole blood, single cells were isolated at a probability of 57 % (MCF-7) and 40 % (SCL-1) (Figure 4A). The determined recovery rates from untreated whole blood at a high purity grade of less than 10 % probability to dispense a WBC with a CTC [25] showcases a fine parameter balance of *CTCelect* compared to other CTC isolation microdevices (Table 2). For example, studies on devices using hydrodynamics, size-based filtration or dielectrophoresis showed indeed cell recovery rates of 70% to 85 % but were only able to process approximately 1 mL/h or lacked CTC isolate purity [5]. In fact, at a flowrate of $2.25*10^{-15}$ L/s and 5 ms nozzle-emptying time, it is theoretically possible to detect, but not dispense, 200 events per second and $4*10^{13}$ cells/chip in 500 µL. The current dispensing limitation is the 500 ms drive time of the object table and the 96-well plate format. *CTCelect* manages a moderate sample throughput of 3.3 mL/h with the current run time of around 2.3 h and 7.5 mL input volume. Additionally, most of the available systems require either sample transfer between different devices or blood pre-processing like density gradient centrifugation for buffy coats. Pre-enriched samples or yielded mononuclear phases of blood to specify the respective research needs can also be sampled in the herein discussed platform. To our knowledge, the possibility to use whole blood samples for automated single cell dispensing of rare cells in only one marker-based device to make them available for corresponding analyzes stands alone.

The workflow for downstream single cell RT-qPCR was simplified to immediate single cell lysis on the well plate. Direct reverse transcription in the cavities of the well plate coming from the device as well as the assay implementation to release detachable beads in the enrichment unit are subjects of future work. This evaluation however included the earliest results of the *CTCelect* device towards isolating single CTCs from a patient with metastatic head and neck squamous cell carcinoma in a clinical environment. In these patient samples, 30 $EpCAM^+$ CTCs and 20 $CD51^+$ CTCs were detected via fluorescence microscopy (Figure 5A). Microfluidic cell singularization enabled single cell RT-qPCR and allowed a distinction in 11 pre- and 13 pEMT CTC subtypes on the basis of different tumor-related markers (Figure 5C). Hence our findings evidence the potential of *CTCelect* to depict cancer plasticity. IVD companies, that is, QIAGEN N.V., offer non-automated CTC isolation/PCR platforms to characterize common tumor entities such as lung, prostate and breast cancer, but not for HNSCC diagnostics. Further, CTC liquid biopsy in HNSCC could elucidate crucial information on early assessment of treatment measures and effectiveness with respect to the detection of micrometastases at the initial diagnosis, complementing well-established ctDNA characterizations. Mouliere et al. recently detected chromosomal mutations of solid tumors in the blood by whole genome copy number variation analysis [26]. Encompassing studies on ctDNA and CTC characterizations have been carried out [27] but, especially in head and neck cancers, the respective literature landscape is sparsely settled and to be addressed in the future with the suggested data.

It is obvious that immuno-biochemical techniques targeting antigens like EpCAM are not infallible for all tumor entities or heterogeneous CTC populations, especially CTCs undergoing epithelial-mesenchymal transition (EMT) which is closely linked to invasive metastasis. Against that, mixtures of antibodies like integrin subtypes, cell surface vimentin or stem cell markers are of assistance to improve the enrichment of partial/post-EMT mesenchymal-like CTCs. Besides these affinity-based techniques to enrich and isolate CTCs, the physical methods base on distinction in cell size, density or even plasticity. Due to the fact that CTCs are a heterogeneous population in blood, they have some characteristics in common with healthy mononuclear blood cells. Thus, methods based on filtration, centrifugation or size exclusion may not be used for a standard clinical test system. Further, it is important to mention that there are other obstacles, i.e. the purity of the CTC fraction, before realizing subsequent applications such as single cell sequencing or copy number variation studies.

The certainly limited patient screening in this study clearly demonstrated the feasibility of downstream applications. The platform enabled fully-automated CTC isolation from HNSCC patient blood and immunofluorescent identification of 18 potential CTCs for proof-of-concept (Figure 6). Several researchers have stated that the presence of CTCs in the blood is of prognostic relevance for overall and progression-free survival in patients with head and neck cancer [28] and that HNSCC exhibits early stage micrometastatic sites and severe intra-tumoral heterogeneity which is closely linked to poor disease outcome. In this context, an important advantage of CTC/DTC isolation over imaging technologies is that minimal residual disease (MRD), for example DTC micrometastases, are undetectable by the latter. Especially bone marrow is intensively studied as a reservoir for dormant DTCs with the capacity to re-enter the circulatory system and trigger MRD in distant tissues [29]. It is easily plausible to broaden the applicability of the *CTCelect* device to process liquid biopsies from bone marrow or dissolved lymph node resections. All of these aspect stress the necessity of an improved cell biological understanding to foremost provide a good care for HNSCC patients. High-resolution of cell heterogeneity, metastatic invasiveness and evolutionary pressure on cancer cells is key to precision medicine. To conclude, the presented results demonstrate the robust technical performance of *CTCelect* and its feasibility as a novel tool for liquid biopsy to make CTCs available for corresponding examinations on a single cell level with respect to head and neck squamous cell carcinoma.

ACKNOWLEDGMENTS

This publication is dedicated to Dr. Ashwin Sriram, member of the Group of Translational Skin Cancer Research, University Duisburg-Essen; German Cancer Research Center (DKFZ) Heidelberg, who sadly passed away during this research. We thank the project team at the Fraunhofer IMM: Peter Spang and Peter Höbel for engineering, Knut Welzel, Jörn Wittek, Matthias Besold and Ivette Krollmann for software and electronics development and Carmen Schwind for biotechnological support and method development.

Open access funding enabled and organized by Projekt DEAL.

CONFLICTS OF INTEREST

The authors have declared no conflicts of interest. All authors have read and agreed to the published version of the manuscript.

DATA AVAILABILITY STATEMENT

The data that support the findings of this study are available on request from the corresponding author. The data are not publicly available due to privacy or ethical restrictions.

ORCID

Janis Stiefel https://orcid.org/0000-0002-1166-4326
Christian Freese https://orcid.org/0000-0001-8411-1573
Nalini Srinivas https://orcid.org/0000-0002-6899-0800
Désirée Gül https://orcid.org/0000-0002-2446-5756
Jan Hagemann https://orcid.org/0000-0002-9846-7850
Jürgen C. Becker https://orcid.org/0000-0001-9183-653X
Michael Baßler https://orcid.org/0000-0003-3911-2897

References

1. Alix-Panabières C, Schwarzenbach H, Pantel K. Circulating tumor cells and circulating tumor DNA. Annu Rev Med. 2012;63:199–215. https://doi.org/10.1146/annurev-med-062310-094219
2. Nolé F, Munzone E, Zorzino L, et al. Variation of circulating tumor cell levels during treatment of metastatic breast cancer: prognostic and therapeutic implications. Ann Oncol. 2008;19:891–897. https://doi.org/10.1093/annonc/mdm558
3. Mentis A-FA, Grivas PD, Dardiotis E, et al. Circulating tumor cells as Trojan Horse for understanding, preventing, and treating cancer: a critical appraisal. Cell Mole Life Sci. 2020;77:3671–3690. https://doi.org/10.1007/s00018-020-03529-4
4. Reduzzi C, Vismara M, Gerratana L, et al. The curious phenomenon of dual-positive circulating cells: longtime overlooked tumor cells. Semin Cancer Biol. 2020;60:344–350. https://doi.org/10.1016/j.semcancer.2019.10.008
5. Lei KF. A review on microdevices for isolating circulating tumor cells. Micromachines. 2020;11. https://doi.org/10.3390/mi11050531
6. Rawal S, Yang YP, Cote R, Agarwal A. Identification and quantitation of circulating tumor cells. Annu Rev Anal Chem (Palo Alto, Calif.). 2017;10:321–343. https://doi.org/10.1146/annurev-anchem-061516-045405
7. Ferreira MM, Ramani VC, Jeffrey SS. Circulating tumor cell technologies†. Mole Oncol. 2016;10:374–394. https://doi.org/10.1016/j.molonc.2016.01.007
8. Hayes DF, Cristofanilli M, Budd GT, et al. Circulating tumor cells at each follow-up time point during therapy of metastatic breast cancer patients predict progression-free and overall survival. Canc Res. 2006;12:4218–4224. https://doi.org/10.1158/1078-0432.CCR-05-2821
9. Cohen SJ, Punt CJA, Iannotti N, et al. Relationship of circulating tumor cells to tumor response, progression-free survival, and overall survival in patients with metastatic colorectal cancer. J Clin Oncol. 2008;26:3213–3221. https://doi.org/10.1200/JCO.2007.15.8923
10. Bono JS, Scher HI, Montgomery RB. et al. Circulating tumor cells predict survival benefit from treatment in metastatic castration-resistant prostate cancer. Clin Canc Res. 2008;14:6302–6309. https://doi.org/10.1158/1078-0432.CCR-08-0872
11. Vokes EE, Agrawal N, Seiwert TY. HPV-Associated head and neck cancer. J Natl Cancer Inst. 2015;107:djv344. https://doi.org/10.1093/jnci/djv344
12. Economopoulou P, Bree R, Kotsantis I, Psyrri A. Diagnostic tumor markers in head and neck squamous cell carcinoma (HNSCC) in the clinical setting. Front Oncol. 2019;9. https://doi.org/10.3389/fonc.2019.00827
13. Bree R, Deurloo EE, Snow GB, Leemans CR. Screening for distant metastases in patients with head and neck cancer. Laryngoscope. 2000;110:397–401. https://doi.org/10.1097/00005537-200003000-00012
14. Siegel R, Naishadham D, Jemal A. Cancer statistics, 2012. CA Cancer J Clin. 2012;62:10–29. https://doi.org/10.3322/caac.20138
15. Boukamp P, Tilgen W, Dzarlieva RT, Breitkreutz D, et al. Phenotypic and genotypic characteristics of a cell line from a squamous cell carcinoma of human skin. J Natl Cancer Inst. 1982;68:415–427.
16. Bulfoni M, Gerratana L, Ben FD, et al. In patients with metastatic breast cancer the identification of circulating tumor cells in epithelial-to-mesenchymal transition is associated with a poor prognosis. Breast Cancer Res. 2016;18:1–15. https://doi.org/10.1186/s13058-016-0687-3
17. Chudziak J, Burt DJ, Mohan S, et al. Clinical evaluation of a novel microfluidic device for epitope-independent enrichment of circulating tumour cells in patients with small cell lung cancer. Analyst. 2016;141:669–678. https://doi.org/10.1039/c5an02156a
18. Gribko A, Stiefel J, Liebetanz L, et al. IsoMAG—an automated system for the immunomagnetic isolation of squamous cell carcinoma-derived circulating tumor cells. Diagnostics (Basel, Switzerland). 2021;11. https://doi.org/10.3390/diagnostics11112040
19. Lee W, Tseng P, Di Carlo D. Microtechnology for Cell Manipulation and Sorting. Springer; 2018.
20. Plyavin YA, Blum EY. Magnetic parameters of blood cells and high gradient paramagnetic and diamagnetic phoresis. Magnetohydrodynamics. 1983;19:349–359.
21. Candas-Green D, Xie B, Huang J, et al. Dual blockade of CD47 and HER2 eliminates radioresistant breast cancer cells. Nat Commun. 11:1–15. https://doi.org/10.1038/s41467-020-18245-7
22. Liu R, Wei H, Gao P, et al. CD47 promotes ovarian cancer progression by inhibiting macrophage phagocytosis. Oncotarget. 2017;8:39021–39032. https://doi.org/10.18632/oncotarget.16547
23. Scheiermann C, Frenette PS, Hidalgo A. Regulation of leucocyte homeostasis in the circulation. Cardiovasc Res. 2015;107:340–351. https://doi.org/10.1093/cvr/cvv099
24. Nelep C, Eberhardt J. Automated rare single cell picking with the ALS cellcelector™. Cytometry. 2018;93:1267–1270. https://doi.org/10.1002/cyto.a.23568
25. Alebrand S, Freese C, Schunck T, Bassler M. Zirkulierende Tumorzellen - voll automatisierte Vereinzelung aus Blut. Biospektrum. 2017;23:766–768. https://doi.org/10.1007/s12268-017-0869-2
26. Mouliere F, Chandrananda D, Piskorz AM, et al. Enhanced detection of circulating tumor DNA by fragment size analysis. Sci Transl Med. 2018;10. https://doi.org/10.1126/scitranslmed.aat4921
27. Shaw JA, Guttery DS, Hills A, et al. Mutation analysis of cell-free DNA and single circulating tumor cells in metastatic breast cancer patients with high circulating tumor cell counts. Clin Cancer Res. 2017;23:88–96. https://doi.org/10.1158/1078-0432.CCR-16-0825
28. Cho J-K, Lee GJ, Kim H-D, et al. Differential impact of circulating tumor cells on disease recurrence and survivals in patients with head and neck squamous cell carcinomas: an updated meta-analysis. PLoS One. 2018;13:e0203758. https://doi.org/10.1371/journal.pone.0203758

29. Alix-Panabières C, Pantel K. Clinical applications of circulating tumor cells and circulating tumor DNA as liquid biopsy. Cancer Discov. 2016;6:479–491. https://doi.org/10.1158/2159-8290.CD-15-1483

SUPPORTING INFORMATION

Additional supporting information may be found in the online version of the article at the publisher's website.

How to cite this article: Stiefel J, Freese C, Sriram A, Alebrand S, Srinivas N, Sproll C, et al. Characterization of a novel microfluidic platform for the isolation of rare single cells to enable CTC analysis from head and neck squamous cell carcinoma patients. Eng Life Sci. 2022;22:391–406. https://doi.org/10.1002/elsc.202100133

2.1.6 SUMMARY

When choosing a CTC enrichment method it is useful to establish a suitable model system for pre-clinical validation. Characterization of the marker expression of HNSCCUM-02T and HNSCCUM-03T by fluorescence microscopy and western blot revealed a more epithelial profile of HNSCCUM-02T cells based on EpCAM, ZO-1, Pan-CK, and E-Cadherin expression. HNSCCUM-03T cells can be considered of a more mesenchymal character based on CSV expression. HNSCCUM-02T were further used to probe the efficacy of manual CTC enrichment by two different positive selection methods, Dynabeads and pluriBeads. Since the pluriBeads generated the more promising results in cell culture medium, they were additionally tested for manual enrichment from whole blood. Recovery rates of around 50 % were achieved from both, medium and blood, but microscopy revealed significant contamination with blood cells after isolation. Automating the process using the *CTCelect* platform in combination with the Dynabeads system was tested with a HNSCC patient sample, generating a recovery of two thirds CTCs and one third non-CTCs/WBCs. Additional tests carried out by collaborators revealed that different CTC/DTC populations can be isolated by the *CTCelect* platform using either EpCAM-based enrichment and staining, or CD51/CD61/CD106-based enrichment and CD51 staining. They could further show that qPCR of dispensed single cells is feasible and CTC expression patterns differ depending on the antigen used for enrichment.

2.2 Exosome Isolation

As introduced, one major hurdle in exosome research and their integration into clinical applications is their successful isolation. When looking at the current body of literature, ultracentrifugation (UC) remains the *gold standard* and is used by 50 % of all researchers. UC is also compatible with various sample types and volumes, making it a favourable method (Chen et al. 2021). Even though UC is a well-established technique with various protocols freely available, a thorough evaluation and validation of exosome isolation is pivotal to ensure that any results generated downstream are in fact related to exosomes. The *MISEV2023* guidelines provide a general workflow for EV characterization that a vast number of researchers from the field have agreed on. It is recommended to show three positive and one negative marker for the respective EV type on protein level. Furthermore, two different but complementary techniques are to be used to characterize single EVs. This shall include image-based methods and single particle analysis techniques assessing biophysical properties. Since the 2018 update, it is also recommended to describe EVs quantitatively, i.e. by particle count, total protein content, or total lipid content (Welsh et al. 2024).

To simplify the validation process, a HEK293T model cell line stably expressing emerald green fluorescent protein (emGFP)-tagged CD63 was used, allowing for quick and easy visual control and protein detection. Figure 16 illustrates the applied UC protocol, including the standard "cleaning" steps at 500x *g*, 3000x *g*, and 12.000x *g* to remove live cells, dead cells, and debris respectively. Exosomes were precipitated at 100.000x *g* and washed once in PBS before further analysis (for detailed protocol see section 4.3.1).

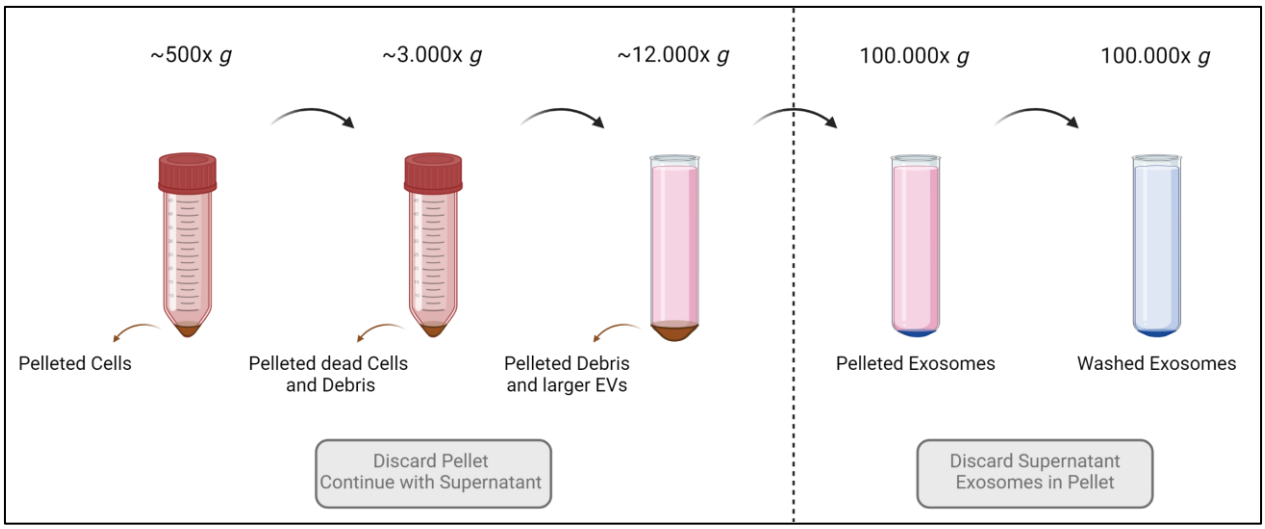

Figure 16. Schematic overview of exosome isolation from cell culture supernatant

2.2.1 Proof of Concept by Fluorescence Analysis

To get a quick and easy first impression of the generated isolates, they were imaged by fluorescence microscopy. Additionally, fluorescence was quantified using a microplate reader. Figure 17A shows representative images of the GFP fluorescence of donor cells and putative exosome isolates. In cells, CD63 is typically localized at the plasma membrane as well as in late endosomes and lysosomes (Pols and Klumperman 2009). Accordingly, the GFP signal in the HEK293T CD63-emGFP cells accumulates at the plasma membrane and appears in dots throughout the cytoplasm, which likely correspond with endosomes or lysosomes. When imaging the putative exosome isolate, small, floating particles and occasional larger aggregates can be observed. When quantifying the fluorescence using a microplate reader, the fluorescence signal was 10-fold higher in UC isolates compared to PBS alone, further confirming the presence of CD63-emGFP in the isolates (Figure 17B).

Whether the observed particles are in fact exosomes, or rather exosome aggregates, cannot be verified by the exploited methods, but the presence of CD63-emGFP motivated further analysis.

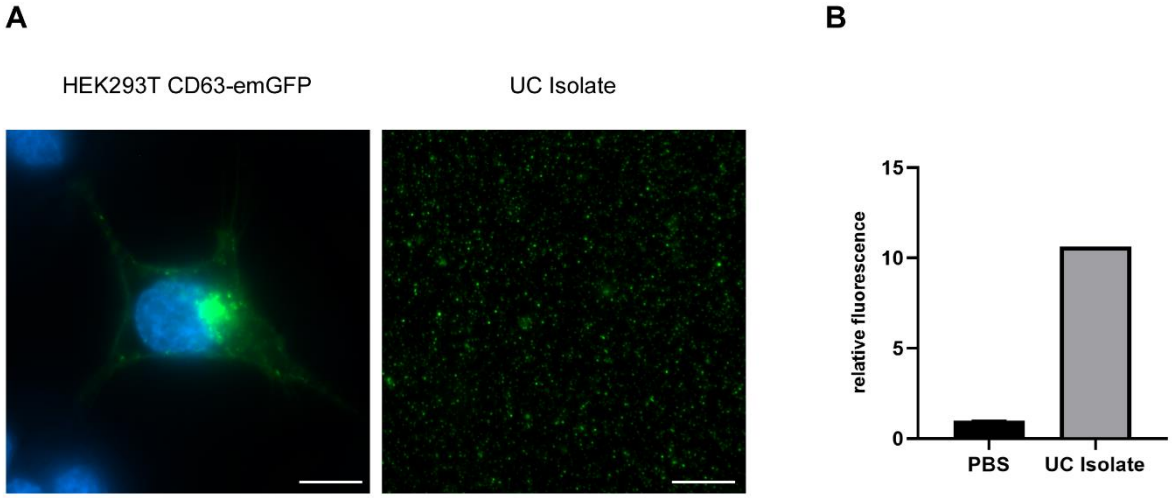

Figure 17. Fluorescence analysis of HEK293T CD63-emGFP cells and their putative exosomes
Putative exosomes were isolated from 40 mL of cell culture supernatant from HEK293T CD63-emGFP cells after 48h of conditioning and resuspended in PBS. **A**) Representative images of HEK293T CD63-emGFP donor cells and respective UC isolates by fluorescence microscopy. Cells were grown in microscopy dishes for 24h before imaging. Nuclei were stained with Hoechst (blue) and CD63 is tagged with emGFP (green). Scale bars 10 µm. **B**) Relative fluorescence of UC isolate normalized to PBS of n=1 experiment.

2.2.2 Single Particle Characterization

Adhering to the *MISEV2023* guidelines, three complementary methods were chosen to analyze the putative exosome preparations on single vesicle level. To assess the biophysical properties of single particles, tunable resistive pulse sensing (TRPS) was applied. TRPS is a technique that can assess size, concentration, and surface charge on single-particle level.

Figure 18A shows the measured particle concentration by particle diameter, with a mean particle diameter of 104 ± 44,3 nm. The mean raw concentration was determined to be 7,89 x 10^{10} particles/mL. The smallest measured particles had a size of 52 nm, while the largest reached 413 nm. 90 % of the measured particles were smaller than 152 nm and 50 % smaller than 68 nm. Thus, particles fall into the typical size range of exosomes. Figure 18B illustrates the particle velocity. When particles of similar size cause different blockade durations, they either differ in shape or surface charge, or smaller particles have formed aggregates. When looking at the blockade durations of the putative exosome isolate, there are only a few outliers, illustrating a uniform size and surface charge of the particles within the sample, with little aggregation.

Size distribution was additionally assayed by dynamic light scattering (DLS). This method relies on the assessment of the Brownian motion, which in turn allows conclusions about the particle size (Stetefeld et al. 2016). Figure 18C shows the measured size distribution with a mean particle diameter of 112 ± 48,2 nm. The smallest measured particles had a size of 58,8 nm, while the largest reached 6440 nm. With 90 % of the particles being smaller than 163 nm and almost 70 % being smaller than 107 nm, they again fit into the typical exosome size range, though there seem to have been some impurities with larger vesicles, aggregates, or debris.

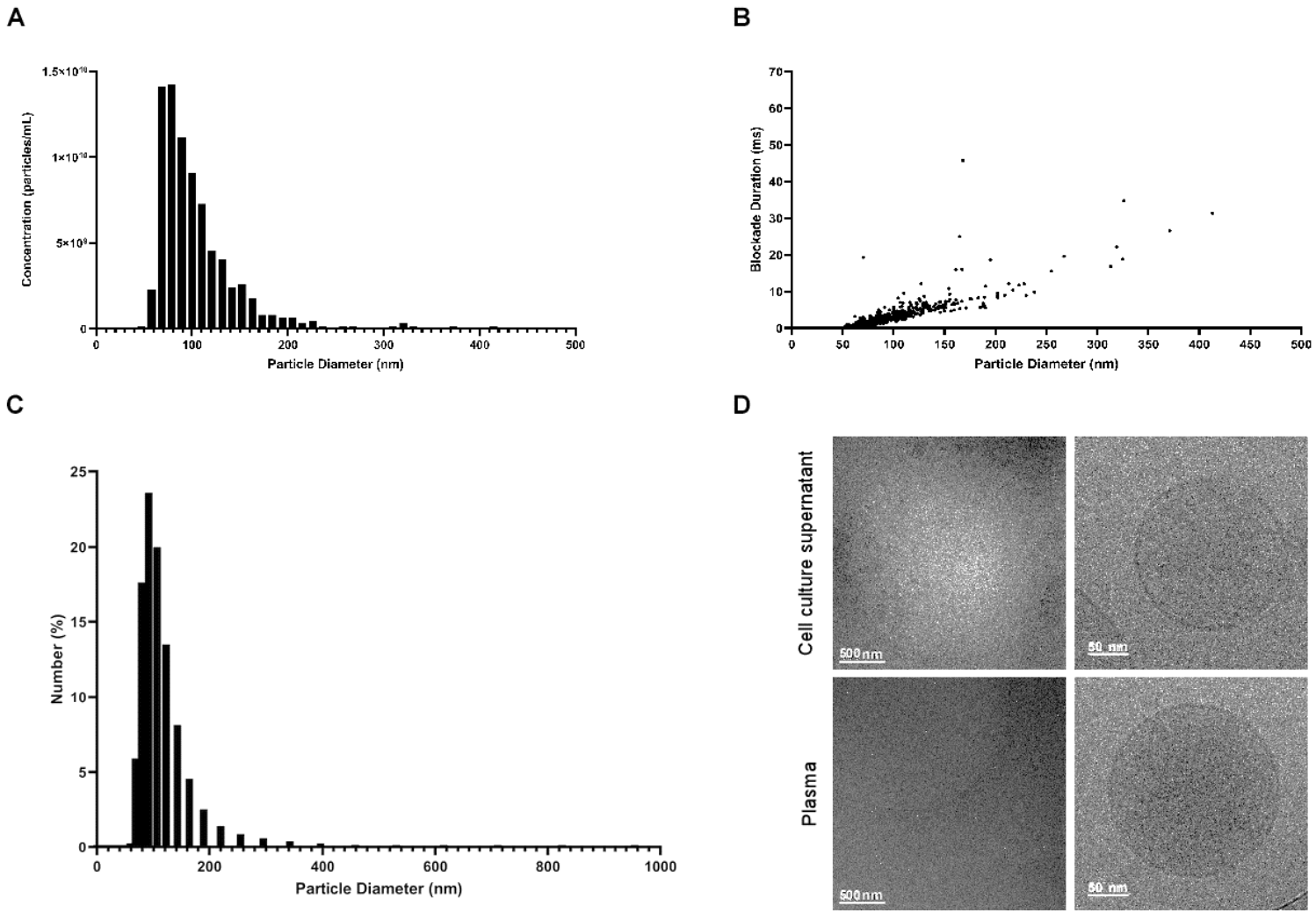

Figure 18. Single particle characterization of putative exosomes
Putative exosomes were isolated from 80 mL (TRPS), 50 mL (DLS), or 160 mL (cryo-TEM) cell culture supernatant of HEK293T CD63-emGFP cells after 48h and resuspended in PBS for analysis. **A)** Particle size distribution as measured by TRPS. **B)** Blockade duration as measured by TRPS. A total of 487 particles were analyzed. **C)** Particle size distribution as measured by DLS. 10 data points lay outside the axis limits and are not displayed. **D)** Putative exosomes were isolated from cell culture supernatant or blood plasma. After storage at 4 °C overnight, samples were fixed and analyzed by cryo-TEM. Scale bars as indicated.

For image-based evaluation, putative exosomes were imaged using cryo-transmission electron microscopy (cryo-TEM). The resulting images are shown in Figure 18D. The isolated vesicles from both, cell culture supernatant and plasma show a round shape and membrane bilayer coating. The speckled appearance of the vesicles' lumens infer an electron dense cargo. Regarding size, the isolated vesicles appear to be in the range of 50-200 nm, with occasional larger vesicles in the cell culture supernatant sample. When looking at the overview images it becomes apparent that the cell culture supernatant sample contained much more vesicles than the plasma sample. This can largely be attributed to the differing starting volumes of the samples (160 mL and 7,5 mL respectively). Overall, the isolated vesicles show great resemblance to exosomes.

Taken together, the single particle characterization by cryo-TEM, TRPS, and DLS reveals membrane-coated vesicles with a round shape and mean diameter of 104 nm (TRPS) and 112 nm (DLS). All these characteristics are in accordance with typical exosome attributes. In cell culture supernatant samples, occasional larger particles with diameters of up to 413 nm (TRPS) and 6440 nm (DLS) were recorded. It should be noted that DLS has a rather low resolution and the CD63-emGFP fluorescence could have interfered with the measurement, as it is based on light detection (Bhattacharjee 2016). Therefore, the TRPS size data can be considered more reliable, plus it is also more in agreement with the cryo-TEM images. Nevertheless, there are some impurities with particles outside of the exosomal size range detectable. When looking at the cryo-TEM images, it seems most likely that larger EVs were co-precipitated, as no aggregation or non-EV particulates are visible. The TRPS data also show little evidence for aggregation based on the blockade duration measurement. Isolating a fully pure exosome population is a rather unrealistic goal, and with 90 % of the particles being smaller than 152 nm as measured by TRPS, the presented EV preparations can likely be identified as exosomes.

2.2.3 Protein and Lipid Content Quantification

It is recommended to give quantitative data on EV preparations. EVs contain nucleic acids, proteins, lipids, and other biomolecules, which can all be exploited for quantification in addition to particle count (Welsh et al. 2024). Protein content is often measured using colorimetric assays, like the Bradford assay. The Bradford assay is based on the ability of Coomassie dye to bind to proteins in acidic conditions. The free, protonated dye absorbs at 465 nm, whereas the dye-protein complex absorbs at 595 nm. This increase in absorption at 595 nm can be measured with a photometer and protein concentrations can be calculated using a standard

curve (Sapan et al. 1999). Lipid content can be measured using the sulfo-phospho-vanillin (SPV) assay. The SPV assay is carried out in two steps.

First, the lipid-containing sample is incubated with sulfuric acid at high temperatures. In the second step, the resulting products react with vanillin in the presence of phosphoric acid. The complex chemical reaction results in the formation of a pink chromophore, if double bonds or free hydroxyl groups are present within the lipid sample. Photometric measurement at 540 nm allows for the calculation of the lipid concentration using a liposome standard curve (McMahon et al. 2013, Visnovitz et al. 2019).

Figure 19A summarizes the quantification data. For lipids, a mean total amount of 14,43 ± 2,81 µg was measured, which translates to a concentration of 288,51 ± 56,18 µg/mL. The mean total protein amount was determined to be 218,88 ± 43,43 µg, which translates to a concentration of 4,38 ± 0,87 µg/µL.

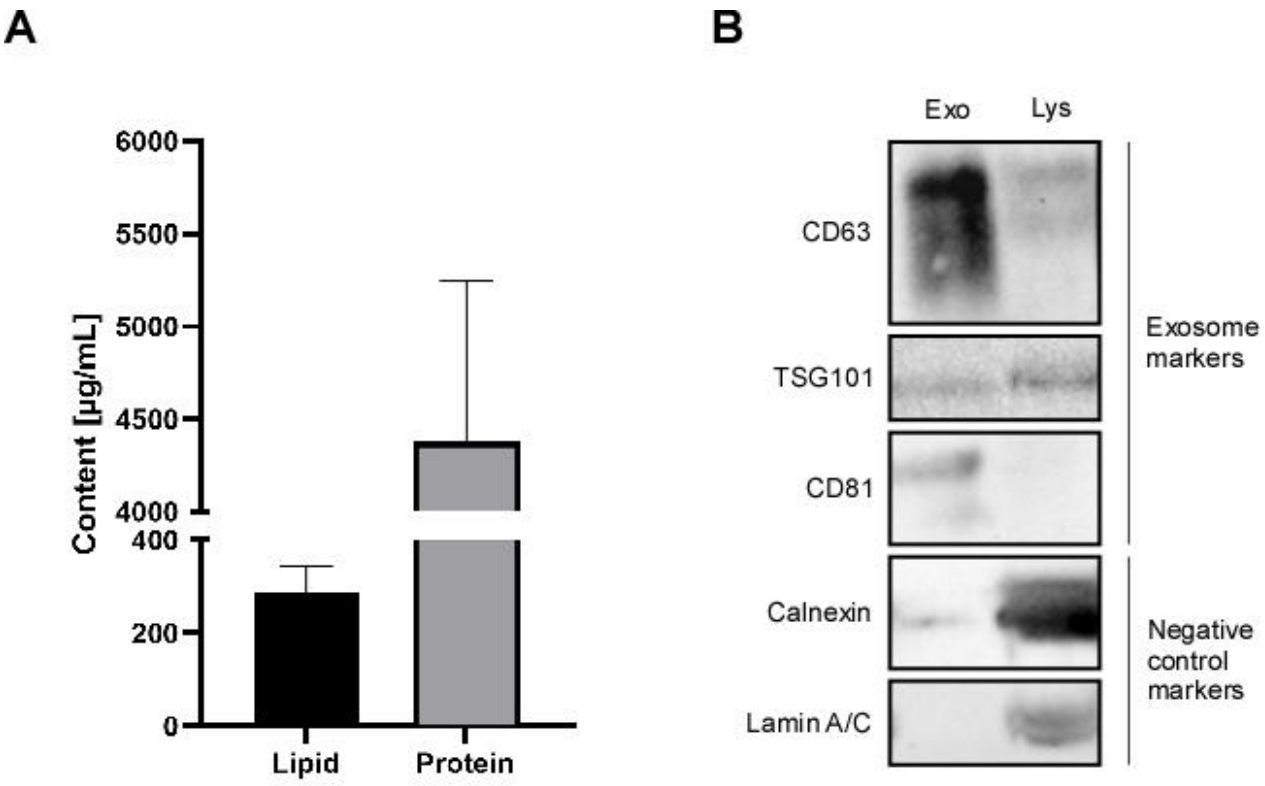

Figure 19. Lipid content quantification and protein content quantification and characterization of putative exosomes

A) Protein and lipid concentration of exosome isolates. Putative exosomes were isolated from ~40 mL cell culture supernatant from HEK293T CD63-emGFP cells after 72h. Protein content was quantified using Bradford assay, while lipid content was determined using the SPV lipid assay. Mean ± SD of n=4 independent isolations. **B)** Western blot analysis of exosomal protein content. Exosomes were isolated from 20 mL HEK293T CD63-emGFP cell culture supernatant after 72h. Exosomes and donor cells were lysed in RIPA buffer, and sonicated. Samples were stored at -80 °C until analysis.

Verifying whether the detected lipid and protein content in fact reflects EVs or exosomes is not possible using the applied methods. When looking at published research, it becomes apparent that different cells produce EVs with differing lipid content. One study found between 2,88 µg and 16,63 µg lipids in 5 µL of a small EV preparation depending on the cell line. Total starting volume for their experiments were 24 mL of cell culture supernatant that had been conditioned for 24h and resulted in a final volume of 30 µL of EVs (Visnovitz et al. 2019). Others only report 0,85 µg/mL lipids in exosome samples from 24h conditioned cell culture medium (Osteikoetxea et al. 2015). Both studies used a combination of gravity driven filtration and differential centrifugation to isolate exosomes, and lipid content was measured by SPV lipid assay. Lipid concentrations can only be calculated reliably within the linear range of the reference curve; otherwise lipid content can be over- or underestimated. It is also not established, whether lipid assays like the SPV assay can detect all EVs independent of their specific lipid composition (Thery et al. 2018). So far, there is only a limited number of publications that disclose lipid quantification in combination with detailed information on the exosome isolation procedure, rendering it impossible to assess whether the results presented in this work are in an appreciable range for exosome isolates. However, being able to detect lipids with appreciable reproducibility is a promising outcome.

When looking at exosomal protein content, one study reports 3,82 µg protein in exosomes from colon cancer cells and 3,02 µg in those from breast cancer cells, as measured by Bradford assay. Data are given per 10^6 cells and exosomes were isolated by UC (Dash et al. 2021). Exosomes isolated from THP-1 cells using different methods revealed total protein amounts between 27,25 µg and 45,5 µg by Bradford assay. Starting volumes for these experiments were 208 mL cell culture supernatant from approximately 4 x 10^9 cells (Wang et al. 2015). Another study reports 46,60 ± 0,9833 µg total protein from leukemia cell exosomes and 38,75 ± 4,57 µg from breast cancer cell exosomes. Here, exosomes were isolated using lyophilisation, but starting volume and cell number are not disclosed (Qazi et al. 2023). When comparing these results, one has to keep in mind the different cell types, specific culture conditions, and isolation methods. Overall, a lot of available data on protein content of EVs is hard to interpret, as key information is not provided. Additionally, the Bradford assay can only detect proteins within the linear range of its reference curve. Highly purified or low concentrated EV preparations might fall outside of this range, leading to underestimation of the protein content. Conversely, overestimation of the protein content can result from co-precipitation of protein contaminants (Thery et al. 2018). Another potential source of error is the use of detergents. SDS is known to lower the sensitivity of the Bradford assay (Friedenauer and Berlet 1989). Other detergents like Triton-X, NP-40, and Na-deoxycholate further contribute to this effect, making the use of

Bradford assay unfavourable in combination with RIPA buffer (Krohn 2011). Indeed, additional protein concentration determination using the DC protein assay revealed significantly lower protein amounts than shown in Figure 19 (~45 µg of total exosomal protein from 240 mL cell culture supernatant). Thus, the here presented results should be viewed with caution.

2.2.4 Protein Content Characterization

The *MISEV2023* guidelines define five different categories of proteins for the protein content-based characterization of EVs. Category 1 contains transmembrane or GPI-anchored proteins associated with the plasma membrane and/or endosomes. These category 1 proteins are further divided into cell or tissue specific and non-tissue specific proteins. Among the non-tissue specific proteins are Integrins, MHC class I, and Tetraspanins (Thery et al. 2018). Exosomes in particular are known to be enriched in Tetraspanins CD63, CD81, and CD9 (Andreu and Yanez-Mo 2014). Category 2 lists cytosolic proteins recovered in EVs, that are sub-grouped into proteins with lipid or membrane protein-binding ability and promiscuously EV incorporated proteins. The first sub-group contains proteins of the ESCRT complex and TSG101, which are involved in the formation of the MVB, and therefore also abundant in exosomes (Vlassov et al. 2012). The second sub-group lists HSP70 and cytoskeleton associated proteins like actin and tubulin. Category 3 contains non-EV co-isolated structures, for example albumin. Category 4 covers proteins associated with intracellular compartments other than endosomes and the plasma membrane, including the nucleus, mitochondria, and the ER. Finally, category 5 lists secreted proteins recovered with EVs, which are of interest if certain functional activities are investigated (Thery et al. 2018).

To verify exosome isolation, putative exosome isolates were analyzed for their protein content by western blot. Figure 19B summarizes the analyzed positive and negative control markers. As expected, the overexpressed CD63-emGFP could be detected in putative exosomes and donor HEK293T cells. To evaluate an endogenously expressed tetraspanin, CD81 was also tested and could be detected in putative exosomes. Additionally, the MVB-associated protein TSG101 was detected in both, putative exosomes and donor cells. With a total of three positive EV markers from categories 1 and 2 found in the putative exosome preparation, EV content of the sample can be confirmed. In order to assess the purity of the preparation, two proteins from category 4 were analyzed. Calnexin, an ER membrane protein, and Lamin A/C, a structural protein of the nucleus, were both detected in the donor cell lysate, as expected. Lamin A/C is completely absent in the putative exosome sample, while there is a faint band detectable for calnexin. This could hint at a contamination with ER components. However, calnexin expression has also been

detected in large EVs, making those another potential contamination source (Saludas et al. 2022). Since exosomes are also known to interact with the ER and calnexin is a membrane bound protein, this would pose an alternative explanation for its appearance in exosomes. Proteins from categories 3 and 5 were not considered, as they are only relevant if exosomes are isolated from biological fluids.

2.2.5 Exosomes in Cancer Progression and Therapy Resistance: Molecular Insights and Therapeutic Opportunities (Review)

Madita Wandrey, Jadwiga Jablonska, Roland H. Stauber, Désirée Gül

Abstract

The development of therapy resistance still represents a major hurdle in treating cancers, leading to impaired treatment success and increased patient morbidity. The establishment of minimally invasive liquid biopsies is a promising approach to improving the early diagnosis, as well as therapy monitoring, of solid tumors. Because of their manifold functions in the tumor microenvironment, tumor-associated small extracellular vesicles, referred to as exosomes, have become a subject of intense research. Besides their important roles in cancer progression, metastasis, and the immune response, it has been proposed that exosomes also contribute to the acquisition and transfer of therapy resistance, mainly by delivering functional proteins and RNAs, as well as facilitating the export of active drugs or functioning as extracellular decoys. Extensive research has focused on understanding the molecular mechanisms underlying the occurrence of resistance and translating these into strategies for early detection. With this review, we want to provide an overview of the current knowledge about the (patho-)biology of exosomes, as well as state-of-the-art methods of isolation and analysis. Furthermore, we highlight the role of exosomes in tumorigenesis and cancer treatment, where they can function as therapeutic agents, biomarkers, and/or targets. By focusing on their roles in therapy resistance, we will reveal new paths of exploiting exosomes for cancer diagnosis and treatment.

life

Review

Exosomes in Cancer Progression and Therapy Resistance: Molecular Insights and Therapeutic Opportunities

Madita Wandrey [1], Jadwiga Jablonska [2,3], Roland H. Stauber [1] and Désirée Gül [1,*]

[1] Nanobiomedicine/ENT Department, University Medical Center Mainz, Langenbeckstraße 1, 55131 Mainz, Germany; wandrey@uni-mainz.de (M.W.); rstauber@uni-mainz.de (R.H.S.)
[2] Translational Oncology/ENT Department, University Hospital Essen, Hufelandstraße 55, 45147 Essen, Germany; jadwiga.jablonska@uk-essen.de
[3] German Cancer Consortium (DKTK) Partner Site Düsseldorf/Essen, 45147 Essen, Germany
* Correspondence: guel@uni-mainz.de

Abstract: The development of therapy resistance still represents a major hurdle in treating cancers, leading to impaired treatment success and increased patient morbidity. The establishment of minimally invasive liquid biopsies is a promising approach to improving the early diagnosis, as well as therapy monitoring, of solid tumors. Because of their manifold functions in the tumor microenvironment, tumor-associated small extracellular vesicles, referred to as exosomes, have become a subject of intense research. Besides their important roles in cancer progression, metastasis, and the immune response, it has been proposed that exosomes also contribute to the acquisition and transfer of therapy resistance, mainly by delivering functional proteins and RNAs, as well as facilitating the export of active drugs or functioning as extracellular decoys. Extensive research has focused on understanding the molecular mechanisms underlying the occurrence of resistance and translating these into strategies for early detection. With this review, we want to provide an overview of the current knowledge about the (patho-)biology of exosomes, as well as state-of-the-art methods of isolation and analysis. Furthermore, we highlight the role of exosomes in tumorigenesis and cancer treatment, where they can function as therapeutic agents, biomarkers, and/or targets. By focusing on their roles in therapy resistance, we will reveal new paths of exploiting exosomes for cancer diagnosis and treatment.

Keywords: exosomes; cancer; cancer therapy; therapy resistance; resistance transmission

Citation: Wandrey, M.; Jablonska, J.; Stauber, R.H.; Gül, D. Exosomes in Cancer Progression and Therapy Resistance: Molecular Insights and Therapeutic Opportunities. *Life* **2023**, *13*, 2033. https://doi.org/10.3390/life13102033

Academic Editor: Juan Pablo Rigalli

Received: 12 September 2023
Revised: 4 October 2023
Accepted: 5 October 2023
Published: 9 October 2023

1. Introduction

Exosomes are nanosized extracellular vesicles (EVs) that were first described as early as 1983 [1,2]. While they were considered a cellular mechanism for waste disposal until the 1990s, research has shown that they carry complex cargoes. By delivering their cargo to neighboring and distant cells, exosomes participate in cell–cell communication and influence the phenotype of recipient cells. The respective cargo is highly dependent on the cell of origin [3–5]. Exosomal communication contributes to fundamental physiological processes like cell homeostasis, immune response regulation, and senescence. As exosomes are released by almost all cell types, aberrant cells, such as cancer cells, also readily shed exosomes. These exosomes are part of the tumor microenvironment (TME) and play an important role in cancer progression, metastasis, immune response, and therapy. They also contribute to the acquisition and transfer of therapy resistance by promoting epithelial–mesenchymal transition (EMT) and delivering functional proteins and non-coding RNAs (ncRNAs) [6,7]. Therapy resistance is one of the major challenges in the treatment of various cancer entities, as it is the main cause of relapses and poor survival outcomes.

2. Exosome Structure and Contents

Exosomes are characterized by their small size (30–200 nm) and endosomal origin, allowing for differentiation from other types of EVs like microvesicles (100–1000 nm) and apoptotic bodies (1–5 µm) [8].

The contents of exosomes are highly complex and include proteins, nucleic acids, metabolites, and lipids (Figure 1B). To date, 41,860 proteins, 7784 RNAs, and 1116 lipids from 286 studies have been entered into the ExoCarta database [9]. Typically, exosomes are enriched in tetraspanins (CD63, CD81, CD9), heat shock proteins (HSP70, HSP90), multivesicular body (MVB)-formation-associated proteins (TSG101, ALG-2-interacting protein X/Alix), and proteins related to membrane transport and fusion (GTPases). These proteins serve as exosome markers, allowing for their distinction from other EVs and even facilitating exosome isolation [10]. Among the RNA species contained in exosomes, microRNAs (miRNAs) are the most abundant in plasma-derived exosomes. Upon their uptake, miRNAs can alter the phenotype of the recipient cell through modifications of its protein expression [11]. As for DNA, it has been shown that more than 90% of cell-free DNA in plasma is associated with exosomes [12]. While DNA of genomic (gDNA) as wells as mitochondrial (mtDNA) origin have been found in exosomes, the packaging mechanisms remain largely unknown. It is thought that the exosomal packaging of DNA is a mechanism of maintaining cell homeostasis but also a means of altering the recipient cell by incorporating the DNA into its genome [13]. Among the metabolites found in exosomes are amino acids and their derivatives, carbohydrates, carbonic acids, and folates [5]. Apart from their cargo, exosomes also have a specific lipid composition. Generally, exosomes are enriched in cholesterol, ceramides, sphingolipids, and phosphatidylserine. Additionally, exosomes can also contain lipolytic enzymes, which can autonomously produce units of bioactive lipids [14,15].

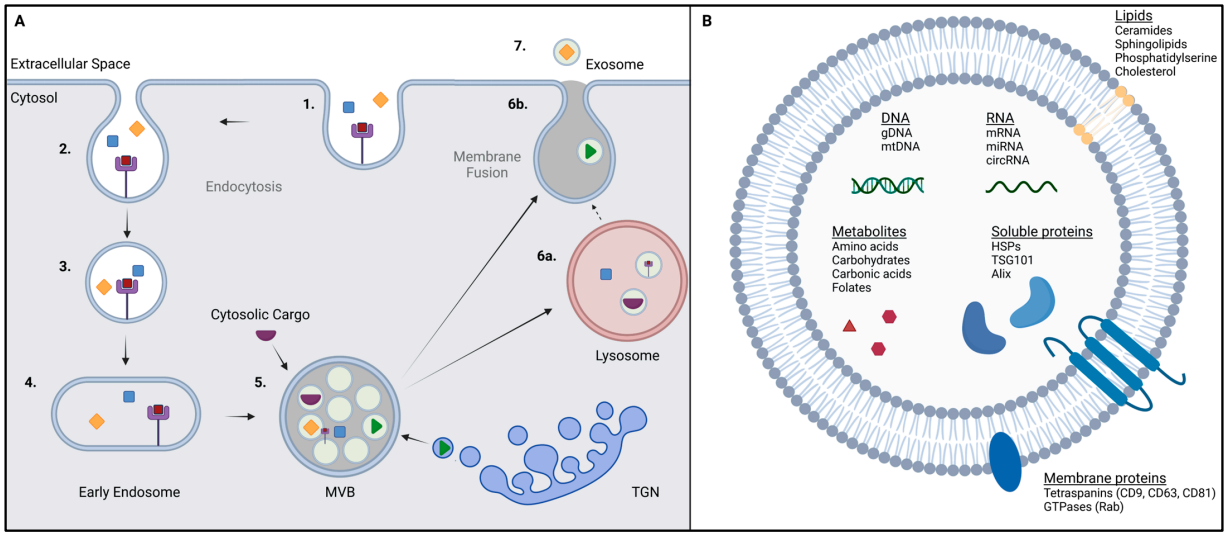

Figure 1. (**A**) Schematic overview of exosome biogenesis via the endosomal pathway. Starting with (receptor-mediated) endocytosis (**1.**,**2.**), intracellular vesicles are formed (**3.**) and converge into early endosomes (**4.**). After maturation to late endosomes, intraluminal vesicles are formed through inward budding of the endosomal membrane, resulting in the MVB (**5.**). Upon fusion of the MVB with lysosomes (**6a.**), contents are typically recycled or degraded. Fusion of the MVB or lysosome with the plasma membrane (**6b.**) leads to the release of exosomes into the extracellular space (**7.**). (**B**) Schematic illustration of a single exosome and its bioactive cargo and components. MVB = Multivesicular body. TGN = Trans-Golgi network. Symbols indicate different endosomal cargoes, such as peptides and proteins, metabolites, and nucleic acids (as depicted in B). Purple squares symbolize ligand for receptor-mediated endocytosis. Created with BioRender.com.

3. Exosome Shaping and Signaling

3.1. Exosome Biogenesis

Exosomes originate from the endosomal pathway, typically starting with the (receptor-mediated) endocytosis of extracellular materials through the invagination of the plasma membrane (Figure 1A). The resulting vesicles converge into early endosomes. These early endosomes not only contain extracellular components but also plasma membrane proteins [15,16]. Through V-ATPase-mediated acidification, they mature into late endosomes. Late endosomes can also receive cargo-loaded vesicles from the Trans-Golgi network [17]. From the inward budding of the endosomal membrane, small intraluminal vesicles (ILVs) are formed. The formation of ILVs requires the activity of the endosomal sorting complex required for transport (ESCRT), which is initiated by the binding of ubiquitinated proteins to the ESCRT-0 subunit in the endosomal membrane [18,19]. Alternatively, there are also ESCRT-independent routes for ILV formation based on ceramide- or tetraspanin-enriched microdomains within the endosomal membrane [20–22]. The ILVs are contained within the MVB, and upon fusion of the MVB with the plasma membrane, they are released into the extracellular space as exosomes [15]. Alternatively, MVBs can fuse with lysosomes, which leads to the degradation of their contents, although there have also been reports of lysosomes fusing with the plasma membrane and releasing exosomes [23]. Other reports also mention exosomes originating directly from the plasma membrane. Budding from endosome-like microdomains, they carry classic exosome markers like CD63 and CD81 [24,25]. However, the amount of evidence is still limited, leaving this route of biogenesis up for debate [8].

3.2. Exosome Distribution and Bioactivity

Exosome biodistribution occurs locally and systemically. Exosomes can undergo multiple cycles of uptake and release, allowing for deep tissue penetration [8]. Most studies on exosome biodistribution come from pharmacokinetic research, meaning they use heterologous exosomes. The oral administration of heterologous exosomes results in their distribution to almost all organs, including the liver, lung, kidney, colon, and brain [26,27]. Intravenous administration leads to the fast elimination of heterologous exosomes from the bloodstream, while nasal administration has been shown to direct them to the brain [28,29]. Exosome biodistribution and cell or organ tropism are considerably influenced by many factors, including the cell of origin, the membrane constitution, and the overall patho-/physiological state of the host, as well as dose and route of administration in the case of heterologous exosomes [30]. It is very likely that the biodistribution of autologous exosomes differs significantly from that of heterologous ones. Nevertheless, autologous exosomes have been found in various bodily fluids, including blood, urine, breast milk, saliva, and interstitial fluid [8].

Upon reaching the recipient cell, there are different possibilities for exosomes to elicit bioactivity (Figure 2). Ligands in the exosomal membrane can bind to cellular receptors, causing downstream signaling cascades. One study has shown that exosomes released by dendritic cells carry tumor necrosis factor (TNF) and TNF-related apoptosis-inducing ligand (TRAIL), which bind to the TNF receptors on tumor cells and activate caspases, eventually resulting in apoptosis [31]. Alternatively, exosomes can be taken up by endocytosis, phagocytosis, or plasma membrane fusion. Fusion with the plasma membrane is most likely Rab- and SNARE-mediated and leads to the direct release of exosomal cargo into the recipient cell [32,33]. However, the primary route for exosome uptake is believed to be internalization by endocytosis or phagocytosis. Typically, endocytosis is receptor-mediated and results in clathrin-coated intracellular vesicles that eventually undergo uncoating and converge into early endosomes. Clathrin-independent endocytosis occurs at lipid rafts, which are membrane microdomains enriched in cholesterol, sphingolipids, and GPI-anchored proteins [16]. Phagocytosis mainly occurs in immune cells like macrophages and dendritic cells. During phagocytosis, the plasma membrane is deformed and engulfs extracellular materials, including bacteria, dead cells, and EVs. The resulting phagosome

is internalized and directed to the endosomal pathway [34]. The typical endpoint of the endosomal pathway is the lysosome, where recycling and degradation take place. In order to achieve signaling, exosomes or their cargo have to bypass lysosomal degradation [8]. Some cargoes, for instance, transforming growth factor (TGF) β-1, can be activated by acidification within the endosome [35]. It has also been shown that cargo can passively diffuse into the cytoplasm [36]. Rab5/Rab7-positive endosomal vesicles have been found to interact with the endoplasmic reticulum (ER). Since protein translation occurs at the ER, this would be a favorable route for exosomes carrying mRNA or miRNA [37,38]. The nucleoplasmic reticulum (NR) is a compartment consisting of invaginations penetrating into the nucleoplasm. Upon the interaction of the NR with late endosomes, exosomal cargo could enter the nucleus [39]. Other possible routes for bypassing degradation are retrograde trafficking from the endosome to the Golgi apparatus, the fusion of endosomal and exosomal membranes, and release into the cytoplasm by endosome or lysosome rupture [8].

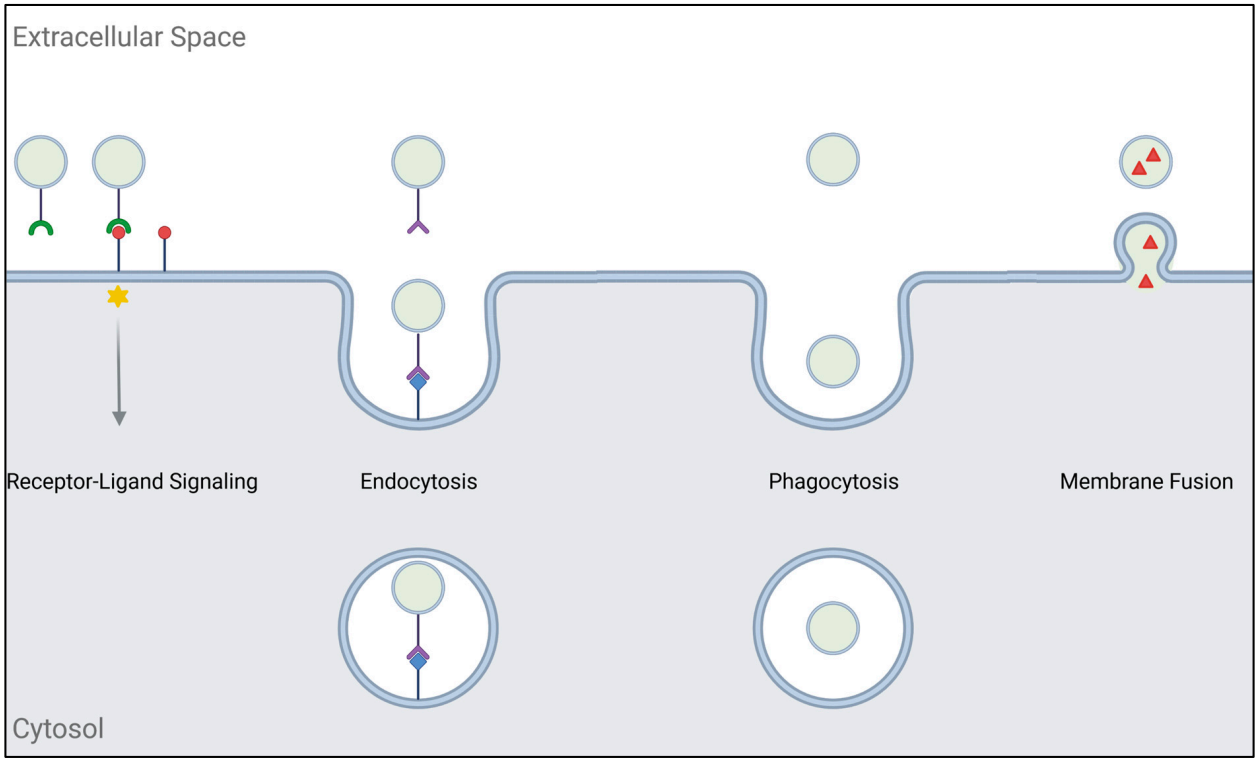

Figure 2. Schematic overview of possible routes for exosome bioactivity. Interaction of exosomal ligands (green) and cellular receptors (red circle) can trigger downstream signaling cascades ((**left**); marked by an asterisk). Alternatively, exosomes can be internalized by endocytosis (receptor-ligand interaction in purple/blue) or phagocytosis (**middle**). Another possibility is the fusion of exosomal and cellular membrane, allowing the direct release of exosomal cargo (red triangle) into the cytoplasm (**right**). Created with BioRender.com.

4. Exosome Isolation and Analysis

4.1. Isolation of Exosomes

One major challenge in studying exosomes is their efficient and reproducible isolation since they are small in size, low in density, and mixed with various other components if isolated from bodily fluids. Depending on the downstream application, there are different techniques in use, with the most common ones being ultracentrifugation, size-based isolation, polymer precipitation, and immunoaffinity capture. There are also numerous commercial exosome isolation kits available that rely on the aforementioned methods [40,41].

Ultracentrifugation (UC), also referred to as differential centrifugation, remains the gold standard of exosome isolation and is used by around 50% of researchers [41]. UC

relies on the differences in size and density between exosomes and other components of the sample [41,42]. Typically, the protocol starts with a series of lower-speed centrifugations to remove live cells, dead cells, and debris (at 300× *g*, 2000× *g*, and 10,000× *g*, respectively). Alternatively, this can be achieved by filtration. Following this are two high-speed centrifugations at 100,000× *g* to precipitate the exosomes [41,43]. The advantages of UC are that it is a well-established method suitable for a variety of sample types and volumes. The downsides of UC are that it is a rather time-consuming method, and due to the high centrifugation speeds, exosomes can be damaged, and their biological functions can be altered. Therefore, UC is more suitable for proteomic or other molecular analyses and less suitable for functional assays. Also, as it is based on size and density, impurities like protein aggregates or organelles can co-precipitate [40,44]. To reduce such impurities, density-gradient UC was introduced, where separation media with different densities are applied. However, this method is rather elaborate and even more time-consuming than classic UC, limiting its application [45,46].

The most common size-based techniques are size-exclusion chromatography (SEC) and ultrafiltration (UF). For SEC, samples are added to columns containing a porous gel (e.g., Sepharose), where larger particles cannot enter the pores and therefore elute faster than the small exosomes trapped in the pores. Since this method works with a low centrifugal force or even gravity, isolated exosomes remain intact and biologically active [47]. However, SEC relies solely on size, which leads to contamination with other particulates in a similar size range. Therefore, SEC is often applied in combination with other methods, like UC [48].

UF uses membranes with different molecular weight cutoffs (MWCOs) to separate exosomes from larger particles. Different forces can be used to drive the sample through the membranes, including centrifugation, pressure, and electric charge. As for SEC, UF suffers from impurities of similar-sized particulates and additionally from low recovery rates due to unspecific binding to or clogging of the membranes [44,49].

Polymer precipitation is a common method for isolating viruses, which share a lot of common features with exosomes [50]. The most commonly used reagent for polymer precipitation is polyethylene glycol (PEG), which reduces the solubility of exosomes, allowing their precipitation at lower centrifugation speeds. While this method is quick and easy, it is also prone to contamination with particles with similar biophysical properties, and it can be difficult to remove the polymer reagent after isolation [40].

Immunoaffinity capture relies on the interaction between antigens and specific antibodies. As described in Section 3.1, exosomes carry a number of general marker proteins that can serve as antigens for capture. The respective antibodies are fixed to a carrier, mostly beads or chromatography matrices. Through the binding of the exosomal antigen to the fixed antibody, exosomes can be separated from contaminants in the sample. Such methods yield high-purity exosomes but are also rather high in cost and time-consuming. Additionally, the isolated exosome population is highly dependent on the choice of antigen(s), thus not reflecting the total exosome population [41,51,52].

Recently, microfluidic devices have emerged as promising tools to combine enrichment and analysis of exosomes. Generally, many of these devices also rely on classic isolation techniques based on physical and biochemical properties. Microfluidic devices based on physical properties contain porous membranes, nanofilters, microvilli, or electrical or acoustic fields to trap and separate exosomes. Biochemical-property-based devices contain mobile or stationary antibody-coated media [41]. There are also devices combining both approaches. Notably, some platforms even offer the possibility of the real-time analysis of the isolated exosomes, for example, by subsequent imaging or biomarker detection [53,54].

The choice of a suitable isolation method is highly dependent on the research focus and downstream application. At the same time, the obtained results may vary depending on the applied isolation method, making this choice pivotal for any exosome research. For more detailed information on methods for exosome isolation and their specific implications, we refer the reader to more thorough reviews on the topic [44,55–57].

4.2. Analysis of Exosomes

To validate successful exosome isolation and gain further insights into their patho-/biological functions, the downstream analysis of exosomes is crucial. Exosomes are typically analyzed for their physical and/or biochemical properties. Physical properties include particle size and concentration, while biochemical properties focus on the exosomes' composition and cargo.

Physical properties can be analyzed using dynamic light scattering (DLS), nanoparticle tracking analysis (NTA), tunable resistive pulse sensing (TRPS), and electron microscopy (EM). DLS is an easy-to-use method that allows the analysis of very small sample volumes. However, DLS has a rather low resolution and tends to skew data toward larger particles [58,59]. NTA is a sensitive method that can readily detect particles in the size range of exosomes, but its major downside is the requirement for rather large sample volumes of around 0.5 mL [59,60]. TRPS is a technique that can assess size, concentration, and surface charge at a single-particle level. While TRPS is suitable for small-sized particles, there are many factors that have to be adjusted for the measurement, like the pore size, current, and choice of calibration particles. When it comes to EM, there are different approaches available, with the most common ones in EV research being transmission EM (TEM) and scanning EM (SEM). Comparing the two, TEM reaches higher resolutions but also needs more advanced sample preparation, as the samples have to be very thin ($\leq$1 µm) to allow the passage of electrons [61,62]. Both methods yield satisfying results for the size assessment of exosomes, but the morphological appearance can differ based on the chosen approach and respective sample preparation [63]. In the Minimal information for studies of extracellular vesicles 2018 (MISEV2018) guidelines published by the International Society of EVs, it is advised to use two complementary techniques to assess EVs at a single-particle level. This should include one image-based method, like EM, and one of the other methods for assessing physical properties [64].

For the analysis of biochemical properties, there are two main groups of methods: immunodetection-based methods and proteomics. Common immunodetection methods include Western blotting and flow cytometry. Western blotting is a quite easy-to-use method that is available in many labs. Western blotting technically allows for the detection of surface markers as well as cargoes since exosomes are lysed before analysis [65]. Unfortunately, Western blotting is highly dependent on the used antibodies when it comes to specificity and reproducibility. Additionally, it only allows for the assessment of a very limited number of proteins in one sample [59]. Flow cytometry requires a single-particle laminar flow of antibody-labeled particles. To achieve this with EVs can be difficult because they are prone to aggregation. As for exosomes, they are also too small to be detected by standard flow cytometers, which detect in a size range of 1–15 µm [66]. Therefore, they are typically bound to beads by either an antibody–antigen interaction or covalent conjugation [67]. Alternatively, the vesicle flow cytometry (VFC) approach is based on staining the vesicle membranes for size and concentration measurements. Antibody staining can give additional information about surface protein expression. To avoid misinterpretation based on aggregation, the measurement of serial dilutions of the sample is advised [68]. Whether VFC can be used for exosomes highly depends on the flow cytometer's detection limit. Flow cytometry generally allows for high-throughput analysis of exosomes and can identify different expression patterns within one sample. However, as for Western blotting, only a limited number of markers can be assessed in one sample, and the outcome might vary depending on the used antibody. As the particles remain intact, analysis is limited to surface markers. Proteomic analysis of exosomes mainly relies on mass spectrometry (MS). Beyond proteomic research, MS is also a suitable method for the analysis of lipids and metabolites, but so far, proteins remain the main focus of MS-driven exosome research [69]. The MISEV2018 guidelines suggest showing at least three positive and one negative marker for the respective EV type on a protein level using any of the aforementioned methods.

Since the 2018 update, the MISEV guidelines also recommend describing EVs quantitatively. One option would be the particle count, as analyzed by DLS, NTA, or TRPS. Other options include total protein content and total lipid content [64]. As mentioned before,

MS can quantify proteins and lipids. However, it is a rather advanced and expensive method, which is hardly used for routine isolation verification. Standard procedures for protein content measurements are colorimetric assays, for example, the Bradford assay. The readout of the Bradford assay is based on a comparison to a reference curve. Accordingly, the Bradford assay can only detect proteins within the linear range of its reference curve. Highly purified or low-concentrated EV preparations might fall outside of this range, leading to an underestimation of the protein content. Conversely, overestimation of the protein content can result from the co-precipitation of protein contaminants like albumin [64]. Other options for colorimetric protein assays include the Pierce BCA assay and the Lowry assay, which both rely on the biuret reaction and the subsequent colorimetric detection of cuprous cations. Lipid content can be measured using the colorimetric sulfo-phospho-vanillin (SPV) assay [70,71]. As for the Bradford assay, the SPV assay uses a reference curve, and lipid concentrations can only be reliably calculated within its linear range; otherwise, lipid content can be over- or underestimated. It is also not established whether lipid assays like the SPV assay can detect all EVs with the same efficacy, independent of their specific lipid composition [64]. Therefore, a conclusive interpretation of protein and lipid content data is nearly impossible, as both require stable input concentrations within the assay's linear range and differ significantly based on the exosome source and isolation method. Unfortunately, the lack of details regarding exosome production and isolation in many publications further contributes to this issue, highlighting the need for standardized procedures.

5. Exosomes in Cancer Development and Progression

Cancer progression is a multi-step process, ultimately resulting in the development of malignancy. Being part of the tumor microenvironment, exosomes have been suggested to regulate multiple different processes of tumorigenesis, such as angiogenesis, metastasis, and immune response.

5.1. Angiogenesis

As cancer cells have a high demand for oxygen and nutrients, angiogenesis is crucial for cancer progression. Angiogenesis is induced by an imbalance between anti- and pro-angiogenic factors, which is favored by hypoxic conditions [72]. Interestingly, exosome release has been found to be elevated in cells exposed to hypoxia [73]. Under hypoxic conditions, cancer cells release exosomes enriched in miR-23a, which promotes angiogenesis by targeting HIF-1α, ZO-1, and prolyl hydroxylase [74,75]. Exosomes also deliver pro-angiogenic miRNAs like miR-9, miR-92a-3p, miR-205, and miR-135b, which are involved in endothelial cell migration and tube formation [76–79]. Melanoma- and glioblastoma-cell-derived exosomes have been shown to carry pro-angiogenic factors like VEGF and IL-6 [80,81]. Exosomes from ovarian cancer cells carry increased levels of soluble E-Cadherin, which activates angiogenic signaling in endothelial cells [82]. Exosomes from nasopharyngeal cancer and myeloma are enriched in matrix metalloproteinases (MMPs) like MMP-9 and MMP-13, which are also involved in angiogenesis induction [83,84]. In head and neck squamous cell carcinoma (HNSSC), small EVs from patients with advanced-stage disease stimulated significantly increased tubulogenesis, migration, and proliferation of endothelial cells compared to those from healthy donors [85]. Upon treatment with exosomes derived from leukemia cells, endothelial cells show increased expression of vascular cell adhesion molecule 1 (VCAM-1) and intercellular adhesion molecule 1 (ICAM-1), which have been associated with neovascularization [86]. The exosomal delivery of surface tetraspanin Tspan8 has also been suggested to promote angiogenesis in colorectal cancer and adenocarcinoma [87].

In summary, exosomes play a significant role in angiogenesis by delivering pro-angiogenic factors and miRNAs, promoting endothelial cell migration, tube formation, and neovascularization in various cancer types.

5.2. Metastasis

Another major step in cancer progression is metastasis, which is responsible for 90% of tumor-related deaths [88]. In order to metastasize, tumor cells need to detach from the original tumor mass and gain migratory potential. This process involves extracellular matrix (ECM) degradation and epithelial–mesenchymal transition (EMT). As mentioned before, tumor-derived exosomes (TDEs) can carry MMPs, which mediate ECM degradation. Additionally, TDEs have been shown to carry miRNAs that promote MMP expression. For example, melanoma-derived exosomes can enhance MMP-2 and MMP-9 expression in fibroblasts through the delivery of miR-21 [89]. In a triple-negative breast cancer (TNBC) model, cancer cells released exosomes enriched in MMP-1. The ingestion of these exosomes by different TNBC cell lines leads to increased MMP-1 secretion, favoring EMT [90]. EMT is a cellular process that leads to a loss of epithelial and a gain of mesenchymal characteristics. During EMT, cells lose their apical–basal polarity, as well as cell–cell and cell–ECM adhesions [91]. There are multiple known signaling pathways that can induce EMT through EMT-promoting transcription factors (EMT-TFs). Prominent examples of EMT-TF families are SNAIL, SLUG, TWIST, and ZEB [92]. A very extensively studied EMT signaling pathway in tumor research is the Wnt/β-catenin pathway. Several Wnt ligands are delivered by TDEs, including Wnt1, Wnt4, and Wnt5a [80,93–95]. Exosomal Wnt10b delivered by fibroblast-derived exosomes induces EMT in breast cancer cells [96]. Exosomal Tenascin-C (TNC), an extracellular matrix protein, has also been shown to induce EMT in breast cancer cells through the Wnt/β-catenin signaling pathway [97]. Exosomes derived from cancer-associated fibroblasts deliver miR-34a-5p, resulting in β-catenin/SNAIL-mediated EMT induction in oral squamous cell carcinoma (OSCC) [98]. The delivery of circABCC1 by colorectal-cancer-cell-derived exosomes also induces EMT through Wnt/ß-catenin signaling [99].

In OSCC, exosomal miR-21 induces EMT, while miR-21 inhibition leads to reversed EMT and cancer stem cell (CSC) phenotype [100]. In bladder cancer, increased levels of exosomal casein kinase II α and annexin A2 were associated with EMT [101]. Another study showed that the treatment of epithelial tumor cells with exosomes from head and neck SCC patients' plasma could induce the expression of mesenchymal markers like Vimentin, N-Cadherin, SNAIL, TWIST, SLUG, and ZEB-1. This effect was lost if exosomes were isolated after patients underwent photodynamic therapy [102]. There are also reports suggesting the involvement of TDEs in pre-metastatic niche formation. Specific integrin patterns and adhesion molecules on the TDEs' surfaces lead to targeted delivery to specific cell types or organs and promote pre-metastatic niche formation [103,104]. In gastric cancer, exosomal delivery of EGFR to liver stromal cells has been associated with the upregulation of hepatocyte growth factor, which represents a binding partner for c-MET and thereby facilitates the landing of metastatic cancer cells [105]. Melanoma-derived exosomes have been shown to prime lymph nodes for metastasis by upregulating proteins involved in melanoma cell recruitment, ECM modification, and angiogenic growth factors [106].

Collectively, a substantial amount of evidence supports the role of exosomes in ECM degradation and EMT, which in turn favors metastasis.

5.3. Cancer Immunity

The immune response against malignant cells is of critical importance for the progression and invasion of the tumor. TDEs have been suggested to take part in both anti- and pro-tumor immune reactions.

The anti-tumor response is mainly based on antigen presentation on the TDEs' surfaces [107]. For example, the presentation of HSP70 on exosomes induces $CD8^+$ T-cells and activates NK cells and macrophages [108–110]. Exosomes from Rab27a-overexpressing lung cancer cells are able to promote $CD4^+$ T-cell proliferation through the activation of MHC-II, CD80, and CD86 on dendritic cells (DCs) [111]. When breast cancer cells are treated with the DNA-double-strand-break-inducing agent Topotecan, they release exosomes that reinforce anti-tumor immunity by activating DCs and $CD8^+$ T-cells [112].

However, the majority of TDEs mediate immune-inhibitory functions. It has been shown that exosomes from head and neck cancer (HNC) patients carry immunosuppressive protein cargoes and mediate suppressive effector T-cell functions [113]. For example, cancer-derived exosomes carry TGFβ and PD-L1 [114–117]. PD-L1 is an immunosuppressive ligand strongly associated with immune evasion in cancer [118]. In agreement, PD-L1-carrying small EVs block the activity of NK cells and T-cells and support apoptosis in $CD8^+$ T-cells in HNSCC [117]. Elevated levels of exosomal PD-L1 have been associated with poor patient prognosis in different cancer entities [119].

Another important immunosuppressive axis in cancer is the Fas/FasL pathway. It is considered crucial for cancer-mediated immunosuppression and T-cell apoptosis [120]. In agreement, exosomal presentation of FasL and galectin-9 has been associated with apoptosis induction in activated T-cells [121,122]. Importantly, small-EV-associated FasL levels are reduced in advanced HNSCCs, while Fas is increased for up to six months after therapy [117].

The downregulation of MHC I plays an important role in cancer immunosurveillance. It has been described in 40–90% of human tumors, often correlating with a worse prognosis [123]. Low levels of MHC-I on glioma-cell-derived exosomes are associated with the dysfunction of $CD8^+$ T-cells, while the upregulation of exosomal MHC-I restored their anti-tumor response [124].

Myeloid cells, such as macrophages, neutrophils, and DCs, strongly influence anti-cancer immune responses. TDEs can inhibit the differentiation of DCs and the function of their cytokines by delivering miR-203. EVs have also been shown to stimulate the pro-tumor activity of neutrophils and to increase their chemotaxis in melanoma [125]. Moreover, there are numerous reports on exosome-driven stimulation of macrophage polarization toward the immunosuppressive and thus cancer-promoting M2 phase [107]. For example, exosomes from SNAIL-expressing HNC cells have been found to be enriched in miR-21. Upon the uptake of the miR-21-containing exosomes by $CD14^+$ monocytes, the expression of M1 markers was suppressed, while that of M2 markers increased [126]. Exosomal delivery of tyrosine kinase with immunoglobulin and epidermal growth factor homology domains 2 (TIE2) from cervical cancer cells to macrophages leads to an M2 phenotype and promotes angiogenesis [127]. TDEs can even influence macrophage polarization in the pre-metastatic niche through TLR2 and NF-κB signaling [128]. Thus, TDEs play an important role in the regulation of anti-tumor immune responses, providing an important target that could be addressed therapeutically in order to impair tumor progression.

By delivering suppressive signals and proteins to immune cells, exosomes substantially contribute to an immunosuppressive microenvironment, ultimately resulting in tumor immune evasion.

6. Exosomes in Cancer Therapy and Treatment

Given the compelling evidence supporting the critical involvement of exosomes in the development and progression of cancer, translating this knowledge into clinical use is a current research interest. Seeing as exosomes can deliver their cargo to specific cells, exploiting them as vehicles for targeted drug or signal delivery is a promising approach. Moreover, TDEs carry distinct markers, allowing their use as biomarkers for cancer detection and therapy monitoring. An alternative treatment approach is to target TDEs to prevent disease progression.

6.1. Exosomes as Drug Carriers and Therapeutic Agents

The targeted delivery of drugs to cancer cells is one of the major challenges in cancer therapy research. A widely studied approach is the use of nanoparticles (NPs) as drug carriers, offering sustained drug release, prolonged bioavailability, an enhanced permeation and retention (EPR) effect on tumors, and few side effects. For example, in a cell spheroid model of HNSCC, the delivery of cisplatin (CDDP) by NPs was able to overcome CDDP resistance and successfully eradicate cancer cells [129]. Copper(II) bis(diethyldithiocarbamate) (CuET)

NPs successfully induced copper-dependent programmed cell death (cuproptosis) in non-small lung cancer cells and showed potent anti-tumor effects in a CDDP-resistant tumor model in vivo [130]. However, the binding of bodily proteins and biomolecules to the NPs, the so-called NP-corona, often limits the desired effects in vivo [131–133]. Exosomes can be viewed as naturally occurring NPs, which have a high bioavailability and few side effects, therefore representing a promising carrier for therapeutic drugs. Loading the respective drugs into exosomes can be achieved by modifying the donor cells to directly incorporate the drug into the exosomes. If this is not possible, purified exosomes can be loaded in vitro using electroporation, sonification, or passive diffusion [134,135]. The delivery of paclitaxel (PTX) via exosomes was shown to be more efficient than free-drug or liposome delivery in a multi-drug-resistant cancer cell model [135]. In mice, coating exosomes with different chemotherapeutics leads to a complete loss of side effects compared to free drugs while effectively inhibiting tumor growth [47]. Chemical or genetic modifications of the exosomal surface also allow for a more targeted delivery of their cargo. The conjugation of ApoA-1 mimetic peptides to lipids allows for the targeted delivery of Methotrexate-loaded exosomes to primary glioma cells [136]. Exosomes engineered to carry a peptide that readily binds to c-Met were successfully targeted to c-Met-overexpressing triple-negative breast cancer cells in vitro and in vivo, leading to increased cellular uptake and tumor apoptosis [137]. Another option for targeting exosomes is the use of antibody mimetics like affibodies. Affibodies are based on the immunoglobulin binding domain of protein A and can bind target proteins with high specificity. Surface Her2-affibody-expressing exosomes from genetically engineered HEK293T donor cells successfully deliver PTX and miR-21 to Her2-expressing colorectal cancer cells and show anti-tumor effects in mice [138]. Genetically engineered exosomes expressing a fragment of IL-3 on their surfaces effectively target IL3-receptor-overexpressing chronic myeloid leukemia cells and inhibit cell growth by delivering Imatinib or BCR-ABL siRNA [139].

Exosomes can also be used as therapeutic agents to induce immunogenic cell death (ICD). Exosomes derived from DCs are known to carry classic antigen-presenting molecules like MHC-I/II and CD1a-d, allowing them to activate the anti-tumor immune response [140]. For example, DC-derived exosomes are able to prime antigen-specific CD4 and CD8 T-cells through MHC-I/II expression and antigen presentation. There are multiple ongoing clinical trials exploring the effectivity of DC exosomes as cancer vaccines [141]. In breast cancer, synthetic multivalent antibody retargeted exosomes (SMART-Exo) have been exploited to activate and redirect T-cells to EGFR- or HER-2-expressing cancer cells by displaying the respective antibodies on their surface [142,143]. CD40-ligand-expressing exosomes from modified lung cancer cells are able to activate DCs in vitro and enhance the anti-tumor activity of T-cells in a mouse model [144]. Engineered A-lactalbumin exosomes loaded with the ICD inducers human neutrophil elastase (ELANE) and Hiltonol specifically induce ICD in breast cancer cells, which in turn leads to the activation of DCs and $CD8^+$ T-cells. ICD can also be triggered by the exosomal delivery of galectin-9 siRNA and the oxaliplatin prodrug in pancreatic ductal adenocarcinoma [145]. In some cases, inflammation can also contribute to tumor growth [146]. Exosomes have also been proposed as decoys for the proinflammatory cytokine TNFα by displaying the TNFα-binding domain of human TNF receptor-1 on their surface [147].

Exploiting exosomes as therapeutic agents is a promising approach, even beyond cancer treatment. However, most studies are still pre-clinical, and further efforts will be necessary to translate the current knowledge into clinical application.

6.2. Exosomes as Biomarkers

Recently, liquid biopsies have emerged as a minimally invasive procedure that can complement the management of cancer patients during standard therapy. Compared to tissue biopsies, liquid biopsies are lower in cost and easily performed, enabling multiple samplings during a patient's treatment [148]. Among the examined biomarkers are circulating tumor cells (CTCs), cell-free DNA, circulating RNA, and exosomes [149,150]. Exosomes

are more abundant and stable in the circulation than CTCs and nucleic acids, making them promising candidates for biomarkers [151]. In breast cancer, a correlation between the total amount of exosomal miRNA and malignancy and prognosis could be established [152]. LncRNA H19 from serum exosomes is significantly elevated in breast cancer patients compared to healthy donors, making it a promising diagnostic marker [153,154]. Exosomal miR-106b is elevated in lung cancer patients compared to healthy individuals and could be linked to cancer cell migration and lymph node metastasis [155]. Upregulation of miR-21 and miR-4257 in exosomes was associated with disease recurrence in non-small-cell lung cancer [156]. In HNSCC, exosome levels are elevated in advanced-stage tumors, with exosome amounts nearly doubling with disease progression [113,157]. One study showed that a high expression of the mesenchymal markers N-cadherin and TGF-β1 on plasma-derived exosomes of HNSCC patients is associated with increased tumor proliferation, migration, and invasion. After photodynamic therapy, they observed a shift to epithelial markers [102]. In a study surveilling HNSCC patients receiving a combination treatment with cetuximab, ipilimumab, and radiation, patients with recurrent disease showed increased levels of total exosome proteins, total exosome ratio, and total $CD3^+$, $CD3^-PD\text{-}L1^+$, and $CD3^+15s^+$ exosomes compared to patients who remained disease-free [158]. Overexpression of EGFR is a common occurrence in HNSCC, which is also reflected in exosomes [150]. Others have shown that exosomal EGFR and pEGFR are reduced in HNSCC patients after cetuximab treatment, allowing for treatment monitoring [159]. In laryngeal SCC, serum exosomal miR-21 and homeobox transcript antisense RNA (HOTAIR) could be associated with disease progression. Patients with lymph node metastasis showed increased levels of exosomal miR-21 and HOTAIR [160]. In patients with stage III colorectal cancer, levels of exosomal 20S proteasome and $MMP9^+$ subpopulations were associated with unfavorable prognostic factors for overall survival [161]. In colon cancer, the lipid profiling of exosomes revealed the molecular species PE 34:2, PE 36:2, pPE 16:0/20:4, and Cer d18:1/24:1 as possible markers for metastasis [162].

Exosomes represent a promising diagnostic and prognostic tool for a variety of different cancer entities and thus have the potential to change the management of cancer patients in the future. However, the lack of standardized isolation methods is hindering the integration of exosomal biomarkers into the clinical routine [163].

6.3. Exosomes as Therapy Targets

Since exosomes have been shown to play a role in multiple steps of cancer progression, they are also interesting targets for therapy. GW4869 is a potent inhibitor of the membrane neutral sphingomyelinase (nSMase), an enzyme that hydrolyzes sphingomyelins and thereby generates ceramides. SMase is found in different cellular compartments, including the Golgi apparatus, endosomes, and the plasma membrane. GW4869-induced Smase inhibition has been shown to also potently inhibit exosome release [164]. GW4869-mediated inhibition of exosome release from cancer-associated fibroblasts can reduce the chemoresistance transfer and thus the survival of pancreatic cancer cells. The combination treatment of gemcitabine and GW4869 also led to reduced tumor growth in a mouse model [165]. Treatment with a CD44-targeting nanounit composed of GW4869 and the ferroptosis inducer FE^{3+} induced an anti-tumor immune response to melanoma cells in mice, while no cytotoxic effects of GW4869 could be observed in vitro [166]. Transfection of pancreatic cancer cells with siRAB27B can also reduce exosome release, resulting in a significant decrease in miR-155-induced gemcitabine resistance [167]. Targeting RAB27A with siRNA led to reduced tumor growth and metastasis in mouse models [168,169]. The blood-pressure-lowering drug dimethyl amiloride has been shown to reduce endocytic recycling and, in turn, also exosome release. Treatment with amiloride can reduce tumor growth in mice by preventing the exosomal delivery of HSP72 to myeloid-derived suppressor cells and increase cyclophosphamide-based chemotherapy efficacy [170]. Inhibition of exosome uptake is another possible route to target exosomes for therapy. Enzymatic depletion of cell surface HSPG has been shown to effectively attenuate exosome uptake [171]. Annexin V

binds to and blocks surface phosphatidylserine, which is important for membrane adhesion and exosome uptake. Treatment with annexin V was shown to reduce the growth rate and metastatic potential of human glioma xenografts in mice [172].

While there is evidence supporting the exploitation of inhibiting exosome release and uptake as a novel therapeutic approach, further in vivo studies will be necessary to explore the systemic effects of such inhibitors. Assuming that interference with Smase activity and phosphatidylserine adhesion is likely to disrupt other cellular processes, achieving the precisely targeted delivery of inhibitors will be crucial.

7. Exosomes in Transmitting Therapy Resistance

The choice of a suitable treatment regimen is highly dependent on the cancer entity, progression stage, and metastasis stage of the tumor. Generally, treatment options include surgical resection, radiotherapy, and systemic therapy, with the ladder including chemotherapy and immunotherapy. Different approaches are often combined to achieve the best possible outcome for the patient. While surgical removal remains a standard procedure for many solid tumors, it is not always an option, depending on the affected anatomical site, and there are also reports suggesting that surgery-induced trauma increases metastasis and recurrence [173]. Non-surgical treatment options are mainly focused on triggering programmed cell death (PD) in cancer cells by inducing cellular stress and DNA damage or enhancing immune surveillance mechanisms [174]. Unfortunately, primary or acquired therapy resistance is a common occurrence, contributing to the nearly 10 million cancer deaths worldwide in 2020 [175]. As intercellular messengers of the TME, exosomes have been suggested to contribute to the development and transfer of therapy resistance in cancer.

7.1. Chemotherapy

The primary goal of chemotherapy is to inhibit tumor cell proliferation and, in turn, prevent invasion and metastasis. Unfortunately, resistance to chemotherapeutic agents is common, accounting for 90% of deaths in patients with metastatic tumors [176]. There are two main routes by which cells achieve chemoresistance: a reduction in the intracellular active drug concentration and the evasion of apoptosis. The intracellular active drug concentration is influenced by drug influx, which depends on transporter expression and membrane constitution, as well as active drug export and intracellular drug detoxification. The evasion of apoptosis is achieved by upregulating pro-survival genes and increasing DNA damage repair activity [177]. Exosomes can contribute to the transmission of chemoresistance mechanisms by delivering functional proteins and miRNAs to neighboring cells and contributing to active drug export from their cell of origin (Figure 3A).

Generally, exosome biogenesis is accelerated by treatment with chemotherapeutic drugs [178,179]. There is evidence that drug export via exosomes contributes to resistance in different cancer entities. In ovarian cancer, exosomes from CDDP-resistant cells were shown to incorporate two-fold more CDDP than those from sensitive cells [180]. In adriamycin (ADM)-resistant breast cancer cells, ADM did not accumulate in the nuclei as expected but instead was exported in exosomes [181]. A similar mechanism was observed in gemcitabine-resistant pancreatic cancer cells [182].

Exosomes can also facilitate the horizontal transfer of proteins. Functional drug exporters like P-gp, multi-drug-resistance-associated proteins (MRPs), and ABC transporters ABCA-3 and ABCG-2 have been found in exosomes [7]. Exosomal delivery of P-gp was shown to transfer a chemoresistant phenotype in breast cancer cells [183,184]. Notably, P-gp functionality could be detected as early as two hours after transfer [185]. Docetaxel-resistant prostate-cancer-cell-derived exosomes show elevated levels of P-gp compared to those from sensitive cells. Likewise, exosomes isolated from patients with docetaxel-resistant pancreatic cancer showed higher P-gp levels than those from therapy-naïve patients [186]. Exosomal transfer of MRP-1 and ABCA-3 could confer a chemoresistant phenotype to leukemia cells [187,188]. Exosomes from CDDP-resistant ovarian cancer cells have been

shown to carry elevated levels of the drug exporters MRP2, ATP7A, and ATP7B [180]. Mesenchymal stem cell (MSC)-derived exosomes could be shown to prevent 5-fluorouracil (5-FU)-induced apoptosis by activating the CaM-Ks/Raf/MEK/ERK pathway and stimulating the expression of MRPs in a gastric cancer mouse model [189].

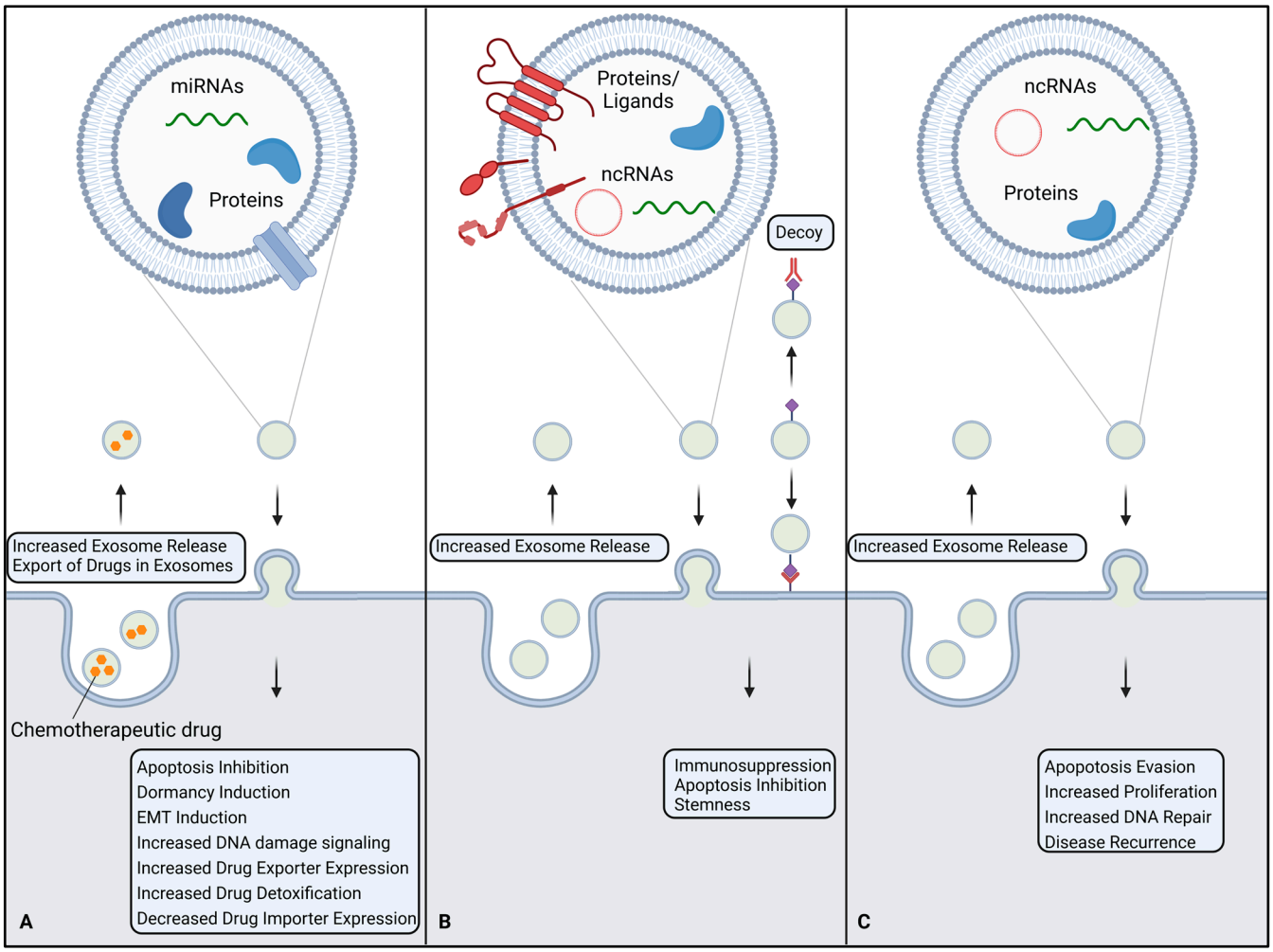

Figure 3. Schematic overview of exosome-related mechanism contributing to therapy resistance. (**A**) Increased release of exosomes and export of active drug within exosomes facilitates chemotherapy resistance. Resistant cells can transfer their resistant phenotype to naïve cells via exosomal delivery of proteins and miRNAs. Upon uptake, this cargo can induce different cellular responses related to chemotherapy resistance. (**B**) Immunotherapy-resistant cells also show an increased release of exosomes. These exosomes can function as decoys for immunotherapeutic drugs or facilitate receptor–ligand signaling that increases therapy resistance. Uptake of exosomes shed by resistant cells can also induce immunotherapy resistance by delivering ncRNAs and proteins. (**C**) Radiotherapy-resistant cells also show an increased amount of exosome release. These exosomes contain ncRNAs and proteins that trigger resistance mechanisms if taken up by naïve cells. Created with BioRender.com.

Exosomes have also been shown to carry pro-survival proteins like survivin and HSPs. Treatment of hepatocellular carcinoma cells with CDDP or Carboplatin increased the exosomal export of HSPs 60, 70, and 90 [179]. High exosomal survivin levels could be associated with relapse after chemotherapy in prostate cancer patients [190]. PTX-resistant breast-cancer-cell-derived exosomes have also been found to contain increased levels of survivin, leading to apoptosis evasion and resistance transfer [191]. Exosomes isolated from hepatitis-B-associated liver cancer cells increased the expression of Lamp2a and, in turn, increased apoptosis evasion and oxaliplatin resistance in naïve liver cancer

cells. However, the details of the underlying mechanism remain unclear [192]. Exosomal transfer of HSP90 from PTX-resistant breast cancer cells to sensitive cells increases their PTX resistance through the degradation of p53. HSP90 was also found to be upregulated in plasma exosomes from patients showing PTX resistance [193].

Among other proteins that are transferred via exosomes is the microsomal triglyceride transfer protein (MTTP), which inhibits ferroptosis and induces resistance to oxaliplatin in colorectal cancer. MTTP levels were found to be increased in the plasma exosomes of colorectal cancer patients with a high body fat ratio, correlating with a poor therapy response [194]. In an esophageal SCC cell model, exosomes from PTX-resistant cells showed higher levels of PD 1 ligand 1 (PDL-1) than those from sensitive cells. Exosomal PDL-1 could transfer the resistant phenotype, putatively by regulating the STAT3/miR-21/PTEN/Akt axis [195]. In an ADM-resistant breast cancer cell model, exosomes transferred resistance via UCH-L1. High levels of UCH-L1 in patient exosomes before therapy onset could be associated with a poor prognosis [181]. Exosomal delivery of CD44 could transfer doxorubicin resistance in a breast cancer cell model. Likewise, exosomal CD44 in the serum of non-responders was significantly higher than in chemotherapy-responsive patients [196]. Exosomes from nasopharyngeal cancer cells treated with CDDP show increased levels of ER-resident protein 44 (ERp44), which enhances the resistant phenotype in recipient cells. The incorporation of ERp44 in exosomes is likely caused by CDDP-induced ER stress [197].

Another mode of resistance transfer via exosomes is the delivery of miRNAs. MiR-21 is one of the most studied oncogenic miRNAs and has been found to play a role in various cancer entities, including glioma, liver cancer, colorectal cancer, prostate cancer, breast cancer, ovarian cancer, and bladder cancer [198]. In oral SCC, exosomal miR-21 was indicated in CDDP resistance transfer by targeting DNA damage signaling [199]. The level of miR-21 is significantly increased in exosomes derived from CDDP-resistant esophageal cancer cells compared to those from sensitive esophageal cancer cells or healthy esophageal cells. Exosomes were also able to transfer the resistant phenotype through miR-21-mediated downregulation of PDCD4 [200]. CDDP-resistant liver cells release exosomes with increased levels of miR-643, which has been shown to transfer resistance to recipient cells by targeting APOL6 and inhibiting apoptosis [201]. In breast cancer cells, Tamoxifen resistance could be transferred to sensitive cells via exosomal miR-221/222 delivery [202]. Exosomal miR-222/223 was shown to induce cancer cell dormancy and subsequent Carboplatin resistance in breast cancer in vitro and in vivo [203]. In another breast cancer model, exosomal miR-451 and miR-326 transferred a P-gp-overexpressing phenotype from donor to recipient cells [204]. When analyzing breast cancer patient exosomes from serum before and after chemotherapy with doxorubicin and paclitaxel, miR-378a-3p and miR-378d could be correlated with therapy resistance. In vitro experiments further revealed that exosomal transfer of miR-378a-3p and miR-378d induced chemoresistance [205]. Exosomes derived from doxorubicin-resistant gastric cancer cells are enriched in miR-501, which can transfer the resistant phenotype to sensitive cells [206]. MiR-196a-3p, which is thought to target the gemcitabine importer hENT1, is upregulated in the exosomes of pancreatic cancer cell lines and in the serum exosomes of patients [207]. Gemcitabine treatment of pancreatic cancer cells can lead to increased amounts of exosomal miR-155, which can induce resistance in recipient cells [167]. Exosomal miR-155-5p has also been associated with EMT induction and the transfer of paclitaxel resistance in gastric cancer cells [208]. Prostate cancer tissue treated with CDDP, doxorubicin, and docetaxel shows increased levels of exosomal miR-27a, which induces chemoresistance by targeting p53. In vitro experiments were able to show that primary prostate fibroblasts co-cultured with cancer cells are a vital source of miR-27a-carrying exosomes [209]. Some miRNAs are also reduced in exosomes upon chemotherapeutic treatment. The miR-30a level is decreased in CDDP-resistant oral SCC cells. Accordingly, exosomal miR-30a was found to be significantly reduced in the serum of oral SCC patients after CDDP treatment, especially those showing recurrent disease [210]. In non-small-cell lung cancer, a reduction in exosomal miR-1273a was found to induce CDDP resistance by increasing Syndecan-binding protein (SDCBP) levels in recipient cells.

Patients receiving platinum-based therapy showing decreased plasma exosomal miR-1273a and increased plasma SDCBP levels experienced worse therapeutic outcomes [211]. Research into exosomal miRNAs and other ncRNAs is a growing field, with novel oncogenic and chemoresistance-related candidates emerging continuously.

While there is a lot of evidence for a pivotal role of exosomes in chemoresistance transfer from in vitro experiments, only a limited number of studies providing in vivo data are available. Conditions in the TME differ significantly from those in vitro, potentially leading to divergent kinetics of exosomal resistance transfer in vivo [7].

Interestingly, some studies also suggest exosomes as enhancers of chemosensitivity. Mesenchymal-stem-cell-derived (MSC) exosomes have been implicated in reversing resistance to taxanes, such as docetaxel, in ovarian cancer by delivering miR-146a [212]. Exosomal miR-451a can inhibit EMT in hepatocellular carcinoma cells, resulting in increased PTX sensitivity [213]. Adipose MSCs release exosomes carrying miR-1236, which increases CDDP sensitivity through SLC9A1 downregulation in breast cancer cells [214].

7.2. Immunotherapy and Targeted Therapy

Ideally, the cells of the immune system recognize and eliminate aberrant cells like cancer cells, thus preventing tumor growth. Unfortunately, cancer cells have evolved different immune-evasive and -suppressive mechanisms to bypass these natural defenses. The aim of immunotherapy is to stimulate the immune response to eradicate cancer cells more effectively. There are different approaches available, including immune checkpoint inhibitors (ICI), cancer vaccines, or adoptive cell transfer. Given their role in cancer immunity, exosomes also contribute to immunotherapy resistance (Figure 3B).

Treatment with immunotherapeutic drugs can increase the number of secreted exosomes and alter their molecular profile [215]. For example, treatment of colorectal cancer cells with cetuximab leads to the release of exosomes with an increased abundance of miRNAs and proteins activating proliferation and inflammation, while those related to immune suppression are reduced [216].

The only FDA-approved ICIs target PD-1, PD-L1, or cytotoxic T-lymphocyte-associated antigen-4 (CTLA-4), all of which are negative regulators of T-cell immune function. CTLA-4 competes with the co-stimulatory CD28 for its ligands CD80 and CD86. Exosomal miR-424 from colorectal cancer cells can inhibit the CD28-CD80/86 pathway, leading to ICI resistance [217]. PD-L1 expression has been found in and on TDEs from different entities [218]. In metastatic melanoma patients, exosomes were found to carry increased levels of PD-L1, contributing to T-cell suppression. The study suggests that high levels of exosomal PD-L1 reflect T-cell exhaustion, rendering anti-PD-1 treatment with Pembrolizumab futile [116]. Exosomal PD-L1 expression can also circumvent anti-PD-L1 treatment. Exosomal PD-L1 can bind to PD-1 on T-cells regardless of PD-L1 inhibition on the tumor cells. Alternatively, PD-L1-expressing exosomes can bind to the respective inhibitor and thus function as a decoy. Both mechanisms are possible explanations for the continuing immunosuppression despite ICI treatment [219].

Currently, there are three therapeutic cancer vaccines and seven adoptive cell transfer treatments approved by the FDA, although the distinction between the two categories is somewhat blurry [220,221]. So far, there is little knowledge about the role of exosomes in these innovative treatment approaches. For example, one study found that EVs expressing CD19 can be used to boost the expansion and efficacy of chimeric-antigen-receptor-modified (CAR) T-cells in vitro and in vivo [222].

Targeted therapy is mostly based on small molecules and monoclonal antibodies. Monoclonal antibodies can block vital cellular processes or help immune cells to recognize and subsequently eliminate cancer cells, leaving them at the intersection of immunotherapy. They are designed to target antigens that are specific to cancer cells. HER-2-positive exosomes from cell culture and breast cancer patients have been shown to express active full-length HER-2 and bind to Trastuzumab, inhibiting its activity [223]. A similar mechanism was observed in B-cell lymphoma, where CD20-expressing exosomes function as a decoy for

Rituximab [224,225]. In a colon cancer model, exosomes could transfer cetuximab resistance to sensitive cells by downregulating PTEN and increasing p-Akt levels [226]. Another study found that exosomes released from MDR colorectal cancer cells increased PD-L1 and Sox2 expression in recipient cells via PI3K/AKT activation and led to the expression of stem-cell-associated markers, resulting in cetuximab resistance [227]. Bevacizumab-resistant colorectal cancer cells and their respective exosomes carry increased levels of the lncRNA SNHG11. SNHG11 increases MRP1 expression via downregulation of miR-1207-5p, resulting in Bevacizumab resistance [228].

Most small molecules used in targeted therapy are protein-kinase inhibitors, thus interfering with cell proliferation signaling. Imatinib-resistant gastrointestinal stromal tumors show an overexpression of Rab25, which leads to the increased release of exosomes. These exosomes have been shown to transfer the resistant phenotype to sensitive cells [229]. Exosomes from Imatinib-resistant chronic myeloid leukemia cells carry elevated levels of IFITM3, CD146, and CD36 and can increase Imatinib tolerance in recipient cells [230]. Exosomes released from lung cancer cells treated with Osimertinib can transfer wildtype EGFR to recipient EGFR-mutated cells, increasing their Osimertinib resistance [231]. Another study found the exosomal transfer of miR-210-3p to be involved in Osimertinib resistance transmission [232]. Exosomal delivery of mir-21 was associated with Gefitinib resistance in lung cancer cells [233]. Another study found that exosomal miR-564 and miR-658 derived from Gefitinib-resistant lung cancer cells can induce resistance in recipient cells [234]. Treatment of melanoma cells with Vemurafenib can enhance miR-211-5p expression in cells and exosomes, allowing for resistance transfer [235]. Another study found circRNA hsa_circ_0001005 to be elevated in Vemurafenib-resistant cells and their respective exosomes. In recipient cells, hsa_circ_0001005 functions as a miRNA sponge, thereby activating canonical pathways related to drug resistance [236].

In summary, more detailed research is needed investigating the effect of exosomes on the outcomes of immune- and targeted therapies. However, given the involvement of exosomes in numerous immunological processes, it is likely that exosomes also contribute to the success or failure of these immunotherapies.

7.3. Radiotherapy

Radiotherapy uses ionizing radiation to damage or kill cancer cells locally. Radiation elicits its toxic effects through the direct damage of hit molecules or indirect effects, mostly due to the ionization of the water contained in the cell plasm, which leads to fission products and radicals with oxidative properties. Both direct and indirect effects induce DNA damage and subsequent cell cycle arrest or cell death. Radiotherapy can be applied with curative intent or as adjuvant or palliative treatment. It is often combined with chemotherapy or surgery [237].

As for chemo- and immunotherapy, radiotherapy also increases the general number of exosomes that are secreted. In non-human primates, the number of plasma-derived exosomes per µL was elevated after irradiation [238]. Breast cancer cells have been shown to release increased amounts of exosomes after irradiation in a dose-dependent manner [239]. A possible explanation is the stress-induced activation of p53, which has been proposed as a regulator of exosome biogenesis in a TSAP6-dependent manner [240,241].

There is also evidence suggesting the role of exosomes in the resistance of cancer cells to radiotherapy (Figure 3C). In lung cancer cells, irradiation leads to increased levels of exosomal miR-208a, which decreases apoptosis and increases proliferation in recipient cells, leading to a radioresistant phenotype [242]. Pancreatic cancer cells dying from irradiation release exosomes carrying miR-194-5p, which induces G1/S arrest and enhances the DNA damage response, promoting the survival of tumor-repopulating cells [243]. Irradiated glioma cells secrete exosomes with elevated levels of miR-889, Notch, and JAK-STAT, favoring the proliferation of recipient cells, while the levels of tumor-suppressive miR-516 and miR-365 are decreased [244]. Exosomal miR-208a from irradiated cells increased the proliferation and radioresistance of lung cancer cells by targeting p21 and the AKT/mTOR

pathway [242]. Radiotherapy-resistant colorectal cancer cells and their respective exosomes show elevated levels of miR-19b. Transfer of miR-19b to naïve cells via exosomes leads to a reduction in apoptosis and an increase in 3D spheroid formation ability, indicating radioresistance and stemness properties [245]. The abundance of the circular RNA circMYC was found to be increased in exosomes from nasopharyngeal cancer and could be associated with disease recurrence. In vitro experiments revealed that the overexpression of circMYC increases resistance to radiotherapy and promotes proliferation, while its knockdown has the opposite effects [246]. Low-dose radiotherapy of glioblastoma cells induces high levels of circMETRN in exosomes, which increases the radioresistance of recipient cells via miR-4709-3p/GRB14/PDGFRα signaling [247]. Using HNSCC cells, one study found 472 proteins that were differentially expressed in exosomes after irradiation. These proteins were mainly involved in the radiation response, radical oxygen species metabolism, DNA repair, chromatin packaging, and protein folding [248]. Exosomes from irradiated cervical cancer cells incorporate increased levels of survivin, promoting recurrence after therapy [249]. Exosomes from LMP1-expressing nasopharyngeal cancer cells can transfer a resistant phenotype to recipient cells via P38 MAPK signaling [250]. In an HNSCC cell model, exosomes from irradiated cells increased DNA double-strand break repair in recipient cells, leading to a higher irradiation tolerance [251]. In rectal cancer, exosomal proteins C8G, CFHR3, and SerpinF2 were elevated in patients with a good response to radiotherapy. The same study found that the exosomal metabolite 1,4-Dithiothreitol is elevated in poor responders, proposing exosomes as possible biomarkers for radiotherapy efficiency in rectal cancer [252]. In human and canine breast cancer cell models, radiotherapy-resistant cells could transfer their resistance to naïve cells via exosomes and additionally increase their resistance to chemotherapy with doxorubicin. The same study also showed that pre-incubation with exosomes derived from radiotherapy resistance increases the 3D-spheroid-forming ability of recipient cells [253]. Glioblastoma cells treated with exosomes from irradiated cells show increased motility [254]. This could explain the local and distant spreading of tumors often observed after radiotherapy [255]. Another major hurdle in radiotherapy is hypoxia, as oxygen is needed to produce free radicals through ionization. Tumors typically contain hypoxic regions distributed throughout the whole tumor mass [256]. As previously mentioned, exosome release is increased under hypoxic conditions [73]. In esophageal SCC cells, hypoxic exosomes were found to be enriched in miR-340-5p, which accelerated DNA damage repair and induced radioresistance in normoxic cells [256].

Another challenge in radiotherapy is the radiotherapy-induced bystander effects (RIBEs), which describe damaging effects on neighboring cells that have not been directly exposed to radiation but received damaging signals through cell–cell communication with affected cells. Exosomes contribute to this intercellular communication and can induce RIBEs. Exosomes from irradiated keratinocytes lead to increased ROS production and cell death in naïve cells [257]. Irradiated fibroblasts release exosomes enriched in miR-21, which induces the formation of micronuclei and enhances DNA damage in bystander cells [258]. Similar effects were observed in keratinocytes [259]. Exosomal miR-1246 from irradiated bronchial epithelial cells also induces micronuclei formation and DNA damage in bystander cells, inhibiting their proliferation [260]. Exosomes from irradiated bronchial epithelial cells can transfer miRNA-7-5p to non-irradiated cells to induce autophagy via the EGFR/Akt/mTOR axis [261]. One study using breast cancer cells showed that even bystander cells that experienced RIBE can transfer the effects further onto naïve cells via exosomes [262].

Radiation therapy can also cause radiation burns. Depending on the dose of radiation, the effects can range from rather benign erythema to chronic non-healing ulcers and fibrosis. A key factor in healing burn wounds is mesenchymal stem cells (MSCs) [263]. MSC-derived exosomes exert immunomodulatory functions, regulating immune cell function and cytokine release [264]. For example, the release of exosomes enriched in miR-146 and miR-34 from MSCs induces M2-like macrophages [265]. MSC-derived exosomes carrying

miR-135a promote epithelial cell migration to the burn site [266]. Exosomes from MSCs can also reduce EMT and thus inhibit fibrosis [267].

In conclusion, not only do exosomes contribute to radiotherapy resistance by increasing DNA damage repair and delivering pro-survival signals, counteracting the toxic effects of radiation, but they can also lead to unwanted RIBE. But on the contrary, exosomes derived from MSCs can also facilitate healing and regeneration of radiotherapy-induced burn wounds.

8. Conclusions and Future Directions

Exosomes are important intercellular messengers, delivering complex cargoes that alter the recipient cells' fate. As such, they also have a pivotal impact on cancer development and progression. There is already a large body of evidence suggesting the involvement of exosomes in cancer progression, metastasis, and therapy response, with new mechanisms emerging continuously. Since therapy response and the development of resistance are still major concerns in cancer treatment, discovering the underlying mechanisms is of critical importance. Exosomes have been shown to transfer drug exporters and pro-survival signals from therapy-resistant to sensitive cells, leading to a reduction in apoptosis and increased survival. There is also a vast amount of evidence that exosomal delivery of miRNAs and other ncRNAs is involved in the evasion of apoptosis, resulting in resistance to chemo-, immuno-, and radiotherapies. Regarding the fact that the majority of studies are focusing on RNAs, further research is urgently needed to clarify the potential functions of other exosomal cargoes, such as membrane and soluble proteins, metabolites, and DNA, in therapy resistance. In chemotherapy, the export of the active drug via exosomes also offers a resistance mechanism, while in immunotherapy, exosomal surface proteins can serve as decoys for drugs, decreasing their efficiency. In radiotherapy, exosomes are not only involved in resistance transfer but also contribute to radiotherapy-induced bystander effects (RIBEs), resulting in unwanted adverse effects on surrounding healthy tissue. On the other hand, exosomes have also been implicated in sensitizing cells to chemotherapy and aiding regeneration in radiotherapy-induced burns.

One of the main goals for future research is to make use of these discoveries to improve the clinical management of cancer patients (Figure 4). While numerous potential applications of exosomes for clinical implementation have already been proposed, including their use as biomarkers for cancer disease in general, as well as for potential drug resistance, as drug carriers, and even as therapy targets, their integration into standard practice is still very limited. This can be attributed to the lack of easy-to-use, standardized isolation and analysis protocols and the rather small amount of in vivo data compared to in vitro studies. Translating the current knowledge about exosomes in cancer progression and therapy response into clinical practice will be the aim of future research. Therefore, there is a high need for (observational) clinical studies evaluating the prognostic power of concurrent exosome analysis during standard cancer treatment (Figure 4B). We suggest that focusing on the development of standardized and potentially automated isolation methods will aid in the successful integration of exosomes as biomarkers into clinical use. Exploiting exosomes as targeted drug carriers is another promising approach, given their high biocompatibility. Further research into the in vivo application of such exosome-based drugs will pave the way for their clinical integration. Analyzing and comparing the biodistribution of heterologous and autologous exosomes will be a pivotal step in this regard. A rather new therapeutic approach is targeting cancer-associated exosomes by inhibiting their release or uptake and, in turn, their cancer- and therapy-resistance-promoting effects. Whether such inhibition can be integrated into clinical practice remains to be elucidated, as it has the potential to interfere with numerous physiological processes in vivo. However, the evidence supporting exosomal involvement in several steps of cancer progression and the transfer of resistant phenotypes renders these vesicles an attractive target to be investigated in depth in future clinical research.

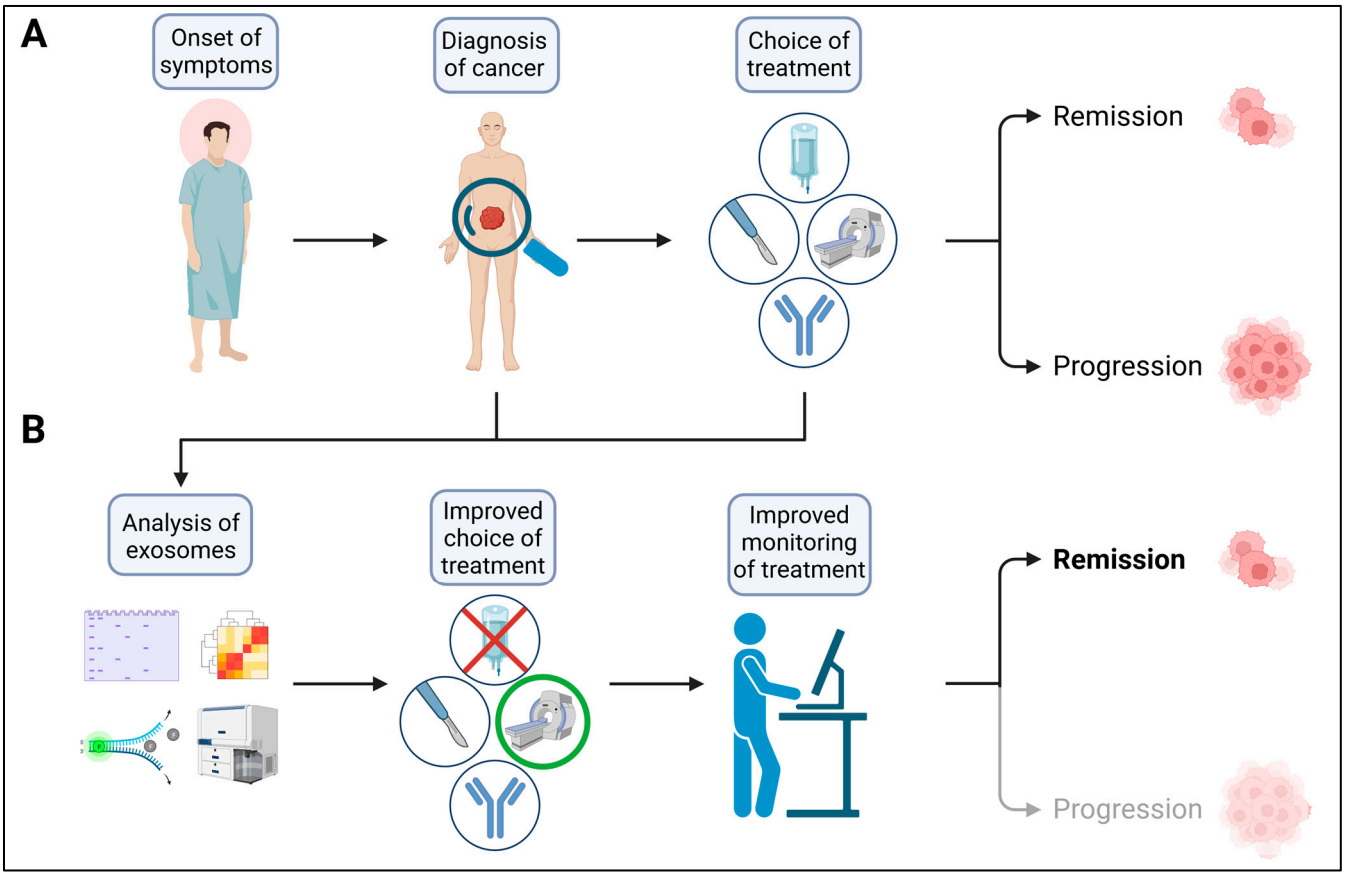

Figure 4. Clinical use of exosomes. (**A**) After the diagnosis of cancer, an appropriate treatment strategy (surgery, chemotherapy, radiotherapy, immunotherapy, or a combination) is chosen based on the clinical gold standard. (**B**) Concurrent and recurrent analyses of exosomes allow treatment choices to be optimized and closely monitored, resulting in higher chances of remission and improved patient survival. Created with BioRender.com.

Author Contributions: Conceptualization, M.W., R.H.S., J.J. and D.G.; writing—original draft preparation, M.W. and D.G.; writing—review and editing, M.W., R.H.S., J.J. and D.G.; visualization, M.W. and D.G.; supervision, R.H.S. and D.G. All authors have read and agreed to the published version of the manuscript.

Funding: This research was funded by the German Research Foundation (DFG), grant number JA 2461/5-1 to JJ, and the Brigitte und Konstanze Wegener Stiftung (project #90).

Institutional Review Board Statement: Not applicable.

Informed Consent Statement: Not applicable.

Data Availability Statement: Not applicable.

Acknowledgments: Figures were created with BioRender.com.

Conflicts of Interest: The authors declare no conflict of interest.

References

1. Pan, B.T.; Johnstone, R.M. Fate of the transferrin receptor during maturation of sheep reticulocytes in vitro: Selective externalization of the receptor. *Cell* **1983**, *33*, 967–978. [CrossRef] [PubMed]
2. Harding, C.; Heuser, J.; Stahl, P. Receptor-mediated endocytosis of transferrin and recycling of the transferrin receptor in rat reticulocytes. *J. Cell Biol.* **1983**, *97*, 329–339. [CrossRef] [PubMed]
3. Valadi, H.; Ekstrom, K.; Bossios, A.; Sjostrand, M.; Lee, J.J.; Lotvall, J.O. Exosome-mediated transfer of mRNAs and microRNAs is a novel mechanism of genetic exchange between cells. *Nat. Cell Biol.* **2007**, *9*, 654–659. [CrossRef] [PubMed]

4. Waldenstrom, A.; Genneback, N.; Hellman, U.; Ronquist, G. Cardiomyocyte microvesicles contain DNA/RNA and convey biological messages to target cells. *PLoS ONE* **2012**, *7*, e34653. [CrossRef]
5. Harmati, M.; Bukva, M.; Boroczky, T.; Buzas, K.; Gyukity-Sebestyen, E. The role of the metabolite cargo of extracellular vesicles in tumor progression. *Cancer Metastasis Rev.* **2021**, *40*, 1203–1221. [CrossRef]
6. Yang, X.; Zhang, Y.; Zhang, Y.; Zhang, S.; Qiu, L.; Zhuang, Z.; Wei, M.; Deng, X.; Wang, Z.; Han, J. The Key Role of Exosomes on the Pre-metastatic Niche Formation in Tumors. *Front. Mol. Biosci.* **2021**, *8*, 703640. [CrossRef]
7. Sharma, A. Chemoresistance in cancer cells: Exosomes as potential regulators of therapeutic tumor heterogeneity. *Nanomedicine* **2017**, *12*, 2137–2148. [CrossRef]
8. Gurung, S.; Perocheau, D.; Touramanidou, L.; Baruteau, J. The exosome journey: From biogenesis to uptake and intracellular signalling. *Cell Commun. Signal.* **2021**, *19*, 47. [CrossRef]
9. Suresh Mathivanan, R.J.S. ExoCarta. Available online: exocarta.org (accessed on 3 July 2023).
10. Vlassov, A.V.; Magdaleno, S.; Setterquist, R.; Conrad, R. Exosomes: Current knowledge of their composition, biological functions, and diagnostic and therapeutic potentials. *Biochim. Biophys. Acta* **2012**, *1820*, 940–948. [CrossRef]
11. Huang, X.; Yuan, T.; Tschannen, M.; Sun, Z.; Jacob, H.; Du, M.; Liang, M.; Dittmar, R.L.; Liu, Y.; Liang, M.; et al. Characterization of human plasma-derived exosomal RNAs by deep sequencing. *BMC Genom.* **2013**, *14*, 319. [CrossRef]
12. Fernando, M.R.; Jiang, C.; Krzyzanowski, G.D.; Ryan, W.L. New evidence that a large proportion of human blood plasma cell-free DNA is localized in exosomes. *PLoS ONE* **2017**, *12*, e0183915. [CrossRef]
13. Elzanowska, J.; Semira, C.; Costa-Silva, B. DNA in extracellular vesicles: Biological and clinical aspects. *Mol. Oncol.* **2021**, *15*, 1701–1714. [CrossRef]
14. Wei, H.; Chen, Q.; Lin, L.; Sha, C.; Li, T.; Liu, Y.; Yin, X.; Xu, Y.; Chen, L.; Gao, W.; et al. Regulation of exosome production and cargo sorting. *Int. J. Biol. Sci.* **2021**, *17*, 163–177. [CrossRef]
15. Zhang, Y.; Liu, Y.; Liu, H.; Tang, W.H. Exosomes: Biogenesis, biologic function and clinical potential. *Cell Biosci.* **2019**, *9*, 19. [CrossRef] [PubMed]
16. Doherty, G.J.; McMahon, H.T. Mechanisms of endocytosis. *Annu. Rev. Biochem.* **2009**, *78*, 857–902. [CrossRef] [PubMed]
17. Huotari, J.; Helenius, A. Endosome maturation. *EMBO J.* **2011**, *30*, 3481–3500. [CrossRef] [PubMed]
18. Minciacchi, V.R.; Freeman, M.R.; Di Vizio, D. Extracellular vesicles in cancer: Exosomes, microvesicles and the emerging role of large oncosomes. *Semin. Cell Dev. Biol.* **2015**, *40*, 41–51. [CrossRef]
19. Henne, W.M.; Buchkovich, N.J.; Emr, S.D. The ESCRT pathway. *Dev. Cell* **2011**, *21*, 77–91. [CrossRef]
20. Airola, M.V.; Hannun, Y.A. Sphingolipid metabolism and neutral sphingomyelinases. *Handb. Exp. Pharmacol.* **2013**, *215*, 57–76. [CrossRef]
21. Castro, B.M.; Prieto, M.; Silva, L.C. Ceramide: A simple sphingolipid with unique biophysical properties. *Prog. Lipid Res.* **2014**, *54*, 53–67. [CrossRef]
22. Perez-Hernandez, D.; Gutierrez-Vazquez, C.; Jorge, I.; Lopez-Martin, S.; Ursa, A.; Sanchez-Madrid, F.; Vazquez, J.; Yanez-Mo, M. The intracellular interactome of tetraspanin-enriched microdomains reveals their function as sorting machineries toward exosomes. *J. Biol. Chem.* **2013**, *288*, 11649–11661. [CrossRef] [PubMed]
23. Buratta, S.; Tancini, B.; Sagini, K.; Delo, F.; Chiaradia, E.; Urbanelli, L.; Emiliani, C. Lysosomal Exocytosis, Exosome Release and Secretory Autophagy: The Autophagic- and Endo-Lysosomal Systems Go Extracellular. *Int. J. Mol. Sci.* **2020**, *21*, 2576. [CrossRef] [PubMed]
24. Booth, A.M.; Fang, Y.; Fallon, J.K.; Yang, J.M.; Hildreth, J.E.; Gould, S.J. Exosomes and HIV Gag bud from endosome-like domains of the T cell plasma membrane. *J. Cell Biol.* **2006**, *172*, 923–935. [CrossRef] [PubMed]
25. Fang, Y.; Wu, N.; Gan, X.; Yan, W.; Morrell, J.C.; Gould, S.J. Higher-order oligomerization targets plasma membrane proteins and HIV gag to exosomes. *PLoS Biol.* **2007**, *5*, e158. [CrossRef]
26. Munagala, R.; Aqil, F.; Jeyabalan, J.; Gupta, R.C. Bovine milk-derived exosomes for drug delivery. *Cancer Lett.* **2016**, *371*, 48–61. [CrossRef]
27. Morishita, M.; Takahashi, Y.; Nishikawa, M.; Takakura, Y. Pharmacokinetics of Exosomes-An Important Factor for Elucidating the Biological Roles of Exosomes and for the Development of Exosome-Based Therapeutics. *J. Pharm. Sci.* **2017**, *106*, 2265–2269. [CrossRef]
28. Smyth, T.; Kullberg, M.; Malik, N.; Smith-Jones, P.; Graner, M.W.; Anchordoquy, T.J. Biodistribution and delivery efficiency of unmodified tumor-derived exosomes. *J. Control. Release* **2015**, *199*, 145–155. [CrossRef]
29. Zhuang, X.; Xiang, X.; Grizzle, W.; Sun, D.; Zhang, S.; Axtell, R.C.; Ju, S.; Mu, J.; Zhang, L.; Steinman, L.; et al. Treatment of brain inflammatory diseases by delivering exosome encapsulated anti-inflammatory drugs from the nasal region to the brain. *Mol. Ther.* **2011**, *19*, 1769–1779. [CrossRef]
30. Choi, H.; Choi, Y.; Yim, H.Y.; Mirzaaghasi, A.; Yoo, J.K.; Choi, C. Biodistribution of Exosomes and Engineering Strategies for Targeted Delivery of Therapeutic Exosomes. *Tissue Eng. Regen. Med.* **2021**, *18*, 499–511. [CrossRef]
31. Munich, S.; Sobo-Vujanovic, A.; Buchser, W.J.; Beer-Stolz, D.; Vujanovic, N.L. Dendritic cell exosomes directly kill tumor cells and activate natural killer cells via TNF superfamily ligands. *Oncoimmunology* **2012**, *1*, 1074–1083. [CrossRef]
32. Jahn, R.; Sudhof, T.C. Membrane fusion and exocytosis. *Annu. Rev. Biochem.* **1999**, *68*, 863–911. [CrossRef] [PubMed]
33. Prada, I.; Meldolesi, J. Binding and Fusion of Extracellular Vesicles to the Plasma Membrane of Their Cell Targets. *Int. J. Mol. Sci.* **2016**, *17*, 1296. [CrossRef] [PubMed]

34. Gordon, S. Phagocytosis: An Immunobiologic Process. *Immunity* **2016**, *44*, 463–475. [CrossRef]
35. Shelke, G.V.; Yin, Y.; Jang, S.C.; Lasser, C.; Wennmalm, S.; Hoffmann, H.J.; Li, L.; Gho, Y.S.; Nilsson, J.A.; Lotvall, J. Endosomal signalling via exosome surface TGFbeta-1. *J. Extracell. Vesicles* **2019**, *8*, 1650458. [CrossRef]
36. Tian, T.; Wang, Y.; Wang, H.; Zhu, Z.; Xiao, Z. Visualizing of the cellular uptake and intracellular trafficking of exosomes by live-cell microscopy. *J. Cell Biochem.* **2010**, *111*, 488–496. [CrossRef]
37. Friedman, J.R.; Dibenedetto, J.R.; West, M.; Rowland, A.A.; Voeltz, G.K. Endoplasmic reticulum-endosome contact increases as endosomes traffic and mature. *Mol. Biol. Cell* **2013**, *24*, 1030–1040. [CrossRef] [PubMed]
38. Heusermann, W.; Hean, J.; Trojer, D.; Steib, E.; von Bueren, S.; Graff-Meyer, A.; Genoud, C.; Martin, K.; Pizzato, N.; Voshol, J.; et al. Exosomes surf on filopodia to enter cells at endocytic hot spots, traffic within endosomes, and are targeted to the ER. *J. Cell Biol.* **2016**, *213*, 173–184. [CrossRef] [PubMed]
39. Santos, M.F.; Rappa, G.; Karbanova, J.; Kurth, T.; Corbeil, D.; Lorico, A. VAMP-associated protein-A and oxysterol-binding protein-related protein 3 promote the entry of late endosomes into the nucleoplasmic reticulum. *J. Biol. Chem.* **2018**, *293*, 13834–13848. [CrossRef]
40. Zhang, Y.; Bi, J.; Huang, J.; Tang, Y.; Du, S.; Li, P. Exosome: A Review of Its Classification, Isolation Techniques, Storage, Diagnostic and Targeted Therapy Applications. *Int. J. Nanomed.* **2020**, *15*, 6917–6934. [CrossRef]
41. Chen, J.; Li, P.; Zhang, T.; Xu, Z.; Huang, X.; Wang, R.; Du, L. Review on Strategies and Technologies for Exosome Isolation and Purification. *Front. Bioeng. Biotechnol.* **2021**, *9*, 811971. [CrossRef]
42. Livshits, M.A.; Khomyakova, E.; Evtushenko, E.G.; Lazarev, V.N.; Kulemin, N.A.; Semina, S.E.; Generozov, E.V.; Govorun, V.M. Isolation of exosomes by differential centrifugation: Theoretical analysis of a commonly used protocol. *Sci. Rep.* **2015**, *5*, 17319. [CrossRef] [PubMed]
43. Thery, C.; Amigorena, S.; Raposo, G.; Clayton, A. Isolation and characterization of exosomes from cell culture supernatants and biological fluids. *Curr. Protoc. Cell Biol.* **2006**, *30*, 3–22. [CrossRef] [PubMed]
44. Yang, D.; Zhang, W.; Zhang, H.; Zhang, F.; Chen, L.; Ma, L.; Larcher, L.M.; Chen, S.; Liu, N.; Zhao, Q.; et al. Progress, opportunity, and perspective on exosome isolation—Efforts for efficient exosome-based theranostics. *Theranostics* **2020**, *10*, 3684–3707. [CrossRef] [PubMed]
45. Gupta, S.; Rawat, S.; Arora, V.; Kottarath, S.K.; Dinda, A.K.; Vaishnav, P.K.; Nayak, B.; Mohanty, S. An improvised one-step sucrose cushion ultracentrifugation method for exosome isolation from culture supernatants of mesenchymal stem cells. *Stem Cell Res. Ther.* **2018**, *9*, 180. [CrossRef]
46. Tauro, B.J.; Greening, D.W.; Mathias, R.A.; Ji, H.; Mathivanan, S.; Scott, A.M.; Simpson, R.J. Comparison of ultracentrifugation, density gradient separation, and immunoaffinity capture methods for isolating human colon cancer cell line LIM1863-derived exosomes. *Methods* **2012**, *56*, 293–304. [CrossRef]
47. Batrakova, E.V.; Kim, M.S. Using exosomes, naturally-equipped nanocarriers, for drug delivery. *J. Control. Release* **2015**, *219*, 396–405. [CrossRef]
48. Boing, A.N.; van der Pol, E.; Grootemaat, A.E.; Coumans, F.A.; Sturk, A.; Nieuwland, R. Single-step isolation of extracellular vesicles by size-exclusion chromatography. *J. Extracell. Vesicles* **2014**, *3*, 23430. [CrossRef]
49. Vergauwen, G.; Dhondt, B.; Van Deun, J.; De Smedt, E.; Berx, G.; Timmerman, E.; Gevaert, K.; Miinalainen, I.; Cocquyt, V.; Braems, G.; et al. Confounding factors of ultrafiltration and protein analysis in extracellular vesicle research. *Sci. Rep.* **2017**, *7*, 2704. [CrossRef]
50. Oh, D.K.; Hyun, C.K.; Kim, J.H.; Park, Y.H. Production of penicillin in a fluidized-bed bioreactor: Control of cell growth and penicillin production by phosphate limitation. *Biotechnol. Bioeng.* **1988**, *32*, 569–573. [CrossRef]
51. Ruivo, C.F.; Adem, B.; Silva, M.; Melo, S.A. The Biology of Cancer Exosomes: Insights and New Perspectives. *Cancer Res.* **2017**, *77*, 6480–6488. [CrossRef]
52. Zhang, M.; Jin, K.; Gao, L.; Zhang, Z.; Li, F.; Zhou, F.; Zhang, L. Methods and Technologies for Exosome Isolation and Characterization. *Small Methods* **2018**, *2*, 1800021. [CrossRef]
53. Chen, B.Y.; Sung, C.W.; Chen, C.; Cheng, C.M.; Lin, D.P.; Huang, C.T.; Hsu, M.Y. Advances in exosomes technology. *Clin. Chim. Acta* **2019**, *493*, 14–19. [CrossRef] [PubMed]
54. Jackson, E.L.; Lu, H. Advances in microfluidic cell separation and manipulation. *Curr. Opin. Chem. Eng.* **2013**, *2*, 398–404. [CrossRef]
55. Jablonska, J.; Pietrowska, M.; Ludwig, S.; Lang, S.; Thakur, B.K. Challenges in the Isolation and Proteomic Analysis of Cancer Exosomes-Implications for Translational Research. *Proteomes* **2019**, *7*, 22. [CrossRef] [PubMed]
56. Liu, W.Z.; Ma, Z.J.; Kang, X.W. Current status and outlook of advances in exosome isolation. *Anal. Bioanal. Chem.* **2022**, *414*, 7123–7141. [CrossRef] [PubMed]
57. Zhu, L.; Sun, H.T.; Wang, S.; Huang, S.L.; Zheng, Y.; Wang, C.Q.; Hu, B.Y.; Qin, W.; Zou, T.T.; Fu, Y.; et al. Isolation and characterization of exosomes for cancer research. *J. Hematol. Oncol.* **2020**, *13*, 152. [CrossRef] [PubMed]
58. Bhattacharjee, S. DLS and zeta potential—What they are and what they are not? *J. Control. Release* **2016**, *235*, 337–351. [CrossRef]
59. Doyle, L.M.; Wang, M.Z. Overview of Extracellular Vesicles, Their Origin, Composition, Purpose, and Methods for Exosome Isolation and Analysis. *Cells* **2019**, *8*, 727. [CrossRef]
60. Filipe, V.; Hawe, A.; Jiskoot, W. Critical evaluation of Nanoparticle Tracking Analysis (NTA) by NanoSight for the measurement of nanoparticles and protein aggregates. *Pharm. Res.* **2010**, *27*, 796–810. [CrossRef]

61. Malatesta, M. Transmission Electron Microscopy as a Powerful Tool to Investigate the Interaction of Nanoparticles with Subcellular Structures. *Int. J. Mol. Sci.* **2021**, *22*, 12789. [CrossRef]
62. Franken, L.E.; Grunewald, K.; Boekema, E.J.; Stuart, M.C.A. A Technical Introduction to Transmission Electron Microscopy for Soft-Matter: Imaging, Possibilities, Choices, and Technical Developments. *Small* **2020**, *16*, e1906198. [CrossRef] [PubMed]
63. Wu, Y.; Deng, W.; Klinke, D.J., 2nd. Exosomes: Improved methods to characterize their morphology, RNA content, and surface protein biomarkers. *Analyst* **2015**, *140*, 6631–6642. [CrossRef]
64. Thery, C.; Witwer, K.W.; Aikawa, E.; Alcaraz, M.J.; Anderson, J.D.; Andriantsitohaina, R.; Antoniou, A.; Arab, T.; Archer, F.; Atkin-Smith, G.K.; et al. Minimal information for studies of extracellular vesicles 2018 (MISEV2018): A position statement of the International Society for Extracellular Vesicles and update of the MISEV2014 guidelines. *J. Extracell. Vesicles* **2018**, *7*, 1535750. [CrossRef] [PubMed]
65. Gallagher, S.; Winston, S.E.; Fuller, S.A.; Hurrell, J.G. Immunoblotting and immunodetection. *Curr. Protoc. Cell Biol.* **2011**, *52*, 6. [CrossRef] [PubMed]
66. Davey, H.M.; Kell, D.B. Flow cytometry and cell sorting of heterogeneous microbial populations: The importance of single-cell analyses. *Microbiol. Rev.* **1996**, *60*, 641–696. [CrossRef]
67. Szatanek, R.; Baj-Krzyworzeka, M.; Zimoch, J.; Lekka, M.; Siedlar, M.; Baran, J. The Methods of Choice for Extracellular Vesicles (EVs) Characterization. *Int. J. Mol. Sci.* **2017**, *18*, 1153. [CrossRef]
68. Nolan, J.P.; Duggan, E. Analysis of Individual Extracellular Vesicles by Flow Cytometry. *Methods Mol. Biol.* **2018**, *1678*, 79–92. [CrossRef]
69. Pocsfalvi, G.; Stanly, C.; Vilasi, A.; Fiume, I.; Capasso, G.; Turiak, L.; Buzas, E.I.; Vekey, K. Mass spectrometry of extracellular vesicles. *Mass Spectrom. Rev.* **2016**, *35*, 3–21. [CrossRef]
70. McMahon, A.; Lu, H.; Butovich, I.A. The spectrophotometric sulfo-phospho-vanillin assessment of total lipids in human meibomian gland secretions. *Lipids* **2013**, *48*, 513–525. [CrossRef]
71. Visnovitz, T.; Osteikoetxea, X.; Sodar, B.W.; Mihaly, J.; Lorincz, P.; Vukman, K.V.; Toth, E.A.; Koncz, A.; Szekacs, I.; Horvath, R.; et al. An improved 96 well plate format lipid quantification assay for standardisation of experiments with extracellular vesicles. *J. Extracell. Vesicles* **2019**, *8*, 1565263. [CrossRef]
72. Olejarz, W.; Kubiak-Tomaszewska, G.; Chrzanowska, A.; Lorenc, T. Exosomes in Angiogenesis and Anti-angiogenic Therapy in Cancers. *Int. J. Mol. Sci.* **2020**, *21*, 5840. [CrossRef] [PubMed]
73. King, H.W.; Michael, M.Z.; Gleadle, J.M. Hypoxic enhancement of exosome release by breast cancer cells. *BMC Cancer* **2012**, *12*, 421. [CrossRef] [PubMed]
74. Hsu, Y.L.; Hung, J.Y.; Chang, W.A.; Lin, Y.S.; Pan, Y.C.; Tsai, P.H.; Wu, C.Y.; Kuo, P.L. Hypoxic lung cancer-secreted exosomal miR-23a increased angiogenesis and vascular permeability by targeting prolyl hydroxylase and tight junction protein ZO-1. *Oncogene* **2017**, *36*, 4929–4942. [CrossRef] [PubMed]
75. Sruthi, T.V.; Edatt, L.; Raji, G.R.; Kunhiraman, H.; Shankar, S.S.; Shankar, V.; Ramachandran, V.; Poyyakkara, A.; Kumar, S.V.B. Horizontal transfer of miR-23a from hypoxic tumor cell colonies can induce angiogenesis. *J. Cell Physiol.* **2018**, *233*, 3498–3514. [CrossRef] [PubMed]
76. Umezu, T.; Ohyashiki, K.; Kuroda, M.; Ohyashiki, J.H. Leukemia cell to endothelial cell communication via exosomal miRNAs. *Oncogene* **2013**, *32*, 2747–2755. [CrossRef]
77. Wozniak, M.; Peczek, L.; Czernek, L.; Duchler, M. Analysis of the miRNA Profiles of Melanoma Exosomes Derived Under Normoxic and Hypoxic Culture Conditions. *Anticancer Res.* **2017**, *37*, 6779–6789. [CrossRef]
78. Chen, S.; Chen, X.; Luo, Q.; Liu, X.; Wang, X.; Cui, Z.; He, A.; He, S.; Jiang, Z.; Wu, N.; et al. Retinoblastoma cell-derived exosomes promote angiogenesis of human vesicle endothelial cells through microRNA-92a-3p. *Cell Death Dis.* **2021**, *12*, 695. [CrossRef]
79. He, L.; Zhu, W.; Chen, Q.; Yuan, Y.; Wang, Y.; Wang, J.; Wu, X. Ovarian cancer cell-secreted exosomal miR-205 promotes metastasis by inducing angiogenesis. *Theranostics* **2019**, *9*, 8206–8220. [CrossRef]
80. Ekstrom, E.J.; Bergenfelz, C.; von Bulow, V.; Serifler, F.; Carlemalm, E.; Jonsson, G.; Andersson, T.; Leandersson, K. WNT5A induces release of exosomes containing pro-angiogenic and immunosuppressive factors from malignant melanoma cells. *Mol. Cancer* **2014**, *13*, 88. [CrossRef]
81. Skog, J.; Wurdinger, T.; van Rijn, S.; Meijer, D.H.; Gainche, L.; Sena-Esteves, M.; Curry, W.T., Jr.; Carter, B.S.; Krichevsky, A.M.; Breakefield, X.O. Glioblastoma microvesicles transport RNA and proteins that promote tumour growth and provide diagnostic biomarkers. *Nat. Cell Biol.* **2008**, *10*, 1470–1476. [CrossRef]
82. Tang, M.K.S.; Yue, P.Y.K.; Ip, P.P.; Huang, R.L.; Lai, H.C.; Cheung, A.N.Y.; Tse, K.Y.; Ngan, H.Y.S.; Wong, A.S.T. Soluble E-cadherin promotes tumor angiogenesis and localizes to exosome surface. *Nat. Commun.* **2018**, *9*, 2270. [CrossRef]
83. Wang, J.; De Veirman, K.; Faict, S.; Frassanito, M.A.; Ribatti, D.; Vacca, A.; Menu, E. Multiple myeloma exosomes establish a favourable bone marrow microenvironment with enhanced angiogenesis and immunosuppression. *J. Pathol.* **2016**, *239*, 162–173. [CrossRef] [PubMed]
84. You, Y.; Shan, Y.; Chen, J.; Yue, H.; You, B.; Shi, S.; Li, X.; Cao, X. Matrix metalloproteinase 13-containing exosomes promote nasopharyngeal carcinoma metastasis. *Cancer Sci.* **2015**, *106*, 1669–1677. [CrossRef] [PubMed]
85. Tengler, L.; Schutz, J.; Tiedtke, M.; Jablonska, J.; Theodoraki, M.N.; Nitschke, K.; Weiss, C.; Seiz, E.; Affolter, A.; Jungbauer, F.; et al. Plasma-derived small extracellular vesicles unleash the angiogenic potential in head and neck cancer patients. *Mol. Med.* **2023**, *29*, 69. [CrossRef] [PubMed]

86. Taverna, S.; Flugy, A.; Saieva, L.; Kohn, E.C.; Santoro, A.; Meraviglia, S.; De Leo, G.; Alessandro, R. Role of exosomes released by chronic myelogenous leukemia cells in angiogenesis. *Int. J. Cancer* **2012**, *130*, 2033–2043. [CrossRef] [PubMed]
87. Nazarenko, I.; Rana, S.; Baumann, A.; McAlear, J.; Hellwig, A.; Trendelenburg, M.; Lochnit, G.; Preissner, K.T.; Zoller, M. Cell surface tetraspanin Tspan8 contributes to molecular pathways of exosome-induced endothelial cell activation. *Cancer Res.* **2010**, *70*, 1668–1678. [CrossRef]
88. Zeeshan, R.; Mutahir, Z. Cancer metastasis—Tricks of the trade. *Bosn. J. Basic Med. Sci.* **2017**, *17*, 172–182. [CrossRef]
89. Wang, C.; Wang, Y.; Chang, X.; Ba, X.; Hu, N.; Liu, Q.; Fang, L.; Wang, Z. Melanoma-Derived Exosomes Endow Fibroblasts with an Invasive Potential via miR-21 Target Signaling Pathway. *Cancer Manag. Res.* **2020**, *12*, 12965–12974. [CrossRef]
90. Zhu, Y.H.; Tao, Z.H.; Chen, Y.; Lin, S.C.; Zhu, M.Y.; Ji, W.; Liu, X.J.; Li, T.; Hu, X.C. Exosomal MMP-1 transfers metastasis potential in triple-negative breast cancer through PAR1-mediated EMT. *Breast Cancer Res. Treat.* **2022**, *193*, 65–81. [CrossRef]
91. Amack, J.D. Cellular dynamics of EMT: Lessons from live in vivo imaging of embryonic development. *Cell Commun. Signal.* **2021**, *19*, 79. [CrossRef]
92. Dongre, A.; Weinberg, R.A. New insights into the mechanisms of epithelial-mesenchymal transition and implications for cancer. *Nat. Rev. Mol. Cell Biol.* **2019**, *20*, 69–84. [CrossRef] [PubMed]
93. Huang, Z.; Feng, Y. Exosomes Derived From Hypoxic Colorectal Cancer Cells Promote Angiogenesis Through Wnt4-Induced beta-Catenin Signaling in Endothelial Cells. *Oncol. Res.* **2017**, *25*, 651–661. [CrossRef] [PubMed]
94. Wang, F.W.; Cao, C.H.; Han, K.; Zhao, Y.X.; Cai, M.Y.; Xiang, Z.C.; Zhang, J.X.; Chen, J.W.; Zhong, L.P.; Huang, Y.; et al. APC-activated long noncoding RNA inhibits colorectal carcinoma pathogenesis through reduction of exosome production. *J. Clin. Investig.* **2021**, *131*, e149666. [CrossRef]
95. Gross, J.C.; Chaudhary, V.; Bartscherer, K.; Boutros, M. Active Wnt proteins are secreted on exosomes. *Nat. Cell Biol.* **2012**, *14*, 1036–1045. [CrossRef] [PubMed]
96. Chen, Y.; Zeng, C.; Zhan, Y.; Wang, H.; Jiang, X.; Li, W. Aberrant low expression of p85alpha in stromal fibroblasts promotes breast cancer cell metastasis through exosome-mediated paracrine Wnt10b. *Oncogene* **2017**, *36*, 4692–4705. [CrossRef]
97. Nagaharu, K.; Zhang, X.; Yoshida, T.; Katoh, D.; Hanamura, N.; Kozuka, Y.; Ogawa, T.; Shiraishi, T.; Imanaka-Yoshida, K. Tenascin C induces epithelial-mesenchymal transition-like change accompanied by SRC activation and focal adhesion kinase phosphorylation in human breast cancer cells. *Am. J. Pathol.* **2011**, *178*, 754–763. [CrossRef]
98. Li, Y.Y.; Tao, Y.W.; Gao, S.; Li, P.; Zheng, J.M.; Zhang, S.E.; Liang, J.; Zhang, Y. Cancer-associated fibroblasts contribute to oral cancer cells proliferation and metastasis via exosome-mediated paracrine miR-34a-5p. *EBioMedicine* **2018**, *36*, 209–220. [CrossRef]
99. Zhao, H.; Chen, S.; Fu, Q. Exosomes from CD133(+) cells carrying circ-ABCC1 mediate cell stemness and metastasis in colorectal cancer. *J. Cell Biochem.* **2020**, *121*, 3286–3297. [CrossRef]
100. Han, M.; Liu, M.; Wang, Y.; Chen, X.; Xu, J.; Sun, Y.; Zhao, L.; Qu, H.; Fan, Y.; Wu, C. Antagonism of miR-21 reverses epithelial-mesenchymal transition and cancer stem cell phenotype through AKT/ERK1/2 inactivation by targeting PTEN. *PLoS ONE* **2012**, *7*, e39520. [CrossRef]
101. Jeppesen, D.K.; Nawrocki, A.; Jensen, S.G.; Thorsen, K.; Whitehead, B.; Howard, K.A.; Dyrskjot, L.; Orntoft, T.F.; Larsen, M.R.; Ostenfeld, M.S. Quantitative proteomics of fractionated membrane and lumen exosome proteins from isogenic metastatic and nonmetastatic bladder cancer cells reveal differential expression of EMT factors. *Proteomics* **2014**, *14*, 699–712. [CrossRef]
102. Theodoraki, M.N.; Yerneni, S.S.; Brunner, C.; Theodorakis, J.; Hoffmann, T.K.; Whiteside, T.L. Plasma-derived Exosomes Reverse Epithelial-to-Mesenchymal Transition after Photodynamic Therapy of Patients with Head and Neck Cancer. *Oncoscience* **2018**, *5*, 75–87. [CrossRef] [PubMed]
103. Hoshino, A.; Costa-Silva, B.; Shen, T.L.; Rodrigues, G.; Hashimoto, A.; Tesic Mark, M.; Molina, H.; Kohsaka, S.; Di Giannatale, A.; Ceder, S.; et al. Tumour exosome integrins determine organotropic metastasis. *Nature* **2015**, *527*, 329–335. [CrossRef] [PubMed]
104. Zomer, A.; Maynard, C.; Verweij, F.J.; Kamermans, A.; Schafer, R.; Beerling, E.; Schiffelers, R.M.; de Wit, E.; Berenguer, J.; Ellenbroek, S.I.J.; et al. In Vivo imaging reveals extracellular vesicle-mediated phenocopying of metastatic behavior. *Cell* **2015**, *161*, 1046–1057. [CrossRef]
105. Zhang, H.; Deng, T.; Liu, R.; Bai, M.; Zhou, L.; Wang, X.; Li, S.; Wang, X.; Yang, H.; Li, J.; et al. Exosome-delivered EGFR regulates liver microenvironment to promote gastric cancer liver metastasis. *Nat. Commun.* **2017**, *8*, 15016. [CrossRef]
106. Hood, J.L.; San, R.S.; Wickline, S.A. Exosomes released by melanoma cells prepare sentinel lymph nodes for tumor metastasis. *Cancer Res.* **2011**, *71*, 3792–3801. [CrossRef]
107. Zhang, L.; Yu, D. Exosomes in cancer development, metastasis, and immunity. *Biochim. Biophys. Acta Rev. Cancer* **2019**, *1871*, 455–468. [CrossRef] [PubMed]
108. Wolfers, J.; Lozier, A.; Raposo, G.; Regnault, A.; Thery, C.; Masurier, C.; Flament, C.; Pouzieux, S.; Faure, F.; Tursz, T.; et al. Tumor-derived exosomes are a source of shared tumor rejection antigens for CTL cross-priming. *Nat. Med.* **2001**, *7*, 297–303. [CrossRef]
109. Vega, V.L.; Rodriguez-Silva, M.; Frey, T.; Gehrmann, M.; Diaz, J.C.; Steinem, C.; Multhoff, G.; Arispe, N.; De Maio, A. Hsp70 translocates into the plasma membrane after stress and is released into the extracellular environment in a membrane-associated form that activates macrophages. *J. Immunol.* **2008**, *180*, 4299–4307. [CrossRef]
110. Gastpar, R.; Gehrmann, M.; Bausero, M.A.; Asea, A.; Gross, C.; Schroeder, J.A.; Multhoff, G. Heat shock protein 70 surface-positive tumor exosomes stimulate migratory and cytolytic activity of natural killer cells. *Cancer Res.* **2005**, *65*, 5238–5247. [CrossRef]

111. Li, W.H.; Mu, D.G.; Tian, F.; Hu, Y.S.; Jiang, T.; Han, Y.; Chen, J.K.; Han, G.L.; Li, X.F. Exosomes derived from Rab27a-overexpressing tumor cells elicit efficient induction of antitumor immunity. *Mol. Med. Rep.* **2013**, *8*, 1876–1882. [CrossRef]
112. Kitai, Y.; Kawasaki, T.; Sueyoshi, T.; Kobiyama, K.; Ishii, K.J.; Zou, J.; Akira, S.; Matsuda, T.; Kawai, T. DNA-Containing Exosomes Derived from Cancer Cells Treated with Topotecan Activate a STING- Dependent Pathway and Reinforce Antitumor Immunity. *J. Immunol.* **2017**, *198*, 1649–1659. [CrossRef] [PubMed]
113. Ludwig, S.; Floros, T.; Theodoraki, M.N.; Hong, C.S.; Jackson, E.K.; Lang, S.; Whiteside, T.L. Suppression of Lymphocyte Functions by Plasma Exosomes Correlates with Disease Activity in Patients with Head and Neck Cancer. *Clin. Cancer Res.* **2017**, *23*, 4843–4854. [CrossRef] [PubMed]
114. Lundholm, M.; Schroder, M.; Nagaeva, O.; Baranov, V.; Widmark, A.; Mincheva-Nilsson, L.; Wikstrom, P. Prostate tumor-derived exosomes down-regulate NKG2D expression on natural killer cells and CD8+ T cells: Mechanism of immune evasion. *PLoS ONE* **2014**, *9*, e108925. [CrossRef]
115. Yang, Y.; Li, C.W.; Chan, L.C.; Wei, Y.; Hsu, J.M.; Xia, W.; Cha, J.H.; Hou, J.; Hsu, J.L.; Sun, L.; et al. Exosomal PD-L1 harbors active defense function to suppress T cell killing of breast cancer cells and promote tumor growth. *Cell Res.* **2018**, *28*, 862–864. [CrossRef] [PubMed]
116. Chen, G.; Huang, A.C.; Zhang, W.; Zhang, G.; Wu, M.; Xu, W.; Yu, Z.; Yang, J.; Wang, B.; Sun, H.; et al. Exosomal PD-L1 contributes to immunosuppression and is associated with anti-PD-1 response. *Nature* **2018**, *560*, 382–386. [CrossRef]
117. Jablonska, J.; Rist, M.; Spyra, I.; Tengler, L.; Domnich, M.; Kansy, B.; Giebel, B.; Thakur, B.K.; Rotter, N.; Lang, S.; et al. Evaluation of Immunoregulatory Biomarkers on Plasma Small Extracellular Vesicles for Disease Progression and Early Therapeutic Response in Head and Neck Cancer. *Cells* **2022**, *11*, 902. [CrossRef]
118. Daassi, D.; Mahoney, K.M.; Freeman, G.J. The importance of exosomal PDL1 in tumour immune evasion. *Nat. Rev. Immunol.* **2020**, *20*, 209–215. [CrossRef]
119. Ye, L.; Zhu, Z.; Chen, X.; Zhang, H.; Huang, J.; Gu, S.; Zhao, X. The Importance of Exosomal PD-L1 in Cancer Progression and Its Potential as a Therapeutic Target. *Cells* **2021**, *10*, 3247. [CrossRef]
120. Whiteside, T.L.; Rabinowich, H. The role of Fas/FasL in immunosuppression induced by human tumors. *Cancer Immunol. Immunother.* **1998**, *46*, 175–184. [CrossRef]
121. Abusamra, A.J.; Zhong, Z.H.; Zheng, X.F.; Li, M.; Ichim, T.E.; Chin, J.L.; Min, W.P. Tumor exosomes expressing Fas ligand mediate CD8(+) T-cell apoptosis. *Blood Cell Mol. Dis.* **2005**, *35*, 169–173. [CrossRef]
122. Klibi, J.; Niki, T.; Riedel, A.; Pioche-Durieu, C.; Souquere, S.; Rubinstein, E.; Moulec, S.L.E.; Guigay, J.; Hirashima, M.; Guemira, F.; et al. Blood diffusion and Th1-suppressive effects of galectin-9-containing exosomes released by Epstein-Barr virus-infected nasopharyngeal carcinoma cells. *Blood* **2009**, *113*, 1957–1966. [CrossRef] [PubMed]
123. Cornel, A.M.; Mimpen, I.L.; Nierkens, S. MHC Class I Downregulation in Cancer: Underlying Mechanisms and Potential Targets for Cancer Immunotherapy. *Cancers* **2020**, *12*, 1760. [CrossRef] [PubMed]
124. Sun, T.; Li, Y.Y.; Wu, J.; Cao, Y.F.; Yang, Y.; He, Y.P.; Huang, W.P.; Liu, B.; Yang, W. Downregulation of exosomal MHC-I promotes glioma cells escaping from systemic immunosurveillance. *Nanomed. Nanotechnol.* **2022**, *46*, 102605. [CrossRef] [PubMed]
125. Guimaraes-Bastos, D.; Frony, A.C.; Barja-Fidalgo, C.; Moraes, J.A. Melanoma-derived extracellular vesicles skew neutrophils into a pro-tumor phenotype. *J. Leukoc. Biol.* **2022**, *111*, 585–596. [CrossRef]
126. Hsieh, C.H.; Tai, S.K.; Yang, M.H. Snail-overexpressing Cancer Cells Promote M2-Like Polarization of Tumor-Associated Macrophages by Delivering MiR-21-Abundant Exosomes. *Neoplasia* **2018**, *20*, 775–788. [CrossRef] [PubMed]
127. Du, S.; Qian, J.; Tan, S.; Li, W.; Liu, P.; Zhao, J.; Zeng, Y.; Xu, L.; Wang, Z.; Cai, J. Tumor cell-derived exosomes deliver TIE2 protein to macrophages to promote angiogenesis in cervical cancer. *Cancer Lett.* **2022**, *529*, 168–179. [CrossRef]
128. Morrissey, S.M.; Zhang, F.; Ding, C.L.; Montoya-Durango, D.E.; Hu, X.L.; Yang, C.H.; Wang, Z.; Yuan, F.; Fox, M.; Zhang, H.G.; et al. Tumor-derived exosomes drive immunosuppressive macrophages in a pre-metastatic niche through glycolytic dominant metabolic reprogramming. *Cell Metab.* **2021**, *33*, 2040–2058. [CrossRef]
129. Siemer, S.; Bauer, T.A.; Scholz, P.; Breder, C.; Fenaroli, F.; Harms, G.; Dietrich, D.; Dietrich, J.; Rosenauer, C.; Barz, M.; et al. Targeting Cancer Chemotherapy Resistance by Precision Medicine-Driven Nanoparticle-Formulated Cisplatin. *ACS Nano* **2021**, *15*, 18541–18556. [CrossRef]
130. Lu, Y.; Pan, Q.; Gao, W.; Pu, Y.; He, B. Reversal of cisplatin chemotherapy resistance by glutathione-resistant copper-based nanomedicine via cuproptosis. *J. Mater. Chem. B* **2022**, *10*, 6296–6306. [CrossRef]
131. Stauber, R.H.; Westmeier, D.; Wandrey, M.; Becker, S.; Docter, D.; Ding, G.B.; Thines, E.; Knauer, S.K.; Siemer, S. Mechanisms of nanotoxicity—Biomolecule coronas protect pathological fungi against nanoparticle-based eradication. *Nanotoxicology* **2020**, *14*, 1157–1174. [CrossRef]
132. Westmeier, D.; Stauber, R.H.; Docter, D. The concept of bio-corona in modulating the toxicity of engineered nanomaterials (ENM). *Toxicol. Appl. Pharmacol.* **2016**, *299*, 53–57. [CrossRef] [PubMed]
133. Docter, D.; Strieth, S.; Westmeier, D.; Hayden, O.; Gao, M.; Knauer, S.K.; Stauber, R.H. No king without a crown--impact of the nanomaterial-protein corona on nanobiomedicine. *Nanomedicine* **2015**, *10*, 503–519. [CrossRef] [PubMed]
134. Liang, Y.J.; Duan, L.; Lu, J.P.; Xia, J. Engineering exosomes for targeted drug delivery. *Theranostics* **2021**, *11*, 3183–3195. [CrossRef] [PubMed]

135. Kim, M.S.; Haney, M.J.; Zhao, Y.; Mahajan, V.; Deygen, I.; Klyachko, N.L.; Inskoe, E.; Piroyan, A.; Sokolsky, M.; Okolie, O.; et al. Development of exosome-encapsulated paclitaxel to overcome MDR in cancer cells. *Nanomedicine* **2016**, *12*, 655–664. [CrossRef] [PubMed]
136. Ye, Z.L.; Zhang, T.; He, W.S.; Jin, H.L.; Liu, C.W.; Yang, Z.; Ren, J.H. Methotrexate-Loaded Extracellular Vesicles Functionalized with Therapeutic and Targeted Peptides for the Treatment of Glioblastoma Multiforme. *ACS Appl. Mater. Inter.* **2018**, *10*, 12341–12350. [CrossRef] [PubMed]
137. Li, S.; Wu, Y.; Ding, F.; Yang, J.; Li, J.; Gao, X.; Zhang, C.; Feng, J. Engineering macrophage-derived exosomes for targeted chemotherapy of triple-negative breast cancer. *Nanoscale* **2020**, *12*, 10854–10862. [CrossRef]
138. Liang, G.F.; Zhu, Y.L.; Ali, D.J.; Tian, T.; Xu, H.T.; Si, K.; Sun, B.; Chen, B.A.; Xiao, Z.D. Engineered exosomes for targeted co-delivery of miR-21 inhibitor and chemotherapeutics to reverse drug resistance in colon cancer. *J. Nanobiotechnol.* **2020**, *18*, 10. [CrossRef]
139. Bellavia, D.; Raimondo, S.; Calabrese, G.; Forte, S.; Cristaldi, M.; Patinella, A.; Memeo, L.; Manno, M.; Raccosta, S.; Diana, P.; et al. Interleukin 3-receptor targeted exosomes inhibit in vitro and in vivo Chronic Myelogenous Leukemia cell growth. *Theranostics* **2017**, *7*, 1333–1345. [CrossRef]
140. Delcayre, A.; Shu, H.; Le Pecq, J.B. Dendritic cell-derived exosomes in cancer immunotherapy: Exploiting nature's antigen delivery pathway. *Expert Rev. Anticancer Ther.* **2005**, *5*, 537–547. [CrossRef]
141. Yao, Y.; Fu, C.; Zhou, L.; Mi, Q.S.; Jiang, A. DC-Derived Exosomes for Cancer Immunotherapy. *Cancers* **2021**, *13*, 3667. [CrossRef]
142. Cheng, Q.; Shi, X.; Han, M.; Smbatyan, G.; Lenz, H.J.; Zhang, Y. Reprogramming Exosomes as Nanoscale Controllers of Cellular Immunity. *J. Am. Chem. Soc.* **2018**, *140*, 16413–16417. [CrossRef]
143. Shi, X.; Cheng, Q.; Hou, T.; Han, M.; Smbatyan, G.; Lang, J.E.; Epstein, A.L.; Lenz, H.J.; Zhang, Y. Genetically Engineered Cell-Derived Nanoparticles for Targeted Breast Cancer Immunotherapy. *Mol. Ther.* **2020**, *28*, 536–547. [CrossRef] [PubMed]
144. Wang, J.; Wang, L.; Lin, Z.; Tao, L.; Chen, M. More efficient induction of antitumor T cell immunity by exosomes from CD40L gene-modified lung tumor cells. *Mol. Med. Rep.* **2014**, *9*, 125–131. [CrossRef]
145. Zhou, W.X.; Zhou, Y.; Chen, X.L.; Ning, T.T.; Chen, H.Y.; Guo, Q.; Zhang, Y.W.; Liu, P.X.; Zhang, Y.J.; Li, C.; et al. Pancreatic cancer-targeting exosomes for enhancing immunotherapy and reprogramming tumor microenvironment. *Biomaterials* **2021**, *268*, 120546. [CrossRef] [PubMed]
146. Mantovani, A.; Allavena, P.; Sica, A.; Balkwill, F. Cancer-related inflammation. *Nature* **2008**, *454*, 436–444. [CrossRef] [PubMed]
147. Duong, N.; Curley, K.; Brown, A.; Campanelli, A.; Do, M.A.; Levy, D.; Tantry, A.; Marriott, G.; Lu, B. Decoy exosomes as a novel biologic reagent to antagonize inflammation. *Int. J. Nanomed.* **2019**, *14*, 3413–3425. [CrossRef]
148. Vaidyanathan, R.; Soon, R.H.; Zhang, P.; Jiang, K.; Lim, C.T. Cancer diagnosis: From tumor to liquid biopsy and beyond. *Lab Chip* **2018**, *19*, 11–34. [CrossRef]
149. Mishra, V.; Singh, A.; Chen, X.; Rosenberg, A.J.; Pearson, A.T.; Zhavoronkov, A.; Savage, P.A.; Lingen, M.W.; Agrawal, N.; Izumchenko, E. Application of liquid biopsy as multi-functional biomarkers in head and neck cancer. *Br. J. Cancer* **2022**, *126*, 361–370. [CrossRef] [PubMed]
150. Xiao, C.; Song, F.; Zheng, Y.L.; Lv, J.; Wang, Q.F.; Xu, N. Exosomes in Head and Neck Squamous Cell Carcinoma. *Front. Oncol.* **2019**, *9*, 894. [CrossRef]
151. Zhou, Y.; Zhang, Y.; Gong, H.; Luo, S.; Cui, Y. The Role of Exosomes and Their Applications in Cancer. *Int. J. Mol. Sci.* **2021**, *22*, 12204. [CrossRef]
152. Joyce, D.P.; Kerin, M.J.; Dwyer, R.M. Exosome-encapsulated microRNAs as circulating biomarkers for breast cancer. *Int. J. Cancer* **2016**, *139*, 1443–1448. [CrossRef] [PubMed]
153. Zhou, W.; Ye, X.L.; Xu, J.; Cao, M.G.; Fang, Z.Y.; Li, L.Y.; Guan, G.H.; Liu, Q.; Qian, Y.H.; Xie, D. The lncRNA H19 mediates breast cancer cell plasticity during EMT and MET plasticity by differentially sponging miR-200b/c and let-7b. *Sci. Signal.* **2017**, *10*, eaak9557. [CrossRef] [PubMed]
154. Zhong, G.; Wang, K.; Li, J.; Xiao, S.; Wei, W.; Liu, J. Determination of Serum Exosomal H19 as a Noninvasive Biomarker for Breast Cancer Diagnosis. *Onco Targets Ther.* **2020**, *13*, 2563–2571. [CrossRef]
155. Sun, S.; Chen, H.; Xu, C.; Zhang, Y.; Zhang, Q.; Chen, L.; Ding, Q.; Deng, Z. Exosomal miR-106b serves as a novel marker for lung cancer and promotes cancer metastasis via targeting PTEN. *Life Sci.* **2020**, *244*, 117297. [CrossRef] [PubMed]
156. Dejima, H.; Iinuma, H.; Kanaoka, R.; Matsutani, N.; Kawamura, M. Exosomal microRNA in plasma as a non-invasive biomarker for the recurrence of non-small cell lung cancer. *Oncol. Lett.* **2017**, *13*, 1256–1263. [CrossRef]
157. Muller, L.; Hong, C.S.; Stolz, D.B.; Watkins, S.C.; Whiteside, T.L. Isolation of biologically-active exosomes from human plasma. *J. Immunol. Methods* **2014**, *411*, 55–65. [CrossRef]
158. Theodoraki, M.N.; Yerneni, S.; Gooding, W.E.; Ohr, J.; Clump, D.A.; Bauman, J.E.; Ferris, R.L.; Whiteside, T.L. Circulating exosomes measure responses to therapy in head and neck cancer patients treated with cetuximab, ipilimumab, and IMRT. *Oncoimmunology* **2019**, *8*, 1593805. [CrossRef]
159. van Dommelen, S.M.; van der Meel, R.; van Solinge, W.W.; Coimbra, M.; Vader, P.; Schiffelers, R.M. Cetuximab treatment alters the content of extracellular vesicles released from tumor cells. *Nanomedicine* **2016**, *11*, 881–890. [CrossRef]
160. Wang, J.; Zhou, Y.; Lu, J.; Sun, Y.; Xiao, H.; Liu, M.; Tian, L. Combined detection of serum exosomal miR-21 and HOTAIR as diagnostic and prognostic biomarkers for laryngeal squamous cell carcinoma. *Med. Oncol.* **2014**, *31*, 148. [CrossRef]

161. Yunusova, N.V.; Zambalova, E.A.; Patysheva, M.R.; Kolegova, E.S.; Afanas'ev, S.G.; Cheremisina, O.V.; Grigor'eva, A.E.; Tamkovich, S.N.; Kondakova, I.V. Exosomal Protease Cargo as Prognostic Biomarker in Colorectal Cancer. *Asian Pac. J. Cancer Prev.* **2021**, *22*, 861–869. [CrossRef]
162. Elmallah, M.I.Y.; Ortega-Deballon, P.; Hermite, L.; Pais-De-Barros, J.P.; Gobbo, J.; Garrido, C. Lipidomic profiling of exosomes from colorectal cancer cells and patients reveals potential biomarkers. *Mol. Oncol.* **2022**, *16*, 2710–2718. [CrossRef] [PubMed]
163. Ebnoether, E.; Muller, L. Diagnostic and Therapeutic Applications of Exosomes in Cancer with a Special Focus on Head and Neck Squamous Cell Carcinoma (HNSCC). *Int. J. Mol. Sci.* **2020**, *21*, 4344. [CrossRef] [PubMed]
164. Catalano, M.; O'Driscoll, L. Inhibiting extracellular vesicles formation and release: A review of EV inhibitors. *J. Extracell. Vesicles* **2020**, *9*, 1703244. [CrossRef] [PubMed]
165. Richards, K.E.; Zeleniak, A.E.; Fishel, M.L.; Wu, J.; Littlepage, L.E.; Hill, R. Cancer-associated fibroblast exosomes regulate survival and proliferation of pancreatic cancer cells. *Oncogene* **2017**, *36*, 1770–1778. [CrossRef] [PubMed]
166. Wang, G.; Xie, L.; Li, B.; Sang, W.; Yan, J.; Li, J.; Tian, H.; Li, W.; Zhang, Z.; Tian, Y.; et al. A nanounit strategy reverses immune suppression of exosomal PD-L1 and is associated with enhanced ferroptosis. *Nat. Commun.* **2021**, *12*, 5733. [CrossRef]
167. Mikamori, M.; Yamada, D.; Eguchi, H.; Hasegawa, S.; Kishimoto, T.; Tomimaru, Y.; Asaoka, T.; Noda, T.; Wada, H.; Kawamoto, K.; et al. MicroRNA-155 Controls Exosome Synthesis and Promotes Gemcitabine Resistance in Pancreatic Ductal Adenocarcinoma. *Sci. Rep.* **2017**, *7*, 42339. [CrossRef]
168. Bobrie, A.; Krumeich, S.; Reyal, F.; Recchi, C.; Moita, L.F.; Seabra, M.C.; Ostrowski, M.; Thery, C. Rab27a supports exosome-dependent and -independent mechanisms that modify the tumor microenvironment and can promote tumor progression. *Cancer Res.* **2012**, *72*, 4920–4930. [CrossRef]
169. Peinado, H.; Aleckovic, M.; Lavotshkin, S.; Matei, I.; Costa-Silva, B.; Moreno-Bueno, G.; Hergueta-Redondo, M.; Williams, C.; Garcia-Santos, G.; Ghajar, C.; et al. Melanoma exosomes educate bone marrow progenitor cells toward a pro-metastatic phenotype through MET. *Nat. Med.* **2012**, *18*, 883–891. [CrossRef]
170. Chalmin, F.; Ladoire, S.; Mignot, G.; Vincent, J.; Bruchard, M.; Remy-Martin, J.P.; Boireau, W.; Rouleau, A.; Simon, B.; Lanneau, D.; et al. Membrane-associated Hsp72 from tumor-derived exosomes mediates STAT3-dependent immunosuppressive function of mouse and human myeloid-derived suppressor cells. *J. Clin. Investig.* **2010**, *120*, 457–471. [CrossRef]
171. Christianson, H.C.; Svensson, K.J.; van Kuppevelt, T.H.; Li, J.P.; Belting, M. Cancer cell exosomes depend on cell-surface heparan sulfate proteoglycans for their internalization and functional activity. *Proc. Natl. Acad. Sci. USA* **2013**, *110*, 17380–17385. [CrossRef]
172. Lima, L.G.; Chammas, R.; Monteiro, R.Q.; Moreira, M.E.; Barcinski, M.A. Tumor-derived microvesicles modulate the establishment of metastatic melanoma in a phosphatidylserine-dependent manner. *Cancer Lett.* **2009**, *283*, 168–175. [CrossRef] [PubMed]
173. Tohme, S.; Simmons, R.L.; Tsung, A. Surgery for Cancer: A Trigger for Metastases. *Cancer Res.* **2017**, *77*, 1548–1552. [CrossRef] [PubMed]
174. Carneiro, B.A.; El-Deiry, W.S. Targeting apoptosis in cancer therapy. *Nat. Rev. Clin. Oncol.* **2020**, *17*, 395–417. [CrossRef] [PubMed]
175. Sung, H.; Ferlay, J.; Siegel, R.L.; Laversanne, M.; Soerjomataram, I.; Jemal, A.; Bray, F. Global Cancer Statistics 2020: GLOBOCAN Estimates of Incidence and Mortality Worldwide for 36 Cancers in 185 Countries. *CA Cancer J. Clin.* **2021**, *71*, 209–249. [CrossRef]
176. Hayatudin, R.; Fong, Z.; Ming, L.C.; Goh, B.H.; Lee, W.L.; Kifli, N. Overcoming Chemoresistance via Extracellular Vesicle Inhibition. *Front. Mol. Biosci.* **2021**, *8*, 629874. [CrossRef]
177. Zhu, H.; Luo, H.; Zhang, W.; Shen, Z.; Hu, X.; Zhu, X. Molecular mechanisms of cisplatin resistance in cervical cancer. *Drug Des. Devel. Ther.* **2016**, *10*, 1885–1895. [CrossRef]
178. Kong, J.N.; He, Q.; Wang, G.; Dasgupta, S.; Dinkins, M.B.; Zhu, G.; Kim, A.; Spassieva, S.; Bieberich, E. Guggulsterone and bexarotene induce secretion of exosome-associated breast cancer resistance protein and reduce doxorubicin resistance in MDA-MB-231 cells. *Int. J. Cancer* **2015**, *137*, 1610–1620. [CrossRef]
179. Lv, L.H.; Wan, Y.L.; Lin, Y.; Zhang, W.; Yang, M.; Li, G.L.; Lin, H.M.; Shang, C.Z.; Chen, Y.J.; Min, J. Anticancer Drugs Cause Release of Exosomes with Heat Shock Proteins from Human Hepatocellular Carcinoma Cells That Elicit Effective Natural Killer Cell Antitumor Responses in Vitro. *J. Biol. Chem.* **2012**, *287*, 15874–15885. [CrossRef]
180. Safaei, R.; Larson, B.J.; Cheng, T.C.; Gibson, M.A.; Otani, S.; Naerdemann, W.; Howell, S.B. Abnormal lysosomal trafficking and enhanced exosomal export of cisplatin in drug-resistant human ovarian carcinoma cells. *Mol. Cancer Ther.* **2005**, *4*, 1595–1604. [CrossRef]
181. Ning, K.; Wang, T.; Sun, X.; Zhang, P.; Chen, Y.; Jin, J.; Hua, D. UCH-L1-containing exosomes mediate chemotherapeutic resistance transfer in breast cancer. *J. Surg. Oncol.* **2017**, *115*, 932–940. [CrossRef]
182. Muralidharan-Chari, V.; Kohan, H.G.; Asimakopoulos, A.G.; Sudha, T.; Sell, S.; Kannan, K.; Boroujerdi, M.; Davis, P.J.; Mousa, S.A. Microvesicle removal of anticancer drugs contributes to drug resistance in human pancreatic cancer cells. *Oncotarget* **2016**, *7*, 50365–50379. [CrossRef] [PubMed]
183. Wang, X.; Xu, C.; Hua, Y.; Sun, L.; Cheng, K.; Jia, Z.; Han, Y.; Dong, J.; Cui, Y.; Yang, Z. Exosomes play an important role in the process of psoralen reverse multidrug resistance of breast cancer. *J. Exp. Clin. Cancer Res.* **2016**, *35*, 186. [CrossRef]
184. Lv, M.M.; Zhu, X.Y.; Chen, W.X.; Zhong, S.L.; Hu, Q.; Ma, T.F.; Zhang, J.; Chen, L.; Tang, J.H.; Zhao, J.H. Exosomes mediate drug resistance transfer in MCF-7 breast cancer cells and a probable mechanism is delivery of P-glycoprotein. *Tumour. Biol.* **2014**, *35*, 10773–10779. [CrossRef] [PubMed]
185. Bebawy, M.; Combes, V.; Lee, E.; Jaiswal, R.; Gong, J.; Bonhoure, A.; Grau, G.E. Membrane microparticles mediate transfer of P-glycoprotein to drug sensitive cancer cells. *Leukemia* **2009**, *23*, 1643–1649. [CrossRef] [PubMed]

186. Kato, T.; Mizutani, K.; Kameyama, K.; Kawakami, K.; Fujita, Y.; Nakane, K.; Kanimoto, Y.; Ehara, H.; Ito, H.; Seishima, M.; et al. Serum exosomal P-glycoprotein is a potential marker to diagnose docetaxel resistance and select a taxoid for patients with prostate cancer. *Urol. Oncol.* **2015**, *33*, 385.e15–385.e20. [CrossRef]
187. Lu, J.F.; Luk, F.; Gong, J.; Jaiswal, R.; Grau, G.E.; Bebawy, M. Microparticles mediate MRP1 intercellular transfer and the re-templating of intrinsic resistance pathways. *Pharmacol. Res.* **2013**, *76*, 77–83. [CrossRef]
188. Chapuy, B.; Koch, R.; Radunski, U.; Corsham, S.; Cheong, N.; Inagaki, N.; Ban, N.; Wenzel, D.; Reinhardt, D.; Zapf, A.; et al. Intracellular ABC transporter A3 confers multidrug resistance in leukemia cells by lysosomal drug sequestration. *Leukemia* **2008**, *22*, 1576–1586. [CrossRef]
189. Ji, R.; Zhang, B.; Zhang, X.; Xue, J.; Yuan, X.; Yan, Y.; Wang, M.; Zhu, W.; Qian, H.; Xu, W. Exosomes derived from human mesenchymal stem cells confer drug resistance in gastric cancer. *Cell Cycle* **2015**, *14*, 2473–2483. [CrossRef]
190. Khan, S.; Jutzy, J.M.; Valenzuela, M.M.; Turay, D.; Aspe, J.R.; Ashok, A.; Mirshahidi, S.; Mercola, D.; Lilly, M.B.; Wall, N.R. Plasma-derived exosomal survivin, a plausible biomarker for early detection of prostate cancer. *PLoS ONE* **2012**, *7*, e46737. [CrossRef]
191. Kreger, B.T.; Johansen, E.R.; Cerione, R.A.; Antonyak, M.A. The Enrichment of Survivin in Exosomes from Breast Cancer Cells Treated with Paclitaxel Promotes Cell Survival and Chemoresistance. *Cancers* **2016**, *8*, 111. [CrossRef]
192. Liu, D.X.; Li, P.P.; Guo, J.P.; Li, L.L.; Guo, B.; Jiao, H.B.; Wu, J.H.; Chen, J.M. Exosomes derived from HBV-associated liver cancer promote chemoresistance by upregulating chaperone-mediated autophagy. *Oncol. Lett.* **2019**, *17*, 323–331. [CrossRef] [PubMed]
193. Tian, T.; Han, J.; Huang, J.; Li, S.; Pang, H. Hypoxia-Induced Intracellular and Extracellular Heat Shock Protein gp96 Increases Paclitaxel-Resistance and Facilitates Immune Evasion in Breast Cancer. *Front. Oncol.* **2021**, *11*, 784777. [CrossRef]
194. Zhang, Q.; Deng, T.; Zhang, H.; Zuo, D.; Zhu, Q.; Bai, M.; Liu, R.; Ning, T.; Zhang, L.; Yu, Z.; et al. Adipocyte-Derived Exosomal MTTP Suppresses Ferroptosis and Promotes Chemoresistance in Colorectal Cancer. *Adv. Sci.* **2022**, *9*, e2203357. [CrossRef]
195. Wang, H.J.; Qi, Y.J.; Lan, Z.J.; Liu, Q.W.; Xu, J.J.; Zhu, M.X.; Yang, T.T.; Shi, R.L.; Gao, S.G.; Liang, G.F. Exosomal PD-L1 confers chemoresistance and promotes tumorigenic properties in esophageal cancer cells via upregulating STAT3/miR-21. *Gene Ther.* **2023**, *30*, 88–100. [CrossRef]
196. Wang, X.; Cheng, K.; Zhang, G.; Jia, Z.; Yu, Y.; Guo, J.; Hua, Y.; Guo, F.; Li, X.; Zou, W.; et al. Enrichment of CD44 in Exosomes From Breast Cancer Cells Treated With Doxorubicin Promotes Chemoresistance. *Front. Oncol.* **2020**, *10*, 960. [CrossRef] [PubMed]
197. Xia, T.; Tian, H.; Zhang, K.W.; Zhang, S.Y.; Chen, W.H.; Shi, S.; You, Y.W. Exosomal ERp44 derived from ER-stressed cells strengthens cisplatin resistance of nasopharyngeal carcinoma. *BMC Cancer* **2021**, *21*, 1003. [CrossRef] [PubMed]
198. Hashemi, M.; Mirdamadi, M.S.A.; Talebi, Y.; Khaniabad, N.; Banaei, G.; Daneii, P.; Gholami, S.; Ghorbani, A.; Tavakolpournegari, A.; Farsani, Z.M.; et al. Pre-clinical and clinical importance of miR-21 in human cancers: Tumorigenesis, therapy response, delivery approaches and targeting agents. *Pharmacol. Res.* **2023**, *187*, 106568. [CrossRef]
199. Liu, T.; Chen, G.; Sun, D.; Lei, M.; Li, Y.; Zhou, C.; Li, X.; Xue, W.; Wang, H.; Liu, C.; et al. Exosomes containing miR-21 transfer the characteristic of cisplatin resistance by targeting PTEN and PDCD4 in oral squamous cell carcinoma. *Acta Biochim. Biophys. Sin.* **2017**, *49*, 808–816. [CrossRef]
200. Yang, Y.C.; Liu, G.J.; Yuan, D.F.; Li, C.Q.; Xue, M.; Chen, L.J. Influence of exosome-derived miR-21 on chemotherapy resistance of esophageal cancer. *Eur. Rev. Med. Pharmacol.* **2019**, *23*, 1513–1519.
201. Raji, G.R.; Poyyakkara, A.; Krishnan, A.K.; Maurya, A.K.; Changmai, U.; Shankar, S.S.; Kumar, V.B.S. Horizontal Transfer of miR-643 from Cisplatin-Resistant Cells Confers Chemoresistance to Recipient Drug-Sensitive Cells by Targeting APOL6. *Cells* **2021**, *10*, 1341. [CrossRef]
202. Wei, Y.; Lai, X.; Yu, S.; Chen, S.; Ma, Y.; Zhang, Y.; Li, H.; Zhu, X.; Yao, L.; Zhang, J. Exosomal miR-221/222 enhances tamoxifen resistance in recipient ER-positive breast cancer cells. *Breast Cancer Res. Treat.* **2014**, *147*, 423–431. [CrossRef] [PubMed]
203. Bliss, S.A.; Sinha, G.; Sandiford, O.A.; Williams, L.M.; Engelberth, D.J.; Guiro, K.; Isenalumhe, L.L.; Greco, S.J.; Ayer, S.; Bryan, M.; et al. Mesenchymal Stem Cell-Derived Exosomes Stimulate Cycling Quiescence and Early Breast Cancer Dormancy in Bone Marrow. *Cancer Res.* **2016**, *76*, 5832–5844. [CrossRef] [PubMed]
204. Jaiswal, R.; Gong, J.; Sambasivam, S.; Combes, V.; Mathys, J.M.; Davey, R.; Grau, G.E.; Bebawy, M. Microparticle-associated nucleic acids mediate trait dominance in cancer. *FASEB J.* **2012**, *26*, 420–429. [CrossRef] [PubMed]
205. Yang, Q.; Zhao, S.; Shi, Z.; Cao, L.; Liu, J.; Pan, T.; Zhou, D.; Zhang, J. Chemotherapy-elicited exosomal miR-378a-3p and miR-378d promote breast cancer stemness and chemoresistance via the activation of EZH2/STAT3 signaling. *J. Exp. Clin. Cancer Res.* **2021**, *40*, 120. [CrossRef]
206. Liu, X.; Lu, Y.; Xu, Y.; Hou, S.; Huang, J.; Wang, B.; Zhao, J.; Xia, S.; Fan, S.; Yu, X.; et al. Exosomal transfer of miR-501 confers doxorubicin resistance and tumorigenesis via targeting of BLID in gastric cancer. *Cancer Lett.* **2019**, *459*, 122–134. [CrossRef]
207. Comandatore, A.; Immordino, B.; Balsano, R.; Capula, M.; Garajova, I.; Ciccolini, J.; Giovannetti, E.; Morelli, L. Potential Role of Exosomes in the Chemoresistance to Gemcitabine and Nab-Paclitaxel in Pancreatic Cancer. *Diagnostics* **2022**, *12*, 286. [CrossRef]
208. Wang, M.; Qiu, R.; Yu, S.R.; Xu, X.Y.; Li, G.; Gu, R.M.; Tan, C.H.; Zhu, W.; Shen, B. Paclitaxel-resistant gastric cancer MGC-803 cells promote epithelial-to-mesenchymal transition and chemoresistance in paclitaxel-sensitive cells via exosomal delivery of miR-155-5p. *Int. J. Oncol.* **2019**, *54*, 326–338. [CrossRef]
209. Cao, Z.; Xu, L.; Zhao, S. Exosome-derived miR-27a produced by PSC-27 cells contributes to prostate cancer chemoresistance through p53. *Biochem. Biophys. Res. Commun.* **2019**, *515*, 345–351. [CrossRef]

210. Kulkarni, B.; Gondaliya, P.; Kirave, P.; Rawal, R.; Jain, A.; Garg, R.; Kalia, K. Exosome-mediated delivery of miR-30a sensitize cisplatin-resistant variant of oral squamous carcinoma cells via modulating Beclin1 and Bcl2. *Oncotarget* **2020**, *11*, 1832–1845. [CrossRef]
211. Zhao, X.; Li, M.; Dai, X.; Yang, Y.; Peng, Y.; Xu, C.; Dai, N.; Wang, D. Downregulation of exosomal miR-1273a increases cisplatin resistance of non-small cell lung cancer by upregulating the expression of syndecan binding protein. *Oncol. Rep.* **2020**, *44*, 2165–2173. [CrossRef]
212. Qiu, L.; Wang, J.; Chen, M.; Chen, F.; Tu, W. Exosomal microRNA-146a derived from mesenchymal stem cells increases the sensitivity of ovarian cancer cells to docetaxel and taxane via a LAMC2-mediated PI3K/Akt axis. *Int. J. Mol. Med.* **2020**, *46*, 609–620. [CrossRef] [PubMed]
213. Dong, B.; Li, S.; Zhu, S.; Yi, M.; Luo, S.; Wu, K. MiRNA-mediated EMT and CSCs in cancer chemoresistance. *Exp. Hematol. Oncol.* **2021**, *10*, 12. [CrossRef] [PubMed]
214. Jia, Z.; Zhu, H.; Sun, H.; Hua, Y.; Zhang, G.; Jiang, J.; Wang, X. Adipose Mesenchymal Stem Cell-Derived Exosomal microRNA-1236 Reduces Resistance of Breast Cancer Cells to Cisplatin by Suppressing SLC9A1 and the Wnt/beta-Catenin Signaling. *Cancer Manag. Res.* **2020**, *12*, 8733–8744. [CrossRef] [PubMed]
215. Bandari, S.K.; Purushothaman, A.; Ramani, V.C.; Brinkley, G.J.; Chandrashekar, D.S.; Varambally, S.; Mobley, J.A.; Zhang, Y.; Brown, E.E.; Vlodavsky, I.; et al. Chemotherapy induces secretion of exosomes loaded with heparanase that degrades extracellular matrix and impacts tumor and host cell behavior. *Matrix Biol.* **2018**, *65*, 104–118. [CrossRef]
216. Ragusa, M.; Statello, L.; Maugeri, M.; Barbagallo, C.; Passanisi, R.; Alhamdani, M.S.; Li Destri, G.; Cappellani, A.; Barbagallo, D.; Scalia, M.; et al. Highly skewed distribution of miRNAs and proteins between colorectal cancer cells and their exosomes following Cetuximab treatment: Biomolecular, genetic and translational implications. *Oncoscience* **2014**, *1*, 132–157. [CrossRef]
217. Zhao, X.; Yuan, C.; Wangmo, D.; Subramanian, S. Tumor-Secreted Extracellular Vesicles Regulate T-Cell Costimulation and Can Be Manipulated To Induce Tumor-Specific T-Cell Responses. *Gastroenterology* **2021**, *161*, 560–574.e11. [CrossRef]
218. Vautrot, V.; Bentayeb, H.; Causse, S.; Garrido, C.; Gobbo, J. Tumor-Derived Exosomes: Hidden Players in PD-1/PD-L1 Resistance. *Cancers* **2021**, *13*, 4537. [CrossRef]
219. Morrissey, S.M.; Yan, J. Exosomal PD-L1: Roles in Tumor Progression and Immunotherapy. *Trends Cancer* **2020**, *6*, 550–558. [CrossRef]
220. Parsonidis, P.; Papasotiriou, I. Adoptive Cellular Transfer Immunotherapies for Cancer. *Cancer Treat. Res. Commun.* **2022**, *32*, 100575. [CrossRef]
221. Le, I.; Dhandayuthapani, S.; Chacon, J.; Eiring, A.M.; Gadad, S.S. Harnessing the Immune System with Cancer Vaccines: From Prevention to Therapeutics. *Vaccines* **2022**, *10*, 816. [CrossRef]
222. Zhang, Y.; Ge, T.; Huang, M.; Qin, Y.; Liu, T.; Mu, W.; Wang, G.; Jiang, L.; Li, T.; Zhao, L.; et al. Extracellular Vesicles Expressing CD19 Antigen Improve Expansion and Efficacy of CD19-Targeted CAR-T Cells. *Int. J. Nanomed.* **2023**, *18*, 49–63. [CrossRef] [PubMed]
223. Ciravolo, V.; Huber, V.; Ghedini, G.C.; Venturelli, E.; Bianchi, F.; Campiglio, M.; Morelli, D.; Villa, A.; Della Mina, P.; Menard, S.; et al. Potential role of HER2-overexpressing exosomes in countering trastuzumab-based therapy. *J. Cell Physiol.* **2012**, *227*, 658–667. [CrossRef] [PubMed]
224. Aung, T.; Chapuy, B.; Vogel, D.; Wenzel, D.; Oppermann, M.; Lahmann, M.; Weinhage, T.; Menck, K.; Hupfeld, T.; Koch, R.; et al. Exosomal evasion of humoral immunotherapy in aggressive B-cell lymphoma modulated by ATP-binding cassette transporter A3. *Proc. Natl. Acad. Sci. USA* **2011**, *108*, 15336–15341. [CrossRef] [PubMed]
225. Aitamer, M.; Akil, H.; Vignoles, C.; Branchaud, M.; Abraham, J.; Gachard, N.; Feuillard, J.; Jauberteau, M.O.; Shirvani, H.; Troutaud, D.; et al. CD20 expression, TrkB activation and functional activity of diffuse large B cell lymphoma-derived small extracellular vesicles. *Br. J. Cancer* **2021**, *125*, 1687–1698. [CrossRef]
226. Zhang, S.; Zhang, Y.; Qu, J.; Che, X.; Fan, Y.; Hou, K.; Guo, T.; Deng, G.; Song, N.; Li, C.; et al. Exosomes promote cetuximab resistance via the PTEN/Akt pathway in colon cancer cells. *Braz. J. Med. Biol. Res.* **2017**, *51*, e6472. [CrossRef]
227. Wei, Z.; Wang, Z.; Chai, Q.; Li, Z.; Zhang, M.; Zhang, Y.; Zhang, L.; Tang, Q.; Zhu, H.; Sui, H. Exosomes derived from MDR cells induce cetuximab resistance in CRC via PI3K/AKT signaling-mediated Sox2 and PD-L1 expression. *Exp. Ther. Med.* **2023**, *25*, 86. [CrossRef]
228. Huang, W.; Zhang, H.; Tian, Y.; Li, Y.; Li, J.; Zhong, X.; Yuan, X. LncRNA SNHG11 enhances bevacizumab resistance in colorectal cancer by mediating miR-1207-5p/ABCC1 axis. *Anticancer Drugs* **2022**, *33*, 575–586. [CrossRef]
229. Li, C.; Gao, Z.; Cui, Z.; Liu, Z.; Bian, Y.; Sun, H.; Wang, N.; He, Z.; Li, B.; Li, F.; et al. Deubiquitylation of Rab35 by USP32 promotes the transmission of imatinib resistance by enhancing exosome secretion in gastrointestinal stromal tumours. *Oncogene* **2023**, *42*, 894–910. [CrossRef]
230. Hrdinova, T.; Toman, O.; Dresler, J.; Klimentova, J.; Salovska, B.; Pajer, P.; Bartos, O.; Polivkova, V.; Linhartova, J.; Machova Polakova, K.; et al. Exosomes released by imatinib-resistant K562 cells contain specific membrane markers, IFITM3, CD146 and CD36 and increase the survival of imatinib-sensitive cells in the presence of imatinib. *Int. J. Oncol.* **2021**, *58*, 238–250. [CrossRef]
231. Wu, S.C.; Luo, M.; To, K.K.W.; Zhang, J.Y.; Su, C.Y.; Zhang, H.; An, S.N.; Wang, F.; Chen, D.; Fu, L.W. Intercellular transfer of exosomal wild type EGFR triggers osimertinib resistance in non-small cell lung cancer. *Mol. Cancer* **2021**, *20*, 17. [CrossRef]

232. Hisakane, K.; Seike, M.; Sugano, T.; Yoshikawa, A.; Matsuda, K.; Takano, N.; Takahashi, S.; Noro, R.; Gemma, A. Exosome-derived miR-210 involved in resistance to osimertinib and epithelial-mesenchymal transition in EGFR mutant non-small cell lung cancer cells. *Thorac. Cancer* **2021**, *12*, 1690–1698. [CrossRef] [PubMed]
233. Jing, C.W.; Cao, H.X.; Qin, X.B.; Yu, S.R.; Wu, J.Z.; Wang, Z.; Ma, R.; Feng, J.F. Exosome-mediated gefitinib resistance in lung cancer HCC827 cells via delivery of miR-21. *Oncol. Lett.* **2018**, *15*, 9811–9817. [CrossRef] [PubMed]
234. Azuma, Y.; Yokobori, T.; Mogi, A.; Yajima, T.; Kosaka, T.; Iijima, M.; Shimizu, K.; Shirabe, K.; Kuwano, H. Cancer exosomal microRNAs from gefitinib-resistant lung cancer cells cause therapeutic resistance in gefitinib-sensitive cells. *Surg. Today* **2020**, *50*, 1099–1106. [CrossRef] [PubMed]
235. Lunavat, T.R.; Cheng, L.; Einarsdottir, B.O.; Bagge, R.O.; Muralidharan, S.V.; Sharples, R.A.; Lasser, C.; Gho, Y.S.; Hill, A.F.; Nilsson, J.A.; et al. BRAF(V600) inhibition alters the microRNA cargo in the vesicular secretome of malignant melanoma cells. *Proc. Natl. Acad. Sci. USA* **2017**, *114*, E5930–E5939. [CrossRef]
236. Wang, X.; Cheng, Q. Suppression of exosomal hsa_circ_0001005 eliminates the Vemurafenib resistance of melanoma. *J. Cancer Res. Clin. Oncol.* **2023**, *149*, 5921–5936. [CrossRef]
237. Schlungbaum, W.; Griszat, H.; Krüger, R. Biologische Wirkung energiereicher Strahlen. In *Medizinische Strahlenkunde: Eine Einführung in die Physikalischen, Technischen und Biologischen Grundlagen der Medizinischen Strahlenanwendung für Mediziner, Medizinisch-Technische Radiologieassistentinnen und -Assistenten*; De Gruyter: Berlin, Germany, 1993. [CrossRef]
238. Cheema, A.K.; Hinzman, C.P.; Mehta, K.Y.; Hanlon, B.K.; Garcia, M.; Fatanmi, O.O.; Singh, V.K. Plasma Derived Exosomal Biomarkers of Exposure to Ionizing Radiation in Nonhuman Primates. *Int. J. Mol. Sci.* **2018**, *19*, 3427. [CrossRef] [PubMed]
239. Jabbari, N.; Nawaz, M.; Rezaie, J. Ionizing Radiation Increases the Activity of Exosomal Secretory Pathway in MCF-7 Human Breast Cancer Cells: A Possible Way to Communicate Resistance against Radiotherapy. *Int. J. Mol. Sci.* **2019**, *20*, 3649. [CrossRef]
240. Lespagnol, A.; Duflaut, D.; Beekman, C.; Blanc, L.; Fiucci, G.; Marine, J.C.; Vidal, M.; Amson, R.; Telerman, A. Exosome secretion, including the DNA damage-induced p53-dependent secretory pathway, is severely compromised in TSAP6/Steap3-null mice. *Cell Death Differ.* **2008**, *15*, 1723–1733. [CrossRef]
241. Yu, X.; Harris, S.L.; Levine, A.J. The regulation of exosome secretion: A novel function of the p53 protein. *Cancer Res.* **2006**, *66*, 4795–4801. [CrossRef]
242. Tang, Y.; Cui, Y.; Li, Z.; Jiao, Z.; Zhang, Y.; He, Y.; Chen, G.; Zhou, Q.; Wang, W.; Zhou, X.; et al. Radiation-induced miR-208a increases the proliferation and radioresistance by targeting p21 in human lung cancer cells. *J. Exp. Clin. Cancer Res.* **2016**, *35*, 7. [CrossRef]
243. Jiang, M.J.; Chen, Y.Y.; Dai, J.J.; Gu, D.N.; Mei, Z.; Liu, F.R.; Huang, Q.; Tian, L. Dying tumor cell-derived exosomal miR-194-5p potentiates survival and repopulation of tumor repopulating cells upon radiotherapy in pancreatic cancer. *Mol. Cancer* **2020**, *19*, 68. [CrossRef] [PubMed]
244. Mrowczynski, O.D.; Madhankumar, A.B.; Sundstrom, J.M.; Zhao, Y.; Kawasawa, Y.I.; Slagle-Webb, B.; Mau, C.; Payne, R.A.; Rizk, E.B.; Zacharia, B.E.; et al. Exosomes impact survival to radiation exposure in cell line models of nervous system cancer. *Oncotarget* **2018**, *9*, 36083–36101. [CrossRef] [PubMed]
245. Sun, T.; Yin, Y.F.; Jin, H.G.; Liu, H.R.; Tian, W.C. Exosomal microRNA-19b targets FBXW7 to promote colorectal cancer stem cell stemness and induce resistance to radiotherapy. *Kaohsiung J. Med. Sci.* **2022**, *38*, 108–119. [CrossRef] [PubMed]
246. Luo, Y.; Ma, J.; Liu, F.; Guo, J.; Gui, R. Diagnostic value of exosomal circMYC in radioresistant nasopharyngeal carcinoma. *Head Neck* **2020**, *42*, 3702–3711. [CrossRef]
247. Wang, X.; Cao, Q.; Shi, Y.; Wu, X.; Mi, Y.; Liu, K.; Kan, Q.; Fan, R.; Liu, Z.; Zhang, M. Identification of low-dose radiation-induced exosomal circ-METRN and miR-4709-3p/GRB14/PDGFRalpha pathway as a key regulatory mechanism in Glioblastoma progression and radioresistance: Functional validation and clinical theranostic significance. *Int. J. Biol. Sci.* **2021**, *17*, 1061–1078. [CrossRef]
248. Abramowicz, A.; Wojakowska, A.; Marczak, L.; Lysek-Gladysinska, M.; Smolarz, M.; Story, M.D.; Polanska, J.; Widlak, P.; Pietrowska, M. Ionizing radiation affects the composition of the proteome of extracellular vesicles released by head-and-neck cancer cells in vitro. *J. Radiat. Res.* **2019**, *60*, 289–297. [CrossRef]
249. Khan, S.; Jutzy, J.M.; Aspe, J.R.; McGregor, D.W.; Neidigh, J.W.; Wall, N.R. Survivin is released from cancer cells via exosomes. *Apoptosis* **2011**, *16*, 1–12. [CrossRef]
250. Zhang, Z.B.; Yu, X.H.; Zhou, Z.; Li, B.; Peng, J.W.; Wu, X.; Luo, X.J.; Yang, L.F. LMP1-positive extracellular vesicles promote radioresistance in nasopharyngeal carcinoma cells through P38 MAPK signaling. *Cancer Med.* **2019**, *8*, 6082–6094. [CrossRef]
251. Mutschelknaus, L.; Peters, C.; Winkler, K.; Yentrapalli, R.; Heider, T.; Atkinson, M.J.; Moertl, S. Exosomes Derived from Squamous Head and Neck Cancer Promote Cell Survival after Ionizing Radiation. *PLoS ONE* **2016**, *11*, e0152213. [CrossRef]
252. Strybel, U.; Marczak, L.; Zeman, M.; Polanski, K.; Mielanczyk, L.; Klymenko, O.; Samelak-Czajka, A.; Jackowiak, P.; Smolarz, M.; Chekan, M.; et al. Molecular Composition of Serum Exosomes Could Discriminate Rectal Cancer Patients with Different Responses to Neoadjuvant Radiotherapy. *Cancers* **2022**, *14*, 993. [CrossRef]
253. Payton, C.; Pang, L.Y.; Gray, M.; Argyle, D.J. Exosomes Derived from Radioresistant Breast Cancer Cells Promote Therapeutic Resistance in Naive Recipient Cells. *J. Pers. Med.* **2021**, *11*, 1310. [CrossRef] [PubMed]
254. Arscott, W.T.; Tandle, A.T.; Zhao, S.; Shabason, J.E.; Gordon, I.K.; Schlaff, C.D.; Zhang, G.; Tofilon, P.J.; Camphausen, K.A. Ionizing radiation and glioblastoma exosomes: Implications in tumor biology and cell migration. *Transl. Oncol.* **2013**, *6*, 638–648. [CrossRef] [PubMed]

255. Ni, J.; Bucci, J.; Malouf, D.; Knox, M.; Graham, P.; Li, Y. Exosomes in Cancer Radioresistance. *Front. Oncol.* **2019**, *9*, 869. [CrossRef] [PubMed]
256. Chen, F.Y.; Xu, B.; Li, J.; Yang, X.; Gu, J.J.; Yao, X.J.; Sun, X.C. Hypoxic tumour cell-derived exosomal miR-340-5p promotes radioresistance of oesophageal squamous cell carcinoma via KLF10. *J. Exp. Clin. Cancer Res.* **2021**, *40*, 38. [CrossRef] [PubMed]
257. Jella, K.K.; Rani, S.; O'Driscoll, L.; McClean, B.; Byrne, H.J.; Lyng, F.M. Exosomes are involved in mediating radiation induced bystander signaling in human keratinocyte cells. *Radiat. Res.* **2014**, *181*, 138–145. [CrossRef] [PubMed]
258. Xu, S.; Wang, J.; Ding, N.; Hu, W.; Zhang, X.; Wang, B.; Hua, J.; Wei, W.; Zhu, Q. Exosome-mediated microRNA transfer plays a role in radiation-induced bystander effect. *RNA Biol.* **2015**, *12*, 1355–1363. [CrossRef] [PubMed]
259. Tian, W.; Yin, X.; Wang, L.; Wang, J.; Zhu, W.; Cao, J.; Yang, H. The key role of miR-21-regulated SOD2 in the medium-mediated bystander responses in human fibroblasts induced by alpha-irradiated keratinocytes. *Mutat. Res.* **2015**, *780*, 77–85. [CrossRef] [PubMed]
260. Mo, L.J.; Song, M.; Huang, Q.H.; Guan, H.; Liu, X.D.; Xie, D.F.; Huang, B.; Huang, R.X.; Zhou, P.K. Exosome-packaged miR-1246 contributes to bystander DNA damage by targeting LIG4. *Br. J. Cancer* **2018**, *119*, 492–502. [CrossRef] [PubMed]
261. Song, M.; Wang, Y.; Shang, Z.F.; Liu, X.D.; Xie, D.F.; Wang, Q.; Guan, H.; Zhou, P.K. Bystander autophagy mediated by radiation-induced exosomal miR-7-5p in non-targeted human bronchial epithelial cells. *Sci. Rep.* **2016**, *6*, 30165. [CrossRef]
262. Al-Mayah, A.; Bright, S.; Chapman, K.; Irons, S.; Luo, P.; Carter, D.; Goodwin, E.; Kadhim, M. The non-targeted effects of radiation are perpetuated by exosomes. *Mutat. Res.* **2015**, *772*, 38–45. [CrossRef]
263. Rodgers, K.; Jadhav, S.S. The application of mesenchymal stem cells to treat thermal and radiation burns. *Adv. Drug Deliv. Rev.* **2018**, *123*, 75–81. [CrossRef] [PubMed]
264. Liu, H.; Liang, Z.; Wang, F.; Zhou, C.; Zheng, X.; Hu, T.; He, X.; Wu, X.; Lan, P. Exosomes from mesenchymal stromal cells reduce murine colonic inflammation via a macrophage-dependent mechanism. *JCI Insight* **2019**, *4*, e131273. [CrossRef] [PubMed]
265. Domenis, R.; Cifu, A.; Quaglia, S.; Pistis, C.; Moretti, M.; Vicario, A.; Parodi, P.C.; Fabris, M.; Niazi, K.R.; Soon-Shiong, P.; et al. Pro inflammatory stimuli enhance the immunosuppressive functions of adipose mesenchymal stem cells-derived exosomes. *Sci. Rep.* **2018**, *8*, 13325. [CrossRef] [PubMed]
266. Gao, S.; Chen, T.; Hao, Y.; Zhang, F.; Tang, X.; Wang, D.; Wei, Z.; Qi, J. Exosomal miR-135a derived from human amnion mesenchymal stem cells promotes cutaneous wound healing in rats and fibroblast migration by directly inhibiting LATS2 expression. *Stem Cell Res. Ther.* **2020**, *11*, 56. [CrossRef]
267. Jiang, X.; Jiang, X.; Qu, C.; Chang, P.; Zhang, C.; Qu, Y.; Liu, Y. Intravenous delivery of adipose-derived mesenchymal stromal cells attenuates acute radiation-induced lung injury in rats. *Cytotherapy* **2015**, *17*, 560–570. [CrossRef]

2.2.6 SUMMARY

In summary, the evaluation of putative exosome isolates by fluorescence microscopy and quantification, TRPS, DLS, cryo-TEM, protein and lipid quantification, and western blot provides all data required by the *MISEV2023* guidelines to validate the respective exosome isolation. Single particle characterization revealed round-shaped, membrane-bilayer coated particles with a mean size of 104 ± 44,3 nm (TRPS) or 112 ± 48,2 nm (DLS) respectively, which is in accordance with typical exosome morphology and size. In cell culture supernatant, the CD63-emGFP exosome marker signal was detectable by fluorescence microscopy and quantification. Particle quantification revealed a particle concentration of 7,89 x 10^{10} particles/mL, 4,38 µg/µL protein content, and 288,51 µg/mL lipid content, though protein content was most likely overestimated due to methodical difficulties. Western blot analysis revealed the presence of overexpressed exosome marker CD63 and endogenous exosome markers CD81 and TSG101, while ER and nucleus markers were (almost) absent. Thus, it can be concluded that the applied UC protocol is suitable for isolation of high purity exosomes, and isolates generated as such will be referred to as exosomes hereafter.

2.3 HNSCC Model Cell Lines for Cisplatin Resistance

As previously discussed, chemoresistance is a major obstacle in the successful treatment of different cancer entities, including HNSCC. Cisplatin represents a suitable model drug for studying chemoresistant HNSCC, as it is a widely used chemotherapeutic, and many patients show a high initial treatment response, however relapses with resistant tumors are common as well (Jou and Hess 2017, Alsahafi et al. 2019). To investigate the role of exosomes in chemoresistant HNSCC, the HPV-negative FaDu model cell line was used. FaDu cells were originally generated from a squamous cell carcinoma of the hypopharynx (Rangan 1972). To increase comparability, single-cell clones of the FaDu cell line were generated to constitute the homogenous $FaDu^{WT}$ cell line. The cisplatin-resistant $FaDu^{CisR}$ cell line was generated by treatment of $FaDu^{WT}$ cells with sublethal cisplatin concentrations (3-5 µM) for 6 months, and subsequent culture in the presence of 3 µM cisplatin, thus provoking the acquisition of heterogeneous mutations by constant mutagen exposure as expected to occur in treated patients. For more details on the generation of the FaDu sub-cell lines refer to section 2.3.3.

2.3.1 Characterization of the Model Cell Lines

The established FaDu sub-cell lines were characterized regarding their morphology and protein marker expression. Both cell lines show comparable morphology and growth in small “islands”, as observed by bright-field microscopy (Figure 20A). Regular passaging revealed that $FaDu^{CisR}$ cells proliferate approximately 50 % slower than $FaDu^{WT}$, even when selective cisplatin pressure is relieved (Data not shown). Since FaDu cells have an epithelial origin, expression of epithelial marker protein EpCAM was tested. EpCAM is readily detectable in both sub-cell lines by fluorescence microscopy (Figure 20B). Furthermore, the expression of known resistance markers was analysed by qPCR. Therefore, cells were seeded in 10 cm dishes at defined numbers and RNA was extracted after 72h. For $FaDu^{CisR}$ cells, the possible influence of cisplatin treatment (3 µM) during the 72h incubation period was considered as well. As shown in Figure 20C, $FaDu^{CisR}$ cells show a significantly decreased expression of ERCC3, a member of the excision repair complex. The decreased expression was detectable regardless of cisplatin treatment before RNA extraction. This is rather counter-intuitive, as cisplatin-resistant cells usually show increased DNA repair activity. However, there are numerous other proteins and pathways relevant to DNA repair, which may play a superior role in this specific model. It is already known that HNSCC chemoresistance is rather based on a shifted balance of DNA repair protein expression, than the expression of a specific singular protein (Bold et al. 2021). Birc5, a member of the inhibitors of apoptosis (IAP) family, is expressed at quite similar levels in both

sub-cell lines. Unfortunately, the standard deviation of Birc5 expression is high in FaDu^{CisR} cells, which may have hampered statistical analysis. As a protein contributing to apoptosis evasion, increased expression of Birc5 has been reported in resistant cells. But like for DNA repair, there are numerous other possible routes of apoptosis evasion that might be at play in FaDu^{CisR} cells.

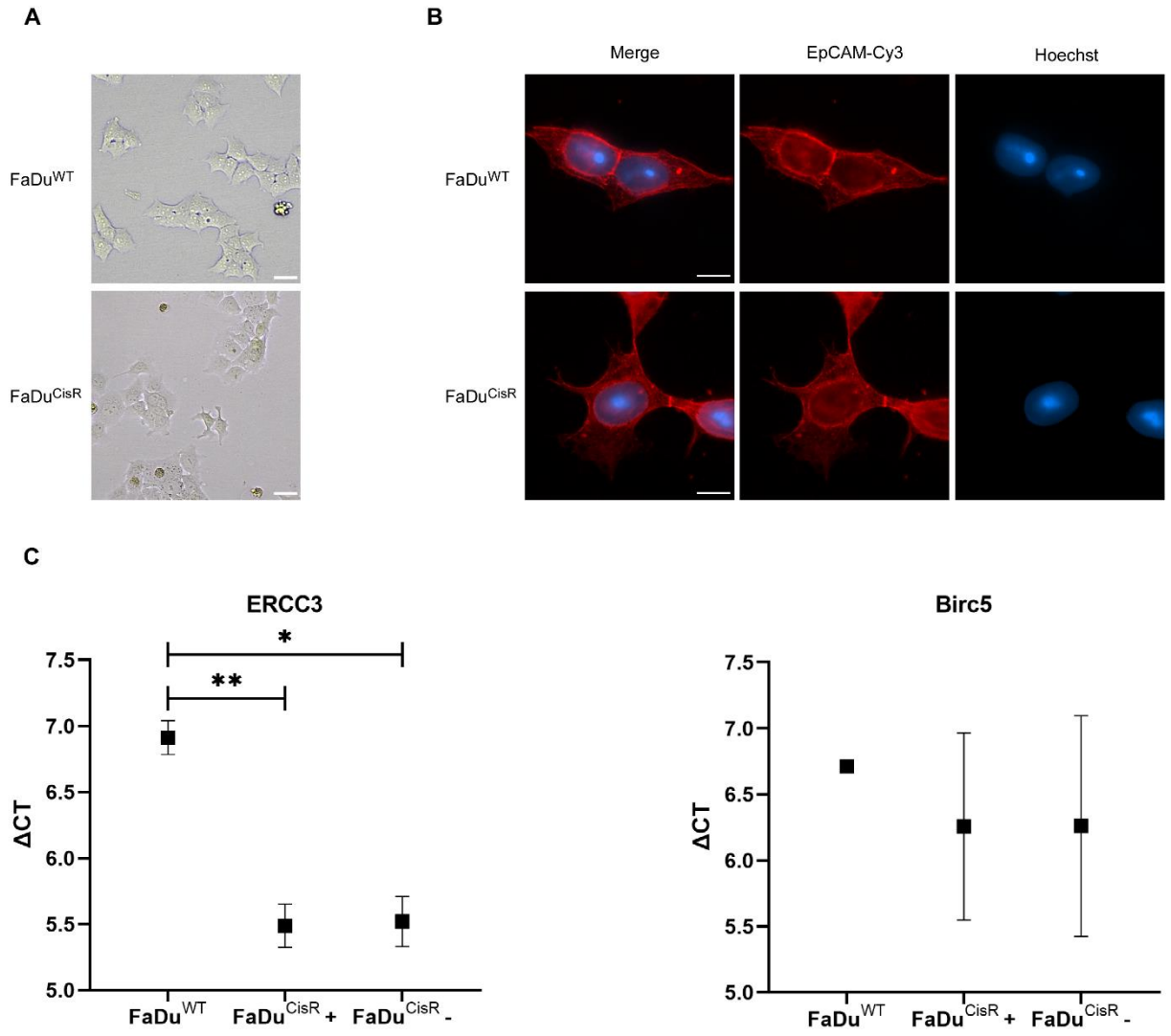

Figure 20. Characterization of newly established FaDu sub-cell lines
A) Representative bright-field images of FaDu^{WT} and FaDu^{CisR} cells. Images were taken 2 days after regular passaging in T25 maintenance flasks. Scale bars 20 µm. **B)** Representative fluorescence microscopy images of FaDu^{WT} and FaDu^{CisR} cells. Cells were grown in microscopy dishes for 24h and then fixed and stained with primary antibody against EpCAM and Cy3-labeled secondary antibody. Nuclei were stained with Hoechst. Scale bars 10 µm. **C)** FaDu cells were seeded at 10^6 cells in 10 cm cell culture dishes. Fadu^{CisR} cells were either treated with 3 µM cisplatin (+) or kept in medium without cisplatin (-). FaDu^{WT} cells were not treated with cisplatin. After 72h, RNA was extracted and transcribed to cDNA for qPCR analysis. cDNA quality was checked by running reactions with and without reverse transcriptase, and subsequent PCR for housekeeping gene actin-ß. Mean ΔCT ± SD of n=3 independent experiments. Statistical analysis by two-way ANOVA and Tukey's multiple comparisons test. * $p < 0,05$; ** $p < 0,01$.

2.3.2 Response of the Model Cell Lines to Cisplatin

To evaluate whether the established FaDu^{CisR} cells were indeed a suitable model for cisplatin resistance, their response to cisplatin treatment was tested using different cell culture techniques and readouts. Assaying the viability in a standard 2D format revealed significantly increased cisplatin tolerance of FaDu^{CisR} cells compared to FaDu^{WT} cells, even at high concentrations (Figure 21A). Applying 3D spheroid culture additionally verified an increased cisplatin tolerance of FaDu^{CisR} cells, even after prolonged cisplatin treatment of 7 days (Figure 21B). In order to determine the effect of cisplatin on the molecular level, induction of DNA double-strand breaks was assayed microscopically. Therefore, the marker protein γH2AX, the phosphorylated form of the histone H2A family member X, was stained. Phosphorylation of H2AX at serine 139 correlates with the amount of DNA double-strand breaks, and has been used for its quantification in several studies (Rogakou et al. 1998, Meyer et al. 2013, Rothkamm et al. 2015). FaDu^{WT} cells treated with 20 µM cisplatin show significant γH2AX staining, while there is no γH2AX detectable in untreated cells, thus proving that cisplatin toxicity is at least partially based on DNA damage in this model (Figure 21C). Additionally, nuclei of cisplatin-treated cells appear larger in comparison to untreated controls. Swelling of the nucleus is characteristic of necrotic cell death (Kwon et al. 2015). Thus, this observation could hint at necrosis or necroptosis as the underlying cell death mechanism.

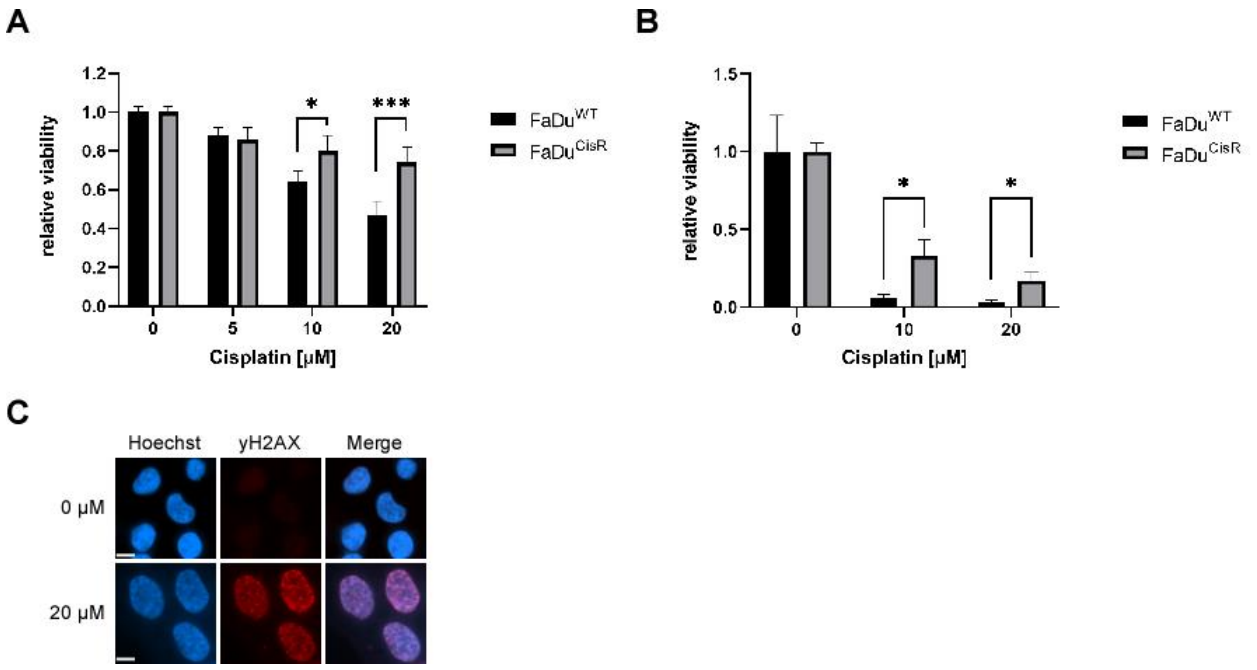

Figure 21. Viability of FaDu sub-cell lines in response to cisplatin
A) Relative viability of FaDu sub-cell lines after 72h of cisplatin treatment as determined by CTG assay. Cells were seeded at defined numbers in 96-well plates and allowed to attach for 24h before onset of treatment. **B)** Relative viability of FaDu spheroids after 7 days of cisplatin treatment as determined by CTG 3D assay. Spheroids were seeded at defined numbers and allowed to form for three days before onset of treatment. **C)** Representative fluorescence microscopy images of cisplatin-induced DNA damage. $FaDu^{WT}$ cells were seeded in microscopy dishes and treated with 0 µM or 20 µM cisplatin for 24h. Then, cells were fixed and stained with Hoechst, primary antibody against γH2AX, and Cy3-labelled secondary antibody. Cells were imaged with fixed exposure times. Scale bars 10 µM.All viability data is given as Mean ± SD of n=3 independent experiments and was normalized to 0 µM controls. Statistical analysis of viability in 2D by two-way ANOVA and Tukey's multiple comparisons test. Statistical analysis of spheroid viability by multiple t-tests and correction for multiple comparisons using the Holm-Sidak method. * $p < 0,05$; *** $p < 0,005$

Beyond viability analysis, spheroids were also evaluated for phenotypic parameters using HCS as described in section 2.1.2, revealing a significantly decreased relative spheroid area in both sub-cell lines in response to cisplatin treatment (Figure 22A). The effect is already visible after four days of treatment in $FaDu^{WT}$, and becomes even more drastic after 7 days, while $FaDu^{CisR}$ only show a significantly decreased spheroid area after 7 days of treatment. Likewise, cisplatin-treated spheroids tend to have a less spherical shape regardless of the sub-cell line, but not to a statistically significant extent (Figure 22B). Even though $FaDu^{WT}$ spheroids display a significantly decreased viability after 10 days of cisplatin treatment, spheroids do not disintegrate, as illustrated by Figure 22C. Nevertheless, especially four days after onset of cisplatin treatment (d7c4) $FaDu^{WT}$ spheroids appear more affected than $FaDu^{CisR}$ spheroids based on the ragged spheroid margin. Spheroid relative intensity generally decreases over time but is not influenced by cisplatin treatment (Supplementary Figure 2). The general decrease in intensity can be

attributed to the increasing cell density as the spheroids grow, resulting in an increased light absorption and subsequent loss of intensity. This is also apparent when looking at the microscopy images, where day 10 spheroids appear darker than those on day three (Figure 22C). Overall, these findings highlight that phenotypic features do not reflect the viability of the spheroids, but can provide additional relevant information.

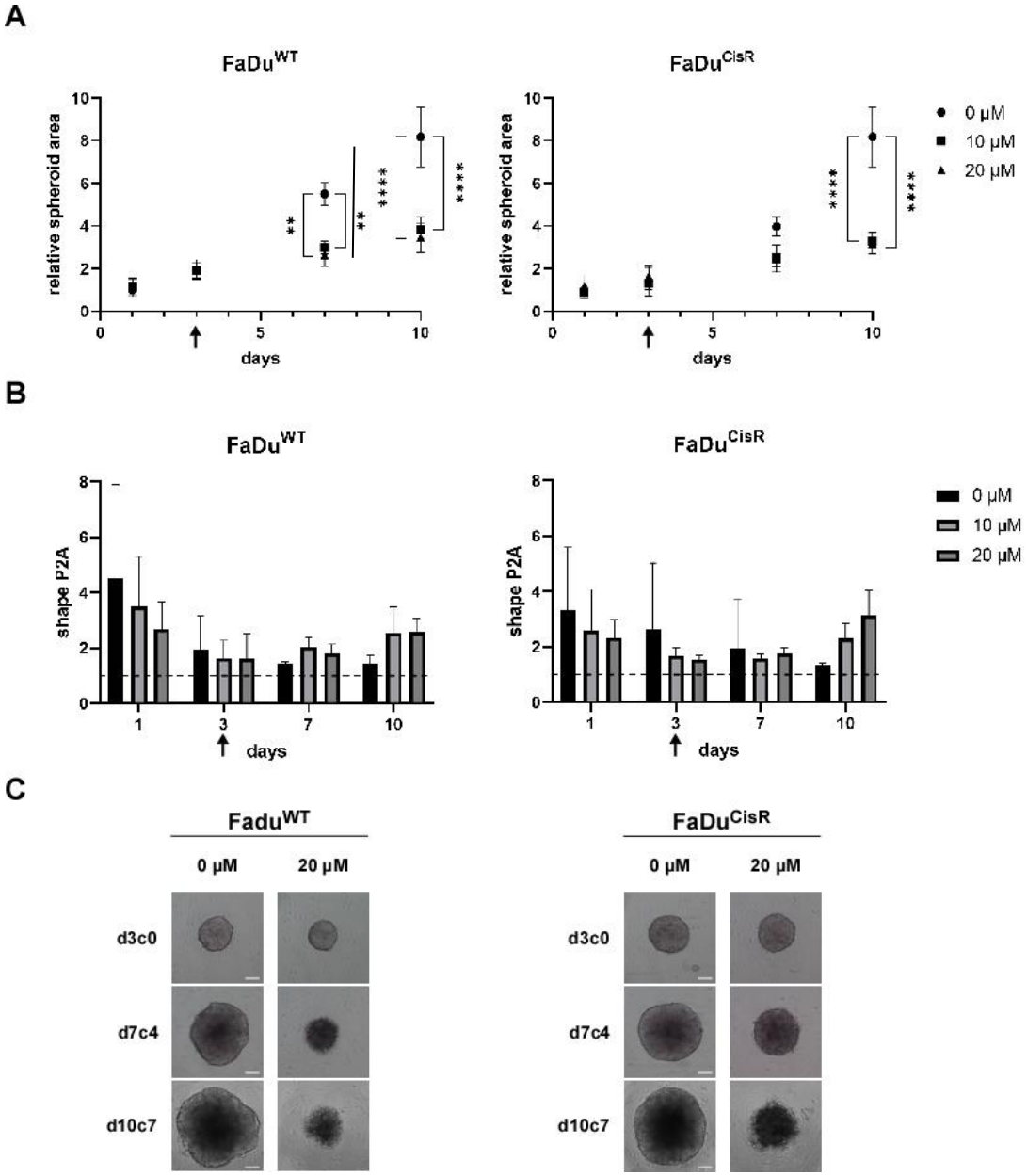

Figure 22. Phenotypic screening of FaDu sub-cell line spheroids in response to cisplatin
A) Relative spheroid area of FaDu spheroids as measured by HCS over 10 days. Data was normalized to day one. Arrows mark beginning of cisplatin treatment. **B)** Shape P2A of FaDu spheroids as measured by HCS over 10 days. Dashed line marks P2A = 1, which equals a perfectly round shape. Arrows mark beginning of cisplatin treatment. **C)** Representative bright-field images of FaDu spheroids in response to cisplatin treatment. d ≙ days since seeding; c ≙ days of cisplatin treatment. Scale bars 50 µm. All data is given as Mean ± SD of n=2 independent experiments. Statistical analysis by two-way ANOVA and Tukey's multiple comparisons test. ** $p < 0,01$; **** $p < 0,001$

2.3.3 A Head and Neck Cancer Spheroid Model for Phenotypic High-Content Screening of Chemoresistance (Book Chapter)

Madita Wandrey, Aya Khamis Hassan, Roland H. Stauber, Désirée Gül

Abstract

Resistances against common treatment regimens like chemotherapy are a major concern in current cancer research and clinical disease management. Moreover, *in vitro* cell culture models cannot always adequately represent the tumor situation *in vivo*, hampering the analysis of the underlying mechanisms. Efforts have been made to establish three-dimensional cancer cell models, such as spheroids or organoids, mimicking the *in vivo* situation of the tumor more closely. Here, we describe the establishment of a three-dimensional spheroid model of head and neck squamous cell carcinoma (HNSCC) allowing for the study of chemoresistance. The analysis of relevant phenotypic readouts by a high-content screening platform enables the objective evaluation and monitoring of spheroids during chemotherapeutic treatment. This model also represents a starting point for the evaluation of a precision medicine-based management of HNSCC patients.

1. Introduction

Head and neck squamous cell carcinoma (HNSCC) is among the ten most common cancer types worldwide. Unfortunately, the 5-year survival rate of patients with advanced disease is only 20%, with 50% of patients developing invasion and metastasis. This is often facilitated by the development of resistances against established treatments [1,2]. Thus, the improvement of traditional treatment strategies, as well as the establishment of novel approaches is urgently needed. To this end, image-based high-content screening (HCS) of *in vitro* cell models is a favorable approach. Modeling resistance to chemotherapeutic drugs in cancer cell lines can be achieved by different means. Inherited or spontaneous mutations can be modeled by directed genetic modifications, whereas resistance with a broad mutational load can be acquired by prolonged exposure to sub-lethal drug doses [3].

Traditionally, cells are cultured as adherent monolayers on flat, two-dimensional (2D) surfaces, which inherently bears significant differences from the situation *in vivo* [4,5]. Within a tumor, cells grow in three-dimensional (3D) structures and constantly engage in communication with neighboring cells and components of the tumor microenvironment. This microarchitecture results in differences in the availability of oxygen, nutrients, or drugs depending on the specific location of the individual cells within the 3D structure. Cultivating cells in 3D cultures, so-called spheroids, gives a better representation of this situation *in vitro*. Additionally, the surrounding cell-cell contacts within spheroids enable cells to develop polarity [6-8]. Such models have already been successfully applied to discover novel treatment regimens to overcome cisplatin resistance [9]. At the same time, 3D cell culture models also allow for a variety of novel phenotypic readouts. Aside from marker expression and cell viability, morphological properties like spheroid shape, volume, diameter, translucency, integrity, and growth kinetics can be assessed. Using image-based HCS platforms, all these

parameters can be analyzed automatically on single spheroid level, enabling the identification of novel drugs or adjuvants, and their effects on the spheroid phenotype (Figure 1) [10].

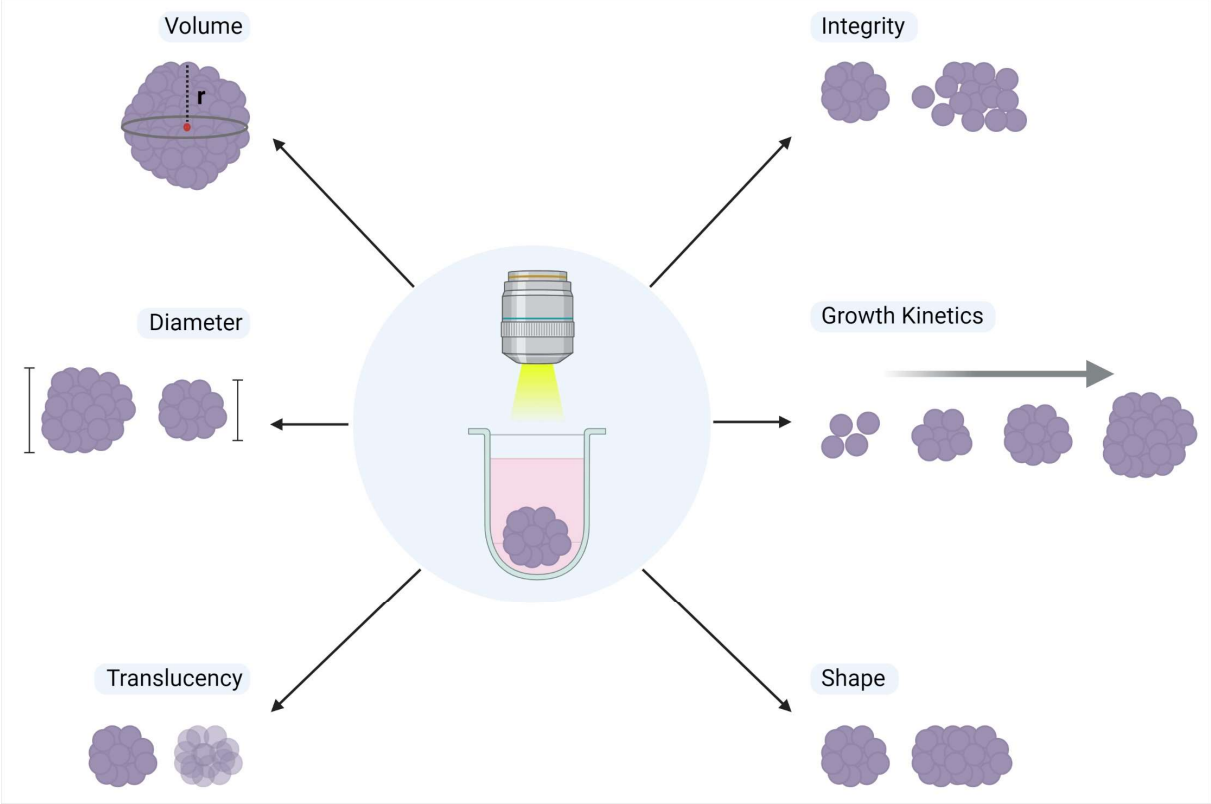

Figure 1: Assessment of phenotypic spheroid properties by high-content screening (HCS) microscopy. Created with BioRender.com.

As a tool for the analysis of chemoresistance, we generated a cisplatin-resistant cell model based on the established human hypopharyngeal squamous cell carcinoma cell line FaDu ($FaDu^{CisR}$). $FaDu^{CisR}$ cells, as well as $FaDu^{WT}$ control cells were used for the generation of 3D spheroids representing a suitable *in vitro* model to analyze the acquisition and maintenance of cellular chemotherapy resistance. We performed a multi-parametric readout of phenotypic properties in response to standard cisplatin treatment using the image-based HCS platform Array Scan VTI, and combined these results with the measurement of cell viability in a 96-well plate format. This model also represents a starting point for the further establishment of HNSCC patient-derived organoids, bridging the gap between *in vivo* and *in vitro* approaches.

2. Materials

2.1 Cell culture and generation of cisplatin-resistant cells

1. HNSCC cell line: FaDu (ATCC-HTB43)
2. Dulbecco's Modified Eagle's Medium (DMEM) containing 4.5 g/L D-Glucose and no Pyruvate, supplemented with 10% fetal calf serum (FCS), 2 mM L-glutamine, 100 U/mL penicillin, and 100 μg/mL streptomycin
3. Trypsin solution
4. Phosphate-buffered saline (PBS) composed of 144 mg/L Potassium Phosphate monobasic, 9000 mg/L Sodium Chloride, and 795 mg/L Sodium Phosphate dibasic. pH 7.4
5. Dimethyl sulfoxide (DMSO)
6. Sterile cell culture flasks, 10 cm dishes, 96-well plates, 24-well plates, pipets, and filter papers
7. Water bath
8. Cell counting device
9. Humidified cell culture incubator set to 37 °C and 5% CO_2
10. Microscope
11. Mycoplasma testing kit or service provider
12. Clinical grade cisplatin (*see* **Note 1**)

2.2 Generation and Assay of spheroids

1. Ultra Low Attachment Round Bottom 96-well cell culture plates (Corning)
2. HCS microscopy platform (Cellomics Array Scan VTI (700 series), Thermo Fisher Scientific) and corresponding data acquisition and analysis software (Cellomics iDEV

Version 7.6.3.1, Thermo Fisher Scientific) or comparable platform providing automated brightfield live cell imaging with 5x objective and corresponding software allowing for phenotypic analysis of three-dimensional structures in regards to object shape and area

3. CellTiter-Glo® 3D Cell Viability Assay (Promega) or comparable viability assay suitable for three-dimensional cell structures
4. Opaque 96-well cell culture plates
5. Horizontal shaker
6. Luminometer or plate reader capable of luminescence readout

3. Methods

FaDu cells should be in culture for at least two weeks and checked for contamination with mycoplasma prior to starting spheroid generation. Standard culture conditions are 37 °C and 5% CO_2 in a humidified atmosphere. Cells should be passaged at least twice a week and medium needs to be exchanged every three to four days.

3.1 Generation of homogenous FaDu^{WT} and cisplatin-resistant FaDu^{CisR} cell lines

To ensure the generation of a homogeneous cell population with uniform resistance characteristics, FaDu single cell clones are prepared as starting material for the FaDu^{WT} sub-cell line. FaDu^{WT} cells are used to establish the cisplatin-resistant FaDu^{CisR} sub-cell line.

3.1.1 Generation of FaDu^{WT} from single cell clones

1. Seed FaDu cells into 10 cm cell culture dishes in serial dilutions (*see* **Note 2**).
2. Over the course of 7-10 days, check cells microscopically for cluster generation from single cells.
3. To separate the cell clusters, wash the plate with PBS and place sterile filter papers soaked in Trypsin on the separate clusters (*see* **Note 3**).

4. After incubation at 37 °C for 5 min, transfer the filter papers and any attached cells to a 24-well plate with fresh medium.
5. After another 7-10 days in culture, check the cells microscopically for successful proliferation and transfer promising populations to cell culture vessels with increasing surface area (*see* **Note 4**).

3.1.2 Generation of FaDu^{CisR} by cisplatin selection

1. Seed FaDu^{WT} cells from section 3.1.1 in a fresh T25-flask and treat with 5 μM cisplatin, which is corresponding to IC90 as determined by cell viability assay.
2. Keep Cells in culture under these conditions for four weeks, and exchange medium every three to four days. Monitor proliferation of clusters closely by microscopy and passage cells whenever they reach 80-90% confluency. Add fresh cisplatin whenever medium is exchanged or cells are passaged.
3. After four weeks, keep the surviving cells under constant selection pressure using 3 μM cisplatin.
4. To ensure a stable resistance phenotype, culture cells for at least 6 months before starting experiments (*see* **Note 5**).

3.2 General protocol for generation and culture of spheroids from FaDu cells

1. Thaw cells from cryo stocks by placing them in a 37 °C water bath until no ice remains in the cell solution.
2. Add FCS in a 5:1 ration and spin down the cells at 500 xg for 5 min.
3. Discard the supernatant and resuspend the cells in medium, then add them to a T25 cell culture flask. Add 3 μM cisplatin for FaDu^{CisR}.
4. Keep cells in culture for one week, then check for mycoplasma contamination.

5. If cells are contamination-free, culture them to 80-90% confluency, then remove medium and wash with PBS once.
6. After addition of trypsin solution, incubate cells at room temperature until they are fully detached (up to 5 min).
7. Resuspend the cells in medium, then count and dilute them to 5,000 cells/mL.
8. Add 200 µL of cell suspension per well to an Ultra Low Attachment Round Bottom 96-well cell culture plate, resulting in a final number of 1,000 cells/well.
9. Keep cells under standard culture conditions (*see* **Note 6**), uniformly shaped spheroids are formed within three days (*see* **Note 7**).
10. Exchange medium every three to four days (*see* **Note 8**).

3.3 Phenotypic HCS of cisplatin-treated spheroids

To assess whether the resistance acquisition has any impact on the reaction to cisplatin treatment on a phenotypic level, $FaDu^{WT}$ and $FaDu^{CisR}$ spheroids are treated with different concentrations of cisplatin for multiple days and analyzed on single spheroid level. Assessment of therapy adjuvants (e.g. Vitamin D) or other chemotherapeutic drugs (e.g. oxaliplatin) can be carried out accordingly.

3.3.1 Spheroid treatment

1. Allow FaDu^{WT} and FaDu^{CisR} spheroids to form for three days prior to treatment.
2. Treat spheroids with different concentrations of cisplatin (*see* **Note 8**) and assay by HSC microscopy for up to 10 days.

3.3.2 HCS microscopy and data analysis

1. Start the iDEV software and load the plate into the device.
2. Select the BioApplication *Morphology V4* and continue to *Configure Acquisition.*
3. Configure the image acquisition by selecting the 5x objective, ORCA-ER camera configuration and standard acquisition camera mode. Set number of channels to 1.
4. For channel specific parameters, select *Brightfield* as detection mode and *XF100 – BRIGHTFIELD* as dye.
5. In the exposure settings, select *Fixed Exposure Time* as exposure type (*see* **Note 9**) and tick the box for *Use This Channel For Autofocus*.
6. Select *AutoFocus* as autofocus camera mode and set the step size to 16.8.
7. For acquisition, set the form factor to the specific plate type you are using.
8. Select one well and autofocus on it. Then acquire an image and save the field for analysis. Repeat this step for one well of each treatment/cell type of the experiment (*see* **Note 10**).
9. Continue to *Configure Assay Parameters* and configure as many groups as there are different treatments/cell types in the experiment and assign the corresponding saved fields from the previous step.
10. For image preprocessing, select *Dark* for the object type and tick the box for background removal using the method *LowPassFilter* with a value of 99.

11. For primary object identification, tick the box for thresholding using the method *Isodata* with a value of 1E -5. Also tick the box for object cleanup.
12. For primary object validation, select the features *Object.BorderObject* (*see* **Note 11**), *Object.ShapeP2A,* and *Object.TotalIntensity*. For *Object.ShapeP2A* the range is set to 0 to 20.
13. Set scan limits to a maximum of one field per well and a minimum of one object per well.
14. Select all possible features to store and save the protocol for further use.
15. Continue to the scan settings and select the appropriate scan area (all wells containing spheroids) and set field pattern type to spiral with starting field 1 (central field), then start the scan.
16. Export all relevant data (in this case shape P2A and object area) to excel or any comparable analysis software.
17. Figure 2C shows example results for spheroid area and shape P2A (*see* **Note 12**) after 10 days of treatment with different cisplatin concentrations (*see* **Note 13**).

3.4 Viability assay for spheroids

To validate the acquired cisplatin resistance of FaDu^{CisR} cells in 3D spheroid culture, spheroids are assayed for their viability using a commercial kit.

1. Place the CellTiter-Glo® 3D Cell Viability reagent at 4 °C overnight.
2. Equilibrate the reagent to room temperature 30 min prior to the assay.
3. Add one volume of the reagent equal to the volume of cell culture medium to each well and mix by pipetting.
4. Incubate on a horizontal shaker at 225 rpm for 5 min in the dark.

5. Incubate at room temperature for 25 min in the dark.

6. Transfer cell solution to an opaque 96-well plate.

7. Measure luminescence (*see* **Note 14**).

8. Example results after 10 days of treatment with different cisplatin concentrations are shown in Figure 2B (*see* **Note 13**).

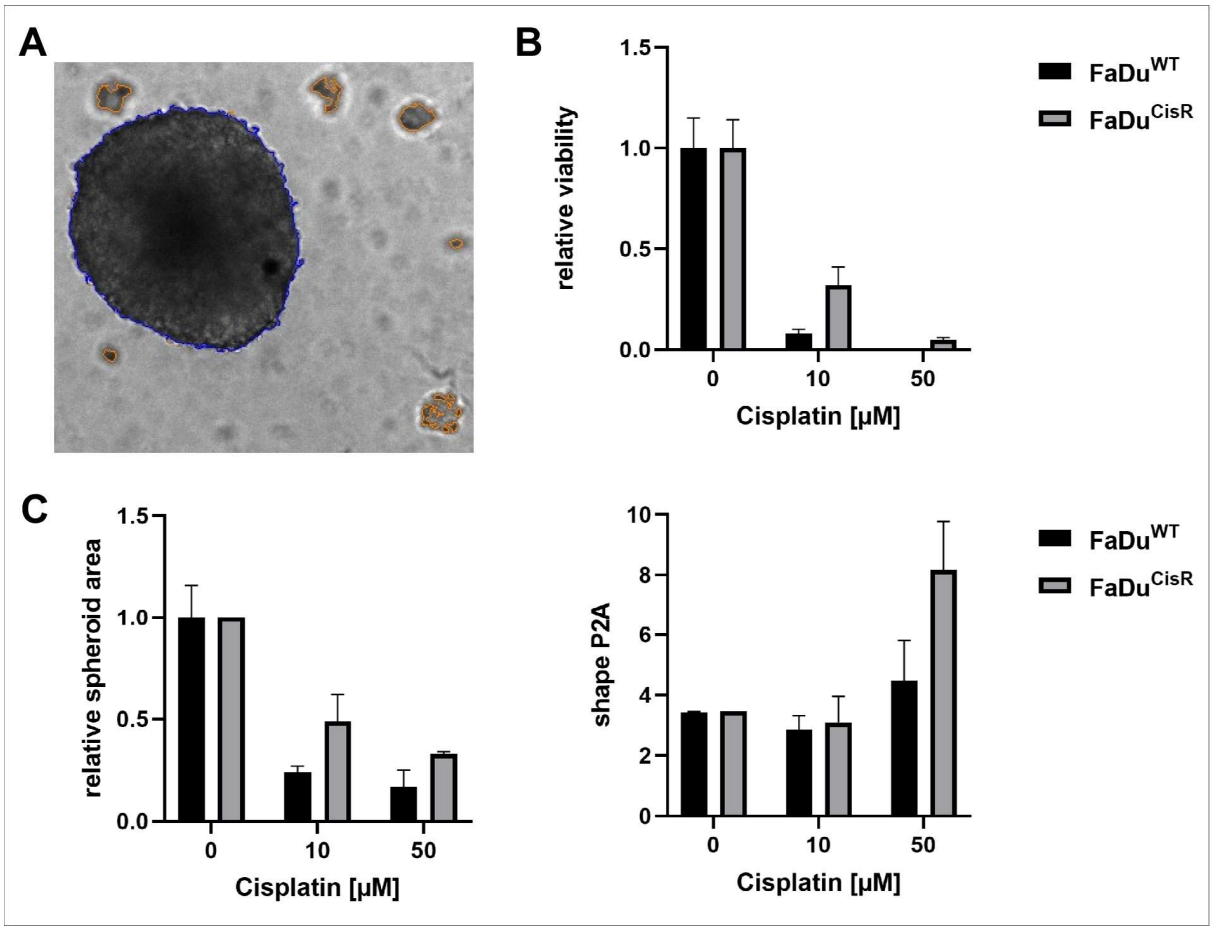

Figure 2: Phenotypic screening of FaDuWT and FaDuCisR spheroids after cisplatin treatment. A) Example image acquired by automated HCS platform. Valid objects are marked in blue, identified objects that did not pass object validation are marked in orange. B) Relative viability as determined by CellTiter-Glo® 3D assay after 10 days of cisplatin treatment. Data was normalized to untreated controls (0 µM). C) Analysis of phenotypic spheroid parameters (area and shape P2A) after 10 days of cisplatin treatment. Spheroid area was normalized to untreated controls (0 µM). All data are shown as mean ± SD of 1-4 biological replicates.

4. Notes

1. Cisplatin stock solution of 1 mg/mL in 0.9% sodium chloride should be stored at -20 °C in aliquots. Do not thaw and refreeze.
2. Start with 5000 cells per 10 cm dish and prepare serial two-fold dilutions thereof.
3. Clusters should have a minimum distance of 2 cm from another.
4. Whenever cells reach ~90% confluency, they can be transferred to a new vessel. We advise to go from 24-well to 12-well, to 6-well, to T25-flask.
5. Regularly preparing cryo-stocks of the sub-cell line during this period is advised, e.g. after 4, 12, and 24 weeks of selection. Stocks are prepared in FCS containing 10% DMSO. Regular validation of cisplatin resistance using viability assays (e.g. CellTiter-Glo® 2.0) is advised.
6. During the initial spheroid formation phase (three days) both, $FaDu^{WT}$ and $FaDu^{CisR}$ spheroids, are cultured in medium without cisplatin.
7. Spheroids should have a round shape (P2A < 2) without any obvious inclusions (non-cellular structures, dark spots) and a diameter of ≥ 200 μm.
8. For medium exchanges or addition of treatments, aspirate and replace ~50% of the total volume within the well. When adding medium containing treatment remember to account for the two-fold dilution after addition to the plate.
9. To define the exposure time during the initial protocol setup, use the auto expose function during acquisition. Then fix the exposure time to the automatically optimized time.
10. As cell type and treatment can influence the phenotypic properties of the spheroids, it is advisable to save one field for each cell type ($FaDu^{WT}$, $FaDu^{CisR}$) and treatment (0 μM, 10 μM, and 50 μM cisplatin) combination and check whether the defined parameters

result in satisfactory object validation for all conditions. In our example, this would result in 6 saved fields/groups.

11. This function ensures that objects intersecting the field border are excluded, which is important to ensure proper measurement of morphological features like shape or area. If the experimental focus is e.g. translucency or stained markers this function might not be necessary.
12. Shape P2A describes the ratio of the perimeter (P) to the area (A) of the validated object using the following formula:

$$P2A = \frac{P^2}{4\pi A}$$

If P2A = 1 the object is perfectly circular.

13. FaDu^{CisR} spheroids show higher viability when treated with cisplatin across both tested concentrations, as expected (Figure 2B). They also elicit a higher spheroid area, indicating continued proliferation during cisplatin treatment as opposed to FaDu^{WT} (Figure 2C). At high cisplatin concentrations (50 μM) all spheroids start to disintegrate and lose their spherical shape due to increased cell death.
14. In our experiment we used an integration time of 1000 ms for the luminescence measurement, however the optimal time might vary based on the specific device used.

5. References

1. Ferlito A, Shaha AR, Silver CE, Rinaldo A, Mondin V (2001) Incidence and sites of distant metastases from head and neck cancer. ORL J Otorhinolaryngol Relat Spec 63 (4):202-207. doi:10.1159/000055740

2. Jemal A, Siegel R, Ward E, Hao Y, Xu J, Murray T, Thun MJ (2008) Cancer statistics, 2008. CA Cancer J Clin 58 (2):71-96. doi:10.3322/CA.2007.0010

3. Siemer S, Fauth T, Scholz P, Al-Zamel Y, Khamis A, Gul D, Freudelsperger L, Wollenberg B, Becker S, Stauber RH, Hagemann J (2021) Profiling Cisplatin Resistance in Head and Neck Cancer: A Critical Role of the VRAC Ion Channel for Chemoresistance. Cancers (Basel) 13 (19). doi:10.3390/cancers13194831

4. Zhu J, Liu B, Wang Z, Wang D, Ni H, Zhang L, Wang Y (2019) Exosomes from nicotine-stimulated macrophages accelerate atherosclerosis through miR-21-3p/PTEN-mediated VSMC migration and proliferation. Theranostics 9 (23):6901-6919. doi:10.7150/thno.37357

5. Guo BB, Bellingham SA, Hill AF (2016) Stimulating the Release of Exosomes Increases the Intercellular Transfer of Prions. J Biol Chem 291 (10):5128-5137. doi:10.1074/jbc.M115.684258

6. Ravi M, Paramesh V, Kaviya SR, Anuradha E, Solomon FD (2015) 3D cell culture systems: advantages and applications. J Cell Physiol 230 (1):16-26. doi:10.1002/jcp.24683

7. Ma HL, Jiang Q, Han S, Wu Y, Cui Tomshine J, Wang D, Gan Y, Zou G, Liang XJ (2012) Multicellular tumor spheroids as an in vivo-like tumor model for three-dimensional imaging of chemotherapeutic and nano material cellular penetration. Mol Imaging 11 (6):487-498

8. Kim JB (2005) Three-dimensional tissue culture models in cancer biology. Semin Cancer Biol 15 (5):365-377. doi:10.1016/j.semcancer.2005.05.002

9. Khamis A, Gul D, Wandrey M, Lu Q, Knauer SK, Reinhardt C, Strieth S, Hagemann J, Stauber RH (2022) The Vitamin D Receptor-BIM Axis Overcomes Cisplatin Resistance in Head and Neck Cancer. Cancers (Basel) 14 (20). doi:10.3390/cancers14205131

10. Koll L, Gul D, Elnouaem MI, Raslan H, Ramadan OR, Knauer SK, Strieth S, Hagemann J, Stauber RH, Khamis A (2023) Exploiting Vitamin D Receptor and Its Ligands to Target

Squamous Cell Carcinomas of the Head and Neck. Int J Mol Sci 24 (5).

doi:10.3390/ijms24054675

2.3.4 SUMMARY

In summary, the established FaDu sub-cell lines do not differ macroscopically and still possess epithelial characteristics based on EpCAM expression. When looking at the expression of cisplatin resistance-relevant proteins ERCC3 and Birc5, ERCC3 is significantly decreased in $FaDu^{CisR}$ cells, while there is no significant difference in Birc5 expression. An acquired cisplatin resistance of $FaDu^{CisR}$ cells could be verified by viability assay in 2D and 3D cell culture. Evaluation of phenotypic spheroid parameters revealed a negative impact of cisplatin treatment on spheroid area, which is apparent after four days in $FaDu^{WT}$ and after 7 days in $FaDu^{CisR}$ cells. Spherical shape also shows a tendency to be negatively affected by cisplatin treatment. Macroscopically, effects of cisplatin treatment appear as ragged spheroid margins on day four of treatment in $FaDu^{WT}$ and on day 7 of treatment in $FaDu^{CisR}$ spheroids. Overall these results confirm that the established FaDu sub-cell lines are a suitable model to investigate cisplatin resistance in HNSCC cells.

2.4 Transcriptomic Characterization of HNSCC Exosomes

Intercellular communication via exosomes is largely attributed to the exosomes' content. Besides their specific lipid membrane composition, exosomes can contain DNA, RNA, proteins, and metabolites (Valadi et al. 2007, Waldenstrom et al. 2012, Elzanowska et al. 2021, Harmati et al. 2021). In the context of chemotherapy resistance, a lot of research has focussed on exosomal ncRNAs, especially miRNAs, and could already identify biomarker candidates among them (Hosseini et al. 2022, Mezher et al. 2023). However, when characterizing tissues or cells, it is more common to analyze the gene expression, i.e. coding RNAs. Since there is little data on the coding RNAs contained in exosomes and their potential role in cisplatin resistance, we chose to focus on coding RNAs contained in exosomes, identifying novel cisplatin resistance biomarker candidates.

2.4.1 Exosomal RNA Content

Total RNA of FaDu^{WT} and FaDu^{CisR} exosomes (Exo^{WT} and Exo^{CisR}) was extracted and analyzed from three independent experiments per group. A total of 16.953 genes was detected after exclusion of those found in less than two of the 6 total samples. Of these genes, 1.811 were upregulated and 1.380 were downregulated in Exo^{CisR}, when considering a $\log_2$ fold change > $\left|1{,}5\right|$ and adjusted p-value < 0,05 as significant (Figure 23A). The 40 most regulated genes according to mean z-scores are shown in Figure 23B.

Notably, the three most upregulated genes in Exos^{CisR} are lncRNAs. Among the coding RNAs upregulated in Exo^{CisR} are several genes with known association to cancer and chemotherapy resistance. Translationally controlled tumor protein 1 (TPT1) is associated with cisplatin resistance in lung cancer cells (Wang et al. 2018). Tissue inhibitor of matrix metalloprotease 1 (TIMP1) overexpression could be associated with gemcitabine resistance and poor overall survival in pancreatic cancer (Tan et al. 2021). TIMP1 levels in saliva and serum have also been suggested as prognostic markers for HNSCC patients. High serum TIMP1 levels are significantly associated with poorer overall and progression-free survival. Saliva TIMP1 levels are significantly higher in tumor patients compared to healthy controls, and high pre-treatment saliva TIMP1 levels could be correlated with poor disease-free survival (Ruokolainen et al. 2005, Carpen et al. 2019, Rinecker et al. 2022). Sperm-associated antigen 9 (SPAG9) expression is positively correlated with mesenchymal markers (Slug and N-cadherin) in endometrial cancer tissue, while SPAG9 knock-down results in enhanced cytotoxicity of paclitaxel (Zhang et al. 2016, Jagadish et al. 2018).

Among the 20 most downregulated genes in Exo^{CisR} is only one ncRNA. Coding RNAs include cyclin-dependent kinase 8 (CDK8), which is known to be involved in EMT via the Wnt/β-catenin pathway (Xu et al. 2015). Overexpression of CDK8 could be associated with short overall survival in laryngeal squamous cell carcinoma (Li et al. 2017). p21-activated kinases (PAKs), including PAK2, are known to be overexpressed in HNSCC cell lines and tumor tissue. Knock-down of PAK2 could be associated with reduced migration and invasion (Park et al. 2015). Integrin-β 6 (ITGB6) is overexpressed in oral cancer tissues and contributes to EMT via TGF-β1 (Zhang et al. 2024). Given their pro-tumor activity, it seems surprising that these genes are expressed at lower levels in Exo^{CisR}. However, exosomal expression levels are not necessarily reflective of the cellular expression. In fact, when looking at the gene expression of FaDu cells from previous work in our lab (Siemer 2021), neither of the three discussed genes is found to be significantly regulated (Supplementary Table 3). Thus it seems that the cisplatin-resistant phenotype of $FaDu^{CisR}$ cells rather influences the specific mRNA packaging into exosomes than the overall expression of these genes.

To check whether certain pathways are enriched or decreased in Exo^{CisR}, reactome analysis was performed, again considering those genes with a $\log_2$ fold change > $|1{,}5|$ and adjusted p-value < 0,05. While there was no clear overrepresentation of pathways in the downregulated genes (FDR > 0,4), the 10 most relevant pathways overrepresented in the upregulated genes are displayed in Table 4. Five pathways can be summarized as immunoregulatory pathways, as they involve interferons (IFNs), cytokines, and interleukin-10. IFNγ has been shown to increase the amount of exosomal PD-L1 shed by melanoma cells (Chen et al. 2018). PD-L1 is overexpressed in many tumors and functions as a suppressor of the immune response (Fan et al. 2022). Exosomal RNAs involved in IFNγ signalling could thus contribute to therapy resistance by facilitating immune evasion. Likewise, IFNα is a cytokine with diverse functions in cancer-related immune response. While it has been used as drug to treat different cancer malignancies, there are also reports of IFNα eliciting immunosuppressive effects (Vidal 2020). Exosomal transmission of RNAs related to IFNα signalling could contribute to a shift towards pro-tumor functions.

Strikingly, four pathways related to mitochondrial RNA processing are also overrepresented in Exo^{CisR}. Mitochondria are involved in the regulation of many vital cellular processes, including energy production, ROS generation, and apoptosis. Shifts in these processes can have considerable consequences (Wallace 2012). As introduced, cisplatin leads to DNA adducts that interfere with DNA function and replication. This is not only true for gDNA, but also for mtDNA. Indeed, mtDNA is especially sensitive to cisplatin-induced DNA damage as it lacks nucleotide excision repair (Cullen et al. 2007). Thus, modifications of mitochondrial pathways could be a

means of protection against cisplatin toxicity. Another common observation in cancer cells is a shift to energy production by “aerobic glycolysis”, which is independent of mitochondria. Opposed to its discoverer’s hypothesis, this so-called Warburg effect is not caused by dysfunctional mitochondria, but rather reflects a metabolic reprogramming that facilitates sustained proliferation and malignant progression of cancer cells (Vaupel and Multhoff 2021). Inhibition of the Warburg effect has been associated with increased cisplatin sensitivity in tongue squamous cell carcinoma, proposing another mechanism of mitochondrial involvement in cisplatin resistance (Liu et al. 2024). Transmission of RNAs related to mitochondrial RNA processing via exosomes could thus contribute to the modification of mitochondrial pathways in the recipient cell, increasing its cisplatin tolerance.

Overrepresentation of genes involved in the endosomal pathway seems generally plausible in exosomes. Their upregulation in Exo^{CisR} compared to Exo^{WT} could hint at a mechanism to increase exosome biogenesis in recipient cells. As introduced, resistant cells typically shed more exosomes than their sensitive counterparts, and export of active drugs via exosomes has been proposed as a resistance mechanism (Safaei et al. 2005, Kong et al. 2015, Wandrey et al. 2023). Thus, modifying the endosomal pathway in recipient cells via exosomal RNA transmission could contribute to resistance acquisition.

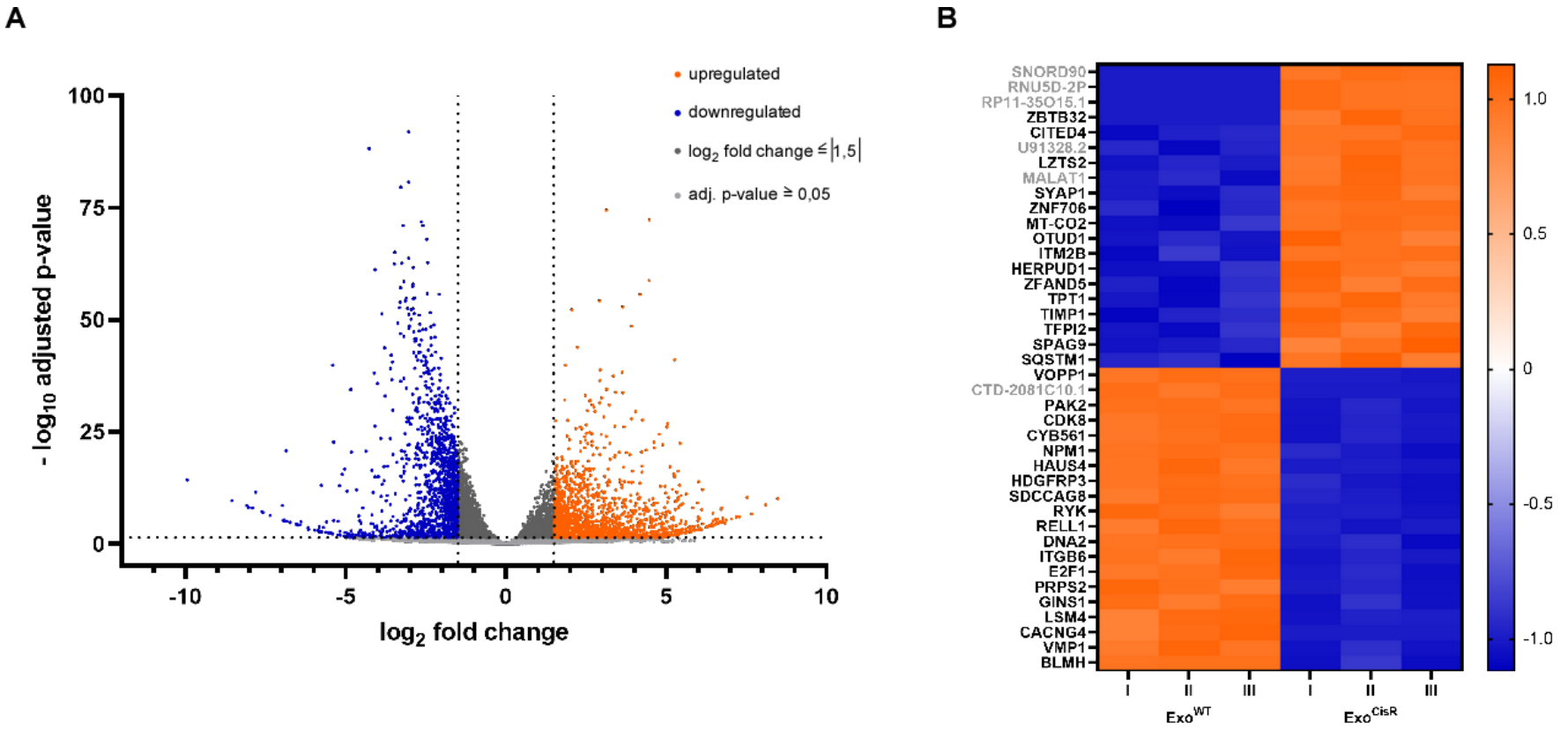

Figure 23. Overview of exosomal RNA content
A) Volcano plot of log_2 fold change against $-log_{10}$ adjusted p-value of FaDu^{CisR} exosomes (Exo^{CisR}) compared to FaDu^{WT} exosomes (Exo^{WT}). A total of 16.953 genes are displayed. Genes were considered significantly regulated if the log_2 fold change > |1,5| and the adjusted p-value < 0,05. **B)** Heatmap analysis of the 40 highest regulated (20 up-, 20 downregulated) genes according to mean z-score. Non-coding RNAs and sequence entries without specific information available (U91328.2) are greyed out.

Table 4. Reactome analysis of genes upregulated (log2 fold change > 1,5) in Exo^{CisR}
The 10 most relevant pathways sorted by p-value are displayed. Statistical analysis by hypergeometric distribution test with correction for multiple testing using the Benjamini-Hochberg method. Analysis was performed using https://reactome.org.

Pathway Name	Entities				Reactions	
	found	ratio	p-value	FDR	found	ratio
Interferon alpha/beta signaling	71/129	0,008	1,11 E-16	2,10 E-16	22/25	0,002
Interferon signaling	111/397	0,025	8,59 E-13	8,12 E-10	69/119	0,008
FASTK family protein regulation and processing of mitochondrial RNAs	15/19	0,001	7,61 E-8	4,72 E-5	4/4	2,67 E-4
Interferon gamma signalling	53/177	0,011	1,00 E-7	4,72 E-5	13/23	0,002
Cytokine signaling in immune system	210/1.099	0,07	1,37 E-7	5,16 E-5	401/785	0,052
Mitochondrial RNA degradation	16/30	0,002	4,57 E-6	0,001	9/10	6,67 E-4
Mitochondrial tRNA processing	19/45	0,003	1,63 E-5	0,004	3/3	2,00 E-4
Endosomal/vacuolar pathway	10/15	9,60 E-4	4,48 E-5	0,011	4/4	2,67 E-4
Interleukin-10 signaling	27/86	0,006	5,82 E-5	0,012	10/15	0,001
Mitochondrial rRNA processing	16/40	0,003	1,35 E-5	0,026	6/6	4,00 E-4

2.4.2 Probing Exosomal RNA Content for Cisplatin Resistance Markers

To find out whether the RNA content of HNSCC exosomes can be exploited as biomarker of cisplatin resistance, cisplatin resistance candidate genes were compiled by literature review (Kelland 2007, Rottenberg et al. 2021). Out of the 99 identified candidate genes, 78 were found in the exosome samples (for full list see Supplementary Table 1), and 45 were significantly regulated in Exo^{CisR} (Figure 24). Interestingly, the majority (28 genes) are downregulated in Exo^{CisR}. A possible explanation for this observation would be a reduction of exosomal packaging to increase the intracellular mRNA abundance and thus expression, resulting in increased cellular cisplatin resistance. A similar effect was already proposed in the previous section.

Among the upregulated genes in Exo^{CisR} is ERCC3, which was shown to be downregulated in FaDu^{CisR} cells (Figure 20). This could hint at increased exosomal packaging of ERCC3 mRNA as the reason behind the differential expression between FaDu^{WT} and FaDu^{CisR}, as well as Exo^{WT} and Exo^{CisR}. Baseline expression could be alike in the donor cells, but differential packaging in exosomes leads to the significant differences in cellular and exosomal abundance. ERCC3 is a member of the excision repair complex, and increased DNA repair activity is a contributing factor in chemotherapy resistance. Uptake of Exo^{CisR} could increase ERCC3 expression in recipient cells, and thus facilitate increased chemotherapy resistance. Likewise, the other 16 upregulated genes in Exo^{CisR} could contribute to the transmission of a cisplatin-resistant phenotype.

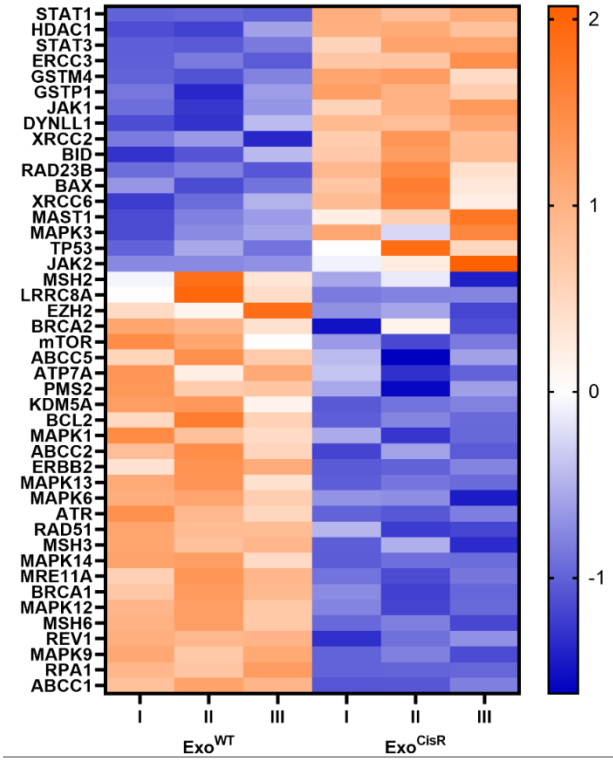

Figure 24. Heatmap analysis of cisplatin resistance candidate genes
Candidate genes were identified by literature review and filtered for those significantly regulated in Exo^{CisR}. Sequencing data is displayed as z-scores. For full list of candidate genes and normalized counts refer to Supplementary Table 1.

Whether the regulated cisplatin resistance markers found in Exo^{CisR} are applicable in a clinical setting remains to be verified, but the compiled list poses a promising starting point for further studies *in vitro* and *in vivo*, and clinical relevance was already probed using *The Cancer Genome Atlas* (TCGA) database (see section 2.4.4).

2.4.3 Probing Exosomal RNA Content for EMT- and CSC-Markers

As introduced, EMT is an important process for the gain of migratory potential, favouring CTC shedding and metastasis. Furthermore, it is also associated with a CSC phenotype, which often elicits higher tolerance to chemotherapeutic treatment (Quail and Joyce 2013, Kisoda et al. 2022). Therefore, exosomal RNA content was analyzed for EMT and CSC candidate genes compiled by literature review (Seton-Rogers 2016, Dongre and Weinberg 2019), investigating the potential involvement of exosomes in the transmission of a more mesenchymal phenotype and exploring the possibility to exploit exosomes as biomarkers for EMT.

Of the 25 probed EMT candidate genes (for full list see Supplementary Table 2), 10 were significantly regulated between Exo^{WT} and Exo^{CisR} (Figure 25). Strikingly, all four mesenchymal markers are upregulated in Exo^{CisR}, though there is considerable heterogeneity among the triplicates. Of the 6 epithelial markers, 50 % are up- and 50 % downregulated in Exo^{CisR}. Considering the overall EMT marker expression (Supplementary Figure 3A) Exo^{WT} represent a more epithelial phenotype, while Exo^{CisR} lean more towards mesenchymal, though both most likely represent intermediate EMT types, as all probed markers were expressed.

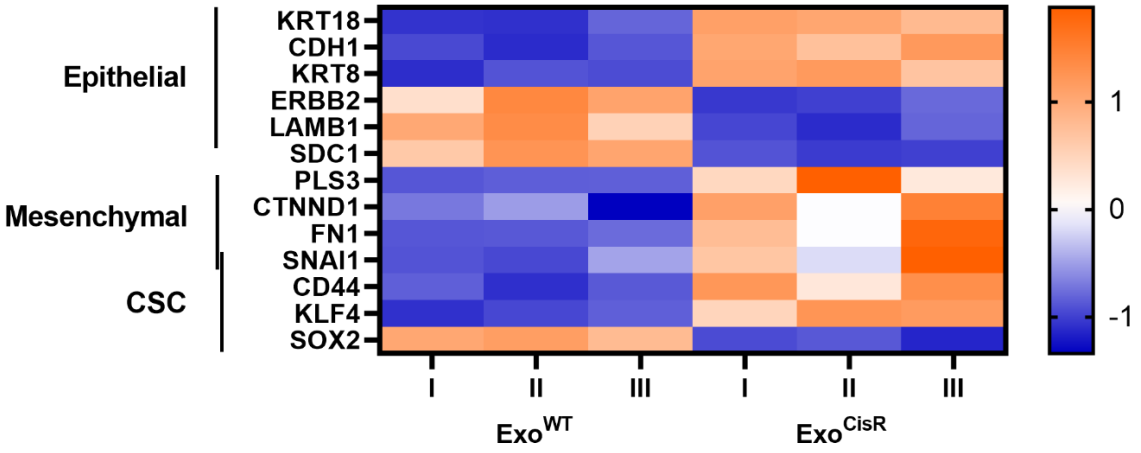

Figure 25. Heatmap analysis of EMT and CSC candidate genes
Candidate genes were identified by literature review and filtered for those significantly regulated in Exo^{CisR}. Sequencing data is displayed as z-scores. For full list of candidate genes and normalized counts refer to Supplementary Table 2.

Probing for 15 CSC candidate genes (for full list see Supplementary Table 2) revealed only four significantly regulated genes in Exo^{CisR}, and one of them (SNAI1) is also considered a mesenchymal marker. Since three of the four genes are upregulated in Exo^{CisR} and they generally show higher expression of CSC markers (Supplementary Figure 3B), they could hold the potential to transmit a CSC phenotype by mRNA delivery.

Involvement of exosomes in EMT stimulation has already been reported, mainly focussing on miRNAs and proteins (Kim et al. 2020, Babaei et al. 2022). The results presented here show that exosomal transmission of coding RNAs could be another contributing factor in triggering EMT in recipient cells, and thus facilitating increased migratory potential, therapy resistance, and a CSC phenotype.

2.4.4 Probing Identified Exosomal RNA Markers for Clinical Relevance

To evaluate the clinical potential of the most regulated genes in Exo^{CisR}, publicly available gene expression and survival data was obtained from *The Cancer Genome Atlas* (TCGA) database, filtering for HNSCC patients with residual disease or remission after primary therapy. Out of the 40 most regulated genes found in FaDu exosomes (Figure 23), only four show a significant influence on treatment success (Figure 26). Tumor protein-, translationally-controlled 1 (TPT1) and Cbp/P300 interacting transactivator with Glu/Asp rich Carboxy-terminal domain 4 (CITED4) are overexpressed in Exo^{CisR}, and could be correlated with residual disease or remission after primary therapy, which can be interpreted as treatment failure. Whether this treatment failure is based on chemotherapy resistance can unfortunately not be verified, but it would pose a plausible explanation. TPT1 is known to be overexpressed in different cancer types and promotes cell survival (Bae et al. 2017). High CITED4 expression has been associated with increased proliferation and invasion (Zhang et al. 2021)(Zhang et al. 2021)(Zhang et al. 2021). Conversely, hepatoma-derived growth factor related protein 3 (HDGFRP3) and DNA replication helicase/nuclease 2 (DNA2) are significantly downregulated in Exo^{CisR}, and could be correlated with treatment success in patient data. DNA2 facilitates DNA replication fork stability, which would typically be associated with therapy resistance through stabilized DNA replication. However, a study using HNSCC cells could show that expression levels of DNA2 and other DNA repair proteins do not reflect resistance (Bold et al. 2021). They concluded that resistance is based on a balanced composition of DNA repair proteins, rather than the overexpression of such. HDGFRP3 is also part of the DNA repair machinery, and is involved in DNA double-strand break (DSB) repair. Knockdown of HDGFRP3 leads to an accumulation of DSBs and subsequent DNA damage hypersensitivity. Thus, it is not surprising that decreased HDGFRP3

expression increases treatment success. Reduced packaging of HDGFRP3 mRNA in Exo^{CisR} could be a means of increasing the cellular expression to increase DBS repair activity and thus cisplatin resistance (Zhang et al. 2023).

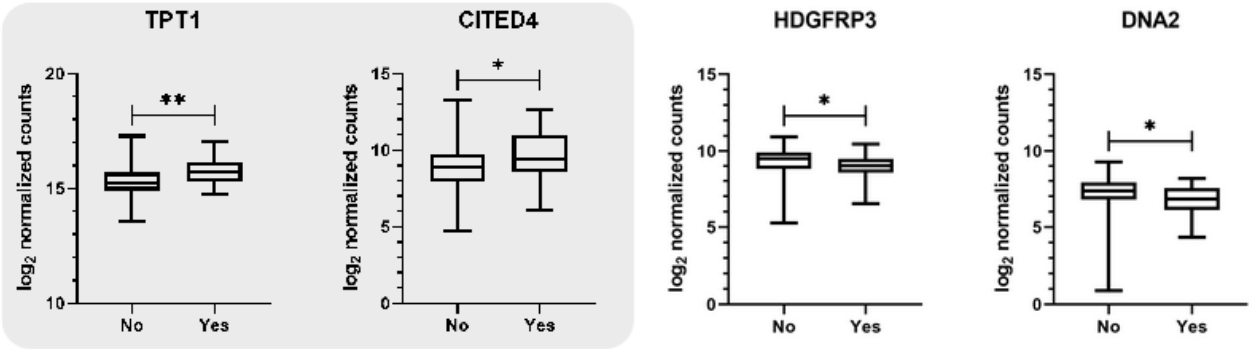

Figure 26. Clinical relevance of selected marker genes for treatment failure
TCGA HNSC data was filtered for patients with residual disease or remission after primary therapy, resulting in a cohort of n=187 patients. Candidate genes displayed in Figure 23B were checked and only significantly influential genes are displayed here. Genes upregulated in Exo^{CisR} are shaded in grey, those downregulated in white. Yes ≙ Treatment failure; No ≙ Treatment success. Statistical analysis by Welch´s t-test. * $p < 0,05$; ** $p < 0,01$

When considering the 5-year survival of patients from the same cohort, four genes that are overexpressed in Exo^{CisR} were found to have a significant impact. While high expression of Zinc finger and BTB domain-containing protein 32 (ZTBT32) and Sperm Associated Antigen 9 (SPAG9) is indicative of increased 5-year survival, high levels of Zinc finger protein 706 (ZNF706) and OTU deubiquitinase 1 (OTUD1) correlate with decreased probability of survival (Figure 27). While there is currently no literature on ZTBT32 involvement in cancer, SPAG9 overexpression could be associated with 5-FU resistance in gastric cancer cells. Contrary to the patient cohort analysed here, high SPAG9 expression correlated with poor prognosis in gastric cancer patients (Miao et al. 2015). However, it has to be kept in mind that high exosomal expression is not necessarily indicative of similar expression levels in the tumor cells. ZNF706 has already been proposed as molecular marker for laryngeal squamous cell carcinoma, while reprogramming of OTUD1 has already been shown in human oral keratinocytes treated with HNSCC and healthy donor exosomes (Colombo et al. 2009, Qadir et al. 2018).

Bleomycin hydrolase (BLMH) expression is decreased in Exo^{CisR}, and low expression correlates with decreased 5-year survival probability in the patient cohort. This is rather surprising, since BLMH inhibits the activity of bleomycin, an antibiotic used in squamous cell carcinoma treatment (Cheng et al. 2021). One study found that the single nucleotide polymorphism (SNP) A1450G of BLMH plays an important role for survival and relapse probability in testicular germ-cell cancer. Patients with the homozygous variant (G/G) have a significantly worse prognosis than those with

wildtype (A/A) or heterozygous (A/G) BLMH (de Haas et al. 2008). Whether this SNP was a contributing factor in the here presented data cannot be verified, but would pose a possible explanation for the counter-intuitive correlation.

Notably, BLMH as wells as SPAG9 expression were only significant indicators when considering the 25 % highest and lowest expression within the cohort.

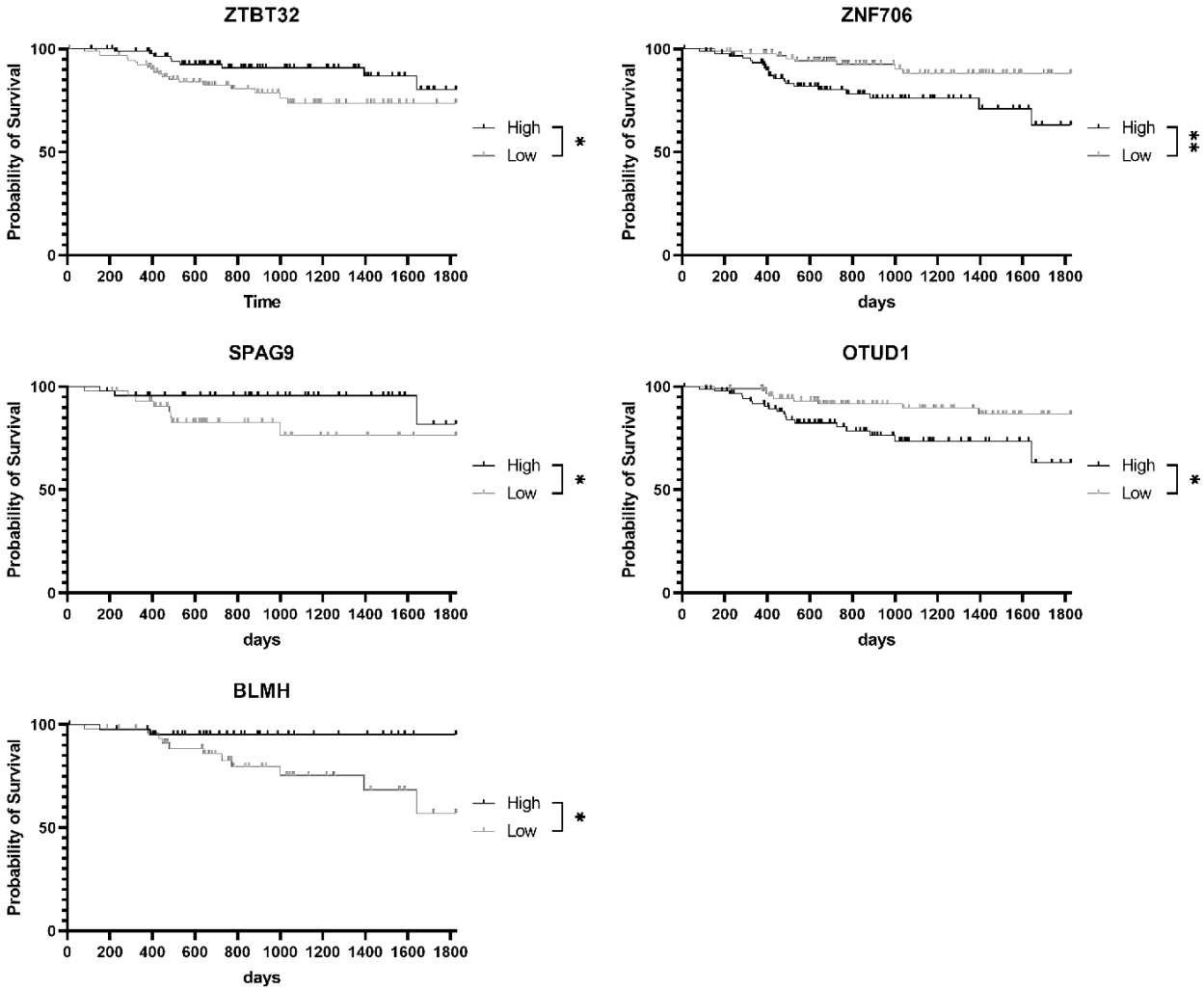

Figure 27. Clinical relevance of selected marker genes for disease specific 5-year survival
TCGA HNSC data was filtered for patients with residual disease or remission after primary therapy, resulting in a cohort of n=187 patients. The follow up period was set to 5 years (1825 days). Candidate genes displayed in Figure 23B were checked and only significantly influential genes are displayed here. For ZTBT32, ZNF706, and OTUD1 the cohort was split into two groups (50 % highest, 50 % lowest expression). For SPAG9 and BLMH the cohort was split into quartiles (25 % highest, 25 % lowest expression). Statistical analysis by Log-rank/Mantel-Cox test. * $p < 0,05$; ** $p < 0,01$

Considering the analysed cisplatin resistance candidate genes found in exosomes (Figure 24), 10 candidates were also significantly relevant for the treatment outcome in the HNSCC patient cohort (Figure 28). Surprisingly, increased expression of all 10 candidates is correlated with treatment success. Signal transducer and activator of transcription 1 (STAT1) and tumor protein 53 (TP53) are the only two among them that are upregulated in Exo^{CisR}. STAT1 is a tumor suppressor, which is activated by cisplatin treatment (Schmitt et al. 2015). Thus, it seems plausible that high STAT1 levels correlate with treatment success. There is currently no data on STAT1 mRNA in exosomes available, but active expulsion could be a means of reducing the cellular STAT1 expression, thus contributing to cisplatin resistance. TP53 mutations are one of the hallmarks of many cancers including HNSCC, while wildtype TP53 is a known positive prognostic marker (Nathan et al. 2022). Transmission of mutated TP53 dsDNA via exosomes has previously been observed between colorectal adenocarcinoma cells and colon epithelial cells, leading to active transcription of mutated p53 in the ladder (Domenis et al. 2021). Exosomal packaging of TP53 mRNA might pose another contributing mechanism to transfer mutated TP53 to naïve cells. There is also evidence for the involvement of p53 in exosome biogenesis and –loading, suggesting that mutated p53 leads to smaller exosomes with differing protein cargo (Sun et al. 2016). Whether the TP53 detected in Exo^{CisR} or the patients was wildtype or mutated is unfortunately unclear. Since high expression correlated with treatment success, it seems more likely that the wildtype variant was more prevalent. For Exo^{CisR}, active transmission of mutated TP53 would appear more plausible.

The other 8 candidate genes are downregulated in Exo^{CisR}, while downregulation is corresponding with treatment failure in the patient cohort. Here it seems most likely that low cellular expression in resistant cells likewise leads to low abundance in the corresponding exosomes, as also apparent in Figure 30.

Surprisingly, none of the EMT markers found in exosomes (Figure 25) could be correlated with treatment success or disease-specific survival in the examined cohort. EMT is generally associated with more aggressive cancer cells, thus a negative impact on patient survival and treatment efficacy would be expected. However, as introduced in section 1.3, cells can also be in intermediate stages of EMT, expressing epithelial and mesenchymal markers simultaneously. Thus, grouping of patients based on one single marker, e.g. a mesenchymal marker, might lead to a mixed population of complete and partial EMT in that group, masking potential effects. Interestingly, a review summarizing previous studies on EMT in HNSCC came to the conclusion that partial EMT gives rise to an even more aggressive phenotype than complete EMT, favouring CTC dissemination, metastasis, and drug resistance (Kisoda et al. 2022). This showcases the complexity of EMT as biomarker and highlights the importance of multiple marker analysis.

Of the CSC markers found differentially regulated in exosomes, none correlate with patient survival and only SOX2 is indicative of treatment outcome. Surprisingly, SOX2 is downregulated in Exo^{CisR} and HNSCC patients with treatment failure. SOX2 is a transcription factor responsible for maintaining the stemness of stem cells. It has also been linked to proliferation and therapy resistance in different cancer entities (Novak et al. 2020). However, for HNSCC the role of SOX2 has been ambiguous, with some studies finding high SOX2 expression to be a positive prognostic marker (Zullig et al. 2013, Chung et al. 2018), and others finding poor outcomes in patients with high SOX2 levels (Du et al. 2011, Schrock et al. 2014).

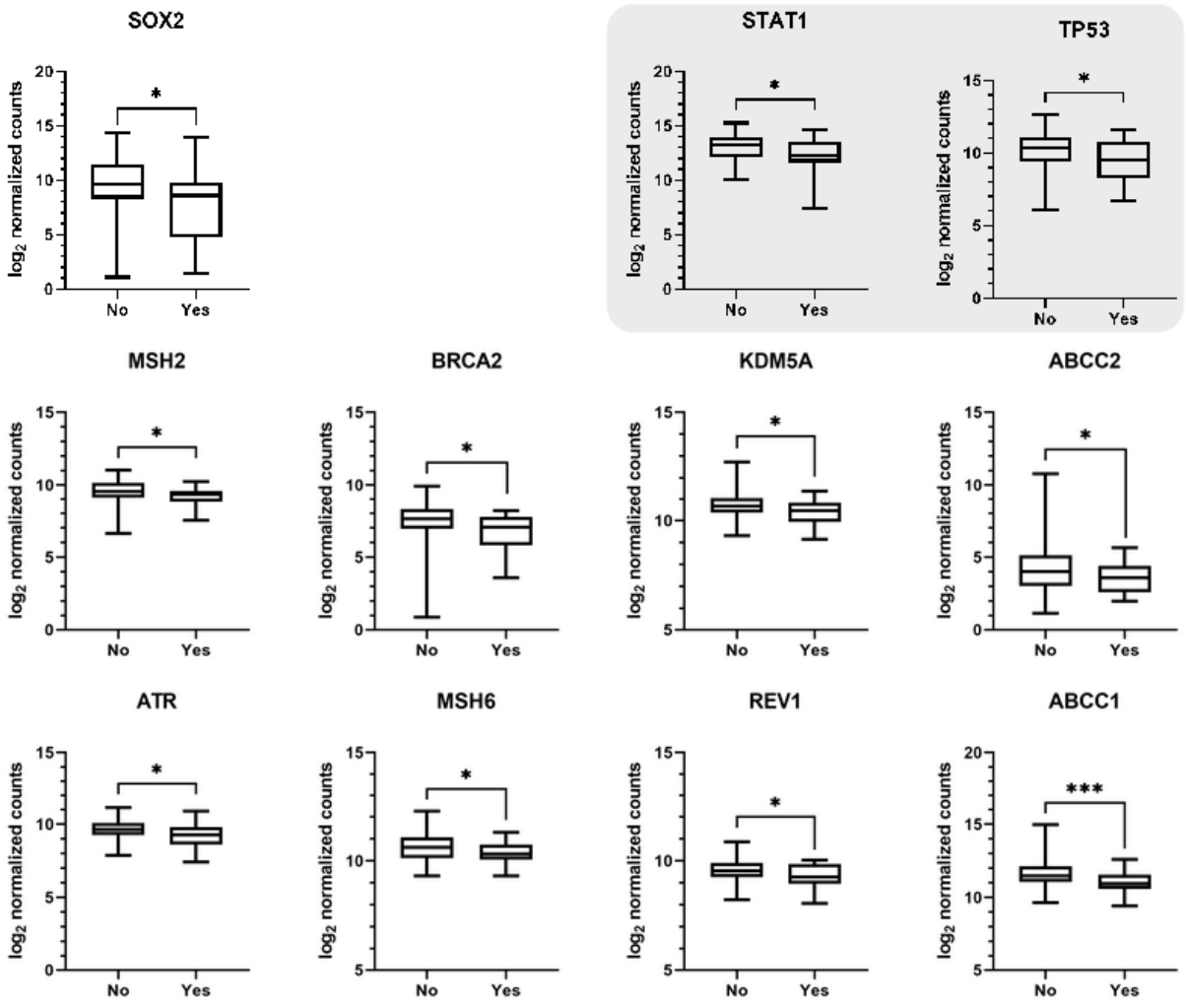

Figure 28. Clinical relevance of cisplatin resistance and CSC candidate genes for treatment failure
TCGA HNSC data was filtered for patients with residual disease or remission after primary therapy, resulting in a cohort of n=187 patients. Candidate genes displayed in Figure 24 and 25 were checked and only significantly influential genes are displayed. Genes upregulated in Exo^{CisR} are shaded in grey. Yes ≙ Treatment failure; No ≙ Treatment success. Statistical analysis by Welch´s t-test. * $p < 0,05$; *** $p < 0,005$

Among the cisplatin resistance candidate genes found in exosomes, six show a significant impact on the 5-year survival in the patient cohort (Figure 29). High expression of all candidate genes is associated with increased probability of survival. Signal transducer and activator of transcription 3 (STAT3) is the only one among them, which is overexpressed in Exo^{CisR}. STAT3 is robustly expressed and activated in HNSCC tissue, and its inhibition sensitizes HNSCC cells to cisplatin and cetuximab *in vitro* (Sun et al. 2018). Given its role in cisplatin resistance, it makes sense to find it highly expressed in Exo^{CisR}, while its positive effect on 5-year survival is counter-intuitive. However, it has to be kept in mind that numerous mechanisms are at play in cancerous cells, and no singular marker can precisely determine treatment outcomes.

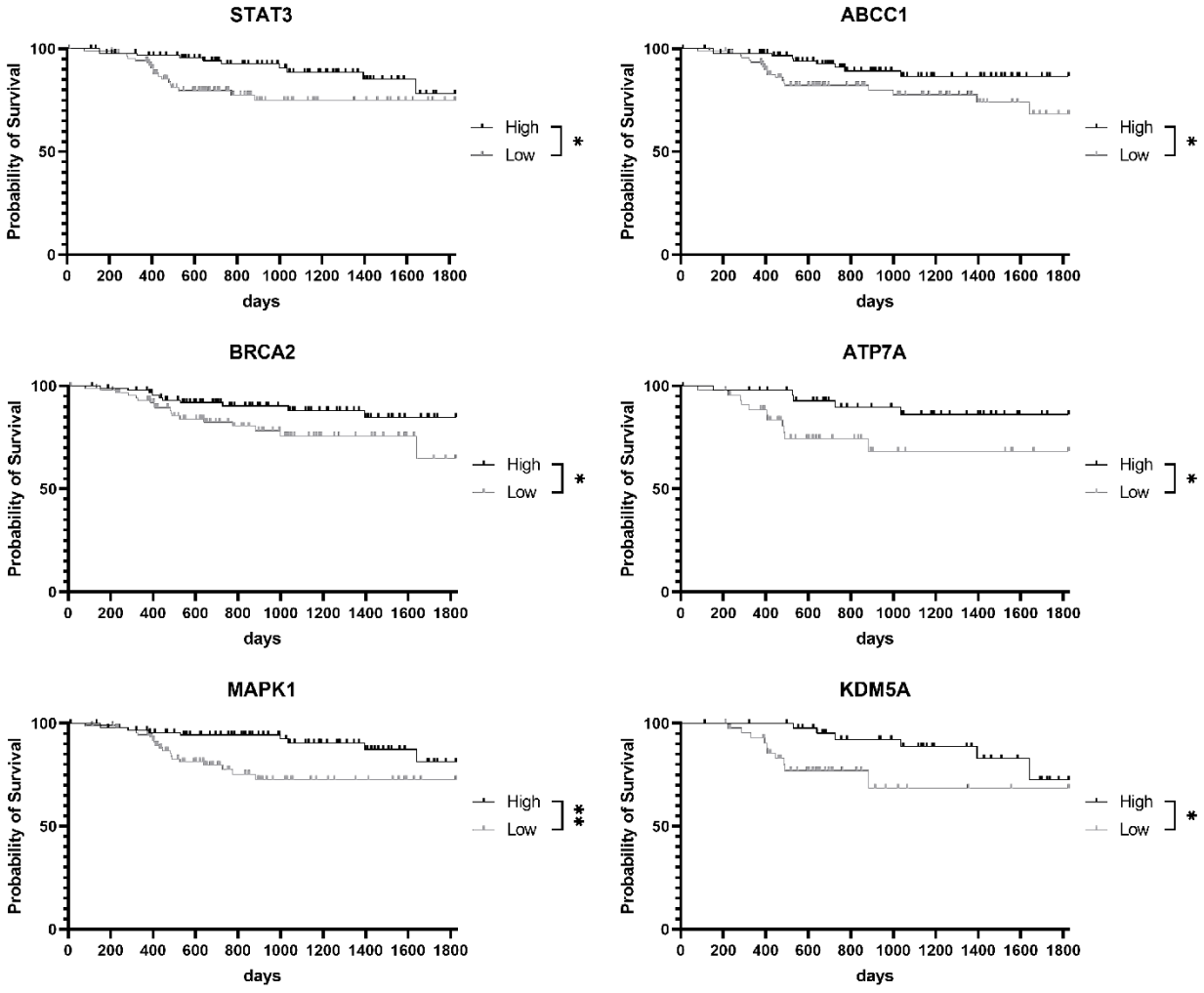

Figure 29. Clinical relevance of cisplatin resistance candidate genes for disease specific 5-year survival

TCGA HNSC data was filtered for patients with residual disease or remission after primary therapy, resulting in a cohort of n=187 patients. The follow up period was set to 5 years (1825 days). Candidate genes displayed in Figure 24 were checked and only significantly influential genes are displayed. For STAT3, BRCA2, MAPK1, and ABCC1 the cohort was split into two groups (50 % highest, 50 % lowest expression). For ATP7A and KDM5A the cohort was split into quartiles (25 % highest, 25 % lowest expression). Statistical analysis by Log-rank/Mantel-Cox test. * $p < 0,05$; ** $p < 0,01$

2.4.5 Transcriptomic Comparison of Exosomes and Donor Cells

To get a better understanding of the role of exosomal RNA packaging in cisplatin resistance and its potential transmission, the gene expression of FaDu donor cells was compared to their respective exosomes. Gene expression data of FaDu sub-cell lines was taken from previous work of our lab (Siemer 2021). Filtering for genes significantly regulated in both, donor cells and exosomes resulted in a list of 246 genes (for full list see Supplementary Table 3). Figure 30 shows a heatmap analysis of the 40 most regulated genes according to mean z-score of $FaDu^{CisR}$ cells (A) or exosomes (B). 10 genes appear in both heatmaps, and out of those only one gene (IFRD1) is regulated differently between cells and exosomes. Interferon-related developmental regulator 1 (IFRD1) is downregulated in $FaDu^{CisR}$ cells, while its expression is upregulated in Exo^{CisR}. IFRD1 is known to be a transcriptional co-regulator. In HNSCC, the IFRD1 locus is hypermethylated while global methylation is decreased, suggesting a pivotal role in maintaining the tumor phenotype (Poage et al. 2011). IFRD1 has also been shown to impair the acetylation of the RelA subunit of NFκB, leading to decreased NF-κB activity (Tummers et al. 2015). However, in many cancers NF-κB is constitutively active, and NF-κB inhibition could counteract cisplatin resistance (Gil da Costa et al. 2023). Coherently, IFDR1 is downregulated in $FaDu^{CisR}$ cells, allowing for NF-κB activity, potentially contributing to the resistant phenotype. As a transcriptional regulator, IFDR1 could also influence other resistance-relevant proteins on an epigenetic level. There is currently no data on IFDR1 expression in exosomes available, but increased efflux of IFDR1 mRNA via Exo^{CisR} could be a mechanism to decrease its cellular expression. This would match the very first theories of exosomes as waste disposal vehicles, but in a way more sophisticated manner than originally assumed (Pan and Johnstone 1983, Thery et al. 2002).

The genes upregulated in $FaDu^{CisR}$ cells and Exo^{CisR} are A-kinase anchor protein 12 (AKAP12), insulin like growth factor binding protein 6 (IGFBP6), transforming growth factor beta 1 (TGFB1), and CD55. AKAP12 is a tumor suppressor, which is downregulated in different cancer types. On the other hand, elevated AKAP12 expression has been found in cisplatin- and paclitaxel-resistant cells (Lopez-Ayllon et al. 2014, Bateman et al. 2015, Liang et al. 2022). IGFBP6 is generally overexpressed in HNSCC cells, while IGFBP6 knock-down has been associated with decreased exosome release (Jeon et al. 2004, Efimova et al. 2023). Whether overexpression of IGFBP6 leads to increased exosome release is currently unknown. Likewise, there is currently no data on IGFBP6 involvement in cisplatin resistance. Exosomal TGFB1 protein levels have been proposed as biomarker for HNSCC disease progression (Ludwig et al. 2023). High expression of TGFBP1 has also been associated with cisplatin resistance in OSCC (Yan and Xu

2021). Overexpression of CD55 has previously been reported in cisplatin-resistant cells, contributing to resistance in a complement-dependant way and via lymphocyte-specific protein tyrosine kinase signaling (Nakamura et al. 2005, Saygin et al. 2017).

Among the downregulated genes in Fadu^{CisR} cells and Exo^{CisR} is discs large MAGUK scaffold protein 3 (DLG3). DLG3 negatively regulates cell proliferation, which plays a pivotal role in sensitivity to Pt-based drugs. High expression of DLG3 was associated with high sensitivity to cisplatin and carboplatin in lymphoblastoid cell lines (Gamazon et al. 2011). Thus, the observed downregulation in Fadu^{CisR} cells and respective exosomes seems plausible. The observed downregulation of sex determining region Y box 2 (SOX2) on the other hand is surprising, as its overexpression is known to contribute to cisplatin resistance, especially in lung cancer (Ashrafizadeh et al. 2021). SCL47A2 codes for multidrug and toxin extrusion 2 (MATE2), a proposed oxaliplatin and cisplatin transporter (Sprowl et al. 2013, Sauzay et al. 2016). Thus, downregulation of SCL47A2 could contribute to cisplatin resistance by decreasing the intracellular drug concentration. Homer scaffolding protein 2 (HOMER2) overexpression has been proposed as a prognostic biomarker for better cancer-specific survival in endometrial adenocarcinoma, but there is currently no evidence for involvement cisplatin sensitivity or HNSCC (Mhawech-Fauceglia et al. 2018). Likewise, there is currently no evidence connecting serine protease 12 (PRSS12) to HNSCC or chemotherapy responsiveness.

Another striking observation is that genes upregulated in cells tend to also be upregulated in the respective exosomes, and genes downregulated in cells are also downregulated in their exosomes (Figure 29A). However, when looking at the most differentially regulated genes in exosomes, there is no clear correlation to the regulation in the respective donor cells (Figure 29B). This again could hint at specific packaging of the mRNAs that are highly abundant in exosomes but not cells, while those overexpressed in the cells naturally also appear at high rates in exosomes, with few exceptions. Likewise, low gene expression in cells is mostly also reflected in the corresponding exosomes, whereas low abundance in exosomes is no definite marker of low cellular expression levels. It is already known that EV RNA content differs substantially from the RNA content of the respective donor cells in terms of abundant RNA types and the relative concentrations of specific RNAs (O'Brien et al. 2020). Molecular changes contributing to cellular cisplatin resistance seem to have an additional impact here.

There are limitations to this study regarding data normalization, which are worth mentioning. The gene expression data of exosomes and donor cells were normalized using different methods, namely DESeq2 (version 1.24.0) for exosomes and fragments per kilobase million (FPKM) for cells. Nevertheless, this should not impact relative expression outcomes. Additionally, there is a 3 year time gap between the RNA sequencing of cells and exosomes, resulting in multiple

freeze/thaw events and passages of the cells in between. These procedures can lead to alterations in the gene expression of cells and subsequently their exosomes (Prasad et al. 2023). Thus, the comparison results should be viewed with caution and simultaneous analysis of exosomes and donor cells should be performed in the future.

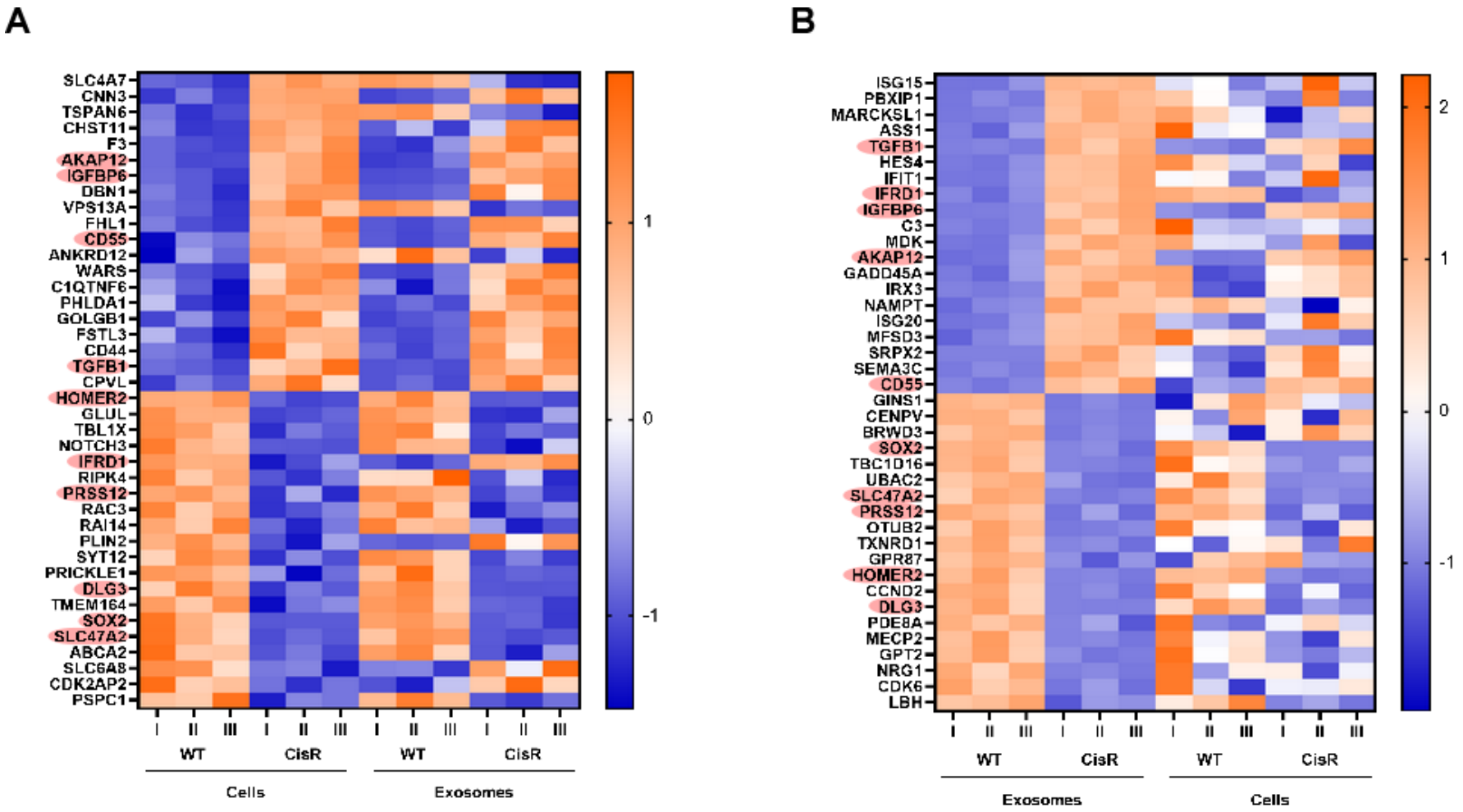

Figure 30. Comparative heatmap analysis of donor cells and exosomes
Sequencing data was filtered for genes significantly regulated in both, cells and exosomes. For full list refer to Supplementary Table 2. **A)** The 40 highest regulated (20 up-, 20 downregulated) genes according to mean z-score of FaDu^{CisR} cells. **B)** The 40 highest regulated (20 up-, 20 downregulated) genes according to mean z-score of Exo^{CisR}. Genes included in both, **A** and **B** are highlighted.

2.4.6 SUMMARY

Transcriptomic characterization of Exo^{WT} and Exo^{CisR} revealed differential expression of a total of 3.191 genes, with 1.811 upregulated and 1.380 downregulated genes in Exo^{CisR}. Out of the 40 most regulated genes in Exo^{CisR}, four show significant correlation with treatment outcomes in HNC patients. Considering the 5-year survival of HNC patients, five of the differentially regulated genes in Exo^{CisR} are indicative of patient survival. Additionally, 45 known cisplatin resistance candidate genes were found to be differentially expressed between Exo^{WT} and Exo^{CisR}, with the majority (28) being downregulated in Exo^{CisR}. When probing their clinical relevance, eight genes had a significant impact on treatment success and six were indicative of the 5-year survival of HNC patients. Probing for EMT and CSC candidate genes revealed that Exo^{CisR} have a more mesenchymal/CSC-like transcriptome compared to Exo^{WT}. Only one of the here considered marker genes was indicative of treatment outcome in the patient cohort. However, gene regulation in Exo^{CisR} did not always correlate with treatment success and 5-year survival in the expected way, highlighting that singular markers cannot reflect patient prognosis, and that the specific role of each gene and its product have to be considered. When looking at the regulation of mRNA content in Exo^{CisR} it appears to have a dual role. On the one hand, exosomal export of specific mRNAs poses a mechanism to decrease intracellular mRNA abundance and subsequent translation of proteins that would sensitize the cell to cisplatin treatment. On the other hand, Exo^{CisR} contain mRNAs encoding for proteins that contribute to cisplatin resistance and are involved in immunomodulatory pathways, hinting at an exosomal mechanism to increase cisplatin resistance through modulation of the recipient cell and the TME. Additionally, comparing exosomes and their respective donor cells revealed, that genes highly regulated in the donor cells often show similar regulation in their respective exosomes. On the contrary, genes highly regulated in exosomes are not necessarily similarly regulated in their donor cells, again highlighting a specific packaging mechanism for those RNAs. However, these results have to be viewed with caution since the time of sampling and the data analysis procedure were different between cells and exosomes.

2.5 *IN VITRO* MODELS FOR EXOSOMAL RESISTANCE TRANSMISSION

After finding that resistance-relevant cargo is upregulated in Exo^{CisR}, the possible transmission of cisplatin resistance via exosomes was to be modelled and analyzed. As introduced, there is a multitude of cell culture techniques available for cancer research. The application of different 2D and 3D cell culture techniques allows for a differentiated picture of the involvement of exosomes in HNSCC chemoresistance transmission.

2.5.1 TWO-DIMENSIONAL CELL CULTURE MODELS

In a first approach, $FaDu^{WT}$ cells were co-cultured with $FaDu^{CisR}$ cells using transwell inserts. This technique allows for the exchange of extracellular messengers without the possibility of direct cell-cell contacts. $FaDu^{WT}$ cells show a significantly higher viability in the presence of $FaDu^{CisR}$ cells after treatment with 20 µM cisplatin, while $FaDu^{CisR}$ cells show s similar viability regardless of the transwell inserts (Figure 31A). Whether this effect can be attributed to exosomes or other extracellular messengers like soluble proteins or other kinds of EVs fitting through the 0,4 µm transwell membrane's pores cannot be determined using this method. Therefore, Exo^{CisR} were deliberately added to $FaDu^{WT}$ cells grown in a standard 96-well format in the next approach. Exosomes were isolated from cell culture supernatant after 72h of conditioning and added to the cells three days before cisplatin treatment. Viability of $FaDu^{WT}$ cells in response to cisplatin treatment was not affected by the addition of exosomes (Figure 31B). This could hint at other extracellular messengers as the responsible agents for resistance transmission in the transwell assay. However, it also has to be considered that co-culture with the transwell inserts lasted for 6 days prior to treatment and continued during cisplatin treatment. The longer and continuous exposure could lead to differences in the signal transmission, and is more in agreement with the *in vivo* situation. It can also not be excluded that the isolation procedure impacted the functionality of the exosomes, even though there was no structural damage visible during the validation process (see section 2.2). Others have found that exosome isolation by UC is associated with reduced protein and RNA recovery, and that the influence of high forces on liquid membranes are not sufficiently investigated (Taylor and Shah 2015).

To investigate the influence of exosomes on the migratory potential of $FaDu^{WT}$ cells, they were seeded in special migration assay dishes and co-incubated with deliberately added exosomes. The dishes contained a silicone insert that created a 500 µm gap in the cell population. After 15 days of co-incubation, the insert was removed and closing of the gap was observed microscopically (Figure 31C). Quantification of the gap width hints at an increased migratory potential of $FaDu^{CisR}$ compared to $FaDu^{WT}$ cells. Exo^{WT} seem to have no impact on $FaDu^{WT}$

migration, while Exo^{CisR} tend to increase the migratory potential of $FaDu^{WT}$, though not reaching the capacity of $FaDu^{CisR}$ (Figure 31D). Whether these results are reproducible and statistically significant cannot be verified at this point, since the migration assay was only performed once. However, others have shown that exosomes from irradiated FaDu cells increased the migration of naïve FaDu cells in a similar experimental setup (Mutschelknaus et al. 2017). Another study revealed that exosomes isolated from the plasma of recurrent HNSCC patients induced higher cell migration *in vitro* than exosomes from disease-free patients after standard of care surgery and adjuvant or primary (chemo)radiation (Hofmann et al. 2022).

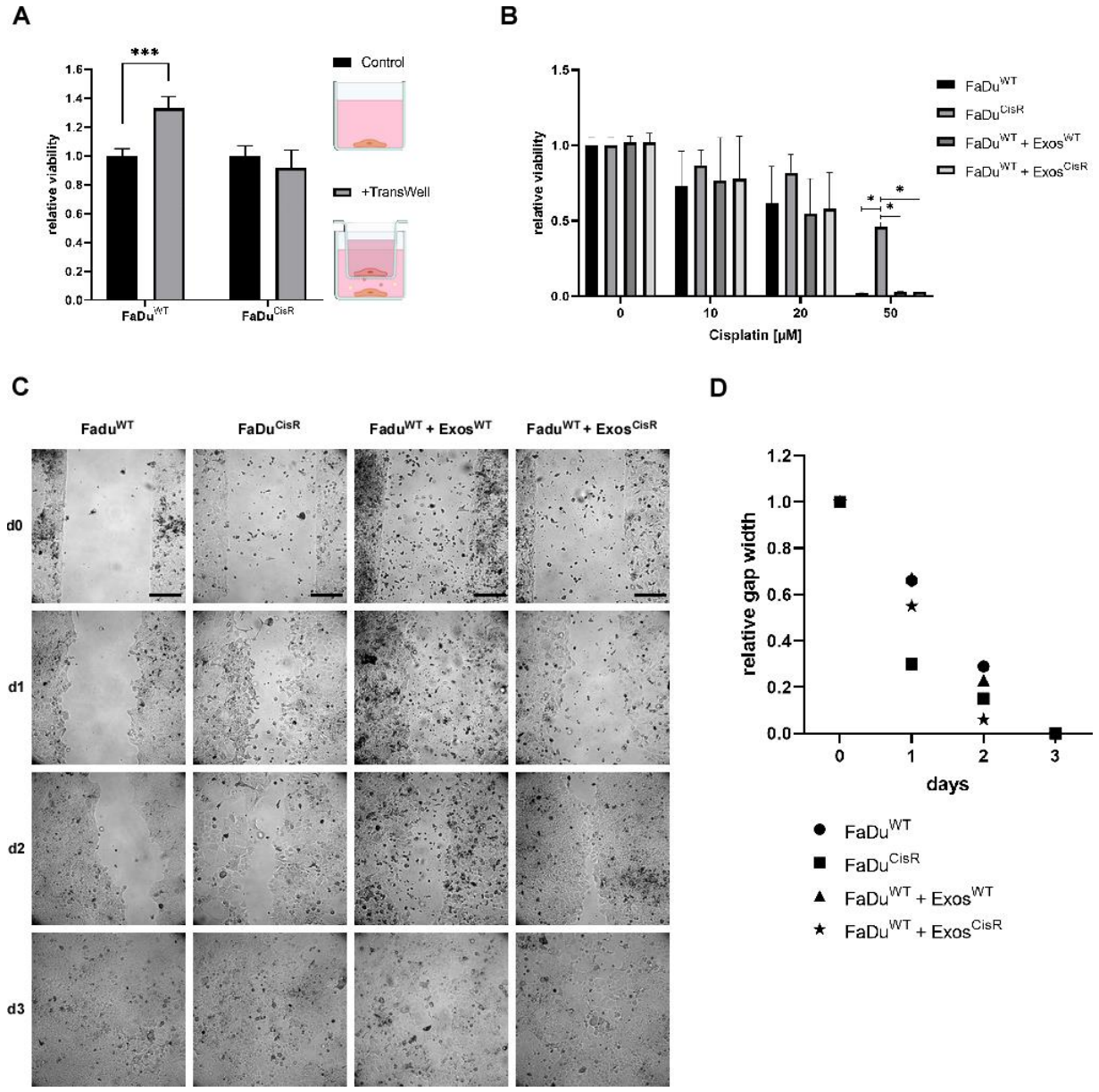

Figure 31. 2D cell culture models for exosomal communication
A) Cells were seeded at defined numbers in 12-well plates and corresponding transwell inserts. Co-culture was started 24h after seeding and lasted for 6 days before treatment with 20 µM cisplatin was started. Transwell inserts remained for the duration of the treatment, viability was determined by alamar blue assay after 72h. Data was normalized to controls without transwells. Data is given as Mean ± SD of n=3 independent experiments. Statistical analysis by two-way ANOVA and multiple comparisons with correction for multiple comparisons using the Dunnett method. *** $p < 0,005$ **B)** Cells were seeded at defined numbers in 96-well plates and exosomes isolated from 72h conditioned cell culture supernatant were added 24h after seeding. After 72h of co-incubation with exosomes, cells were treated with cisplatin. Viability was determined by CTG assay after 72h. Data was normalized to untreated controls. Data is given as Mean ± SD of n=3 independent experiments. Statistical analysis by two-way ANOVA and Tukey's multiple comparisons test. * $p < 0,05$ **C-D)** Cells were seeded at defined numbers in migration assay dishes and exosomes isolated from 72h conditioned cell culture supernatant were added 24h after seeding. Medium was exchanged every three to four days, continuously adding exosomes. After 15 days, the silicone divider was removed and cells were imaged daily for three days. Representative bright-field images are displayed. Scale bars 200 µm (**C**). Gaps were measured using AxioVision software and data was normalized to day zero. Data is given as Mean of n=1 experiment with 1-2 biological replicates (**D**).

2.5.2 THREE-DIMENSIONAL CELL CULTURE MODEL

As previously discussed, 3D cell culture models have gained significant popularity over the past years, as they give a better representation of the conditions *in vivo* than 2D cultures. Thus, different modes of adding exosomes to 3D cell culture were tested in a preliminary experiment (Figure 32). Compared to FaDu^{WT} spheroids, FaDu^{WT} spheroids formed in the presence of Exo^{CisR} show an increased viability after cisplatin treatment. Co-treating FaDu^{WT} spheroids with a combination of Exo^{CisR} and cisplatin lead to reduced viability. Pre-treating FaDu^{WT} spheroids with Exo^{CisR} for three days before cisplatin treatment had no effect on spheroid viability.

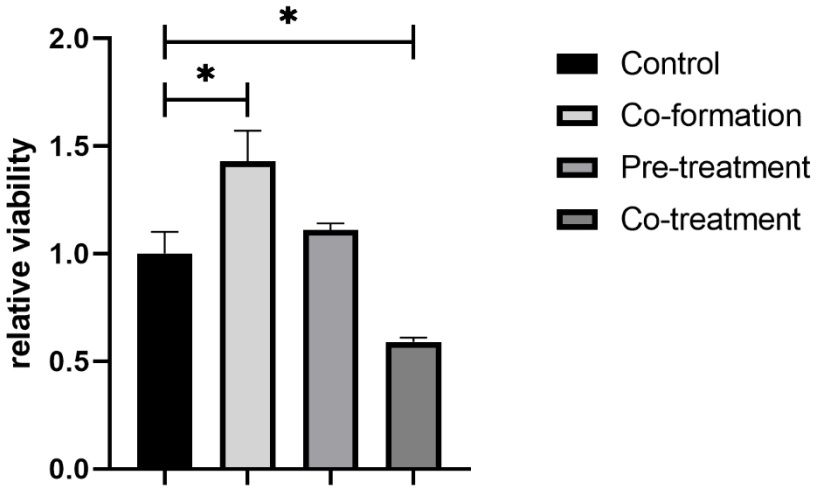

Figure 32. Influence of different exosome treatments on FaDu spheroid viability
FaDu^{WT} cells were seeded at defined numbers and treated with exosomes and cisplatin at different time points. Control spheroids were allowed to form for 7 days before treatment with 20 µM cisplatin. The co-formation group was seeded in the presence of Exo^{CisR} and allowed to grow for four days before treatment with 20 µM cisplatin. The pre-treatment group was allowed to grow for four days before addition of Exo^{CisR}. Another three days later treatment with 20 µM cisplatin started. The co-treatment group was allowed to grow for four days before simultaneous addition of Exo^{CisR} and 20 µM cisplatin. Viability was assayed by CTG 3D 72h after onset of cisplatin treatment. Data was normalized to the control group and is given as Mean ± SD of n=1 experiment with 2-3 biological replicates. Statistical analysis by one-way ANOVA and Tukey's multiple comparisons test. * $p < 0,05$

Given the observed increase in cisplatin tolerance in the co-formation group, the impact of exosomes on the phenotype of 3D spheroids was tested. Exosomes were isolated from cell culture supernatant after 72h of conditioning and deliberately added to the cells upon seeding. Thus, the spheroids formed in the presence of (externally added) exosomes. Staining of the exosomes with membrane dye revealed their integration into the 3D structure, with the signal still readily detectable after 10 days (Figure 33B). When observing the spheroids microscopically, those formed in the presence of exosomes appear larger regardless of the exosome-donor cells (Figure 33A). Quantification of phenotypic parameters by HCS revealed significant differences in

relative spheroid area after 10 days of culture. FaDu^{CisR} spheroids are significantly smaller than FaDu^{WT} spheroids, regardless of the presence of exosomes during formation. This was not observed during initial assessment of the established sub-cell lines (see section 2.3.2). As previously discussed, spheroid area is not a reliable singular parameter. Experiments with the HPV-positive SCC-154 cell line in our lab even revealed shrinkage of spheroids over time, as spheroids did not grow in surface area but became more dense (data not shown). Whether the contradicting observations made here are based on similar phenomena, represent artefacts, or are based on different batches of cells in use cannot be clarified. FaDu^{WT} spheroids formed in the presence of Exo^{CisR} tend to be the largest, though not significantly different from the other FaDu^{WT} spheroids (Figure 33C). Spheroids are generally less spherical during the first three days of culture and then approach a nearly round shape (Supplementary Figure 4). The addition of exosomes tends to disrupt spheroid formation based on an even less spherical shape in the first days of formation. On day one, FaDu^{WT} spheroids formed in the presence of Exos^{WT} are significantly less round than FaDu^{CisR} spheroids, though there are no statistically significant differences among the other groups. On day 10 all spheroids reach an almost perfectly round shape (Figure 33D). Assaying the average spheroid intensity by HCS revealed a general decrease over time, but no significant differences based on sub-cell line or exosome addition (Supplementary Figure 5).

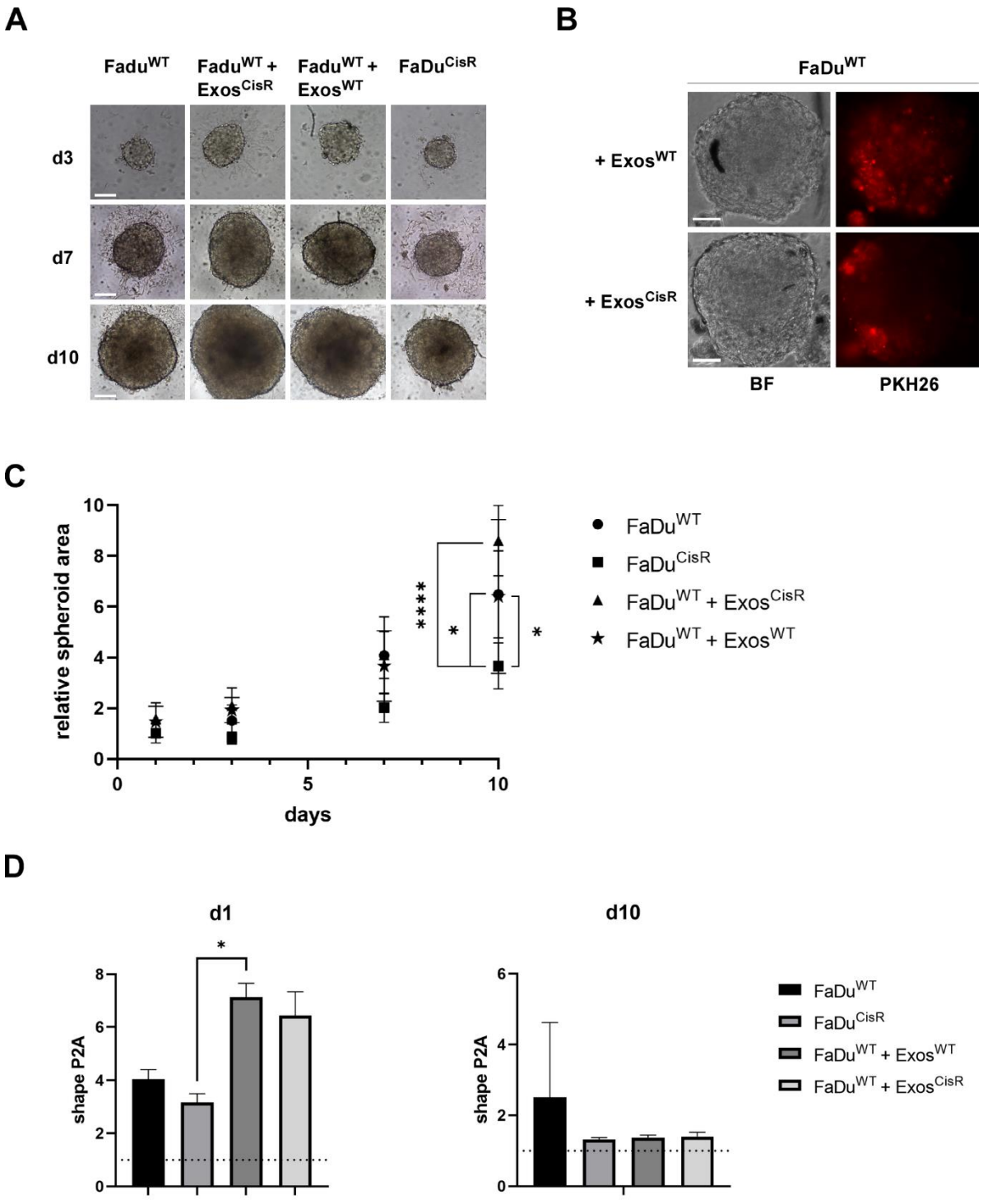

Figure 33. Phenotypic assessment of spheroids formed in the presence of exosomes
A) Representative bright-field images of FaDu spheroids formed in the presence or absence of exosomes over 10 days. Scale bars 50 µm. **B)** Representative images of FaDu^{WT} spheroids formed in the presence of PKH26-labeled exosomes on day 10. Scale bars 50 µm. **C)** Relative spheroid area of FaDu spheroids formed in the presence or absence of exosomes as measured by HCS over 10 days. Data was normalized to day one controls. **D)** Shape P2A of FaDu spheroids formed in the presence or absence of exosomes as measured by HCS on day one (left) and day 10 (right). Dashed lines mark P2A = 1, which equals a perfectly round shape. All data is given as Mean ± SD of n=3 independent experiments. Statistical analysis by two-way ANOVA and Tukey's multiple comparisons test. * $p < 0,05$; **** $p < 0,001$

When considering the impact of cisplatin treatment on the relative spheroid area, $FaDu^{WT}$ spheroids formed in the presence of Exo^{CisR} show a significantly decreased area on day three of cisplatin treatment, in a seemingly concentration dependent manner. $FaDu^{CisR}$ spheroids are significantly smaller after treatment with 50 µM cisplatin compared to untreated controls (Supplementary Figure 6). $FaDu^{CisR}$ cells generally grow slower than $FaDu^{WT}$ cells in 2D (section 2.2.3.1) and 3D (Figure 33C). This is also known for other cisplatin resistant cells (Duan et al. 2017). Reduced proliferation has been proposed as a protective mechanism against cisplatin toxicity, as cells go through the sensitive S phase less frequently (Ijichi et al. 2014, Yano et al. 2014). Exosomes from esophageal squamous cell carcinoma cells have been shown to reduce proliferation in recipient cells and increase the ratio of cells in G1 phase (Matsumoto et al. 2020). A similar, potentially cisplatin-induced mechanism might be at play here. However, the relative spheroid area on day three of 50 µM cisplatin treatment (day 10 of culture) does not differ significantly among the groups (Figure 34B). When looking at Figure 34A, it again becomes apparent that cisplatin treatment leads to frayed spheroid margins in $FaDu^{WT}$ spheroids, regardless of the presence of exosomes, while $FaDu^{CisR}$ spheroids seem rather unaffected even at 50 µM cisplatin. Surprisingly, automated microscopic analysis did not pick up any significant differences in spheroid intensity based on the cisplatin treatment (Supplementary Figure 5), even though treated spheroids appear darker in Figure 34A. Spheroid shape appears to be unaffected by cisplatin treatment (Figure 34C). Viability assay revealed significantly higher cisplatin tolerance of $FaDu^{CisR}$ spheroids at 50 µM cisplatin compared to $FaDu^{WT}$ and $FaDu^{WT}$ formed in the presence of $Exos^{WT}$. $FaDu^{WT}$ spheroids formed in the presence of $Exos^{CisR}$ neither significantly differ from $FaDu^{WT}$ spheroids ($p = 0{,}9612$) nor $FaDu^{CisR}$ ($p = 0{,}0691$), but $FaDu^{CisR}$ clearly exhibit the highest cisplatin tolerance (Figure 34D). Testing of longer cisplatin treatment durations and different treatment starting times did also not reveal a clear influence of exosomes on spheroid viability or area (Supplementary Figure 7A,B). Starting 20 µM cisplatin treatment on day three of culture seems to have disrupted the spherical shape regardless of exosome presence in this experiment, though this was not observed previously and may be an artefact of this specific experimental run (Supplementary Figure 7C).

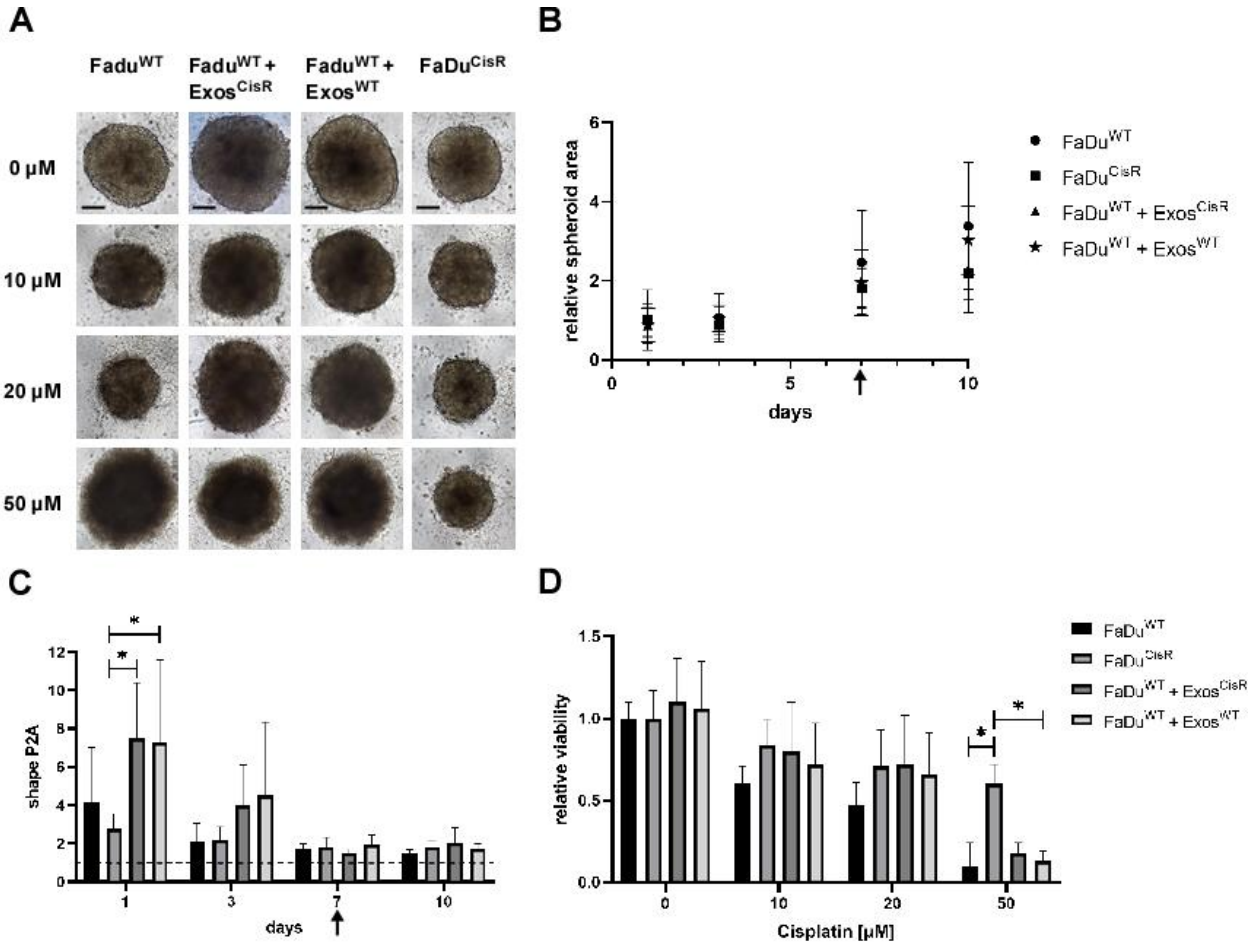

Figure 34. Cisplatin-response of spheroids formed in the presence of exosomes
Cells were seeded in the presence or absence of exosomes and spheroids were allowed to grow for 7 days before treatment with different concentrations of cisplatin. Phenotypic parameters were assayed by HCS over 10 days. **A)** Representative bright-field images of FaDu spheroids on day 10. Scale bars 50 µm. **B)** Relative spheroid area of FaDu spheroids treated with 50 µM cisplatin. Arrow marks onset of treatment. **C)** Shape P2A of FaDu spheroids treated with 50 µM cisplatin. Arrow marks onset of treatment. Dashed line marks P2A = 1, which equals a perfectly round shape. **D)** Relative viability of FaDu spheroids in response to cisplatin treatment. Viability was assayed on day three of treatment using the CTG assay. All data is given as Mean ± SD of n=3 independent experiments. Statistical analysis by two-way ANOVA and Tukey's multiple comparisons test. * $p < 0,05$.

2.5.3 SUMMARY

Applying different cell culture techniques to model exosomal cisplatin resistance transmission generated different perspectives on the impact of exosomes on cell viability, migratory behavior, and phenotypic parameters.

The 2D cell culture approaches revealed that the co-culture of cisplatin-sensitive $FaDu^{WT}$ cells with cisplatin-resistant $FaDu^{CisR}$ cells increases the cisplatin tolerance of $FaDu^{WT}$. The effect could not be reproduced by directly adding Exo^{CisR} to $FaDu^{WT}$ in standard 2D cell culture. However, it has to be considered that the prolonged co-incubation before cisplatin treatment (6 days) and the continuous co-culture during the treatment may have led to a more intense (exosomal) communication between $FaDu^{CisR}$ and $FaDu^{WT}$ cells than the addition of Exo^{CisR} three days before cisplatin treatment, with no exosomes present during treatment. The migratory potential of $FaDu^{WT}$ cells was increased by the addition of exosomes, especially the addition of Exo^{CisR}.

3D spheroid culture revealed that exosomes are readily incorporated into cell spheroids when present since seeding. $FaDu^{WT}$ spheroids formed in the presence of exosomes tend to have a less spherical shape during the first days, and an overall increased size. $FaDu^{WT}$ spheroids formed in the presence of Exo^{CisR} elicit a reduced area in response to cisplatin treatment, suggesting reduced proliferation as a potential resistance mechanism. Effects of Exo^{CisR} on $FaDu^{WT}$ spheroid susceptibility to cisplatin treatment could neither be verified nor ruled out. Further experimental adjustments could shed more light on this.

3 CONCLUSIONS AND OUTLOOK

3.1 EXPLOITING CTCS AS BIOMARKER FOR HNSCC

Standardized, easy-to-use procedures are pivotal for the integration of new methods into clinical use. A valuable step in that direction is automation, as it increases reproducibility and reduces the time and expertise required from users. Given their role in metastasis, it is not surprising that CTCs have already been successfully integrated into the staging of breast cancer, and the *American Society of Clinical Oncology* supports their use as biomarker for cancer in general. Nevertheless, *CellSearch* remains the only FDA-approved platform for automated CTC enrichment and analysis, hindering the broader integration of CTC-based biomarkers into cancer detection and monitoring.

Comparing two bead-based positive selection methods with different protocol variations revealed striking differences in the achievable recovery rates. Manual isolation of HNSCCUM-02T cells spiked into cell culture medium was most successful using the pluriBeads system (49,5 ± 15,7 % recovery). However, tests with whole blood revealed significant contamination with non-target cells, making clinical application unfavourable. The DynaBead-compatible prototype *IsoMAG* achieved a recovery rate of 95 ± 15 % in a first study (Gribko et al. 2021), however these results could not be reproduced here. Nevertheless, the “human factor” has to be kept in mind here, especially for manual isolation. Operation of the *IsoMAG* platform was only performed once in the here presented study, thus lack of experience in its operation is a considerable source of variance. The successor platform *CTCelect* achieved 56,7 ± 18,9 % recovery of SCL-1 cells spiked into cell culture medium and 40,0 ± 5,0 % of cells were recovered from blood. Initial tests using HNSCC patient blood revealed that approximately 66 % of the isolated cells were CTCs, while 33 % were identified as non-CTCs/WBCs based immunofluorescent staining. Applying different antigens for enrichment and analysis of dispensed single cells by qPCR was also successful, allowing for the characterization of different CTC subpopulations.

Overall, the spiking experiments using relevant HNSCC cell lines have proven to be a useful tool in validating CTC isolation. Efforts to automate the process using the *CTCelect* platform generated the first promising results using HNSCC patient blood. Further clinical tests with significantly larger patient cohorts will be necessary to validate the clinical applicability of the automated isolation, and to correlate single cell characteristics with clinical parameters. Analyzing patient CTCs on single cell level (e.g. by qPCR) will generate new insights into CTC-specific biomarkers. Additionally, *ex vivo* culture of CTCs in standard or 3D cell culture could be

a next step towards personalized therapy. Different drugs could be tested on the patient's CTCs *in vitro* to identify possible resistances early on and aid informed treatment decisions.

3.2 Modelling Exosomal Chemoresistance Transmission *In Vitro*

In vitro models are an important tool to unravel the molecular mechanisms contributing to chemotherapy resistance and its transmission. Insights generated from such models can aid the early detection and optimized treatment of HNSCC patients suffering from chemoresistance. Exosomes as extracellular messengers have been implied as transmission vehicles for different molecular cargo contributing to the occurrence of chemoresistance. To understand how exosomes can transmit a resistant phenotype and how their uptake influences the recipient cells, a cell model for cisplatin resistance was established and exosomal communication was evaluated using different *in vitro* cell culture techniques.

To increase the reproducibility and avoid any possible genetic heterogeneity, a single-cell derived sub-cell line was generated from the established hypopharyngeal squamous cell carcinoma cell line FaDu ($FaDu^{WT}$). Starting from $FaDu^{WT}$ cells, the cisplatin-resistant $FaDu^{CisR}$ sub-cell line was generated by constant exposure to sublethal cisplatin concentrations over a period of 6 months before onset of experiments, thus preventing further genetic drift in between observations. As opposed to directed genetic modifications of known contributors to chemoresistance, long term exposure to cisplatin likely leads to a broad mutational load. This method was chosen to mimic the acquisition of cisplatin resistance as occurring when patients undergo cisplatin therapy, though it has to be kept in mind that cisplatin is typically not applied as single agent but in combination with radiotherapy in the clinic. Evaluation of cell viability after cisplatin treatment revealed a significantly higher resistance of $FaDu^{CisR}$ cells to cisplatin when compared to $FaDu^{WT}$, verifying an acquired chemoresistance phenotype. The effect was consistent using 2D and 3D cell culture models.

To assess whether $FaDu^{CisR}$ cells are able to transfer their resistance to sensitive $FaDu^{WT}$ cells via exosomes, different 2D and 3D cell culture methods were applied. Co-culture of $FaDu^{WT}$ and $FaDu^{CisR}$ cells using trans-well inserts revealed an increased cisplatin tolerance of $FaDu^{WT}$ cells after co-culture. To find out whether this effect was caused by exosomes, $FaDu^{WT}$ cells were cultured as traditional 2D monolayers, and pre-treated with exosomes from $FaDu^{CisR}$ cells (Exo^{CisR}) prior to cisplatin treatment. However, this did not impact their cisplatin tolerance. It cannot be ruled out that the increased tolerance observed in the co-culture set-up was based on other extracellular messengers besides exosomes. As mentioned before, it is also possible that the isolation procedure lead to changes in the exosome constitution and functionality, as it uses high force. Nonetheless, other studies have already shown that transmission of cisplatin resistance is possible using similar experimental setups. As evidenced by the transcriptomic characterization of Exo^{CisR}, they also hold the potential to modulate the immune response. Even

though they did not influence FaDu^{WT} cisplatin tolerance directly, they could potentially increase tumor cell survival through TME modulation. However, this effect was not investigated here. Nevertheless, the addition of exosomes, especially Exo^{CisR}, appeared to have a positive impact on the migratory potential of FaDu^{WT} cells in a gap-closing assay. These results highlight that exosomal function is at least not completely lost during the isolation procedure, and signaling via exosomes does occur. Future experiments focusing on other extracellular messengers would be beneficial to rule out or identify additional modes of chemoresistance transmission. Integrating other cell types, e.g. immune cells, into the model would be another valuable step towards a better representation of the *in vivo* situation, and it would allow for additional conclusions about exosomal communication with the TME.

To get a more realistic representation of the situation within a tumor, 3D spheroid culture was applied. Here, cells can develop polarity, and nutrient, oxygen, and drug supply differ depending on the individual cell's location within the 3D structure. Establishment of a HCS protocol allowed for the quantification of phenotypic parameters as additional readout to viability assessment. Automated analysis of spheroid morphology, including area, shape, and intensity, can generate new insights into the impact of genetic modifications and molecular communication in a broader context. The addition of exosomes to spheroids upon formation lead to the incorporation of those exosomes into the 3D structure. Automated assessment of phenotypic spheroid parameters revealed that FaDu^{WT} spheroids formed in the presence of exosomes tend to be larger, and reaching a spherical shape takes them longer than without exosomes. In response to cisplatin treatment, FaDu^{WT} spheroids formed in the presence of Exo^{CisR} exert a decreased spheroid area compared to untreated controls. The decrease is strongest after treatment with 50 µM cisplatin, suggesting a concentration dependent area reduction. Other than that, exosomes did not affect spheroid morphology after cisplatin treatment. Considering the viability, there was no striking effect of exosome addition, though FaDu^{WT} spheroids formed in the presence of Exo^{CisR} may have a slightly increased cisplatin tolerance, but not reaching FaDu^{CisR} spheroids' resistance. Further experimental adjustments may help to clarify the validity of this observation.

In conclusion, the presented cell culture models are a solid basis to explore the molecular mechanisms of cisplatin resistance and its transmission via exosomes and other extracellular messengers. The different applied *in vitro* cell culture techniques allow for diverse readouts related to cisplatin resistance and beyond. As such, the models can be applied to answer a broad spectrum of basic chemoresistance research questions in the future. Even though there was no definite effect of Exo^{CisR} on the cisplatin tolerance of FaDu^{WT} spheroids measureable, the established 3D model and HCS protocol offer many possibilities for further experiments. Modifications of exosome dose, spheroid growth before treatment, and cisplatin treatment

duration may deliver new, potentially different results. The model is also very versatile, allowing for the assessment of other chemotherapeutics, adjuvants, and drug carriers. Even the application of (chemo-) radiation would be possible and advisable, as cisplatin is typically administered in combination with radiation. To increase the scientific value, it would be beneficial to apply a similar “protocol” to additional HNSCC cell lines or primary cells for comparison. Adding patient-derived exosomes would pose another valuable option. The use of heterogeneous 3D models including additional cell types or even patient derived organoids will be another critical step towards a realistic and personalized model to answer basic research questions and to aid informed treatment decisions.

3.3 Exploiting Exosomes as (Chemoresistance-) Biomarker for HNSCC

The main goal of *in vitro* experiments is to translate the generated results into clinical applications. Since the introduction of liquid biopsy into cancer diagnostics, exosomes have been proposed as potential biomarker. Exploiting exosomes in the early detection of chemotherapy-resistant patients could significantly improve treatment success and patient well-being.

To identify potential exosomal biomarkers for cisplatin resistance, exosomes were isolated from cell culture supernatant of $FaDu^{WT}$ and $FaDu^{CisR}$ cells, and exosomal RNA was extracted and sequenced. RNA sequencing revealed differential expression of 3.191 genes between Exo^{WT} and Exo^{CisR}, with 1.811 upregulated and 1.380 downregulated genes in Exo^{CisR}. Among the 40 most regulated genes were several with known association to cancer and chemotherapy resistance. Interestingly, there is no definite pattern of expression of those genes in Exo^{CisR}, as some are up- and some are downregulated. Similarly, when probing for known cisplatin resistance candidate genes, roughly 60 % were downregulated in Exo^{CisR}, while the rest was upregulated. Probing for EMT and CSC markers revealed, that Exo^{CisR} show a more mesenchymal/CSC-like expression pattern compared to Exo^{WT}. This is in agreement with the general assumption that EMT and stemness facilitate more aggressive, therapy-resistant cancer. Comparison of RNA sequencing data of donor cells and exosomes revealed that genes upregulated in cells tend to also be upregulated in the respective exosomes, and genes downregulated in cells are also downregulated in their respective exosomes. However, when looking at the genes highly regulated in exosomes, there is no clear correlation to the expression in the respective donor cells. Thus, it seems that mRNA abundance in exosomes is influenced by two factors: The donor cell's expression level and the specific regulation of exosomal packaging. The ladder group could be of high interest in terms of exosomal contribution to maintenance and transmission of chemoresistance.

Reactome analysis of genes overexpressed in Exo^{CisR} revealed two prevalent groups of pathways: immunoregulatory pathways and pathways related to mitochondrial RNA processing. Both can be considered relevant to cisplatin resistance. Regulation of immunological pathways via exosomes is a known resistance mechanism, shaping the TME and systemic responses. Mitochondria are also affected by cisplatin toxicity, suggesting alterations in mitochondrial pathways as protective mechanisms.

Correlating the sequencing data with clinical parameters from a HNSCC cohort retrieved from the TCGA database revealed that four of the most differentially regulated genes in Exo^{CisR} are predictive of treatment success. Genes strongly upregulated in Exo^{CisR} (TPT1, CITED4) are correlated with treatment failure, while those strongly downregulated in Exo^{CisR} (HDGFRP3, DNA2) are indicative of treatment success. Considering the cisplatin resistance candidate genes significantly downregulated in Exo^{CisR}, low expression of 8 genes (MSH2, BRCA2, ABCC2, ATR, MSH6, REV1, ABCC1) was also associated with treatment failure in the analyzed patient cohort. Assessment of the patients' 5-year survival revealed that high expression of ZNF706 and OTUD1 is associated with decreased survival. Both genes were upregulated in Exo^{CisR}. Low expression of BRCA2, MAPK1, ABCC1, ATP7A, and KDM5A correlates with decreased 5-year survival. These genes are downregulated in Exo^{CisR}. Thus, these 16 genes are promising candidates for further validation in a clinical setting.

In order to verify the significance of these findings for HNSCC patients, future experiments using patient-derived exosomes will be necessary. Here, the use of exosomes derived from relevant biological fluids such as blood or saliva would be an option. Knowing the patients' history and treatment regimen in detail will contribute to a more precise evaluation of the biomarker candidates. Furthermore, reducing the time and equipment requirements for the exosome isolation procedure would accommodate clinical implementation. Methods like polymer precipitation pose a promising approach in this regard, significantly reducing necessary centrifugation speeds and overall isolation time. As with CTCs, automating the exosome isolation procedure would be the optimal long-term solution. If the here presented results can be confirmed in patient exosomes, it would be a solid basis for novel exosomal biomarkers of treatment success and patient survival in correlation with cisplatin resistance. Such biomarkers could help to identify high risk patients at an early stage and allow for timely treatment adjustments.

4 MATERIALS AND METHODS

4.1 MATERIALS

4.1.1 INSTRUMENTS

Table 5: Instruments

Instrument	Model	Manufacturer
Agarose Gel System		peqLab, VWR, Darmstadt
Array Scan	VTI	Thermo Fisher Scientific, Dreieich
Autoclave	5050 ELV	Tuttnauer, Breda
Cell Counting Device	CASY TTC	OMNI Life Science, Hamburg
Cell Culture Hood	Hera safe	Heraeus Holding GmbH, Hanau
Cell Freezing Container	CoolCell	Biocision, USA
Centrifuge, Benchtop	Mini Spin	Eppendorf, Hamburg
Centrifuge, Benchtop	Centrifuge 5415D	Eppendorf, Hamburg
Centrifuge, Falcons	Heraeus Multifuge 1L-R	Thermo Scientific, Tuttlingen
Centrifuge, High-Speed	Avanti JXN-30	Beckman-Coulter, Krefeld
Chemidoc	MP Imaging System	Bio-Rad Laboratories, München
Crushed Ice Machine	AF 80	Scotsman, Vernon Hills, USA
Fluorescence Reader	Tecan Spark	Tecan, Crailsheim
Freezer (-20 °C)		Liebherr, Bulle, Schweiz
Freezer (-80 °C)	TSX	Thermo Scientific, Dreieich
Fridge		Liebherr, Bulle, Schweiz
Gel Documentation	Multi Genius	Syngene
Heating Block	Thermomixer	Eppendorf, Hamburg
Incubator	Hera Cell	Thermo Fisher Scientifc, Dreieich

Instrument	Model	Manufacturer
	CB 60	Binder, Tuttlingen
Magnetic rack	DynaMag-15	Thermo Fisher Scientific, Dreieich
Micro Scale	PCB250-3	Kern&Sohn, Balingen-Frommern
	PCB8000-1	
Microscope, Flourescence	Axiovert 200M	Zeiss, Oberkochen
Microscope, Fluorescence	Eclipse TE2000-U	Nikon, Düsseldorf
Microscope, Cell Culture	Nikon TMS	Nikon, Düsseldorf
Microwave	M730	Philips, Hamburg
Nanophotometer	NanoDrop	Thermo Fisher Scientific, Dreieich
Nitrogen Tank	GT 38	Omnilab AG, Mettmennstetten
pH-Meter	EasyFive	Mettler Toledo, Gießen
Pipette (Multi Channel)	Research plus	Eppendorf, Hamburg
Pipettes	Pipetman Neo	Gilson, Limburg-Offenheim
	P2N, P200N, P1000N, P5000N	
Pipette	Pipetboy acu	INTEGRA Biosciences, Fernwald
High-Speed Centrifugation Tubes	Polypropylene Centrifuge Tubes (25 x 89 mm)	Beckman Coulter, USA
Power Supply	PowerPac	Bio-Rad Laboratories, München
Rollermixer	RollerMixer SRT6	Stuart Scientific, Asbach
Scale	ABT 120-SDM	Kern&Sohn, Balingen
SDS Gel System	Mini Protean Cell	Bio-Rad Laboratories, München
Shaker	WS 10	Edmung Bühler GmbH, Hechingen
	Rocker 2D digital	IKA, Staufen
	3D Rocking Shaker	StarLab, Hamburg
Sonicator	Sonoplus mini20	Bandelin, Berlin

Instrument	Model	Manufacturer
Stirring Plate	Ikama RCT	Ika, Staufen
Thermocycler	T Personal	Biometra, Jena
Thermocycler	One Cycler	VWR, Darmstadt
Turbo-Blotter	Trans-Blot Turbo Transfer System	Bio-Rad Laboratories, München
Ultra fine scale	ABT 120-5DM	Kern&Sohn, Balingen-Frommern
Vortex Mixer	VWR VV3	VWR, Darmstadt
	REAX 2000	Heidolph, Schwabach

4.1.2 CONSUMABLES

Table 6: Consumables

Type	Supplier
Acrylamid (Rotiphorese 30)	Carl Roth, Karslruhe
Agarose	Invitrogen, Karlsruhe
Amicon® Ultra Centrifugal Filters (10 kDa MWCO)	Sigma Aldrich, Merck, Darmstadt
Ammoniumpersulfat (APS)	AppliChem, Darmstadt
Bovine Serum Albumin (BSA)	AppliChem, Darmstadt
Bradford Protein Assay	Bio-Rad, Dreieich
Bromphenolblau	Sigma Aldrich, Merck, Darmstadt
Casy-Blue	OMNI Life Science, Hamburg
Casy-Ton	OMNI Life Science, Hamburg
Cell Culture Bottles T25, T75, T225	Greiner Bio-One, Österreich
Cell Culture Dish, microscopy	Mattek, USA
Cell Culture Dish, migration assay	Ibidi, Martinsried
Cell Culture Plates 10 cm	Greiner Bio-One, Österreich
Cell Culture Plates 96 well, half-area	Greiner Bio-One, Österreich
Cell Culture Plates 96/24/12/6 well	Greiner Bio-One, Österreich
Cell Culture Plates, low adhesion, round bottom	Corning, USA
Cell Culture Slides, 8 well	Ibidi, Martinsried
Cisplatin, clinical grade	University Medical Center Mainz Pharmacy

Type	Supplier
Complete Protease Inhibitor	Roche, Penzberg
Cryoconservation Tubes	Biozym Scientific GmbH, Hessisch Oldendorf
Dimethylsulfoxid (DMSO)	AppliChem, Darmstadt
Dithiothreitol (DTT)	Carl Roth, Karslruhe
DMEM	Gibco, Invitrogen, Karlsruhe
DMEM/F12	c. c. pro GmbH, Oberdorla
dNTP Mix, 10 mM	Roche, Penzberg
Ethanol	Carl Roth, Karlsruhe
Ethanol, denatured	Höfer Chemie, Kleinblittersdorf
Ethidium Bromide	Sigma Aldrich, Merck, Darmstadt
Ethyldiamintetaacetat-Dinatriumsalt (EDTA)	AppliChem, Darmstadt
Falcon Tubes (15 mL, 50 mL)	Greiner Bio-One, Austria
Fetal Calf Serum (FCS)	Gibco, Invitrogen, Karlsruhe
GeneRuler 1 kb DNA Ladder	Thermo Fisher Scientific, Dreieich
Glutamine solution (200 mM)	Gibco, Invitrogen, Karlsruhe
Glycine	AppliChem, Darmstadt
Hoechst 33342	Sigma Aldrich, Merck, Darmstadt
HEPES (1 M)	Sigma Aldrich, Merck, Darmstadt
InstantBlue Protein Stain	Expedeon, Heidelberg
Isopropanol	Fisher Scientific, Schwerte
JetPRIME	Polyplus Transfection, France
KCl	Carl Roth, Karslruhe
KH_2PO_4	Carl Roth, Karslruhe
Lipofectamin 2000	Invitrogen, Karlsruhe
Lysogeny broth (LB) medium	Carl Roth, Karlsruhe
Mercaptoethanol	Carl Roth, Karslruhe
Methanol	Carl Roth, Karslruhe
$MgSO_4$	AppliChem, Darmstadt
Microreaction tubes (0,5 mL, 1,5 mL, 2 mL)	Ratiolab, Dreieich
Microreaction tubes (5 mL)	Eppendorf, Hamburg

Type	Supplier
Mini-PROTEAN TGX Precast Gels	Bio-Rad Laboratories, Dreieich
NaCl	Carl Roth, Karlsruhe
$NaHCO_3$	Carl Roth, Karlsruhe
$NaHCO_3$ solution (7,5 %)	Gibco, Invitrogen, Karlsruhe
NEAA (100x)	Gibco, Invitrogen, Karlsruhe
OptiMEM	Gibco, Invitrogen, Karlsruhe
Paclitaxel	Sigma Aldrich, Merck, Darmstadt
PageRuler Plus Prestained Protein Ladder	Thermo Fisher Scientific, Dreieich
Paraformaldehyd	Serva Electrophoresis, Heidelberg
PBS, sterile	Gibco, Invitrogen, Karlsruhe
Penicillin/Streptomycin (PenStrep) (10.000 U/mL Pen, 10 mg/mL Strep)	Gibco, Invitrogen, Karlsruhe
Pipette Tips (10 µL)	Starlab, Hamburg
Pipette Tips (200 µL, 1.000 µL, 5.000 µL)	Falcon, Corning, USA
Pipettes (2 mL)	Corning, USA
Pipettes (5 mL, 10 mL, 25 mL)	Greiner Bio-One, Austria
Polypropylene Tube (38,5 mL)	Beckman-Coulter, Krefeld
qEVoriginal / 35 nm columns	Izon Science, Christchurch
ReBlot strong (10x) Stripping Buffer	Chemicon International
RPMI	Gibco, Invitrogen, Karlsruhe
Skim Milk Powder	AppliChem, Darmstadt
Sodiumdodecylsulfat (SDS)	Carl Roth, Karslruhe
Syringe Filter (sterile, 0,22 µm pore size)	Merck Milipore, Darmstadt
Tetramethylethylendiamin (TEMED)	Serva Electrophoresis, Heidelberg
TransWell inserts (0,4 µM pore size)	Greiner Bio-One, Austria
Tris(hydroxymethyl)-aminomethan (Tris)	Neolab, Heidelberg
Triton X-100	Sigma Aldrich, Merck, Darmstadt
Trypsin LE Express	Gibco, Invitrogen, Karlsruhe
Tween 20	AppliChem, Darmstadt
Urea	Merck, Darmstadt

4.1.3 BUFFERS AND SOLUTIONS

Table 7: Buffers and Solutions

Type	Composition
0,2 % Tween	0,2 % Tween 20 in PBS
1 % Agarose gel	1 % agarose in TAE
1 x Dissociation Buffer	62,5 mM Tris, 10 % glycerine, 2 % SDS, 50 mM DTT, 0,01 % bromphenol blue
6 x Dissociation Buffer	350 mM Tris-HCl, 30 % β-mercaptoethanol, 10 % SDS, 30 % glycerine, 0,02 % bromphenol blue
DNA Loading Buffer	15 % glycerine (87 %), 3 mM EDTA, 600 mg/l bromphenol blue
Lysis Buffer	8 M urea, 2 % CHAPS, 0,01 % bromphenol blue
Milk/PBS	5 % skim milk powder in PBS
PBS	4,3 mM Na_2HPO_4, 1,4 mM KH_2PO_4, 137 mM NaCl, 2,7 mM KCl, pH 7,4
PBS-T	0,1 % Tween 20 in PBS
RIPA Buffer	150 mM NaCl, 50 mM Tris-HCl, 1 mM EDTA, 1 % NP-40, 1 % Na-desoxycholat, 0,5 mM PMSF, Complete 1/50 mL 0,1 % SDS
SDS Buffer (Stacking gel)	26,6 ml Rotiphorese 30, 125 mM Tris-HCl (pH 6,8), 0,1 % SDS, *ad* 200 mL
SDS Buffer	3 g/l Tris, 14,4 g/l Tris, 1 g/l SDS
Tris-Acetat-EDTA-Puffer (TAE)	4,84 g/l Tris, 2,29 g/l Na·3 H_2O, 1 mM EDTA, pH 8 (HCl)
Tris-HCl	0,5 M Tris, pH 6,8 (HCl)

4.1.4 COMMERCIAL KITS

Table 8: Commercial Kits

Type	Supplier
AlamarBlue	Thermo Fisher Scientific, Dreieich
CellTiterGlo 2.0	Promega, Mannheim
CellTiterGlo 3D	Promega, Mannheim
Clarity Western ECL	Bio-Rad Laboratories, Dreieich
Dynabeads FlowComp Flexi	Thermo Fisher Scientific, Dreieich
PKH26 Red Fluorescent Cell Linker Mini Kit for General Cell Membrane Labeling	Sigma Aldrich, Merck, Darmstadt
Plasmid Plus Maxi Kit	Qiagen, Hilden
Plasmid Plus Mini Kit	Qiagen, Hilden
pluriBeads S	pluriSelect, Leipzig
QIAquick Gel Extraction Kit	Qiagen, Hilden
TaqMan Fast Advanced Master Mix	Thermo Fisher Scientific, Dreieich
TaqMan Assays	Thermo Fisher Scientific, Dreieich
Total Exosome RNA and Protein Isolation Kit	Invitrogen, Karlsruhe
Trans-Blot Turbo RTA Mini PVDF Transfer Kit	Bio-Rad Laboratories, Dreieich

4.1.5 CELL LINES

Table 9: Cell Lines

Name	Organism, Entity	Medium	ATCC/Reference
293T	Human embryonic kidney	DMEM, 10 % FCS, 2 mM Glutamin, 1x PenStrep	CRL-11268 CVCL_0063
FaDu	Human hypopharyngeal squamous cell carcinoma	DMEM, 10 % FCS, 2 mM Glutamin, 1x PenStrep, 1x NEAA, 10 mM HEPES, 1,5 mg $NaHCO_3$	ATCC-HTB43 CVCL_1218
HNSCCUM-02T	Human squamous cell carcinoma, base of the tongue	DMEM:F12, 10 % FCS, 2 mM Glutamin, 1x PenStrep	Welkoborsky et al. 2003
HNSCCUM-03T	Human squamous cell carcinoma, pyriform sinus	DMEM:F12, 10 % FCS, 2 mM Glutamin, 1x PenStrep	Welkoborsky et al. 2003

4.1.6 OLIGONUCLEOTIDES

Table 10: Oligonucleotides

Primer -No.	Name	Sequence (5‘ → 3‘)	Application
3221	ACTB for	GTGGGGCGCCCCAGGCACCA	cDNA control
3222	ACTB rev	CTCCTTAATGTCACGCACGATTTC	cDNA control

4.1.7 PLASMIDS

Table 11: Plasmids

Name	Features	Encoded Resistance
Bio CD63-emGFP	emGFP-tagged CD63	Ampicillin, Puromycin

4.1.8 ENZYMES

Table 12: Enzymes

Enzyme	Supplier
KAPA HiFi-DNA-Polymerase	Roche, Penzberg
RNase-free DNase	Qiagen, Hilden
Taq-DNA-Polymerase	BioAxis Genecraft Products, Köln

4.1.9 ANTIBODIES

Table 13: Antibodies

No.	Antigen	Host	Dilution Western Blot	Dilution Immunofluorescence
Primary Antibodies				
F101	**TSG101**	mouse	1:1.000	
F64	**CD63**	mouse	1:1.000	
F63	**CD81**	mouse	1:1.000	
F102	**Calnexin**	rabbit	1:1.000	
31	**GAPDH**	mouse	1:1.000	
35	**GFP (FL)**	rabbit	1:1.000	
B19	**Lamin A/C**	rabbit	1:1.000	
221	**Pan-CK-PE**	mouse		1:50
219	**EpCAM-PE**	mouse		1:50
223	**ZO-1-Alexa 594**	mouse		1:50
222	**E-Cadherin-Alexa 594**	rabbit		1:50
225	**CSV-PE**	mouse		1:50
59	**CD45-FITC**	mouse		1:50
209	**γH2AX**	rabbit		1:200
Secondary Antibodies				
B73	**α-mouse (HRP)**	horse	1:5.000	
S31/B74	**α-rabbit (HRP)**	goat	1:5.000	
S25	**α-rabbit (TexasRed)**	goat		1:200
-	**α-rabbit (Cy3)**	goat		1:300

4.1.10 SOFTWARE

Table 14: Software

Program	Supplier/Reference
Axiovision	Zeiss, Oberkochen
BioEdit	BioEdit, available from https://bioedit.software.informer.com/7.2/.
BLAST, GeneBank	National Center for Biotechnology Information (NCBI). Bethesda (MD): National Library of Medicine (US), National Center for Biotechnology Information. Available from https://www.ncbi.nlm.nih.gov/
Canvas	Canvas GFX, Inc., Boston, USA
Fiji/ImageJ	See Schindelin et al., 2012
GraphPad PRISM 8	Graphpad Software, Inc., San Diego, USA
Ingenuity Pathway Analysis (IPA)	Qiagen, Hilden
Leica Image Suite	Leica, Wetzlar
NEBioCalculator	New England Biolabs, Inc., Ipswich, USA. Available from: https://nebiocalculator.neb.com

4.2 Working with Mammalian Cells

4.2.1 Cell Culture and Storage

Cell lines were stored in liquid nitrogen and thawed in a water bath at 37 °C for usage. Every cell line was cultured in its respective medium (Table 5) at 37 °C and 5 % CO_2 under humidified conditions. For passaging, cells were washed with PBS and detached by incubation with Trypsin at 37 °C. After a maximum of 5 min of co-incubation with Trypsin, detached cells were resuspended in fresh medium and the desired amount of cells was transferred to a new cell culture flask. Cells were passaged every 2 to 5 days, according to doubling time and experimental needs. To prepare stocks, cells were expanded to bigger flasks (T75 for 3 stocks, T125 for 5 stocks) at an early passage after thawing. When cells reached confluency, they were detached using Trypsin and pelleted at 1.500 rpm for 5 min. Cell pellets were resuspended in FCS containing 10 % DMSO. Aliquots of 1 mL were cooled down using a cell freezing container at -80 °C and then transferred to a liquid nitrogen tank for long term storage.

4.2.2 Viable Cell Count

Viable cell count was determined using the Casy TTC (Roche Innovatis, Bielefeld). Specific measurement parameters were established for every cell line. Therefore 50-100 µL of the respective cell suspension were incubated with 200 µL CasyBlue for 10 min and then mixed with 10 mL CasyTon to determine live/dead cells. For regular measurements 50-100 µL of cells in solution were mixed with 10 mL CasyTon and analysed using the established parameters.

4.2.3 TransWell Co-Culture

Cells were seeded in 12-well plates at a density of 5 x 10^3 cells/well and corresponding transwell inserts at 2,5 x 10^3 cells/transwell. After 24h, co-culture was started. After 6 days of incubation, cells were treated with 20 µM cisplatin. Viability was assayed 72h after onset of treatment. Viability was normalized to controls without transwell inserts.

4.2.4 Spheroid Cell Culture

To generate three-dimensional cell spheroids, cells were seeded at a density of 1000 cells/well in special Ultra Low Attachment Round Bottom 96-well cell culture plates (Corning). Approximately 50 % of the medium was aspirated and exchanged for fresh medium every 3 to 5 days according to experimental needs. Spheroids were allowed to form for at least 3 days before any experiments/treatments were performed.

4.2.5 Cell Transfection

For transfection, cells were seeded in the desired cell culture plate or dish at defined numbers and plasmid DNA was introduced into the cells using the JetPrime transfection reagent. The transfection mixture was prepared according to Table 15. First, the desired amount of plasmid DNA was diluted in JetPrime buffer and vortexed for 10 sec. Then the JetPrime reagent was added and the sample was vortexed again. After 10 min incubation at RT, the mixture was added to the cells. After 5 h or overnight incubation the medium was exchanged.

Table 15 JetPrime transfection mixture

Format	JetPrime buffer [µL]	DNA [µg]	JetPrime reagent [µL]
6-Well	200	1-2	2-4
24-Well	50	0,5	1
96-Well	10	0,1	0,2

4.2.6 Preparation of Cells for Microscopy

For microscopy, cells were seeded into glass-bottom microscopy dishes at defined numbers. Imaging was either performed on live cells or fixed cells. For fixation, medium was aspirated and cells were washed with PBS. 4 % PFA was added and cells were incubated for 20 min at RT, followed by three PBS washes. If necessary, cells were also permeabilized with 0,2 % Triton-X 100 in PBS for 5 min at RT and then blocked in 0,5 % BSA in PBS for 30 min at RT.

4.2.6.1 Staining of the Nucleus

Nuclear staining was achieved with Hoechst 33342. Cells were co-incubated with Hoechst at a final concentration of 0,5 ng/mL for 10 min at RT (fixed cells) or in the incubator (live cells).

4.2.6.2 Immunofluorescence Staining

For immunofluorescence staining cells needed to be fixed and potentially permeabilized as described in section 4.2.1.5. The primary antibody was diluted in 0,5 % BSA in PBS and incubated with the cells at 4 °C overnight. After three PBS washes the secondary, fluorescently labelled antibody diluted in PBS was added. After 1-2 h incubation at RT the cells were washed three times with PBS and then either directly imaged or stored at 4 °C. Respective antibody dilutions can be found in Table 13.

4.2.6.3 Migration Assay

For the migration assay, cells were seeded at 10^4 cells per chamber in migration assay dishes (ibidi, Martinsried) and incubated until they reached confluency. Medium was exchanged every three to four days. Then, the silicone insert was removed, creating a 500 µM gap in the cell population. Closure of this gap was observed microscopically and quantified using the AxioVision software.

4.2.6.4 Carboxyfluoresceinsuccinimidylester (CFSE) Staining

Cells were detached and pelleted at 400x *g* for 5 min. Afterwards the cells were resuspended in 1 mL prewarmed PBS and 2 µL CFSE staining solution were added. After 15 min incubation at 37 °C cells were pelleted again and washed twice with cell culture medium. Cells were finally resuspended in 1 mL cell culture medium. For spiking experiments, stained cells were transferred into microscopy dishes and incubated for 10-15 min until cells sedimented. Then cells were counted and spiked into medium or whole blood using a fluorescence microscope.

4.2.7 Fluorescence Microscopy

Fluorescence microscopy was performed on a Zeiss Axiovert microscope either with optimal or fixed excitation times depending on the experiment. Image analysis was performed using Leica image suite and imageJ.

4.2.8 Determination of Cell Viability

4.2.8.1 CellTiterGlo Assay

To determine cell viability in two-dimensional cultures the CellTiter-Glo® 2.0 Viability Assay kit (Promega) was applied according to the manufacturer's instructions. For three-dimensional cultures, the CellTiter-Glo® 3D Viability Assay kit (Promega) was used according to the manufacturer's instructions. Luminescence was measured using a Tecan Spark multiplate reader. Viability was normalized to control samples incubated under the same conditions.

4.2.8.2 Alamar Blue Assay

To determine cell viability by Alamar Blue Assay, cell culture medium was changed to fresh medium containing 10 % Alamar Blue and incubated for 30-60 min. The fluorescence of resorufin was detected using a Tecan Spark multiplate reader with 550 nm excitation and 595 nm emission wave lengths. Viability was normalized to control samples incubated under the same conditions.

4.2.9 High-Content-Analysis

High content analysis (HCA) was performed at an Array Scan VTI (Thermo Fisher). To determine phenotypic spheroid parameters, the *Morphology* assay was used in bright light mode on live spheroids. A more detailed description of the protocol can be found in section 2.3.3. Data was exported as mean value per well. Further analysis was performed using Microsoft Excel and Graphpad Prism.

4.2.10 CTC ISOLATION

4.2.10.1 DYNABEADS FLOWCOMP FLEXI

50 µg of EpCAM or CSV antibodies were coupled to DSB-X biotin according to manufacturer's instructions. For EpCAM based isolation 25 µL, for EpCAM plus CSV based isolation 15 µL each of biotinylated antibodies were added to 5 or 7,5 mL samples and cells were enriched according to the manufacturer's instructions using the DynaMag-15 (Thermo Fisher Scientific, Dreieich). For the reduction of magnetic forces on the cells a protocol using weaker magnets was applied. For automated enrichment using the *IsoMAG* platform, samples were transferred to the instrument after incubation with the beads. Detachment from the beads was performed manually. After release from the beads cells were resuspended in 200 µL cell culture medium and transferred to 8-well slides for microscopic evaluation.

4.2.10.2 PLURIBEADS

For self-coupled beads, 10 µg EpCAM antibody were coupled to 400 µL of pluriBeads according to manufacturer's instructions. Isolation was carried out using 160 µL of beads in 5 or 7,5 mL samples according to manufacturer's instructions. After release from the beads cells were resuspended in 200 µL cell culture medium and transferred to 8-well slides for microscopic evaluation.

4.3 Working with Exosomes

4.3.1 Exosome Isolation by Ultracentrifugation (UC)

4.3.1.1 Exosome Isolation from Cell Culture Medium

For exosome isolation, cells were seeded in 10 cm or 20 cm cell culture dishes. When cells reached 80-90 % confluency, medium was exchanged to FCS-free medium to avoid contamination with serum exosomes. Cells were cultured in FCS-free medium for 48-72h. Then, conditioned medium was collected and subjected to a series of centrifugations at 4 °C. The first centrifugation was carried out at 500x *g* for 10 min to pellet any remaining cells. The supernatant was transferred to a fresh tube and centrifuged at 3.000x *g* for 20 min to remove dead cells and debris. Next, the supernatant was transferred to a polypropylene tube and weighed in to exactly balance out the centrifuge. High speed centrifugation was carried out in an Avanti JXN-30 at 12.000x *g* for 20 min without break to remove any remaining debris from the sample. Finally the supernatant was transferred to a fresh polypropylene tube and exosomes were pelleted at 100.000x *g* for 90 min. Afterwards the supernatant was removed and the exosomes were resuspended in PBS. After pelleting the exosomes again at 100.000x *g* for 90 min, they were resuspended in PBS, cell culture medium, or lysis buffer according to experimental needs. They were either used directly or stored at 4 °C or -20 °C overnight. Storage duration never exceeded 20 h.

4.3.1.2 Exosome Isolation from Blood

Blood samples were collected in EDTA tubes and stored at 4 °C for up to 24h. For plasma separation, samples were centrifuged at 2.000x *g* for 15 min at 4 °C. Afterwards exosomes were isolated by ultracentrifugation as described in the previous section.

4.3.2 PKH26 Staining of Exosomes

For PKH26 staining exosomes were diluted in PBS. Staining was performed using a commercial kit (Sigma Aldrich, Darmstadt). The exosome sample was mixed 1:1 with diluent C. Afterwards 0,6 µL PKH26 dye per 100 µL sample were added and mixed in by pipetting for 30 sec. After 5 min incubation at RT the reaction was stopped by adding 1:2 10 % BSA in PBS. The sample was transferred to a ultracentrifuge tube and filled up to 30 mL with PBS. Then a 5,25 mL 0,9 M sucrose cushion was added and the sample was centrifuged at 100.000x *g* for 90 min. Pelleted exosomes were resuspended according to experimental needs.

4.3.3 Sulfo-Phospho-Vanillin (SPV) Lipid Assay

Exosomes were isolated from cell culture supernatant as described in section 4.3.1 and diluted in PBS. Phospho-Vanillin solution was prepared according to Table 16. To generate a standard curve, a liposome standard stock was prepared. 1 mg of 1,2-Dioleoyl-sn-glycero-3-phosphocholine (DOPC) liposomes in chloroform was incubated at 60 °C under a fume hood until chloroform had evaporated. After resuspending in 1 mL PBS, the solution was vortexed vigorously for 2 min. Then it was sonicated at 30 kHz at 45 °C for 10 min and vortexed again for 2 min. The resulting liposome standard solution was stored at 4 °C and vortexed before usage. For the assay, 40 µL of sample or standard were mixed with 200 µL 96 % sulfuric acid, vortexed and incubated at 90 °C for 20 min with open lid under a fume hood. After cooling down at 4 °C for 5 min, 120 µL Phospho-Vanillin were added to the samples and vortexed. Then 100 µL sample mix were added to a 96-Well plate in triplicates. After incubation at 37 °C for 1h, the absorbance was measured at 540 nm in a Tecan Spark multiplate reader. Lipid concentrations were calculated from the liposome standard curve.

Table 16 Phospho-Vanillin Composition

Component	Amount
Vanillin	50 mg
Water	40 mL
85 % phosphoric acid	10 mL

4.3.4 Cryo-Transmission Electron Microscopy

Exosomes were isolated from cell culture supernatant and blood plasma as described above and diluted in PBS. Samples were stored at 4 °C overnight until imaging. Cryo-transmission electron microscopy (TEM) and sample preparation were carried out at the Max Planck Institute for Polymer Research. 3 µL of each sample were applied to a Quantifoil or a lacey carbon coated TEM grid, that had been glow discharged in an oxygen plasma cleaner (Diener electronic, Ebhausen) shortly before. Excess sample was removed with a filter paper. Then, the sample was vitrified by plunging the grid into liquid ethane using a Vitrobot Mark V (Thermo Fisher, Hilsboro Oregon). For subsequent examination the sample was transferred to a TEM (FEI Titan Krios G4) keeping cryogenic conditions. Imaging was done using an acceleration voltage of 300 kV.

4.3.5 Tunable Resistive Pulse Sensing (TRPS) Analysis

Exosome were characterized by Tunable Resistive Pulse Sensing (TRPS) by Izon Science Limited ©, Lyon, France. Exosomes were isolated from cell culture supernatant as described in 4.3.1 and diluted in PBS. Measurement was carried out using the Izon qNano.

4.3.6 Dynamic Light Scattering (DLS) Analysis

Exosome size was measured by Dynamic Light Scattering (DLS) using the Malvern Nano S90. Exosomes were isolated from cell culture supernatant as described in section 4.3.1.1 and diluted in PBS. Measurement was carried out at the Max Planck Institute for Polymer Research.

4.4 Working with Proteins

4.4.1 Preparation of Protein Lysates from Mammalian Cells

For protein lysates, mammalian cells were grown in 10 cm culture dishes or in 6-well plates and harvested by scraping. The detached cells were taken up in cold PBS and centrifuged at 1500 rpm for 5 min at 4 °C. The cell pellet was then resuspended in 1 mL cold PBS and pelleted again. Thereafter the cell pellet was resuspended in 50-200 µL RIPA buffer according to pellet size. Samples were incubated on ice for 20 min. During this incubation time the samples were sonicated (amplitude 50 %, 0,5 s pulses for 30 s per interval) in three intervals with 5 min breaks in between. After sonication, the samples were centrifuged at 13.000 rpm for 20 min at 4 °C to clear out any remaining cell debris. The supernatants were collected in fresh tubes and either used directly or stored at -80 °C.

4.4.2 Preparation of Protein Lysates from Exosomes

Exosomes were isolated as described in section 4.3.1. After the second centrifugation at 100.000x *g* the pelleted exosomes were resuspended in 50-60 µL RIPA buffer. Samples were incubated on ice for 20 min. During this incubation time the samples were sonicated (amplitude 50 %, 0,5 s pulses for 30 s per interval) in three intervals with 5 min breaks in between. Samples were either used directly or stored at -80 °C. For gel separation samples were mixed with Laemmli buffer and boiled for 5 min at 95 °C.

4.4.3 Determination of Protein Concentration

4.4.3.1 Bradford Assay

Protein concentrations were determined using a commercial Bradford stock solution (Bio-Rad, Dreieich). The stock solution was diluted 5-fold with water before use. 10 µL of sample were mixed with 90 µL of Bradford solution in a 96-Well plate. After 10 min of incubation at RT the absorption at 595 nm was measured using a Tecan Spark multiplate reader. Protein concentration was calculated using a standard curve generated by measuring BSA samples of known concentration under the same conditions.

4.4.3.2 DC ASSAY

For samples containing detergents, using Lowry-based assays is advised. DC assay components were purchased from Bio-Rad (Dreieich) and used according to manufacturer's instructions. After 15 min of incubation at RT the absorption at 750 nm was measured using a Tecan Spark multiplate reader. Protein concentration was calculated using a standard curve generated by measuring BSA samples of known concentration under the same conditions.

4.4.4 PROTEIN ANALYSIS VIA SDS-PAGE

SDS gels were poured in glass chambers with a distance of 1,5 mm (Bio-Rad, Dreieich). Gel compositions are shown in Table 17. The separation gel was poured first and topped off with a small volume of methanol to generate an even surface. After polymerization for 1h, the methanol was removed and the stacking gel was added. A comb was introduced to generate pockets for sample application. After another hour of polymerization, the gels were stored at 4 °C under moist conditions. Alternatively commercial gels (Mini-PROTEAN TGX Precast Gel, Bio-Rad Laboratories, Dreieich) were used.

Table 17: SDS-Page Gel Composition

Component	Separation gel (10 %)	Stacking gel
SDS buffer	3,3 mL	-
Stacking gel buffer	-	5 mL
Acrylamide	2,5 mL	-
Water	4,2 mL	-
APS (10 %)	100 µL	50 µL
TEMED	10 µL	5 µL

Samples were prepared by mixing with dissociation buffer and boiling at 95 °C for 5 min. Afterwards samples were centrifuged at 13000 rpm for 5 min to remove any aggregates. Supernatants were applied to the gel. Additionally a protein ladder (PageRuler Plus Prestained Protein Ladder, Thermo Fisher Scientific) was added to the gel for size comparison. The gel was run at 60 V until samples passed through the stacking gel, then voltage was increased to 90 V. Commercial gels were run at 90 V. After the electrophoresis was finished, gels were removed from the chamber and further analyzed by Western Blot.

4.4.5 Western Blot Analysis

For Western Blot analysis, proteins separated by SDS-PAGE were transferred onto PVDF membranes. Therefore the membrane was activated by incubation in methanol for 2 min. Then, whatman paper soaked in transblot buffer, the membrane, the SDS gel and another soaked whatman paper were stacked in the cassette of a turbo blotter and additional transblot buffer was added to ensure semi-dry conditions. Blotting was carried out at 20 V and 0.8 Amp for 30 min. Afterwards the membrane was transferred to 5 % milk in PBS for blocking. After 1h incubation with mild shaking at RT the primary antibody diluted in 5 % milk in PBS was added and the membrane was incubated at 4 °C with mild shaking overnight. Then the membrane was washed three times for 5 min each. The first washing step was carried out using 0,1 % Tween in PBS, the following two with just PBS. Then the secondary antibody diluted in 5 % milk in PBS was added and the membrane was incubated at RT with mild shaking for 1h. After three washes with PBS, the protein bands were visualized by adding a thin layer of ECL substrate and detecting luminescence with a ChemiDoc. Additionally a colorimetric image of the membrane was taken to visualize the protein ladder for size comparison. To detect further proteins on the same membrane, it was stripped by incubation with Reblot buffer for 10 min at RT. After three washes in PBS the whole procedure was started again beginning with the blocking step. The respective antibody dilutions can be found in Table 13.

4.5 Working with Nucleic Acids

4.5.1 Extraction of RNA from Mammalian Cells

Cells were seeded in 10 cm dishes at defined numbers and allowed to grow for 48-72h before RNA extraction. Cells were washed twice with cold PBS. 1 mL of Trizol was added per plate and cells were scraped off of the surface and collected in a 2 mL tube. After homogenization by vortexing, 200 µL Chloroform were added and samples were vortexed again. After a 3 min incubation at RT samples were centrifuged at 12.000x *g* for 15 min at 4 °C. Supernatants were transferred to a fresh tube and one volume of 100 % ethanol was added. Now the samples were transferred onto RNeasy Mini Kit columns and spun down at 8.000x *g* for 15 sec. Then 350 µL RW1 from the kit were added and samples were spun down at 8.000x *g* for 15 sec again. Then 10 µL of DNAse were added for 15 min at RT to degrade any contaminating DNA. Afterwards the procedure was carried out according to the manufacturer's instructions. RNA was eluted in 30-50 µL RNAse-free water and concentration as wells as purity were determined using a nanophotometer. RNA was immediately reverse-transcribed into cDNA if A260/280 was greater than 1.9 and left-over RNA was stored at -80 °C.

4.5.2 Extraction of RNA from Exosomes

Exosomes were isolated according to 4.3.1 and diluted in 200 µL PBS. RNA was isolated and enriched for small RNA using the Total Exosome RNA and Protein Isolation Kit (Invitrogen, Karlsruhe) according to manufacturer's instructions, with an additional DNA degradation after the first washing step. For DNA degradation DNAse was added to the column and incubated for 15 min at RT.

4.5.3 cDNA Synthesis

For cDNA synthesis starting from 1 µg of isolated RNA, the SuperScript IV VILO kit (Thermo Fisher Scientific, Dreieich) was used according to manufacturer's instructions. Reaction mix and thermocycler program can be taken from Tables 18 and 19. To check the isolated RNA for contaminations with DNA, reactions with and without reverse transcriptase were prepared for each sample. PCR analysis of housekeeping gene Actin-β (ACTB) was performed on the synthesized cDNA samples. Samples containing reverse transcriptase should show a band at 657 bp, while samples not containing reverse transcriptase should show no band when separated in an agarose gel after performance of PCR.

Table 18: SuperScript IV VILO Reaction Mix

Component	Amount [µL]
5x VILO reaction mix	4
RNA-free water	*ad* 20

Table 19: Thermocycler program SuperScript IV VILO

Temperature [°C]	Time [min]
25	5
50	60
85	5

4.5.4 Polymerase Chain Reaction (PCR)

The Taq polymerase was used for analytical PCR. Reaction mix and Thermocycler program can be taken from Tables 20 and 21.

Table 20: Taq Polymerase Reaction Mix

Component	Amount [µL]
DNA	x
Primer I	1
Primer II	1
dNTPs	0,5
Buffer	2
Taq polymerase	0,5
Water	*ad* 20

Table 21: Thermocycler program Taq

Temperature [°C]	Time [mm:ss]	Number of Cycles
95	10:00	1
95	00:30	
x	00:30	30
72	01:00	
72	07:00	1
4	∞	

4.5.5 Gel Electrophoresis

Agarose gel electrophoresis was used to separate DNA fragments according to their size. For gel preparation, 35 mL of 1 % agarose in TAE buffer were heated until boiling in a microwave. After cooling, 7 µL ethidium bromide were added to the solution and it was poured into a gel chamber, where it was left to solidify. For DNA sample preparation, DNA was mixed with loading buffer (6x) and then transferred into the gel pockets. A size standard was applied to the gel for comparison. The gel was then run at 90 V for up to 60 min. Afterwards bands were visualized on a UV table.

4.5.6 Quantitative PCR (qPCR)

TaqMan assays and master mix were purchased from Thermo Fisher Scientific. For qPCR a reaction mix containing 1-4 µL of cDNA was prepared according to Table 22. Samples were analyzed using a QuantStudio 1 Real-Time PCR cycler (Thermo Fisher Scientific, Dreieich) applying the comparative Ct method (ΔΔ Ct). ACTB was used as endogenous control (ECr). Target and ECr were multiplexed in one well. Wildtype (WT) or untreated samples were used as reference samples. The Thermocycler program can be taken from Table 23.

Table 22: TaqMan Reaction Mix

Component	Amount [µL]
20x TaqMan Assay Target	1
20x TaqMan Assay ECr	1
2x TaqMan Master Mix	10
cDNA template	1-4
Water	*ad* 20

Table 23: Thermocycler program TaqMan

Temperature [°C]	Time [mm:ss]	Number of Cycles
50	02:00	1
95	10:00	1
95	00:15	40
60	01:00	

4.5.7 RNA Sequencing

Total RNA sequencing was performed by CeGaT GmbH, Tuebingen. RNA was extracted from exosomes as described in section 4.5.2 in three independent experiments per group. DNA contamination was checked by performing cDNA transcription with and without addition of reverse transcriptase and subsequent control for amplification of housekeeping gene actin-β in a PCR reaction. Samples were shipped on dry ice. Differential expression analysis between groups was performed with DESeq2 (version 1.24.0). Adjusted p-values were calculated with Benjamini-Hochberg correction. Z-scores were calculated from normalized counts.

4.5.8 Patient Gene Expression Analysis

Publicly available gene expression and survival data was obtained from *The Cancer Genome Atlas* (TCGA), filtering for patients with HNSCCs (TCGA HNSC). Patient data was accessed via the USCS Xena server and further analysed using GraphPad Prism software. Phenotypic parameters were set to “disease_after_curative_tx” to filter for patients with residual disease or remission after primary therapy. Genotypic parameters were set as indicated. Statistical evaluation of gene expression data was achieved by Welch’s t-test. Survival data was analysed using Log-rank/Mantel–Cox test.

4.5.9 Reactome Analysis

Reactome analysis was performed using the publicly available online platform reactome.org. Statistical analysis by hypergeometric distribution test with correction for multiple testing using the Benjamini-Hochberg method was performed.

5 LITERATURE

Abels, E. R. and Breakefield, X. O. (2016). "Introduction to Extracellular Vesicles: Biogenesis, RNA Cargo Selection, Content, Release, and Uptake." Cell Mol Neurobiol **36**(3): 301-312.

Aceto, N., Bardia, A., Miyamoto, D. T., Donaldson, M. C., Wittner, B. S., Spencer, J. A., Yu, M., Pely, A., Engstrom, A., Zhu, H. L., Brannigan, B. W., Kapur, R., Stott, S. L., Shioda, T., Ramaswamy, S., Ting, D. T., Lin, C. P., Toner, M., Haber, D. A. and Maheswaran, S. (2014). "Circulating Tumor Cell Clusters Are Oligoclonal Precursors of Breast Cancer Metastasis." Cell **158**(5): 1110-1122.

Airola, M. V. and Hannun, Y. A. (2013). "Sphingolipid metabolism and neutral sphingomyelinases." Handb Exp Pharmacol(215): 57-76.

Allard, W. J., Matera, J., Miller, M. C., Repollet, M., Connelly, M. C., Rao, C., Tibbe, A. G., Uhr, J. W. and Terstappen, L. W. (2004). "Tumor cells circulate in the peripheral blood of all major carcinomas but not in healthy subjects or patients with nonmalignant diseases." Clin Cancer Res **10**(20): 6897-6904.

Alsahafi, E., Begg, K., Amelio, I., Raulf, N., Lucarelli, P., Sauter, T. and Tavassoli, M. (2019). "Clinical update on head and neck cancer: molecular biology and ongoing challenges." Cell Death Dis **10**(8): 540.

Alves, A. C., Ribeiro, D., Nunes, C. and Reis, S. (2016). "Biophysics in cancer: The relevance of drug-membrane interaction studies." Biochim Biophys Acta **1858**(9): 2231-2244.

Amack, J. D. (2021). "Cellular dynamics of EMT: lessons from live in vivo imaging of embryonic development." Cell Commun Signal **19**(1): 79.

Amjad, M. T., Chidharla, A. and Kasi, A. (2022). Cancer Chemotherapy. StatPearls. Treasure Island (FL).

Anand, S., Samuel, M., Kumar, S. and Mathivanan, S. (2019). "Ticket to a bubble ride: Cargo sorting into exosomes and extracellular vesicles." Biochim Biophys Acta Proteins Proteom **1867**(12): 140203.

Andree, K. C., van Dalum, G. and Terstappen, L. W. (2016). "Challenges in circulating tumor cell detection by the CellSearch system." Mol Oncol **10**(3): 395-407.

Andreu, Z. and Yanez-Mo, M. (2014). "Tetraspanins in extracellular vesicle formation and function." Front Immunol **5**: 442.

Ashrafizadeh, M., Zarrabi, A., Hushmandi, K., Hashemi, F., Moghadam, E. R., Owrang, M., Hashemi, F., Makvandi, P., Goharrizi, M., Najafi, M. and Khan, H. (2021). "Lung cancer cells and their sensitivity/resistance to cisplatin chemotherapy: Role of microRNAs and upstream mediators." Cell Signal **78**: 109871.

Ashworth, T. R. (1869). "A case of cancer in which cells similar to those in the tumors were seen in the blood after death." Australasian Medical Journal **14**: 146-149.

Babaei, G., Asghari Vostakolaei, M., Rajabi Bazl, M., Gholizadeh-Ghaleh Aziz, S., Gholipour, E. and Nejati-Koshki, K. (2022). "The role of exosomes in the molecular mechanisms of metastasis: Focusing on EMT and cancer stem cells." Life Sci **310**: 121103.

Bae, S. Y., Byun, S., Bae, S. H., Min, D. S., Woo, H. A. and Lee, K. (2017). "TPT1 (tumor protein, translationally-controlled 1) negatively regulates autophagy through the BECN1 interactome and an MTORC1-mediated pathway." Autophagy **13**(5): 820-833.

Bakir, B., Chiarella, A. M., Pitarresi, J. R. and Rustgi, A. K. (2020). "EMT, MET, Plasticity, and Tumor Metastasis." Trends Cell Biol **30**(10): 764-776.

Balasubramanian, P., Lang, J. C., Jatana, K. R., Miller, B., Ozer, E., Old, M., Schuller, D. E., Agrawal, A., Teknos, T. N., Summers, T. A., Jr., Lustberg, M. B., Zborowski, M. and Chalmers, J. J. (2012). "Multiparameter analysis, including EMT markers, on negatively enriched blood samples from patients with squamous cell carcinoma of the head and neck." PLoS One **7**(7): e42048.

Banko, P., Lee, S. Y., Nagygyorgy, V., Zrinyi, M., Chae, C. H., Cho, D. H. and Telekes, A. (2019). "Technologies for circulating tumor cell separation from whole blood." J Hematol Oncol **12**(1): 48.

Bateman, N. W., Jaworski, E., Ao, W., Wang, G., Litzi, T., Dubil, E., Marcus, C., Conrads, K. A., Teng, P. N., Hood, B. L., Phippen, N. T., Vasicek, L. A., McGuire, W. P., Paz, K., Sidransky, D., Hamilton, C. A., Maxwell, G. L., Darcy, K. M. and Conrads, T. P. (2015). "Elevated AKAP12 in paclitaxel-resistant serous ovarian cancer cells is prognostic and predictive of poor survival in patients." J Proteome Res **14**(4): 1900-1910.

Bebawy, M., Combes, V., Lee, E., Jaiswal, R., Gong, J., Bonhoure, A. and Grau, G. E. (2009). "Membrane microparticles mediate transfer of P-glycoprotein to drug sensitive cancer cells." Leukemia **23**(9): 1643-1649.

Beltz, A., Gosswein, D., Zimmer, S., Limburg, I., Wunsch, D., Gribko, A., Deichelbohrer, M., Hagemann, J., Stauber, R. H. and Kunzel, J. (2019). "Staging of oropharyngeal squamous cell carcinoma of the head and neck: Prognostic features and power of the 8th edition of the UICC staging manual." Eur J Surg Oncol **45**(6): 1046-1053.

Bhattacharjee, S. (2016). "DLS and zeta potential - What they are and what they are not?" J Control Release **235**: 337-351.

Bierie, B., Pierce, S. E., Kroeger, C., Stover, D. G., Pattabiraman, D. R., Thiru, P., Liu Donaher, J., Reinhardt, F., Chaffer, C. L., Keckesova, Z. and Weinberg, R. A. (2017). "Integrin-beta4 identifies cancer stem cell-enriched populations of partially mesenchymal carcinoma cells." Proc Natl Acad Sci U S A **114**(12): E2337-E2346.

Bledsoe, T. J., Park, H. S., Stahl, J. M., Yarbrough, W. G., Burtness, B. A., Decker, R. H. and Husain, Z. A. (2017). "Hypofractionated Radiotherapy for Patients with Early-Stage Glottic Cancer: Patterns of Care and Survival." J Natl Cancer Inst **109**(10).

Boase, N. A. and Kumar, S. (2015). "NEDD4: The founding member of a family of ubiquitin-protein ligases." Gene **557**(2): 113-122.

Bold, I. T., Specht, A. K., Droste, C. F., Zielinski, A., Meyer, F., Clauditz, T. S., Munscher, A., Werner, S., Rothkamm, K., Petersen, C. and Borgmann, K. (2021). "DNA Damage Response during Replication Correlates with CIN70 Score and Determines Survival in HNSCC Patients." Cancers (Basel) **13**(6).

Booth, A. M., Fang, Y., Fallon, J. K., Yang, J. M., Hildreth, J. E. and Gould, S. J. (2006). "Exosomes and HIV Gag bud from endosome-like domains of the T cell plasma membrane." J Cell Biol **172**(6): 923-935.

Buglione, M., Grisanti, S., Almici, C., Mangoni, M., Polli, C., Consoli, F., Verardi, R., Costa, L., Paiar, F., Pasinetti, N., Bolzoni, A., Marini, M., Simoncini, E., Nicolai, P., Biti, G. and Magrini, S. M. (2012). "Circulating tumour cells in locally advanced head and neck cancer: preliminary report about their possible role in predicting response to non-surgical treatment and survival." Eur J Cancer **48**(16): 3019-3026.

Buratta, S., Tancini, B., Sagini, K., Delo, F., Chiaradia, E., Urbanelli, L. and Emiliani, C. (2020). "Lysosomal Exocytosis, Exosome Release and Secretory Autophagy: The Autophagic- and Endo-Lysosomal Systems Go Extracellular." Int J Mol Sci **21**(7).

Burtness, B., Harrington, K. J., Greil, R., Soulieres, D., Tahara, M., de Castro, G., Jr., Psyrri, A., Baste, N., Neupane, P., Bratland, A., Fuereder, T., Hughes, B. G. M., Mesia, R., Ngamphaiboon, N., Rordorf, T., Wan Ishak, W. Z., Hong, R. L., Gonzalez Mendoza, R., Roy, A., Zhang, Y., Gumuscu, B., Cheng, J. D., Jin, F., Rischin, D. and Investigators, K.-. (2019). "Pembrolizumab alone or with chemotherapy versus cetuximab with chemotherapy for recurrent or metastatic squamous cell carcinoma of the head and neck (KEYNOTE-048): a randomised, open-label, phase 3 study." Lancet **394**(10212): 1915-1928.

Carpen, T., Sorsa, T., Jouhi, L., Tervahartiala, T., Haglund, C., Syrjanen, S., Tarkkanen, J., Mohamed, H., Makitie, A., Hagstrom, J. and Mattila, P. S. (2019). "High levels of tissue inhibitor of metalloproteinase-1 (TIMP-1) in the serum are associated with poor prognosis in HPV-negative squamous cell oropharyngeal cancer." Cancer Immunol Immunother **68**(8): 1263-1272.

Castro, B. M., Prieto, M. and Silva, L. C. (2014). "Ceramide: a simple sphingolipid with unique biophysical properties." Prog Lipid Res **54**: 53-67.

Chapuy, B., Koch, R., Radunski, U., Corsham, S., Cheong, N., Inagaki, N., Ban, N., Wenzel, D., Reinhardt, D., Zapf, A., Schweyer, S., Kosari, F., Klapper, W., Truemper, L. and Wulf, G. G. (2008). "Intracellular ABC transporter A3 confers multidrug resistance in leukemia cells by lysosomal drug sequestration." Leukemia **22**(8): 1576-1586.

Chen, G., Huang, A. C., Zhang, W., Zhang, G., Wu, M., et al. (2018). "Exosomal PD-L1 contributes to immunosuppression and is associated with anti-PD-1 response." Nature **560**(7718): 382-386.

Chen, J., Li, P., Zhang, T., Xu, Z., Huang, X., Wang, R. and Du, L. (2021). "Review on Strategies and Technologies for Exosome Isolation and Purification." Front Bioeng Biotechnol **9**: 811971.

Chen, W. X., Liu, X. M., Lv, M. M., Chen, L., Zhao, J. H., Zhong, S. L., Ji, M. H., Hu, Q., Luo, Z., Wu, J. Z. and Tang, J. H. (2014). "Exosomes from drug-resistant breast cancer cells transmit chemoresistance by a horizontal transfer of microRNAs." PLoS One **9**(4): e95240.

Cheng, S., Khan, M., Luo, L., Wang, L., Liu, S., Ping, J., Lin, J. M. and Hu, Q. (2021). "Detection of bleomycin and its hydrolase by the cationic surfactant-doped liquid crystal-based sensing platform." Anal Chim Acta **1150**: 338247.

Choi, H., Choi, Y., Yim, H. Y., Mirzaaghasi, A., Yoo, J. K. and Choi, C. (2021). "Biodistribution of Exosomes and Engineering Strategies for Targeted Delivery of Therapeutic Exosomes." Tissue Eng Regen Med **18**(4): 499-511.

Choromanska, A., Chwilkowska, A., Kulbacka, J., Baczynska, D., Rembialkowska, N., Szewczyk, A., Michel, O., Gajewska-Naryniecka, A., Przystupski, D. and Saczko, J. (2021). "Modifications of Plasma Membrane Organization in Cancer Cells for Targeted Therapy." Molecules **26**(7).

Chung, J. H., Jung, H. R., Jung, A. R., Lee, Y. C., Kong, M., Lee, J. S. and Eun, Y. G. (2018). "SOX2 activation predicts prognosis in patients with head and neck squamous cell carcinoma." Sci Rep **8**(1): 1677.

Colombo, J., Fachel, A. A., De Freitas Calmon, M., Cury, P. M., Fukuyama, E. E., Tajara, E. H., Cordeiro, J. A., Verjovski-Almeida, S., Reis, E. M. and Rahal, P. (2009). "Gene expression profiling reveals molecular marker candidates of laryngeal squamous cell carcinoma." Oncol Rep **21**(3): 649-663.

Coumans, F. A., van Dalum, G., Beck, M. and Terstappen, L. W. (2013). "Filter characteristics influencing circulating tumor cell enrichment from whole blood." PLoS One **8**(4): e61770.

Cramer, J. D., Burtness, B., Le, Q. T. and Ferris, R. L. (2019). "The changing therapeutic landscape of head and neck cancer." Nat Rev Clin Oncol **16**(11): 669-683.

Cristofanilli, M., Budd, G. T., Ellis, M. J., Stopeck, A., Matera, J., Miller, M. C., Reuben, J. M., Doyle, G. V., Allard, W. J., Terstappen, L. W. M. M. and Hayes, D. F. (2004). "Circulating tumor cells, disease progression, and survival in metastatic breast cancer." New England Journal of Medicine **351**(8): 781-791.

Cullen, K. J., Yang, Z., Schumaker, L. and Guo, Z. (2007). "Mitochondria as a critical target of the chemotheraputic agent cisplatin in head and neck cancer." J Bioenerg Biomembr **39**(1): 43-50.

D'Alterio, C., Scala, S., Sozzi, G., Roz, L. and Bertolini, G. (2020). "Paradoxical effects of chemotherapy on tumor relapse and metastasis promotion." Semin Cancer Biol **60**: 351-361.

Dasari, S. and Tchounwou, P. B. (2014). "Cisplatin in cancer therapy: molecular mechanisms of action." Eur J Pharmacol **740**: 364-378.

Dasgupta, A., Lim, A. R. and Ghajar, C. M. (2017). "Circulating and disseminated tumor cells: harbingers or initiators of metastasis?" Mol Oncol **11**(1): 40-61.

Dash, M., Palaniyandi, K., Ramalingam, S., Sahabudeen, S. and Raja, N. S. (2021). "Exosomes isolated from two different cell lines using three different isolation techniques show variation in physical and molecular characteristics." Biochim Biophys Acta Biomembr **1863**(2): 183490.

de Haas, E. C., Zwart, N., Meijer, C., Nuver, J., Boezen, H. M., Suurmeijer, A. J., Hoekstra, H. J., van der Steege, G., Sleijfer, D. T. and Gietema, J. A. (2008). "Variation in bleomycin

hydrolase gene is associated with reduced survival after chemotherapy for testicular germ cell cancer." J Clin Oncol **26**(11): 1817-1823.

Dejima, H., Iinuma, H., Kanaoka, R., Matsutani, N. and Kawamura, M. (2017). "Exosomal microRNA in plasma as a non-invasive biomarker for the recurrence of non-small cell lung cancer." Oncol Lett **13**(3): 1256-1263.

Doherty, G. J. and McMahon, H. T. (2009). "Mechanisms of endocytosis." Annu Rev Biochem **78**: 857-902.

Domenis, R., Cifu, A., Mio, C., Fabris, M. and Curcio, F. (2021). "Pro-Inflammatory Microenvironment Modulates the Transfer of Mutated TP53 Mediated by Tumor Exosomes." Int J Mol Sci **22**(12).

Dong, Y., Skelley, A. M., Merdek, K. D., Sprott, K. M., Jiang, C., Pierceall, W. E., Lin, J., Stocum, M., Carney, W. P. and Smirnov, D. A. (2013). "Microfluidics and circulating tumor cells." J Mol Diagn **15**(2): 149-157.

Dongre, A. and Weinberg, R. A. (2019). "New insights into the mechanisms of epithelial-mesenchymal transition and implications for cancer." Nat Rev Mol Cell Biol **20**(2): 69-84.

Du, L., Yang, Y., Xiao, X., Wang, C., Zhang, X., Wang, L., Zhang, X., Li, W., Zheng, G., Wang, S. and Dong, Z. (2011). "Sox2 nuclear expression is closely associated with poor prognosis in patients with histologically node-negative oral tongue squamous cell carcinoma." Oral Oncol **47**(8): 709-713.

Duan, G., Tang, Q., Yan, H., Xie, L., Wang, Y., Zheng, X. E., Zhuge, Y., Shen, S., Zhang, B., Zhang, X., Wang, J., Wang, W. and Zou, X. (2017). "A Strategy to Delay the Development of Cisplatin Resistance by Maintaining a Certain Amount of Cisplatin-Sensitive Cells." Sci Rep **7**(1): 432.

Ebnoether, E. and Muller, L. (2020). "Diagnostic and Therapeutic Applications of Exosomes in Cancer with a Special Focus on Head and Neck Squamous Cell Carcinoma (HNSCC)." Int J Mol Sci **21**(12).

Efimova, A. S., Antipenko, I. D., Evtushenko, E. A., Balan, P. V. and Tonevitskaya, S. A. (2023). "Effect of IGFBP6 Knockdown on Proteins Regulating Exosome Synthesis and Secretion in MDA-MB-231 Cell Line." Bull Exp Biol Med **175**(1): 157-161.

Elzanowska, J., Semira, C. and Costa-Silva, B. (2021). "DNA in extracellular vesicles: biological and clinical aspects." Mol Oncol **15**(6): 1701-1714.

Fan, Z., Wu, C., Chen, M., Jiang, Y., Wu, Y., Mao, R. and Fan, Y. (2022). "The generation of PD-L1 and PD-L2 in cancer cells: From nuclear chromatin reorganization to extracellular presentation." Acta Pharm Sin B **12**(3): 1041-1053.

Fang, Y., Wu, N., Gan, X., Yan, W., Morrell, J. C. and Gould, S. J. (2007). "Higher-order oligomerization targets plasma membrane proteins and HIV gag to exosomes." PLoS Biol **5**(6): e158.

Ferlito, A., Shaha, A. R., Silver, C. E., Rinaldo, A. and Mondin, V. (2001). "Incidence and sites of distant metastases from head and neck cancer." ORL J Otorhinolaryngol Relat Spec **63**(4): 202-207.

Ferreira, M. M., Ramani, V. C. and Jeffrey, S. S. (2016). "Circulating tumor cell technologies." Mol Oncol **10**(3): 374-394.

Forastiere, A., Koch, W., Trotti, A. and Sidransky, D. (2001). "Head and neck cancer." N Engl J Med **345**(26): 1890-1900.

Friedenauer, S. and Berlet, H. H. (1989). "Sensitivity and variability of the Bradford protein assay in the presence of detergents." Anal Biochem **178**(2): 263-268.

Fuertes, M. A., Castilla, J., Alonso, C. and Perez, J. M. (2003). "Cisplatin biochemical mechanism of action: from cytotoxicity to induction of cell death through interconnections between apoptotic and necrotic pathways." Curr Med Chem **10**(3): 257-266.

Galluzzi, L., Senovilla, L., Vitale, I., Michels, J., Martins, I., Kepp, O., Castedo, M. and Kroemer, G. (2012). "Molecular mechanisms of cisplatin resistance." Oncogene **31**(15): 1869-1883.

Gamazon, E. R., Im, H. K., O'Donnell, P. H., Ziliak, D., Stark, A. L., Cox, N. J., Dolan, M. E. and Huang, R. S. (2011). "Comprehensive evaluation of the contribution of X chromosome genes to platinum sensitivity." Mol Cancer Ther **10**(3): 472-480.

Garzetti, G. G., Ciavattini, A., Provinciali, M., Di Stefano, G., Lucarini, G., Goteri, G. and Biagini, G. (1996). "Expression of p53 and apoptosis of tumor cells in locally advanced cervical carcinoma after cisplatin based neoadjuvant chemotherapy." Anticancer Res **16**(5B): 3229-3234.

Gascoyne, P. R., Noshari, J., Anderson, T. J. and Becker, F. F. (2009). "Isolation of rare cells from cell mixtures by dielectrophoresis." Electrophoresis **30**(8): 1388-1398.

Ghosh, S. (2019). "Cisplatin: The first metal based anticancer drug." Bioorg Chem **88**: 102925.

Gil da Costa, R. M., Levesque, C., Bianchi-Frias, D., Chatterjee, P., Lam, H. M., Santos, C., Coleman, I. M., Ferreirinha, P., Vilanova, M., Pinto da Cunha, N., Carvalho, H., Moreira-Pais, A., Faustino-Rocha, A., Neto, T., Batista da Costa, J., Wright, J. L., Ferreira, R., Oliveira, P. A., Mendes, J., Bastos, M., Colaco, B., Lopes, C., Black, P. C., Sweeney, C. J. and Nelson, P. S. (2023). "Pharmacological NF-kappaB inhibition decreases cisplatin chemoresistance in muscle-invasive bladder cancer and reduces cisplatin-induced toxicities." Mol Oncol **17**(12): 2709-2727.

Goel, P., Manning, J. A. and Kumar, S. (2015). "NEDD4-2 (NEDD4L): the ubiquitin ligase for multiple membrane proteins." Gene **557**(1): 1-10.

Gordon, S. (2016). "Phagocytosis: An Immunobiologic Process." Immunity **44**(3): 463-475.

Gradilone, A., Naso, G., Raimondi, C., Cortesi, E., Gandini, O., Vincenzi, B., Saltarelli, R., Chiapparino, E., Spremberg, F., Cristofanilli, M., Frati, L., Agliano, A. M. and Gazzaniga, P. (2011). "Circulating tumor cells (CTCs) in metastatic breast cancer (MBC): prognosis, drug resistance and phenotypic characterization." Ann Oncol **22**(1): 86-92.

Gribko, A., Kunzel, J., Wunsch, D., Lu, Q., Nagel, S. M., Knauer, S. K., Stauber, R. H. and Ding, G. B. (2019). "Is small smarter? Nanomaterial-based detection and elimination of circulating tumor cells: current knowledge and perspectives." Int J Nanomedicine **14**: 4187-4209.

Gribko, A., Stiefel, J., Liebetanz, L., Nagel, S. M., Künzel, J., Wandrey, M., Hagemann, J., Stauber, R. H., Freese, C. and Gül, D. (2021). "IsoMAG-An Automated System for the Immunomagnetic Isolation of Squamous Cell Carcinoma-Derived Circulating Tumor Cells." Diagnostics **11**(11).

Guo, B. B., Bellingham, S. A. and Hill, A. F. (2016). "Stimulating the Release of Exosomes Increases the Intercellular Transfer of Prions." Journal of Biological Chemistry **291**(10): 5128-5137.

Guo, W., Keckesova, Z., Donaher, J. L., Shibue, T., Tischler, V., Reinhardt, F., Itzkovitz, S., Noske, A., Zurrer-Hardi, U., Bell, G., Tam, W. L., Mani, S. A., van Oudenaarden, A. and Weinberg, R. A. (2012). "Slug and Sox9 cooperatively determine the mammary stem cell state." Cell **148**(5): 1015-1028.

Gurung, S., Perocheau, D., Touramanidou, L. and Baruteau, J. (2021). "The exosome journey: from biogenesis to uptake and intracellular signalling." Cell Commun Signal **19**(1): 47.

Harmati, M., Bukva, M., Boroczky, T., Buzas, K. and Gyukity-Sebestyen, E. (2021). "The role of the metabolite cargo of extracellular vesicles in tumor progression." Cancer Metastasis Rev **40**(4): 1203-1221.

Harrach, S. and Ciarimboli, G. (2015). "Role of transporters in the distribution of platinum-based drugs." Front Pharmacol **6**: 85.

Hayatudin, R., Fong, Z., Ming, L. C., Goh, B. H., Lee, W. L. and Kifli, N. (2021). "Overcoming Chemoresistance via Extracellular Vesicle Inhibition." Front Mol Biosci **8**: 629874.

Henne, W. M., Buchkovich, N. J. and Emr, S. D. (2011). "The ESCRT pathway." Dev Cell **21**(1): 77-91.

Hofmann, L., Waizenegger, M., Roth, R., Schmitteckert, S., Engelhardt, D., Schuler, P. J., Laban, S., Hoffmann, T. K., Brunner, C. and Theodoraki, M. N. (2022). "Treatment dependent impact of plasma-derived exosomes from head and neck cancer patients on the epithelial-to-mesenchymal transition." Front Oncol **12**: 1043199.

Hosokawa, M., Hayata, T., Fukuda, Y., Arakaki, A., Yoshino, T., Tanaka, T. and Matsunaga, T. (2010). "Size-selective microcavity array for rapid and efficient detection of circulating tumor cells." Anal Chem **82**(15): 6629-6635.

Hosseini, K., Ranjbar, M., Pirpour Tazehkand, A., Asgharian, P., Montazersaheb, S., Tarhriz, V. and Ghasemnejad, T. (2022). "Evaluation of exosomal non-coding RNAs in cancer using high-throughput sequencing." J Transl Med **20**(1): 30.

Hristozova, T., Konschak, R., Stromberger, C., Fusi, A., Liu, Z., Weichert, W., Stenzinger, A., Budach, V., Keilholz, U. and Tinhofer, I. (2011). "The presence of circulating tumor cells (CTCs) correlates with lymph node metastasis in nonresectable squamous cell carcinoma of the head and neck region (SCCHN)." Ann Oncol **22**(8): 1878-1885.

Hsieh, J. C., Lin, H. C., Huang, C. Y., Hsu, H. L., Wu, T. M., Lee, C. L., Chen, M. C., Wang, H. M. and Tseng, C. P. (2015). "Prognostic value of circulating tumor cells with podoplanin expression in patients with locally advanced or metastatic head and neck squamous cell carcinoma." Head Neck **37**(10): 1448-1455.

Hu, Y. B., Dammer, E. B., Ren, R. J. and Wang, G. (2015). "The endosomal-lysosomal system: from acidification and cargo sorting to neurodegeneration." Transl Neurodegener **4**: 18.

Huang, S. H. and O'Sullivan, B. (2017). "Overview of the 8th Edition TNM Classification for Head and Neck Cancer." Curr Treat Options Oncol **18**(7): 40.

Huotari, J. and Helenius, A. (2011). "Endosome maturation." EMBO J **30**(17): 3481-3500.

Ijichi, K., Adachi, M., Ogawa, T., Hasegawa, Y. and Murakami, S. (2014). "Cell-cycle distribution and Thymidilate Synthatase (TS) expression correlate with 5-FU resistance in head and neck carcinoma cells." Anticancer Res **34**(6): 2907-2911.

Jagadish, N., Fatima, R., Sharma, A., Devi, S., Suri, V., Kumar, V. and Suri, A. (2018). "Sperm associated antigen 9 (SPAG9) a promising therapeutic target of ovarian carcinoma." Tumour Biol **40**(5): 1010428318773652.

Jatana, K. R., Balasubramanian, P., Lang, J. C., Yang, L., Jatana, C. A., White, E., Agrawal, A., Ozer, E., Schuller, D. E., Teknos, T. N. and Chalmers, J. J. (2010). "Significance of circulating tumor cells in patients with squamous cell carcinoma of the head and neck: initial results." Arch Otolaryngol Head Neck Surg **136**(12): 1274-1279.

Jemal, A., Siegel, R., Ward, E., Hao, Y., Xu, J., Murray, T. and Thun, M. J. (2008). "Cancer statistics, 2008." CA Cancer J Clin **58**(2): 71-96.

Jeon, G. A., Lee, J. S., Patel, V., Gutkind, J. S., Thorgeirsson, S. S., Kim, E. C., Chu, I. S., Amornphimoltham, P. and Park, M. H. (2004). "Global gene expression profiles of human head and neck squamous carcinoma cell lines." Int J Cancer **112**(2): 249-258.

Johnson, D. E., Burtness, B., Leemans, C. R., Lui, V. W. Y., Bauman, J. E. and Grandis, J. R. (2020). "Head and neck squamous cell carcinoma." Nat Rev Dis Primers **6**(1): 92.

Jou, A. and Hess, J. (2017). "Epidemiology and Molecular Biology of Head and Neck Cancer." Oncol Res Treat **40**(6): 328-332.

Joyce, D. P., Kerin, M. J. and Dwyer, R. M. (2016). "Exosome-encapsulated microRNAs as circulating biomarkers for breast cancer." Int J Cancer **139**(7): 1443-1448.

Kannan, A., Hertweck, K. L., Philley, J. V., Wells, R. B. and Dasgupta, S. (2017). "Genetic Mutation and Exosome Signature of Human Papilloma Virus Associated Oropharyngeal Cancer." Sci Rep **7**: 46102.

Kawada, T., Takahashi, H., Sakakura, K., Ida, S., Mito, I., Toyoda, M. and Chikamatsu, K. (2017). "Circulating tumor cells in patients with head and neck squamous cell carcinoma: Feasibility of detection and quantitation." Head Neck **39**(11): 2180-2186.

Kelland, L. (2007). "The resurgence of platinum-based cancer chemotherapy." Nat Rev Cancer **7**(8): 573-584.

Khan, S., Jutzy, J. M., Valenzuela, M. M., Turay, D., Aspe, J. R., Ashok, A., Mirshahidi, S., Mercola, D., Lilly, M. B. and Wall, N. R. (2012). "Plasma-derived exosomal survivin, a plausible biomarker for early detection of prostate cancer." PLoS One **7**(10): e46737.

Kim, H., Lee, S., Shin, E., Seong, K. M., Jin, Y. W., Youn, H. and Youn, B. (2020). "The Emerging Roles of Exosomes as EMT Regulators in Cancer." Cells **9**(4).

Kim, J. B. (2005). "Three-dimensional tissue culture models in cancer biology." Semin Cancer Biol **15**(5): 365-377.

Kisoda, S., Mouri, Y., Kitamura, N., Yamamoto, T., Miyoshi, K. and Kudo, Y. (2022). "The role of partial-EMT in the progression of head and neck squamous cell carcinoma." J Oral Biosci **64**(2): 176-182.

Kong, J. N., He, Q., Wang, G., Dasgupta, S., Dinkins, M. B., Zhu, G., Kim, A., Spassieva, S. and Bieberich, E. (2015). "Guggulsterone and bexarotene induce secretion of exosome-associated breast cancer resistance protein and reduce doxorubicin resistance in MDA-MB-231 cells." Int J Cancer **137**(7): 1610-1620.

Krebs, M. G., Metcalf, R. L., Carter, L., Brady, G., Blackhall, F. H. and Dive, C. (2014). "Molecular analysis of circulating tumour cells-biology and biomarkers." Nat Rev Clin Oncol **11**(3): 129-144.

Krohn, R. I. (2011). "The colorimetric detection and quantitation of total protein." Curr Protoc Cell Biol **Appendix 3**: 3H.

Kunzel, J., Gribko, A., Lu, Q., Stauber, R. H. and Wunsch, D. (2019). "Nanomedical detection and downstream analysis of circulating tumor cells in head and neck patients." Biol Chem **400**(11): 1465-1479.

Kwon, H. K., Lee, J. H., Shin, H. J., Kim, J. H. and Choi, S. (2015). "Structural and functional analysis of cell adhesion and nuclear envelope nano-topography in cell death." Sci Rep **5**: 15623.

Lanzi, C., Perego, P., Supino, R., Romanelli, S., Pensa, T., Carenini, N., Viano, I., Colangelo, D., Leone, R., Apostoli, P., Cassinelli, G., Gambetta, R. A. and Zunino, F. (1998). "Decreased drug accumulation and increased tolerance to DNA damage in tumor cells with a low level of cisplatin resistance." Biochem Pharmacol **55**(8): 1247-1254.

Leidal, A. M. and Debnath, J. (2020). "Unraveling the mechanisms that specify molecules for secretion in extracellular vesicles." Methods **177**: 15-26.

Li, M., Zhao, X., Liu, Y., An, J., Xiao, H. and Wang, C. (2017). "Aberrant expression of CDK8 regulates the malignant phenotype and associated with poor prognosis in human laryngeal squamous cell carcinoma." Eur Arch Otorhinolaryngol **274**(5): 2205-2213.

Li, S. P., Lin, Z. X., Jiang, X. Y. and Yu, X. Y. (2018). "Exosomal cargo-loading and synthetic exosome-mimics as potential therapeutic tools." Acta Pharmacol Sin **39**(4): 542-551.

Liang, Q., Peng, J., Xu, Z., Li, Z., Jiang, F., Ouyang, L., Wu, S., Fu, C., Liu, Y., Liu, Y. and Yan, Y. (2022). "Pan-cancer analysis of the prognosis and immunological role of AKAP12: A potential biomarker for resistance to anti-VEGF inhibitors." Front Genet **13**: 943006.

Lim, S., Becker, A., Zimmer, A., Lu, J., Buettner, R. and Kirfel, J. (2013). "SNAI1-mediated epithelial-mesenchymal transition confers chemoresistance and cellular plasticity by regulating genes involved in cell death and stem cell maintenance." PLoS One **8**(6): e66558.

Lin, D., Shen, L., Luo, M., Zhang, K., Li, J., Yang, Q., Zhu, F., Zhou, D., Zheng, S., Chen, Y. and Zhou, J. (2021). "Circulating tumor cells: biology and clinical significance." Signal Transduct Target Ther **6**(1): 404.

Liu, T., Chen, G., Sun, D., Lei, M., Li, Y., Zhou, C., Li, X., Xue, W., Wang, H., Liu, C. and Xu, J. (2017). "Exosomes containing miR-21 transfer the characteristic of cisplatin resistance by targeting PTEN and PDCD4 in oral squamous cell carcinoma." Acta Biochim Biophys Sin (Shanghai) **49**(9): 808-816.

Liu, X., Li, Z., Zhao, Q., Zhou, X., Wang, Y., Zhao, G. and Guo, X. (2024). "Capsaicin reverses cisplatin resistance in tongue squamous cell carcinoma by inhibiting the Warburg effect and facilitating mitochondrial-dependent apoptosis via the AMPK/AKT/mTOR axis." Cell Biol Int.

Lopez-Ayllon, B. D., Moncho-Amor, V., Abarrategi, A., Ibanez de Caceres, I., Castro-Carpeno, J., Belda-Iniesta, C., Perona, R. and Sastre, L. (2014). "Cancer stem cells and cisplatin-resistant cells isolated from non-small-lung cancer cell lines constitute related cell populations." Cancer Med **3**(5): 1099-1111.

Lord, C. J. and Ashworth, A. (2012). "The DNA damage response and cancer therapy." Nature **481**(7381): 287-294.

Lou, X. L., Sun, J., Gong, S. Q., Yu, X. F., Gong, R. and Deng, H. (2015). "Interaction between circulating cancer cells and platelets: clinical implication." Chinese Journal of Cancer Research **27**(5): 450-460.

Lu, J. F., Luk, F., Gong, J., Jaiswal, R., Grau, G. E. and Bebawy, M. (2013). "Microparticles mediate MRP1 intercellular transfer and the re-templating of intrinsic resistance pathways." Pharmacological Research **76**: 77-83.

Ludwig, S., Floros, T., Theodoraki, M. N., Hong, C. S., Jackson, E. K., Lang, S. and Whiteside, T. L. (2017). "Suppression of Lymphocyte Functions by Plasma Exosomes Correlates with Disease Activity in Patients with Head and Neck Cancer." Clin Cancer Res **23**(16): 4843-4854.

Ludwig, S., Sharma, P., Theodoraki, M. N., Pietrowska, M., Yerneni, S. S., Lang, S., Ferrone, S. and Whiteside, T. L. (2018). "Molecular and Functional Profiles of Exosomes From HPV(+) and HPV(-) Head and Neck Cancer Cell Lines." Front Oncol **8**: 445.

Lv, L. H., Wan, Y. L., Lin, Y., Zhang, W., Yang, M., Li, G. L., Lin, H. M., Shang, C. Z., Chen, Y. J. and Min, J. (2012). "Anticancer drugs cause release of exosomes with heat shock proteins from human hepatocellular carcinoma cells that elicit effective natural killer cell antitumor responses in vitro." Journal of Biological Chemistry **287**(19): 15874-15885.

Lv, M. M., Zhu, X. Y., Chen, W. X., Zhong, S. L., Hu, Q., Ma, T. F., Zhang, J., Chen, L., Tang, J. H. and Zhao, J. H. (2014). "Exosomes mediate drug resistance transfer in MCF-7 breast cancer

cells and a probable mechanism is delivery of P-glycoprotein." Tumour Biol **35**(11): 10773-10779.

Ma, H. L., Jiang, Q., Han, S., Wu, Y., Cui Tomshine, J., Wang, D., Gan, Y., Zou, G. and Liang, X. J. (2012). "Multicellular tumor spheroids as an in vivo-like tumor model for three-dimensional imaging of chemotherapeutic and nano material cellular penetration." Mol Imaging **11**(6): 487-498.

Maqsood, M. I., Matin, M. M., Bahrami, A. R. and Ghasroldasht, M. M. (2013). "Immortality of cell lines: challenges and advantages of establishment." Cell Biol Int **37**(10): 1038-1045.

Martin, L. P., Hamilton, T. C. and Schilder, R. J. (2008). "Platinum resistance: the role of DNA repair pathways." Clin Cancer Res **14**(5): 1291-1295.

Matsumoto, Y., Kano, M., Murakami, K., Toyozumi, T., Suito, H., Takahashi, M., Sekino, N., Shiraishi, T., Kamata, T., Ryuzaki, T., Hirasawa, S., Kinoshita, K. and Matsubara, H. (2020). "Tumor-derived exosomes influence the cell cycle and cell migration of human esophageal cancer cell lines." Cancer Sci **111**(12): 4348-4358.

McMahon, A., Lu, H. and Butovich, I. A. (2013). "The spectrophotometric sulfo-phospho-vanillin assessment of total lipids in human meibomian gland secretions." Lipids **48**(5): 513-525.

Meyer, B., Voss, K. O., Tobias, F., Jakob, B., Durante, M. and Taucher-Scholz, G. (2013). "Clustered DNA damage induces pan-nuclear H2AX phosphorylation mediated by ATM and DNA-PK." Nucleic Acids Res **41**(12): 6109-6118.

Mezher, M., Abdallah, S., Ashekyan, O., Shoukari, A. A., Choubassy, H., Kurdi, A., Temraz, S. and Nasr, R. (2023). "Insights on the Biomarker Potential of Exosomal Non-Coding RNAs in Colorectal Cancer: An In Silico Characterization of Related Exosomal lncRNA/circRNA-miRNA-Target Axis." Cells **12**(7).

Mhawech-Fauceglia, P., Walia, S., Yessaian, A., Machida, H., Matsuo, K. and Lawrenson, K. (2018). "Overexpression of HOMER2 predicts better outcome in low-grade endometrioid endometrial adenocarcinoma." Pathology **50**(5): 499-503.

Miao, Z. F., Wang, Z. N., Zhao, T. T., Xu, Y. Y., Wu, J. H., Liu, X. Y., Xu, H., You, Y. and Xu, H. M. (2015). "Overexpression of SPAG9 in human gastric cancer is correlated with poor prognosis." Virchows Arch **467**(5): 525-533.

Minciacchi, V. R., Freeman, M. R. and Di Vizio, D. (2015). "Extracellular vesicles in cancer: exosomes, microvesicles and the emerging role of large oncosomes." Semin Cell Dev Biol **40**: 41-51.

Mishra, V., Singh, A., Chen, X., Rosenberg, A. J., Pearson, A. T., Zhavoronkov, A., Savage, P. A., Lingen, M. W., Agrawal, N. and Izumchenko, E. (2022). "Application of liquid biopsy as multi-functional biomarkers in head and neck cancer." Br J Cancer **126**(3): 361-370.

Moreno-Gonzalo, O., Villarroya-Beltri, C. and Sanchez-Madrid, F. (2014). "Post-translational modifications of exosomal proteins." Front Immunol **5**: 383.

Muller, L., Hong, C. S., Stolz, D. B., Watkins, S. C. and Whiteside, T. L. (2014). "Isolation of biologically-active exosomes from human plasma." J Immunol Methods **411**: 55-65.

Muraro, E., Fanetti, G., Lupato, V., Giacomarra, V., Steffan, A., Gobitti, C., Vaccher, E. and Franchin, G. (2021). "Cetuximab in locally advanced head and neck squamous cell carcinoma: Biological mechanisms involved in efficacy, toxicity and resistance." Crit Rev Oncol Hematol **164**: 103424.

Mutschelknaus, L., Azimzadeh, O., Heider, T., Winkler, K., Vetter, M., Kell, R., Tapio, S., Merl-Pham, J., Huber, S. M., Edalat, L., Radulovic, V., Anastasov, N., Atkinson, M. J. and Moertl, S. (2017). "Radiation alters the cargo of exosomes released from squamous head and neck cancer cells to promote migration of recipient cells." Sci Rep **7**(1): 12423.

Nakamura, M., Nakatani, K., Uzawa, K., Ono, K., Uesugi, H., Ogawara, K., Shiiba, M., Bukawa, H., Yokoe, H., Wada, T., Fujita, S. and Tanzawa, H. (2005). "Establishment and characterization of a cisplatin-resistant oral squamous cell carcinoma cell line, H-1R." Oncol Rep **14**(5): 1281-1286.

Nathan, C. A., Khandelwal, A. R., Wolf, G. T., Rodrigo, J. P., Makitie, A. A., Saba, N. F., Forastiere, A. A., Bradford, C. R. and Ferlito, A. (2022). "TP53 mutations in head and neck cancer." Mol Carcinog **61**(4): 385-391.

Novak, D., Huser, L., Elton, J. J., Umansky, V., Altevogt, P. and Utikal, J. (2020). "SOX2 in development and cancer biology." Semin Cancer Biol **67**(Pt 1): 74-82.

O'Brien, K., Breyne, K., Ughetto, S., Laurent, L. C. and Breakefield, X. O. (2020). "RNA delivery by extracellular vesicles in mammalian cells and its applications." Nat Rev Mol Cell Biol **21**(10): 585-606.

Oosting, S. F. and Haddad, R. I. (2019). "Best Practice in Systemic Therapy for Head and Neck Squamous Cell Carcinoma." Front Oncol **9**: 815.

Osazuwa-Peters, N., Simpson, M. C., Zhao, L., Boakye, E. A., Olomukoro, S. I., Deshields, T., Loux, T. M., Varvares, M. A. and Schootman, M. (2018). "Suicide risk among cancer survivors: Head and neck versus other cancers." Cancer **124**(20): 4072-4079.

Osteikoetxea, X., Balogh, A., Szabo-Taylor, K., Nemeth, A., Szabo, T. G., Paloczi, K., Sodar, B., Kittel, A., Gyorgy, B., Pallinger, E., Matko, J. and Buzas, E. I. (2015). "Improved characterization of EV preparations based on protein to lipid ratio and lipid properties." PLoS One **10**(3): e0121184.

Pan, B. T. and Johnstone, R. M. (1983). "Fate of the transferrin receptor during maturation of sheep reticulocytes in vitro: selective externalization of the receptor." Cell **33**(3): 967-978.

Papadaki, M. A., Stoupis, G., Theodoropoulos, P. A., Mavroudis, D., Georgoulias, V. and Agelaki, S. (2019). "Circulating Tumor Cells with Stemness and Epithelial-to-Mesenchymal Transition Features Are Chemoresistant and Predictive of Poor Outcome in Metastatic Breast Cancer." Mol Cancer Ther **18**(2): 437-447.

Park, J., Kim, J. M., Park, J. K., Huang, S., Kwak, S. Y., Ryu, K. A., Kong, G., Park, J. and Koo, B. S. (2015). "Association of p21-activated kinase-1 activity with aggressive tumor behavior and poor prognosis of head and neck cancer." Head Neck **37**(7): 953-963.

Payne, K., Brooks, J., Spruce, R., Batis, N., Taylor, G., Nankivell, P. and Mehanna, H. (2019). "Circulating Tumour Cell Biomarkers in Head and Neck Cancer: Current Progress and Future Prospects." Cancers **11**(8).

Pereira-Veiga, T., Schneegans, S., Pantel, K. and Wikman, H. (2022). "Circulating tumor cell-blood cell crosstalk: Biology and clinical relevance." Cell Rep **40**(9): 111298.

Perez-Hernandez, D., Gutierrez-Vazquez, C., Jorge, I., Lopez-Martin, S., Ursa, A., Sanchez-Madrid, F., Vazquez, J. and Yanez-Mo, M. (2013). "The intracellular interactome of tetraspanin-enriched microdomains reveals their function as sorting machineries toward exosomes." Journal of Biological Chemistry **288**(17): 11649-11661.

Poage, G. M., Houseman, E. A., Christensen, B. C., Butler, R. A., Avissar-Whiting, M., McClean, M. D., Waterboer, T., Pawlita, M., Marsit, C. J. and Kelsey, K. T. (2011). "Global hypomethylation identifies Loci targeted for hypermethylation in head and neck cancer." Clin Cancer Res **17**(11): 3579-3589.

Pols, M. S. and Klumperman, J. (2009). "Trafficking and function of the tetraspanin CD63." Exp Cell Res **315**(9): 1584-1592.

Prada, I. and Meldolesi, J. (2016). "Binding and Fusion of Extracellular Vesicles to the Plasma Membrane of Their Cell Targets." Int J Mol Sci **17**(8).

Praharaj, P. P., Bhutia, S. K., Nagrath, S., Bitting, R. L. and Deep, G. (2018). "Circulating tumor cell-derived organoids: Current challenges and promises in medical research and precision medicine." Biochim Biophys Acta Rev Cancer **1869**(2): 117-127.

Prasad, C. P., Tripathi, S. C., Kumar, M. and Mohapatra, P. (2023). "Passage number of cancer cell lines: Importance, intricacies, and way-forward." Biotechnol Bioeng **120**(8): 2049-2055.

Prigge, E. S., Arbyn, M., von Knebel Doeberitz, M. and Reuschenbach, M. (2017). "Diagnostic accuracy of p16(INK4a) immunohistochemistry in oropharyngeal squamous cell carcinomas: A systematic review and meta-analysis." Int J Cancer **140**(5): 1186-1198.

Qadir, F., Aziz, M. A., Sari, C. P., Ma, H., Dai, H., Wang, X., Raithatha, D., Da Silva, L. G. L., Hussain, M., Poorkasreiy, S. P., Hutchison, I. L., Waseem, A. and Teh, M. T. (2018). "Transcriptome reprogramming by cancer exosomes: identification of novel molecular targets in matrix and immune modulation." Molecular Cancer **17**(1): 97.

Qazi, R. E. M., Sajid, Z., Zhao, C., Hussain, I., Iftikhar, F., Jameel, M., Rehman, F. U. and Mian, A. A. (2023). "Lyophilization Based Isolation of Exosomes." Int J Mol Sci **24**(13).

Quail, D. F. and Joyce, J. A. (2013). "Microenvironmental regulation of tumor progression and metastasis." Nature Medicine **19**(11): 1423-1437.

Rangan, S. R. (1972). "A new human cell line (FaDu) from a hypopharyngeal carcinoma." Cancer **29**(1): 117-121.

Ravi, M., Paramesh, V., Kaviya, S. R., Anuradha, E. and Solomon, F. D. (2015). "3D cell culture systems: advantages and applications." J Cell Physiol **230**(1): 16-26.

Rinecker, J., Roesch, R., Krippgans, S., Nieberler, M., Stark, L., Stangl, S., Haller, B., Fritsche, K., Multhoff, G., Knopf, A., Winter, C., Wollenberg, B. and Wirth, M. (2022). "Comparing TIMP-1 and Hsp70 in Blood and Saliva as Potential Prognostic Markers in HNSCC." Biomedicines **10**(12).

Rogakou, E. P., Pilch, D. R., Orr, A. H., Ivanova, V. S. and Bonner, W. M. (1998). "DNA double-stranded breaks induce histone H2AX phosphorylation on serine 139." Journal of Biological Chemistry **273**(10): 5858-5868.

Rossi, E. and Fabbri, F. (2019). "CTCs 2020: Great Expectations or Unreasonable Dreams." Cells **8**(9).

Rothkamm, K., Barnard, S., Moquet, J., Ellender, M., Rana, Z. and Burdak-Rothkamm, S. (2015). "DNA damage foci: Meaning and significance." Environ Mol Mutagen **56**(6): 491-504.

Rottenberg, S., Disler, C. and Perego, P. (2021). "The rediscovery of platinum-based cancer therapy." Nat Rev Cancer **21**(1): 37-50.

Ruokolainen, H., Paakko, P. and Turpeenniemi-Hujanen, T. (2005). "Tissue inhibitor of matrix metalloproteinase-1 is prognostic in head and neck squamous cell carcinoma: comparison of the circulating and tissue immunoreactive protein." Clin Cancer Res **11**(9): 3257-3264.

Safaei, R., Larson, B. J., Cheng, T. C., Gibson, M. A., Otani, S., Naerdemann, W. and Howell, S. B. (2005). "Abnormal lysosomal trafficking and enhanced exosomal export of cisplatin in drug-resistant human ovarian carcinoma cells." Mol Cancer Ther **4**(10): 1595-1604.

Saludas, L., Garbayo, E., Ruiz-Villalba, A., Hernandez, S., Vader, P., Prosper, F. and Blanco-Prieto, M. J. (2022). "Isolation methods of large and small extracellular vesicles derived from cardiovascular progenitors: A comparative study." Eur J Pharm Biopharm **170**: 187-196.

Santarelli, A., Mascitti, M., Lo Russo, L., Sartini, D., Troiano, G., Emanuelli, M. and Lo Muzio, L. (2018). "Survivin-Based Treatment Strategies for Squamous Cell Carcinoma." Int J Mol Sci **19**(4).

Santos, M. F., Rappa, G., Karbanova, J., Kurth, T., Corbeil, D. and Lorico, A. (2018). "VAMP-associated protein-A and oxysterol-binding protein-related protein 3 promote the entry of late endosomes into the nucleoplasmic reticulum." Journal of Biological Chemistry **293**(36): 13834-13848.

Sapan, C. V., Lundblad, R. L. and Price, N. C. (1999). "Colorimetric protein assay techniques." Biotechnol Appl Biochem **29**(2): 99-108.

Satelli, A., Brownlee, Z., Mitra, A., Meng, Q. H. and Li, S. (2015). "Circulating tumor cell enumeration with a combination of epithelial cell adhesion molecule- and cell-surface vimentin-based methods for monitoring breast cancer therapeutic response." Clin Chem **61**(1): 259-266.

Sauzay, C., White-Koning, M., Hennebelle, I., Deluche, T., Delmas, C., Imbs, D. C., Chatelut, E. and Thomas, F. (2016). "Inhibition of OCT2, MATE1 and MATE2-K as a possible mechanism of drug interaction between pazopanib and cisplatin." Pharmacological Research **110**: 89-95.

Saygin, C., Wiechert, A., Rao, V. S., Alluri, R., Connor, E., Thiagarajan, P. S., Hale, J. S., Li, Y., Chumakova, A., Jarrar, A., Parker, Y., Lindner, D. J., Nagaraj, A. B., Kim, J. J., DiFeo, A., Abdul-

Karim, F. W., Michener, C., Rose, P. G., DeBernardo, R., Mahdi, H., McCrae, K. R., Lin, F., Lathia, J. D. and Reizes, O. (2017). "CD55 regulates self-renewal and cisplatin resistance in endometrioid tumors." J Exp Med **214**(9): 2715-2732.

Schmitt, N. C., Trivedi, S. and Ferris, R. L. (2015). "STAT1 Activation Is Enhanced by Cisplatin and Variably Affected by EGFR Inhibition in HNSCC Cells." Mol Cancer Ther **14**(9): 2103-2111.

Schrock, A., Bode, M., Goke, F. J., Bareiss, P. M., Schairer, R., Wang, H., Weichert, W., Franzen, A., Kirsten, R., van Bremen, T., Queisser, A., Kristiansen, G., Heasley, L., Bootz, F., Lengerke, C. and Perner, S. (2014). "Expression and role of the embryonic protein SOX2 in head and neck squamous cell carcinoma." Carcinogenesis **35**(7): 1636-1642.

Seton-Rogers, S. (2016). "Epithelial-mesenchymal transition: Untangling EMT's functions." Nat Rev Cancer **16**(1): 1.

Shang, C., Feng, L., Gu, Y., Hong, H., Hong, L. and Hou, J. (2021). "Impact of Multidisciplinary Team Management on the Survival Rate of Head and Neck Cancer Patients: A Cohort Study Meta-analysis." Front Oncol **11**: 630906.

Sharkey Ochoa, I., O'Regan, E., Toner, M., Kay, E., Faul, P., O'Keane, C., O'Connor, R., Mullen, D., Nur, M., O'Murchu, E., Barry-O'Crowley, J., Kernan, N., Tewari, P., Keegan, H., O'Toole, S., Woods, R., Kennedy, S., Feeley, K., Sharp, L., Gheit, T., Tommasino, M., O'Leary, J. J. and Martin, C. M. (2022). "The Role of HPV in Determining Treatment, Survival, and Prognosis of Head and Neck Squamous Cell Carcinoma." Cancers (Basel) **14**(17).

Sharma, A. (2017). "Chemoresistance in cancer cells: exosomes as potential regulators of therapeutic tumor heterogeneity." Nanomedicine (Lond) **12**(17): 2137-2148.

Sharma, S., Zhuang, R., Long, M., Pavlovic, M., Kang, Y., Ilyas, A. and Asghar, W. (2018). "Circulating tumor cell isolation, culture, and downstream molecular analysis." Biotechnol Adv **36**(4): 1063-1078.

Siemer, S. Evaluation of Nanoparticular Cancer Treatment Strategies to Overcome Clinical Resistances. **2021**.

Siemer, S., Bauer, T. A., Scholz, P., Breder, C., Fenaroli, F., Harms, G., Dietrich, D., Dietrich, J., Rosenauer, C., Barz, M., Becker, S., Strieth, S., Reinhardt, C., Fauth, T., Hagemann, J. and Stauber, R. H. (2021). "Targeting Cancer Chemotherapy Resistance by Precision Medicine-Driven Nanoparticle-Formulated Cisplatin." ACS Nano **15**(11): 18541-18556.

Siemer, S., Fauth, T., Scholz, P., Al-Zamel, Y., Khamis, A., Gul, D., Freudelsperger, L., Wollenberg, B., Becker, S., Stauber, R. H. and Hagemann, J. (2021). "Profiling Cisplatin Resistance in Head and Neck Cancer: A Critical Role of the VRAC Ion Channel for Chemoresistance." Cancers (Basel) **13**(19).

Sprowl, J. A., Ness, R. A. and Sparreboom, A. (2013). "Polymorphic transporters and platinum pharmacodynamics." Drug Metab Pharmacokinet **28**(1): 19-27.

Stavrovskaya, A. A. (2000). "Cellular mechanisms of multidrug resistance of tumor cells." Biochemistry (Mosc) **65**(1): 95-106.

Stetefeld, J., McKenna, S. A. and Patel, T. R. (2016). "Dynamic light scattering: a practical guide and applications in biomedical sciences." Biophys Rev **8**(4): 409-427.

Stiefel, J., Freese, C., Sriram, A., Alebrand, S., Srinivas, N., Sproll, C., Wandrey, M., Gul, D., Hagemann, J., Becker, J. C. and Bassler, M. (2022). "Characterization of a novel microfluidic platform for the isolation of rare single cells to enable CTC analysis from head and neck squamous cell carcinoma patients." Eng Life Sci **22**(5): 391-406.

Strati, A., Koutsodontis, G., Papaxoinis, G., Angelidis, I., Zavridou, M., Economopoulou, P., Kotsantis, I., Avgeris, M., Mazel, M., Perisanidis, C., Sasaki, C., Alix-Panabieres, C., Lianidou, E. and Psyrri, A. (2017). "Prognostic significance of PD-L1 expression on circulating tumor cells in patients with head and neck squamous cell carcinoma." Ann Oncol **28**(8): 1923-1933.

Sun, S., Wu, Y., Guo, W., Yu, F., Kong, L., Ren, Y., Wang, Y., Yao, X., Jing, C., Zhang, C., Liu, M., Zhang, Y., Zhao, M., Li, Z., Wu, C., Qiao, Y., Yang, J., Wang, X., Zhang, L., Li, M. and Zhou, X. (2018). "STAT3/HOTAIR Signaling Axis Regulates HNSCC Growth in an EZH2-dependent Manner." Clin Cancer Res **24**(11): 2665-2677.

Sun, Y., Zheng, W., Guo, Z., Ju, Q., Zhu, L., Gao, J., Zhou, L., Liu, F., Xu, Y., Zhan, Q., Zhou, Z., Sun, W. and Zhao, X. (2016). "A novel TP53 pathway influences the HGS-mediated exosome formation in colorectal cancer." Sci Rep **6**: 28083.

Sung, H., Ferlay, J., Siegel, R. L., Laversanne, M., Soerjomataram, I., Jemal, A. and Bray, F. (2021). "Global Cancer Statistics 2020: GLOBOCAN Estimates of Incidence and Mortality Worldwide for 36 Cancers in 185 Countries." CA Cancer J Clin **71**(3): 209-249.

Tan, Y., Li, X., Tian, Z., Chen, S., Zou, J., Lian, G., Chen, S., Huang, K. and Chen, Y. (2021). "TIMP1 down-regulation enhances gemcitabine sensitivity and reverses chemoresistance in pancreatic cancer." Biochem Pharmacol **189**: 114085.

Tang, Y. T., Huang, Y. Y., Zheng, L., Qin, S. H., Xu, X. P., An, T. X., Xu, Y., Wu, Y. S., Hu, X. M., Ping, B. H. and Wang, Q. (2017). "Comparison of isolation methods of exosomes and exosomal RNA from cell culture medium and serum." Int J Mol Med **40**(3): 834-844.

Taylor, D. D. and Shah, S. (2015). "Methods of isolating extracellular vesicles impact down-stream analyses of their cargoes." Methods **87**: 3-10.

Theodoraki, M. N., Yerneni, S., Gooding, W. E., Ohr, J., Clump, D. A., Bauman, J. E., Ferris, R. L. and Whiteside, T. L. (2019). "Circulating exosomes measure responses to therapy in head and neck cancer patients treated with cetuximab, ipilimumab, and IMRT." Oncoimmunology **8**(7): 1593805.

Theodoraki, M. N., Yerneni, S. S., Brunner, C., Theodorakis, J., Hoffmann, T. K. and Whiteside, T. L. (2018). "Plasma-derived Exosomes Reverse Epithelial-to-Mesenchymal Transition after Photodynamic Therapy of Patients with Head and Neck Cancer." Oncoscience **5**(3-4): 75-87.

Thery, C., Witwer, K. W., Aikawa, E., Alcaraz, M. J., Anderson, J. D., et al. (2018). "Minimal information for studies of extracellular vesicles 2018 (MISEV2018): a position statement of the International Society for Extracellular Vesicles and update of the MISEV2014 guidelines." J Extracell Vesicles **7**(1): 1535750.

Thery, C., Zitvogel, L. and Amigorena, S. (2002). "Exosomes: composition, biogenesis and function." Nat Rev Immunol **2**(8): 569-579.

Tian, T., Wang, Y., Wang, H., Zhu, Z. and Xiao, Z. (2010). "Visualizing of the cellular uptake and intracellular trafficking of exosomes by live-cell microscopy." J Cell Biochem **111**(2): 488-496.

Tinhofer, I., Konschak, R., Stromberger, C., Raguse, J. D., Dreyer, J. H., Johrens, K., Keilholz, U. and Budach, V. (2014). "Detection of circulating tumor cells for prediction of recurrence after adjuvant chemoradiation in locally advanced squamous cell carcinoma of the head and neck." Ann Oncol **25**(10): 2042-2047.

Torii, Y., Kato, R., Minami, Y., Hasegawa, K., Fujii, T. and Udagawa, Y. (2014). "ERCC1 expression and chemosensitivity in uterine cervical adenocarcinoma cells." Anticancer Res **34**(1): 107-115.

Tummers, B., Goedemans, R., Pelascini, L. P., Jordanova, E. S., van Esch, E. M., Meyers, C., Melief, C. J., Boer, J. M. and van der Burg, S. H. (2015). "The interferon-related developmental regulator 1 is used by human papillomavirus to suppress NFkappaB activation." Nat Commun **6**: 6537.

Vaidyanathan, R., Soon, R. H., Zhang, P., Jiang, K. and Lim, C. T. (2018). "Cancer diagnosis: from tumor to liquid biopsy and beyond." Lab Chip **19**(1): 11-34.

Valadi, H., Ekstrom, K., Bossios, A., Sjostrand, M., Lee, J. J. and Lotvall, J. O. (2007). "Exosome-mediated transfer of mRNAs and microRNAs is a novel mechanism of genetic exchange between cells." Nat Cell Biol **9**(6): 654-659.

van Dommelen, S. M., van der Meel, R., van Solinge, W. W., Coimbra, M., Vader, P. and Schiffelers, R. M. (2016). "Cetuximab treatment alters the content of extracellular vesicles released from tumor cells." Nanomedicine (Lond) **11**(8): 881-890.

Vaupel, P. and Multhoff, G. (2021). "Revisiting the Warburg effect: historical dogma versus current understanding." J Physiol **599**(6): 1745-1757.

Vidal, P. (2020). "Interferon alpha in cancer immunoediting: From elimination to escape." Scand J Immunol **91**(5): e12863.

Villarroya-Beltri, C., Gutierrez-Vazquez, C., Sanchez-Cabo, F., Perez-Hernandez, D., Vazquez, J., Martin-Cofreces, N., Martinez-Herrera, D. J., Pascual-Montano, A., Mittelbrunn, M. and Sanchez-Madrid, F. (2013). "Sumoylated hnRNPA2B1 controls the sorting of miRNAs into exosomes through binding to specific motifs." Nat Commun **4**: 2980.

Visnovitz, T., Osteikoetxea, X., Sodar, B. W., Mihaly, J., Lorincz, P., Vukman, K. V., Toth, E. A., Koncz, A., Szekacs, I., Horvath, R., Varga, Z. and Buzas, E. I. (2019). "An improved 96 well plate format lipid quantification assay for standardisation of experiments with extracellular vesicles." J Extracell Vesicles **8**(1): 1565263.

Vlassov, A. V., Magdaleno, S., Setterquist, R. and Conrad, R. (2012). "Exosomes: current knowledge of their composition, biological functions, and diagnostic and therapeutic potentials." Biochim Biophys Acta **1820**(7): 940-948.

Waldenstrom, A., Genneback, N., Hellman, U. and Ronquist, G. (2012). "Cardiomyocyte microvesicles contain DNA/RNA and convey biological messages to target cells." PLoS One **7**(4): e34653.

Wallace, D. C. (2012). "Mitochondria and cancer." Nat Rev Cancer **12**(10): 685-698.

Wandrey, M., Jablonska, J., Stauber, R. H. and Gul, D. (2023). "Exosomes in Cancer Progression and Therapy Resistance: Molecular Insights and Therapeutic Opportunities." Life (Basel) **13**(10).

Wang, H. M., Wu, M. H., Chang, P. H., Lin, H. C., Liao, C. D., Wu, S. M., Hung, T. M., Lin, C. Y., Chang, T. C., Tzu-Tsen, Y. and Hsieh, J. C. (2019). "The change in circulating tumor cells before and during concurrent chemoradiotherapy is associated with survival in patients with locally advanced head and neck cancer." Head Neck **41**(8): 2676-2687.

Wang, J., Yao, Y., Wu, J. and Li, G. (2015). "Identification and analysis of exosomes secreted from macrophages extracted by different methods." Int J Clin Exp Pathol **8**(6): 6135-6142.

Wang, J., Zhou, Y., Lu, J., Sun, Y., Xiao, H., Liu, M. and Tian, L. (2014). "Combined detection of serum exosomal miR-21 and HOTAIR as diagnostic and prognostic biomarkers for laryngeal squamous cell carcinoma." Med Oncol **31**(9): 148.

Wang, X., Xu, C., Hua, Y., Sun, L., Cheng, K., Jia, Z., Han, Y., Dong, J., Cui, Y. and Yang, Z. (2016). "Exosomes play an important role in the process of psoralen reverse multidrug resistance of breast cancer." J Exp Clin Cancer Res **35**(1): 186.

Wang, Z., Liu, L., Guo, X., Guo, C. and Wang, W. (2018). "microRNA-1236-3p Regulates DDP Resistance in Lung Cancer Cells." Open Med (Wars) **14**: 41-51.

Wei, H., Chen, Q., Lin, L., Sha, C., Li, T., Liu, Y., Yin, X., Xu, Y., Chen, L., Gao, W., Li, Y. and Zhu, X. (2021). "Regulation of exosome production and cargo sorting." Int J Biol Sci **17**(1): 163-177.

Wei, Y., Lai, X., Yu, S., Chen, S., Ma, Y., Zhang, Y., Li, H., Zhu, X., Yao, L. and Zhang, J. (2014). "Exosomal miR-221/222 enhances tamoxifen resistance in recipient ER-positive breast cancer cells." Breast Cancer Res Treat **147**(2): 423-431.

Weiswald, L. B., Bellet, D. and Dangles-Marie, V. (2015). "Spherical cancer models in tumor biology." Neoplasia **17**(1): 1-15.

Welkoborsky, H. J., Jacob, R., Riazimand, S. H., Bernauer, H. S. and Mann, W. J. (2003). "Molecular biologic characteristics of seven new cell lines of squamous cell carcinomas of the head and neck and comparison to fresh tumor tissue." Oncology **65**(1): 60-71.

Weller, P., Nel, I., Hassenkamp, P., Gauler, T., Schlueter, A., Lang, S., Dountsop, P., Hoffmann, A. C. and Lehnerdt, G. (2014). "Detection of circulating tumor cell subpopulations in patients with head and neck squamous cell carcinoma (HNSCC)." PLoS One **9**(12): e113706.

Welsh, J. A., Goberdhan, D. C. I., O'Driscoll, L., Buzas, E. I., Blenkiron, C., et al. (2024). "Minimal information for studies of extracellular vesicles (MISEV2023): From basic to advanced approaches." J Extracell Vesicles **13**(2): e12404.

Windon, M. J., D'Souza, G., Rettig, E. M., Westra, W. H., van Zante, A., Wang, S. J., Ryan, W. R., Mydlarz, W. K., Ha, P. K., Miles, B. A., Koch, W., Gourin, C., Eisele, D. W. and Fakhry, C. (2018). "Increasing prevalence of human papillomavirus-positive oropharyngeal cancers among older adults." Cancer **124**(14): 2993-2999.

Xiao, C., Song, F., Zheng, Y. L., Lv, J., Wang, Q. F. and Xu, N. (2019). "Exosomes in Head and Neck Squamous Cell Carcinoma." Front Oncol **9**: 894.

Xin, Y., Chen, X., Tang, X., Li, K., Yang, M., Tai, W. C., Liu, Y. and Tan, Y. (2019). "Mechanics and Actomyosin-Dependent Survival/Chemoresistance of Suspended Tumor Cells in Shear Flow." Biophys J **116**(10): 1803-1814.

Xu, W., Wang, Z., Zhang, W., Qian, K., Li, H., Kong, D., Li, Y. and Tang, Y. (2015). "Mutated K-ras activates CDK8 to stimulate the epithelial-to-mesenchymal transition in pancreatic cancer in part via the Wnt/beta-catenin signaling pathway." Cancer Lett **356**(2 Pt B): 613-627.

Xu, Z., Chen, Y., Ma, L., Chen, Y., Liu, J., Guo, Y., Yu, T., Zhang, L., Zhu, L. and Shu, Y. (2022). "Role of exosomal non-coding RNAs from tumor cells and tumor-associated macrophages in the tumor microenvironment." Mol Ther **30**(10): 3133-3154.

Yan, J. and Xu, H. (2021). "Regulation of transforming growth factor-beta1 by circANKS1B/miR-515-5p affects the metastatic potential and cisplatin resistance in oral squamous cell carcinoma." Bioengineered **12**(2): 12420-12430.

Yang, L., Lang, J. C., Balasubramanian, P., Jatana, K. R., Schuller, D., Agrawal, A., Zborowski, M. and Chalmers, J. J. (2009). "Optimization of an enrichment process for circulating tumor cells from the blood of head and neck cancer patients through depletion of normal cells." Biotechnol Bioeng **102**(2): 521-534.

Yano, S., Zhang, Y., Miwa, S., Tome, Y., Hiroshima, Y., Uehara, F., Yamamoto, M., Suetsugu, A., Kishimoto, H., Tazawa, H., Zhao, M., Bouvet, M., Fujiwara, T. and Hoffman, R. M. (2014). "Spatial-temporal FUCCI imaging of each cell in a tumor demonstrates locational dependence of cell cycle dynamics and chemoresponsiveness." Cell Cycle **13**(13): 2110-2119.

Yap, T. A., Lorente, D., Omlin, A., Olmos, D. and de Bono, J. S. (2014). "Circulating tumor cells: a multifunctional biomarker." Clin Cancer Res **20**(10): 2553-2568.

Zhang, C., Xu, C., Gao, X. and Yao, Q. (2022). "Platinum-based drugs for cancer therapy and anti-tumor strategies." Theranostics **12**(5): 2115-2132.

Zhang, L., Wang, Y., Sha, Y., Zhang, B., Zhang, R., Zhang, H., Xu, S., Wang, H., Xu, Y., Chen, Y., Zhao, X., Zhu, J., Zhang, Z. and Wang, C. (2021). "CITED4 enhances the metastatic potential of lung adenocarcinoma." Thorac Cancer **12**(9): 1291-1302.

Zhang, L., Yan, L., Cao, M., Zhang, H., Li, C., Bai, Y., Yu, P., Li, M. and Zhao, X. (2016). "SPAG9 promotes endometrial carcinoma cell invasion through regulation of genes related to the epithelial-mesenchymal transition." Eur J Gynaecol Oncol **37**(3): 312-319.

Zhang, Y., Liu, Y., Liu, H. and Tang, W. H. (2019). "Exosomes: biogenesis, biologic function and clinical potential." Cell Biosci **9**: 19.

Zhang, Y., Shu, Y. M., Wang, S. F., Da, B. H., Wang, Z. H. and Li, H. B. (2010). "Stabilization of mismatch repair gene PMS2 by glycogen synthase kinase 3beta is implicated in the treatment of cervical carcinoma." Bmc Cancer **10**: 58.

Zhang, Z., Samsa, W. E., De, Y., Zhang, F., Reizes, O., Almasan, A. and Gong, Z. (2023). "HDGFRP3 interaction with 53BP1 promotes DNA double-strand break repair." Nucleic Acids Res **51**(5): 2238-2256.

Zhang, Z., Wang, Z., Liu, T., Tang, J., Liu, Y., Gou, T., Chen, K., Wang, L., Zhang, J., Yang, Y. and Zhang, H. (2024). "Exploring the role of ITGB6: fibrosis, cancer, and other diseases." Apoptosis **29**(5-6): 570-585.

Zhu, H., Luo, H., Zhang, W., Shen, Z., Hu, X. and Zhu, X. (2016). "Molecular mechanisms of cisplatin resistance in cervical cancer." Drug Des Devel Ther **10**: 1885-1895.

Zhu, J., Liu, B., Wang, Z., Wang, D., Ni, H., Zhang, L. and Wang, Y. (2019). "Exosomes from nicotine-stimulated macrophages accelerate atherosclerosis through miR-21-3p/PTEN-mediated VSMC migration and proliferation." Theranostics **9**(23): 6901-6919.

Zisowsky, J., Koegel, S., Leyers, S., Devarakonda, K., Kassack, M. U., Osmak, M. and Jaehde, U. (2007). "Relevance of drug uptake and efflux for cisplatin sensitivity of tumor cells." Biochem Pharmacol **73**(2): 298-307.

Zullig, L., Roessle, M., Weber, C., Graf, N., Haerle, S. K., Jochum, W., Stoeckli, S. J., Moch, H. and Huber, G. F. (2013). "High sex determining region Y-box 2 expression is a negative predictor of occult lymph node metastasis in early squamous cell carcinomas of the oral cavity." Eur J Cancer **49**(8): 1915-1922.

6 APPENDIX

6.1 SUPPLEMENTARY MATERIALS

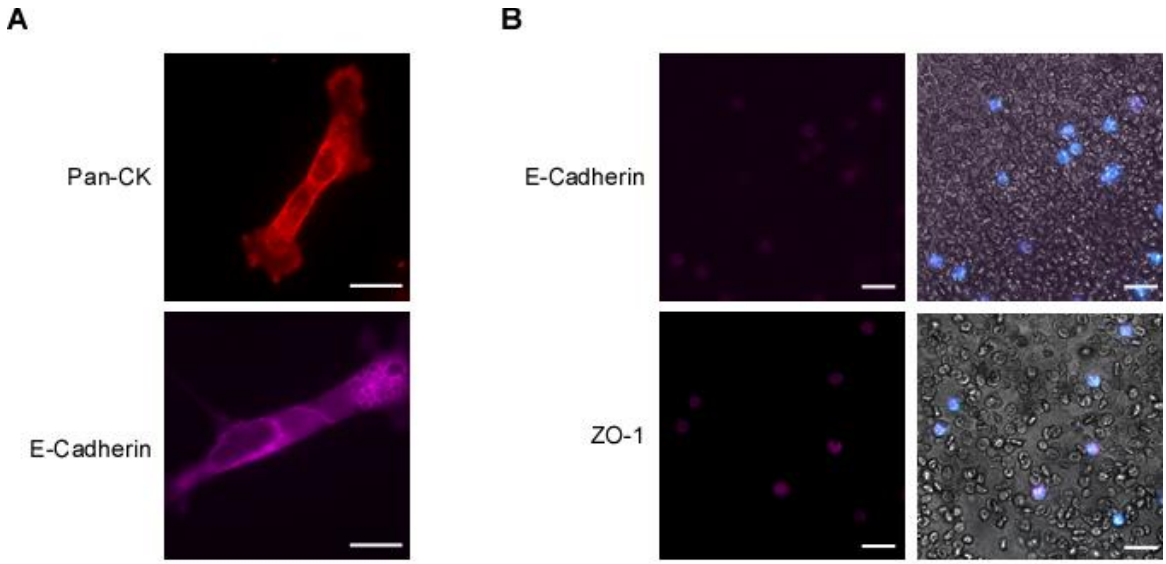

Supplementary Figure 1. Marker analysis of HNSCCUM-02T cells by fluorescence microscopy.
A) Cells were seeded in microscopy dishes and fixed with PFA before staining with Pan-CK-PE or E-Cadherin-594 antibodies. **B)** Cells were spiked into 7,5 mL whole blood from a healthy donor and enriched using pluriBeads. Afterwards, cells were fixed and stained with Hoechst and E-Cadherin-594 or ZO-1-594 antibodies. Scale bars 20 µM.

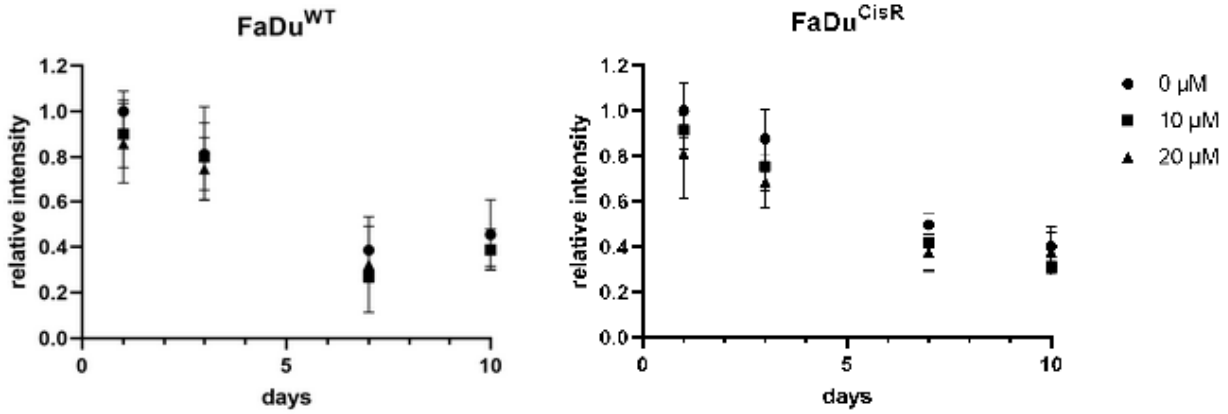

Supplementary Figure 2. Relative intensity of FaDu spheroids
Cells were seeded at defined numbers and spheroids were allowed to form for three days before onset of cisplatin treatment (arrows). Spheroid average intensity was assayed by HCS and normalized to untreated controls on day one. Data is given as Mean ± SD of n=3 independent experiments. Statistical analysis by two-way ANOVA and Tukey's multiple comparisons test revealed no significant differences based on cisplatin treatment.

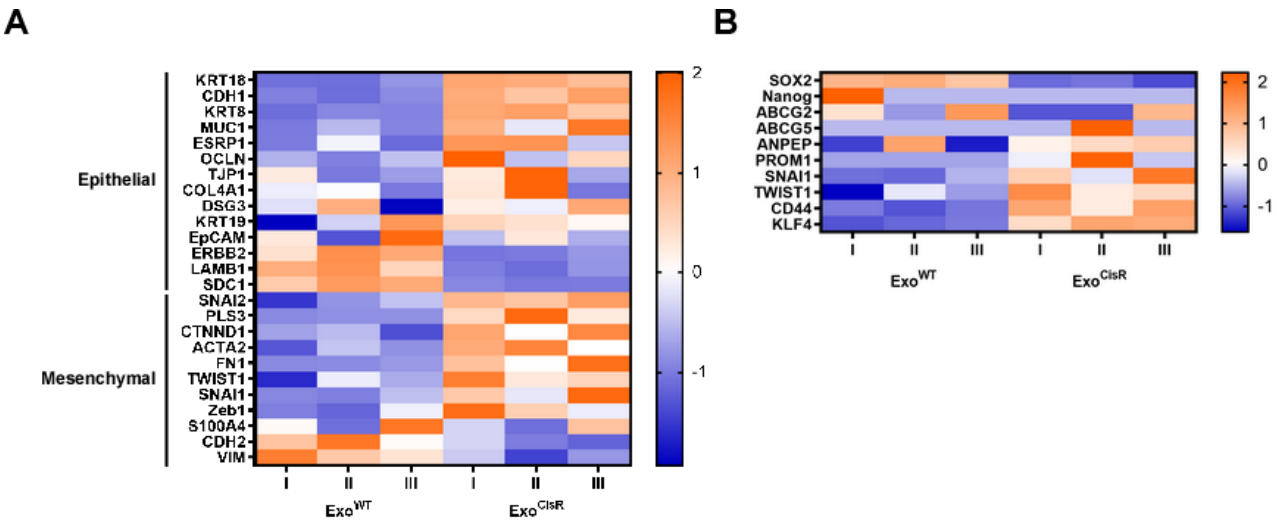

Supplementary Figure 3. Heatmap analysis of full set of EMT candidate genes
Candidate genes were identified by literature review. Sequencing data is displayed as z-scores. For full list of candidate genes and normalized counts refer to Supplementary Table 2.

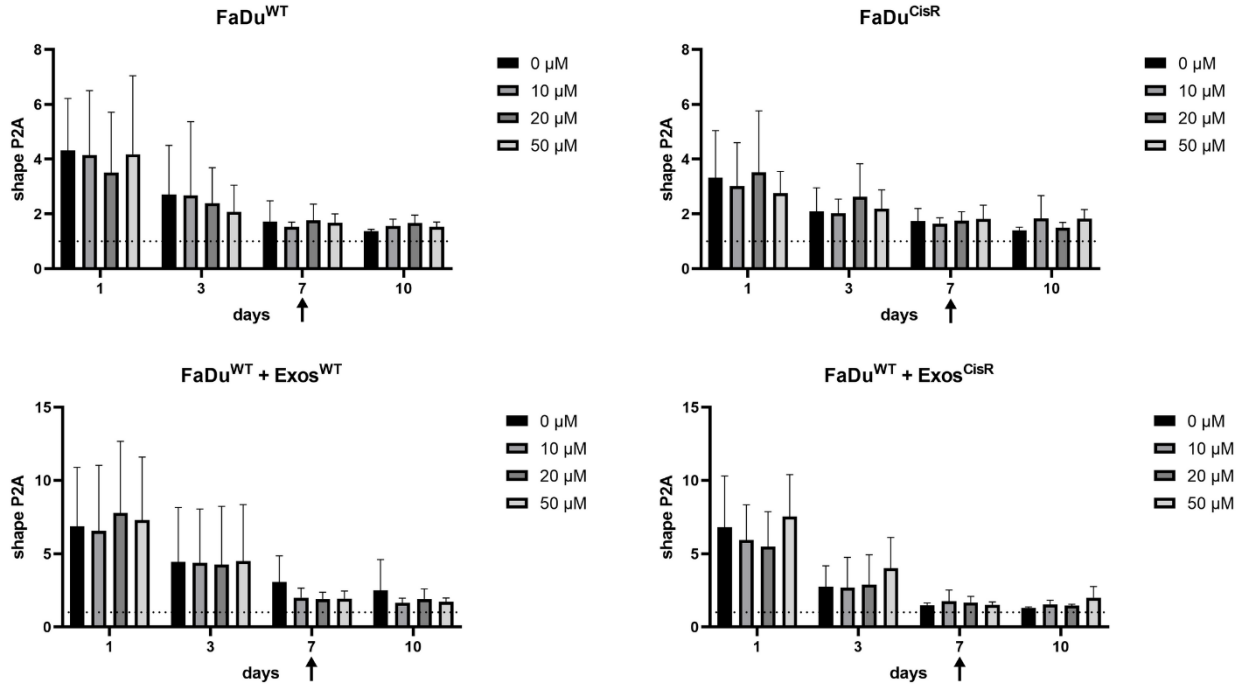

Supplementary Figure 4. Shape of spheroids formed in the presence or absence of exosomes
Spheroids were seeded in the presence or absence of exosomes and allowed to grow for 7 days before treatment with different concentrations of cisplatin. Spheroid shape P2A was assayed by HCS. Arrows mark onset of treatment. Dashed line marks P2A=1, which equals a perfectly round shape. Data is given as Mean ± SD of n=3 independent experiments. Statistical analysis by two-way ANOVA and Tukey's multiple comparisons test revealed no significant differences based on cisplatin treatment.

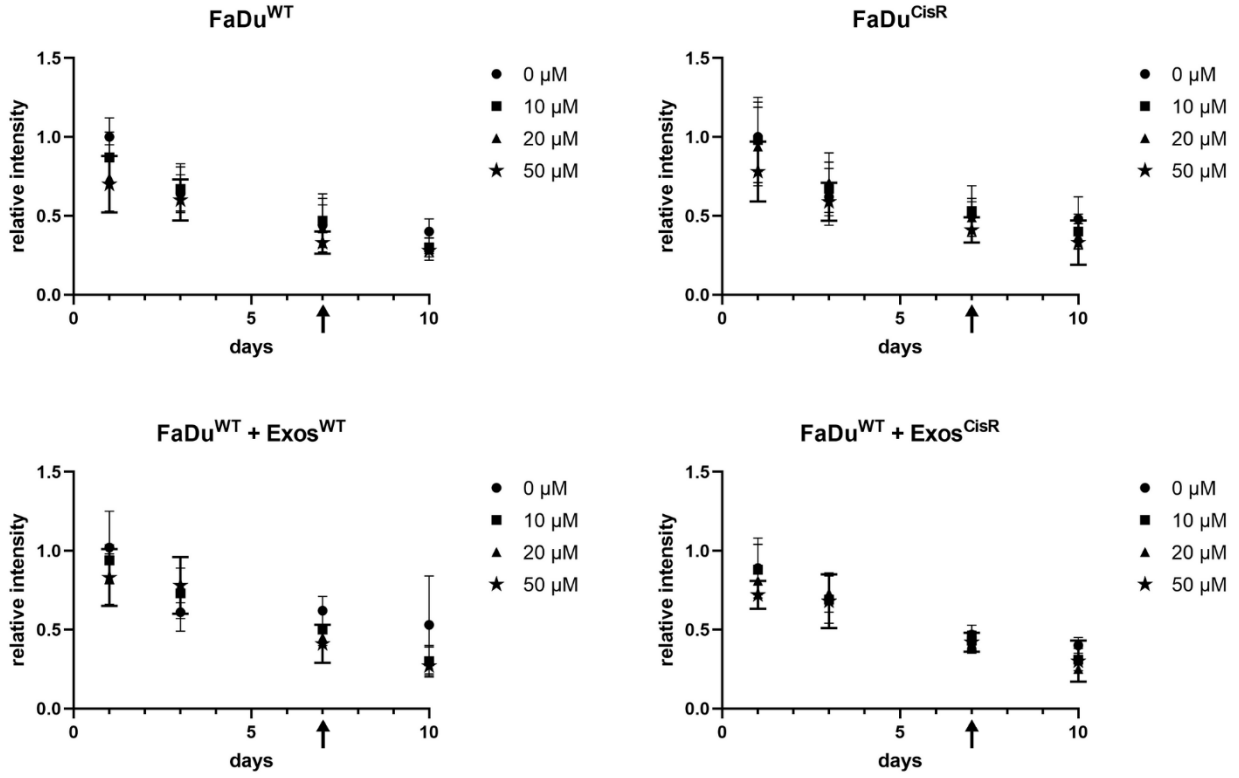

Supplementary Figure 5. Relative intensity of spheroids formed in the presence or absence of exosomes

Spheroids were seeded in the presence or absence of exosomes and allowed to grow for 7 days before treatment with different concentrations of cisplatin. Spheroid average intensity was assayed by HCS and normalized to untreated controls on day one. Arrows mark onset of treatment. Data is given as Mean ± SD of n=3 independent experiments. Statistical analysis by two-way ANOVA and Tukey's multiple comparisons test revealed no significant differences based on cisplatin treatment.

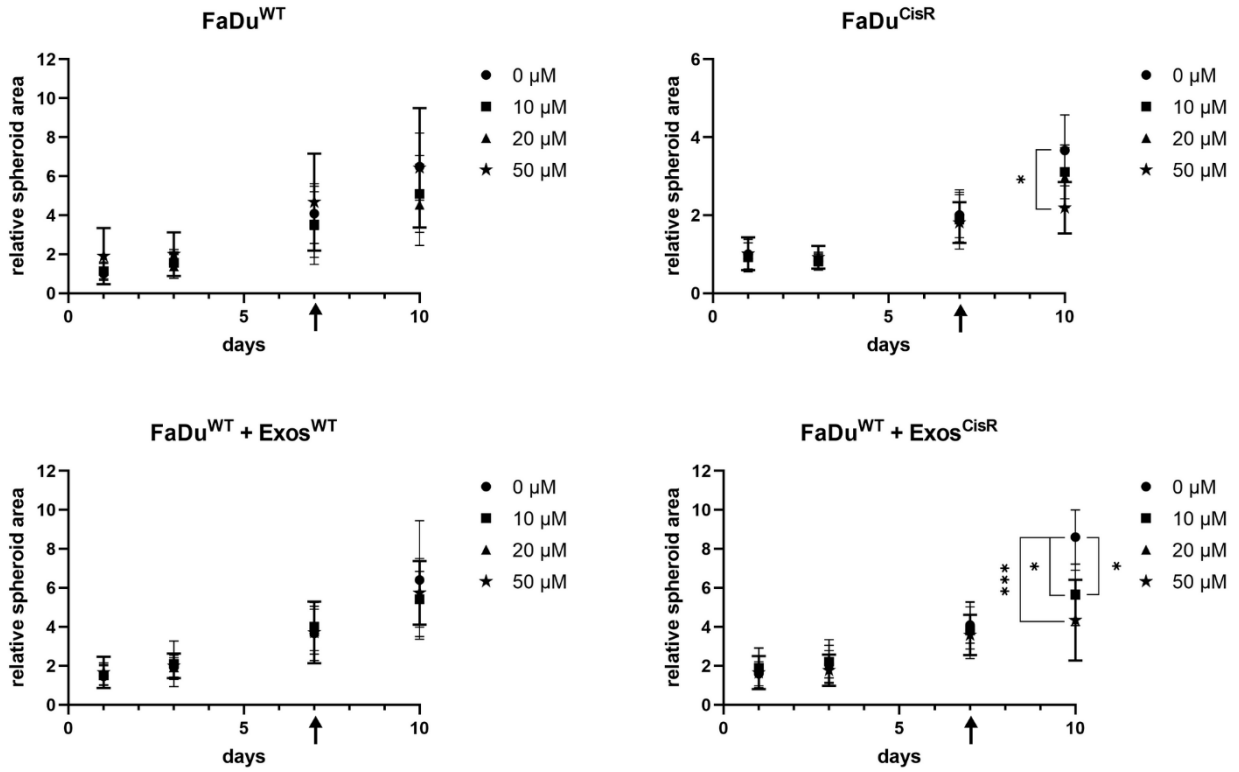

Supplementary Figure 6. Relative area of spheroids formed in the presence or absence of exosomes

Spheroids were seeded in the presence or absence of exosomes and allowed to grow for 7 days before treatment with different concentrations of cisplatin. Spheroid area was assayed by HCS and normalized to untreated controls on day one. Arrows mark onset of treatment. All data is given as Mean ± SD of n=3 independent experiments. Statistical analysis by two-way ANOVA and Tukey's multiple comparisons test. * $p < 0,05$; *** $p < 0,005$

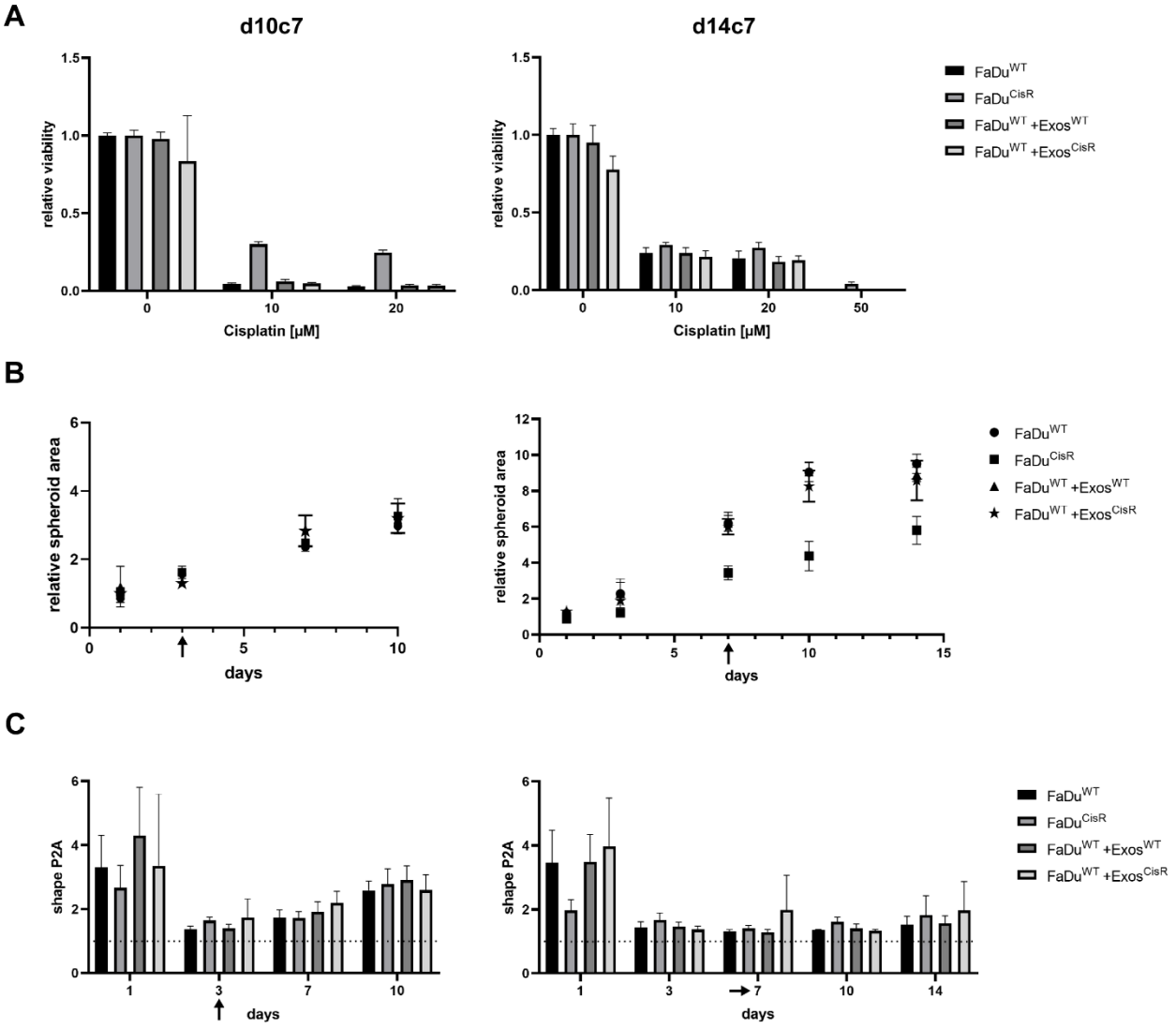

Supplementary Figure 7. Influence of treatment start and duration on spheroids formed in the presence or absence of exosomes

Spheroids were seeded at defined numbers and allowed to grow for three (left) or 7 (right) days before cisplatin treatment. Medium was exchanged once during the 7 day treatment phase. **A)** Relative spheroid viability as determined by CTG assay on d10c7 or d14c7. Data was normalized to untreated controls. **B)** Relative spheroid area in response to 20 µM (left) and 50 µM (right) cisplatin treatment for seven days. Arrows mark onset of treatment. Data was normalized to untreated controls on day 1. **C)** Shape P2A of spheroids in response to 20 µM (left) and 50 µM (right) cisplatin treatment for seven days. Arrows mark onset of treatment. Dashed line marks P2A = 1, which equals a perfectly round shape. All data is given as Mean ± SD of n=1 experiment with 6 biological replicates.

Supplementary Table 1. RNA Sequencing Results of Cisplatin Resistance Candidate Genes
Values are given as normalized counts. Significantly regulated genes based on adjusted p-value < 0,05 are shaded in grey. All significantly regulated genes are included in the heatmap (Figure 17). n.a. ≙ gene not detected.

Gene	Exo^{WT} 1	Exo^{WT} 2	Exo^{WT} 3	Exo^{CisR} 1	Exo^{CisR} 2	Exo^{CisR} 3
MAPK3	-1,138	-1,138	-1,138	-1,138	-1,138	-1,138
ABCC1	0,819	1,195	0,957	-1,086	-1,069	-0,815
RPA1	0,950	0,736	1,277	-0,996	-0,988	-0,978
REV1	1,048	0,923	0,978	-1,326	-0,914	-0,708
MSH6	0,996	1,247	0,703	-0,961	-0,815	-1,171
BRCA1	0,719	1,298	0,910	-0,740	-1,213	-0,975
MRE11a	0,609	1,366	0,941	-0,895	-1,144	-0,876
MAPK14	1,190	1,251	0,458	-1,041	-0,923	-0,934
MSH3	1,148	0,797	0,948	-1,030	-0,512	-1,351
RAD51	1,157	0,873	0,860	-0,467	-1,247	-1,177
ATR	1,440	0,920	0,525	-1,002	-1,062	-0,820
ERBB2	0,372	1,401	1,076	-1,051	-1,005	-0,793
ABCC2	0,843	1,458	0,535	-1,192	-0,597	-1,048
JAK1	-0,933	-0,933	-0,933	-0,933	-0,933	-0,933
BCL2	0,502	1,681	0,583	-1,025	-0,784	-0,958
KDM5A	1,272	1,338	0,147	-1,060	-0,891	-0,806
PMS2	1,349	0,665	0,740	-0,559	-1,581	-0,615
ATP7A	1,366	0,213	1,106	-0,372	-1,320	-0,993
ABCC5	0,540	1,440	0,676	-0,434	-1,620	-0,602
mTOR	1,482	1,146	0,027	-0,645	-1,168	-0,842
BRCA2	1,150	0,972	0,381	-1,516	0,139	-1,127
EZH2	0,457	0,128	1,882	-0,705	-0,578	-1,184
LRRC8A	0,014	1,967	0,432	-0,839	-0,798	-0,776
CHD4	0,308	1,610	0,396	-0,904	-1,525	0,114
JAK2	-0,762	-0,762	-0,762	-0,762	-0,762	-0,762
TAZ	0,586	1,369	0,231	0,251	-1,809	-0,628
GSTO2	2,024	-0,280	0,436	-0,685	-0,901	-0,594
MSH2	-0,070	1,871	0,337	-0,567	-0,143	-1,427
ABCC3	0,547	1,975	-0,531	-0,571	-1,014	-0,405
ERCC2	1,972	-0,358	0,364	-0,113	-1,156	-0,708
ERCC4	0,349	1,816	-0,286	-0,452	-1,513	0,086
FOXO1	-0,733	1,521	0,672	-1,454	0,536	-0,543
LRRC8D	0,527	0,487	-0,486	-0,966	1,672	-1,233
ATP7B	0,243	-0,351	0,616	-1,691	1,561	-0,377
GSTT1	-0,245	0,326	-0,259	1,126	-1,897	0,949
NRP2	-0,674	1,032	-0,541	-0,048	-1,327	1,557
GSTK1	-0,912	-1,035	1,702	0,908	-0,054	-0,610
MLH1	-1,686	-0,493	1,629	-0,142	0,336	0,356

Gene	Exo^{WT} 1	Exo^{WT} 2	Exo^{WT} 3	Exo^{CisR} 1	Exo^{CisR} 2	Exo^{CisR} 3
MGST2	-0,004	-1,141	0,573	-0,657	1,876	-0,647
XPC	-0,387	1,533	-1,737	0,664	0,108	-0,181
XPC	-0,387	1,533	-1,737	0,664	0,108	-0,181
MGST1	-0,273	-1,752	1,299	-0,255	-0,069	1,050
TP73	-0,243	-0,512	-0,137	-0,536	-0,762	2,189
TIE1	-0,447	-0,447	-0,447	-0,447	-0,447	2,236
ERCC1	-0,798	-0,934	0,384	0,944	-1,095	1,500
ABCB1	-0,510	-0,510	-0,510	2,220	-0,510	-0,180
GTF2H5	-0,756	-0,945	-0,320	0,017	-0,099	2,103
GSTM2	-0,705	-0,705	-0,705	1,552	1,267	-0,705
GSTM3	-0,707	-0,707	-0,707	1,450	-0,707	1,378
ERCC5	-0,582	-1,160	-0,397	0,098	0,005	2,037
STAT6	-1,082	-0,039	-1,138	-0,144	0,644	1,760
GSTZ1	-0,301	-1,217	-0,774	1,106	-0,382	1,569
MGST3	-0,986	-1,536	0,107	1,033	0,127	1,254
XPA	-0,525	-0,039	-1,855	0,999	0,337	1,082
TP53	-0,994	-0,557	-0,890	0,014	1,907	0,521
MAST1	-1,155	-0,813	-0,641	0,214	0,613	1,781
GSTO1	-1,054	-0,857	-0,738	1,413	-0,035	1,270
XRCC6	-1,240	-0,946	-0,489	0,882	1,583	0,210
BAX	-0,670	-1,144	-0,895	0,733	1,678	0,298
RAD23B	-0,940	-0,813	-1,078	0,918	1,513	0,400
BID	-1,308	-1,093	-0,449	0,694	1,288	0,867
XRCC2	-0,847	-0,650	-1,367	0,660	1,355	0,849
MAPK12	0,955	0,955	0,955	0,955	0,955	0,955
DYNLL1	-1,137	-1,305	-0,437	0,893	0,842	1,143
GSTP1	-0,872	-1,374	-0,635	1,239	1,003	0,639
GSTM4	-0,992	-1,100	-0,796	1,154	1,277	0,457
ERCC3	-1,019	-0,844	-1,042	0,719	0,732	1,453
STAT3	-1,024	-1,050	-0,856	0,562	1,185	1,182
HDAC1	-1,130	-1,204	-0,600	1,027	1,100	0,807
STAT1	-1,003	-0,964	-1,023	1,050	0,837	1,103
MAPK6	1,060	1,060	1,060	1,060	1,060	1,060
MAPK13	1,098	1,098	1,098	1,098	1,098	1,098
MAPK9	1,130	1,130	1,130	1,130	1,130	1,130
MAPK14	1,190	1,190	1,190	1,190	1,190	1,190
MAPK1	1,504	1,504	1,504	1,504	1,504	1,504
CTR1	n.a.	n.a.	n.a.	n.a.	n.a.	n.a.
REV7	n.a.	n.a.	n.a.	n.a.	n.a.	n.a.
VEGF	n.a.	n.a.	n.a.	n.a.	n.a.	n.a.
P21	n.a.	n.a.	n.a.	n.a.	n.a.	n.a.

Gene	Exo^{WT} 1	Exo^{WT} 2	Exo^{WT} 3	Exo^{CisR} 1	Exo^{CisR} 2	Exo^{CisR} 3
OCT1	n.a.	n.a.	n.a.	n.a.	n.a.	n.a.
OCT3	n.a.	n.a.	n.a.	n.a.	n.a.	n.a.
OCTN1	n.a.	n.a.	n.a.	n.a.	n.a.	n.a.
MRP2	n.a.	n.a.	n.a.	n.a.	n.a.	n.a.
PTIP	n.a.	n.a.	n.a.	n.a.	n.a.	n.a.
YAP	n.a.	n.a.	n.a.	n.a.	n.a.	n.a.
CD133	n.a.	n.a.	n.a.	n.a.	n.a.	n.a.
TLR9	n.a.	n.a.	n.a.	n.a.	n.a.	n.a.
NOX2	n.a.	n.a.	n.a.	n.a.	n.a.	n.a.
PD1	n.a.	n.a.	n.a.	n.a.	n.a.	n.a.
GSTM1	n.a.	n.a.	n.a.	n.a.	n.a.	n.a.
GSTT2	n.a.	n.a.	n.a.	n.a.	n.a.	n.a.
OCTN2	n.a.	n.a.	n.a.	n.a.	n.a.	n.a.
53BP1	n.a.	n.a.	n.a.	n.a.	n.a.	n.a.
MEK1	n.a.	n.a.	n.a.	n.a.	n.a.	n.a.
NER	n.a.	n.a.	n.a.	n.a.	n.a.	n.a.
GSTA4	n.a.	n.a.	n.a.	n.a.	n.a.	n.a.

Supplementary Table 2. RNA Sequencing Results of EMT and CSC Candidate Genes
Values are given as normalized counts. Significantly regulated genes based on adjusted p-value < 0,05 are shaded in grey. All significantly regulated genes are included in the heatmap (Figure 25). n.a. ≙ gene not detected; E ≙ epithelial; M ≙ mesenchymal; C ≙ CSC

Gene	Exo^{WT} 1	Exo^{WT} 2	Exo^{WT} 3	Exo^{CisR} 1	Exo^{CisR} 2	Exo^{CisR} 3	Marker
KRT18	-1,074	-1,091	-0,810	1,116	1,045	0,814	E
CDH1	-0,959	-1,117	-0,889	1,038	0,730	1,197	E
KRT8	-1,108	-0,906	-0,945	1,079	1,190	0,691	E
MUC1	-1,015	-0,537	-0,931	0,983	-0,178	1,678	E
ESRP1	-0,998	-0,093	-1,128	1,311	1,346	-0,438	E
OCLN	-0,595	-0,967	-0,472	2,005	-0,469	0,498	E
TJP1	0,242	-1,023	-0,758	0,258	1,951	-0,671	E
COL4A1	-0,141	-0,023	-1,029	0,291	1,939	-1,037	E
DSG3	-0,237	1,003	-1,928	0,208	-0,123	1,077	E
KRT19	-1,938	-0,348	1,301	0,529	0,377	0,080	E
EpCAM	0,275	-1,314	1,869	-0,494	0,281	-0,617	E
ERBB2	0,372	1,401	1,076	-1,051	-1,005	-0,793	E
LAMB1	1,019	1,353	0,528	-0,973	-1,117	-0,810	E
SDC1	0,636	1,255	1,057	-0,908	-1,031	-1,008	E
SNAI2	-1,535	-0,818	-0,460	0,888	0,714	1,211	M
PLS3	-0,891	-0,850	-0,843	0,458	1,871	0,254	M
CTNND1	-0,712	-0,522	-1,340	1,111	-0,015	1,480	M
ACTA2	-1,288	-0,441	-0,842	1,051	1,528	-0,007	M
FN1	-0,892	-0,882	-0,779	0,774	-0,015	1,794	M
TWIST1	-1,624	-0,149	-0,633	1,609	0,271	0,526	M
SNAI1	-0,909	-0,966	-0,486	0,672	-0,186	1,876	M/C
Zeb1	-0,971	-1,170	-0,123	1,818	0,590	-0,144	M
S100A4	0,070	-1,096	1,712	-0,334	-1,096	0,744	M
CDH2	0,741	1,719	0,046	-0,331	-0,991	-1,184	M
VIM	1,608	0,684	0,331	-0,402	-1,431	-0,791	M
SOX2	1,030	1,143	0,802	-0,947	-0,883	-1,146	C
Nanog	2,236	-0,447	-0,447	-0,447	-0,447	-0,447	C
ABCG2	0,408	-0,656	1,434	-1,088	-1,088	0,989	C
ABCG5	-0,447	-0,447	-0,447	-0,447	2,236	-0,447	C
ANPEP	-1,211	1,281	-1,455	0,180	0,511	0,694	C
PROM1	-0,582	-0,582	-0,582	-0,104	2,202	-0,351	C
TWIST1	-1,624	-0,149	-0,633	1,609	0,271	0,526	C
CD44	-0,846	-1,095	-0,876	1,225	0,272	1,320	C
KLF4	-1,091	-0,967	-0,844	0,486	1,246	1,171	C
ALDH1	n.a.	n.a.	n.a.	n.a.	n.a.	n.a.	C
OCT4	n.a.	n.a.	n.a.	n.a.	n.a.	n.a.	C
DPP4	n.a.	n.a.	n.a.	n.a.	n.a.	n.a.	C
c-Met	n.a.	n.a.	n.a.	n.a.	n.a.	n.a.	C
Bmi-1	n.a.	n.a.	n.a.	n.a.	n.a.	n.a.	C

Supplementary Table 3. Genes significantly regulated in FaDu cells and exosomes
Values are given as z-scores. Genes included in the heatmap analysis (Figure 18) are shaded in grey.

	Cells						Exosomes					
gene	**WT1**	**WT2**	**WT3**	**CisR1**	**CisR2**	**CisR3**	**WT1**	**WT2**	**WT3**	**CisR1**	**CisR2**	**CisR3**
HOMER2	0,92	0,90	1,16	-0,88	-1,08	-1,02	0,91	1,34	0,70	-0,97	-0,94	-1,04
GLUL	1,23	0,86	0,88	-1,08	-1,01	-0,88	1,18	0,97	0,74	-1,17	-1,21	-0,52
TBL1X	1,24	1,07	0,61	-1,22	-0,77	-0,94	1,23	1,35	0,20	-1,06	-0,79	-0,93
NOTCH3	1,44	0,81	0,67	-0,95	-0,96	-1,01	1,23	0,79	0,77	-1,10	-1,41	-0,28
IFRD1	1,15	0,86	0,89	-1,34	-1,03	-0,54	-0,94	-1,15	-0,87	0,92	0,81	1,23
RIPK4	1,36	0,57	0,96	-0,97	-1,18	-0,74	0,38	0,40	1,76	-1,00	-0,30	-1,23
PRSS12	0,97	1,15	0,77	-1,17	-0,48	-1,24	1,17	1,00	0,78	-1,08	-0,71	-1,16
RAC3	1,35	0,54	1,00	-1,19	-1,00	-0,70	0,85	1,45	0,54	-1,31	-0,86	-0,65
RAI14	0,97	0,55	1,36	-0,85	-1,26	-0,77	1,37	0,69	0,80	-0,55	-1,31	-0,99
PLIN2	0,86	1,24	0,79	-0,99	-1,36	-0,53	-0,88	-0,95	-0,89	1,47	0,09	1,17
SYT12	0,48	1,30	1,09	-1,19	-0,67	-1,02	1,28	1,12	0,48	-1,05	-0,72	-1,12
PRICKLE1	1,15	1,03	0,69	-0,58	-1,45	-0,84	0,71	1,62	0,48	-0,98	-0,89	-0,94
DLG3	0,51	1,43	0,92	-1,17	-0,74	-0,95	1,02	1,31	0,60	-0,97	-0,99	-0,98
TMEM164	1,08	0,59	1,20	-1,41	-0,79	-0,67	1,11	1,25	0,56	-0,88	-0,91	-1,13
SOX2	1,51	0,86	0,49	-0,97	-0,95	-0,95	1,03	1,14	0,80	-0,95	-0,88	-1,15
SLC47A2	1,52	0,88	0,44	-1,03	-0,85	-0,97	0,64	1,22	1,09	-0,95	-1,04	-0,96
ABCA2	1,59	0,60	0,64	-0,99	-0,77	-1,07	1,06	1,32	0,45	-0,97	-1,31	-0,55
SLC6A8	1,25	1,20	0,36	-0,77	-0,71	-1,33	-0,72	-0,70	-1,14	1,05	-0,10	1,61
CDK2AP2	1,59	0,51	0,69	-0,81	-1,19	-0,79	-1,00	-1,30	-0,35	0,58	1,63	0,44
PSPC1	0,67	0,57	1,55	-1,31	-0,69	-0,79	0,75	1,42	0,74	-0,95	-1,14	-0,82
NEDD9	1,44	0,88	0,47	-1,37	-0,56	-0,85	-1,19	-0,78	-0,82	0,26	1,16	1,37
CAPG	1,27	0,92	0,60	-1,44	-1,00	-0,34	-1,10	-1,05	-0,76	0,63	0,92	1,37
NIPAL2	1,18	1,40	0,19	-0,93	-0,84	-1,01	1,25	1,07	0,44	-1,45	-0,40	-0,90
ELF4	1,39	0,60	0,78	-1,06	-1,37	-0,34	0,98	0,71	1,24	-1,27	-0,93	-0,73
NEIL2	0,35	0,90	1,50	-0,52	-1,26	-0,97	0,92	1,56	0,31	-0,86	-1,05	-0,88
GAMT	1,66	0,47	0,62	-1,09	-1,01	-0,66	-0,85	-0,69	-1,23	0,79	1,58	0,40
SNCG	0,63	0,68	1,45	-1,13	-1,29	-0,33	-1,09	-1,05	-0,74	0,70	0,69	1,48
TRIB3	1,66	0,31	0,77	-1,09	-0,81	-0,84	-1,32	-1,32	0,10	0,62	0,59	1,33
SNX12	0,78	0,70	1,25	-1,38	-1,18	-0,18	1,32	0,48	1,09	-0,89	-0,90	-1,11
UBAC2	0,30	1,71	0,72	-0,94	-0,90	-0,88	0,76	1,02	1,17	-0,74	-1,08	-1,14
BMP7	1,72	0,58	0,42	-0,91	-0,76	-1,05	1,16	0,09	1,47	-0,91	-0,91	-0,91
FGFR2	1,71	0,53	0,48	-0,79	-0,76	-1,16	1,19	1,20	0,54	-0,96	-0,93	-1,03
LBH	0,26	0,77	1,68	-0,96	-0,69	-1,06	0,78	0,91	1,25	-1,30	-0,78	-0,86
ADD2	1,77	0,50	0,42	-1,00	-0,77	-0,92	1,23	1,17	0,48	-0,70	-1,04	-1,14
PCK2	1,74	0,38	0,56	-1,03	-0,62	-1,04	-0,91	-1,04	-0,97	0,52	1,11	1,28
TSPAN1	0,56	1,18	0,91	-1,01	-0,09	-1,56	-0,91	-1,15	-0,84	0,58	0,90	1,42
SBDSP1	0,95	0,35	1,34	-0,52	-1,62	-0,50	0,68	0,11	1,67	-0,40	-0,58	-1,49
B3GALT6	0,90	0,71	1,04	-0,86	-1,69	-0,09	0,61	1,57	0,65	-1,10	-0,74	-0,99

	Cells						Exosomes					
gene	**WT1**	**WT2**	**WT3**	**CisR1**	**CisR2**	**CisR3**	**WT1**	**WT2**	**WT3**	**CisR1**	**CisR2**	**CisR3**
SYNM	0,87	1,27	0,47	-1,74	-0,44	-0,42	0,49	1,56	0,63	-0,89	-1,42	-0,37
EGLN3	1,35	1,28	-0,06	-1,34	-0,66	-0,56	-1,04	-1,23	-0,33	0,60	0,31	1,69
MFSD3	1,88	0,24	0,42	-0,74	-0,73	-1,06	-1,22	-0,94	-0,79	0,82	0,89	1,24
ANKRD2	1,61	-0,23	1,12	-0,83	-0,71	-0,96	0,40	1,38	1,06	-0,63	-1,10	-1,10
FUNDC2	-0,17	1,44	1,20	-0,77	-1,31	-0,39	0,71	0,87	1,04	-1,25	0,08	-1,45
NCS1	1,61	0,21	0,64	-0,92	-1,45	-0,08	1,13	1,35	0,38	-0,97	-0,81	-1,08
AMER1	0,91	0,25	1,24	0,24	-1,38	-1,26	1,46	0,84	0,32	-1,43	-0,18	-1,00
PEX6	1,76	0,85	-0,20	-1,10	-0,43	-0,88	0,83	0,54	1,49	-1,10	-0,88	-0,89
TBC1D16	1,98	0,08	0,35	-0,79	-0,95	-0,66	1,00	1,24	0,72	-0,95	-0,97	-1,05
GPT2	1,95	-0,02	0,44	-0,80	-1,02	-0,55	0,92	1,35	0,66	-0,85	-1,08	-1,00
CCND2	1,75	0,61	-0,01	-1,08	-0,08	-1,18	1,13	1,21	0,59	-0,98	-0,88	-1,08
NGFRAP1	0,74	1,84	-0,25	-0,70	-1,11	-0,52	-1,25	-1,22	-0,32	1,13	0,55	1,12
PGK1	0,21	0,77	1,32	-0,88	-1,67	0,25	-0,79	-1,32	-0,75	0,98	0,53	1,35
IFRD2	1,46	0,15	0,68	-0,70	-1,70	0,12	0,53	1,47	0,78	-0,48	-1,27	-1,05
NDRG1	1,40	0,78	0,09	-0,74	-1,68	0,16	-1,02	-1,01	-0,51	0,44	0,24	1,86
NAMPT	0,61	1,07	0,57	-0,47	-1,98	0,19	-1,15	-0,93	-0,87	1,30	0,82	0,83
FAT2	1,90	0,68	-0,33	-0,77	-0,46	-1,01	1,35	1,25	0,16	-0,98	-1,04	-0,74
PVRL4	1,12	1,20	-0,12	-1,46	0,30	-1,04	-0,94	-0,67	-0,61	0,54	-0,30	1,98
RAPGEF3	2,03	-0,14	0,28	-0,59	-0,50	-1,09	0,67	1,84	0,03	-0,83	-0,79	-0,92
CORO2A	2,10	0,21	-0,21	-0,64	-0,56	-0,89	0,79	1,43	0,49	-1,23	-0,25	-1,24
HCAR2	1,56	0,84	-0,32	-1,11	0,23	-1,21	1,39	0,50	0,89	-1,21	-1,20	-0,36
IRAK1	1,98	-0,27	0,36	-0,84	-1,08	-0,15	0,76	1,52	0,59	-0,92	-0,89	-1,06
SLC7A11	0,98	-0,10	1,18	-1,90	-0,10	-0,06	1,48	1,18	-0,12	-0,71	-0,60	-1,23
GDF15	2,10	0,09	-0,14	-0,97	-0,43	-0,65	-0,92	-1,03	-0,79	0,52	0,50	1,72
ASS1	2,13	-0,16	0,04	-0,93	-0,49	-0,59	-1,00	-1,21	-0,76	1,03	0,91	1,03
IGBP1	-0,39	0,34	2,04	-0,54	-1,05	-0,40	-1,02	-0,57	-1,27	0,56	0,97	1,33
MECP2	1,69	-0,09	0,38	-0,83	-1,48	0,33	0,87	1,37	0,70	-0,96	-0,91	-1,06
SLC19A1	1,90	0,00	0,08	-0,72	-1,36	0,10	1,60	0,76	0,23	-0,87	-1,39	-0,34
BCL11A	0,73	1,91	-0,66	-0,46	-0,87	-0,64	1,35	0,70	0,87	-0,95	-0,81	-1,16
OTUB2	1,76	0,16	0,03	-0,86	-1,42	0,33	0,71	1,31	0,93	-1,04	-1,00	-0,91
COL4A2	1,90	0,74	-0,73	-0,64	-0,42	-0,85	0,55	1,94	-0,11	-0,59	-0,90	-0,88
RPS4X	-0,80	1,08	1,60	-0,82	-0,97	-0,08	-0,95	-1,24	-0,64	0,87	0,49	1,47
MAGEA4	-0,69	0,93	1,63	-0,80	-1,16	0,08	-1,22	-1,27	-0,38	0,94	0,95	0,98
CYGB	2,14	-0,16	-0,14	-1,00	-0,30	-0,54	1,18	0,35	1,29	-0,70	-0,85	-1,26
CLDN1	1,82	0,33	-0,33	-1,00	0,34	-1,17	-0,73	-0,98	-0,54	0,40	2,01	-0,15
ATP11C	-0,40	1,04	1,17	-0,69	0,51	-1,63	0,88	1,49	0,45	-0,69	-0,97	-1,17
SEMA3B	2,12	-0,31	-0,02	-0,32	-0,40	-1,07	-1,21	-0,87	-0,84	0,81	0,74	1,38
RPL36A	-0,95	1,07	1,66	-0,44	-0,92	-0,41	-0,80	-0,80	-0,66	-0,33	1,93	0,67
RASGEF1A	0,43	1,65	-0,32	-1,64	0,30	-0,43	0,52	0,86	1,47	-1,18	-0,66	-1,01
MARCKSL1	1,28	0,58	-0,11	-1,83	-0,52	0,60	-1,05	-1,01	-0,93	0,84	1,18	0,96

	Cells						Exosomes					
gene	**WT1**	**WT2**	**WT3**	**CisR1**	**CisR2**	**CisR3**	**WT1**	**WT2**	**WT3**	**CisR1**	**CisR2**	**CisR3**
NFIX	1,69	0,43	-0,37	-0,36	-1,62	0,23	0,82	1,68	0,19	-0,78	-0,85	-1,06
HES4	1,56	0,49	-0,33	-0,87	0,59	-1,45	-1,03	-1,08	-0,86	0,83	0,90	1,23
COX7B	-1,07	1,38	1,26	-0,25	-0,22	-1,11	-0,99	-1,52	-0,29	0,94	1,02	0,84
PLAG1	0,84	0,56	0,13	-0,86	1,08	-1,75	1,04	1,28	0,56	-0,77	-1,32	-0,79
TMEM132A	2,19	-0,28	-0,39	-0,80	-0,53	-0,20	-0,90	-1,02	-0,82	0,37	0,64	1,72
SOX9	1,21	0,98	-0,71	-0,50	-1,57	0,59	-1,07	-0,92	-0,66	0,38	0,46	1,80
NCDN	1,93	-0,36	-0,14	-0,87	-1,05	0,49	-0,56	-1,01	-1,12	1,42	0,09	1,18
BLVRB	1,68	-0,91	0,59	-1,02	-0,85	0,51	-1,21	-1,22	-0,41	1,28	0,83	0,73
SASH1	1,79	0,60	-1,10	-0,34	0,09	-1,04	0,62	0,67	1,41	-0,54	-1,60	-0,57
FSD1	1,87	0,15	-0,72	-0,28	0,33	-1,34	-1,04	-1,21	-0,59	0,89	1,42	0,54
NRG1	1,85	-0,78	0,20	0,22	-1,37	-0,11	1,18	0,56	1,19	-0,98	-0,91	-1,04
ELF2	-1,02	0,32	1,94	-1,04	-0,12	-0,08	1,00	0,92	0,88	-0,74	-0,43	-1,63
C3	2,21	-0,45	-0,57	-0,49	-0,13	-0,57	-0,97	-1,06	-0,93	1,08	0,68	1,20
LCN2	2,18	-0,47	-0,52	-0,54	0,05	-0,69	-0,86	-0,92	-0,46	1,25	-0,53	1,54
CD99L2	-0,42	0,12	1,42	-1,42	1,07	-0,78	1,35	0,60	0,96	-0,77	-1,13	-1,02
NAA10	0,38	-0,49	1,15	-0,47	-1,69	1,11	0,36	1,40	1,06	-0,80	-1,23	-0,80
CXCL1	2,19	-0,61	-0,66	-0,23	-0,10	-0,59	-1,10	-0,71	-0,89	0,33	0,65	1,72
HAGHL	1,59	-0,16	-0,51	0,02	0,71	-1,64	-0,97	-0,57	-1,06	0,28	0,52	1,81
HDAC8	-0,80	1,34	0,33	-1,71	0,12	0,71	-0,16	1,31	1,43	-0,75	-0,92	-0,91
GAL	-0,49	0,02	1,25	-0,06	-1,76	1,04	-0,78	-0,87	-0,55	1,10	1,67	-0,57
MDK	1,25	-0,23	-0,26	-0,77	1,38	-1,36	-1,05	-1,09	-0,82	0,72	1,22	1,01
ST3GAL2	1,87	0,27	-1,46	-0,45	0,09	-0,31	-0,89	-0,73	-1,00	-0,06	1,57	1,10
ZC3H12A	2,10	-0,81	-0,70	-0,32	0,25	-0,52	-0,87	-0,80	-0,37	0,53	-0,49	1,99
C20orf194	0,75	0,72	-0,90	-0,40	1,32	-1,49	1,09	0,46	1,34	-0,91	-1,02	-0,96
MORF4L2	-1,67	0,87	1,35	0,23	-0,02	-0,76	-1,29	-0,76	-0,80	1,41	0,51	0,93
KREMEN2	2,11	-0,96	-0,60	-0,52	-0,02	0,00	-0,96	-1,07	-0,88	0,56	1,39	0,96
FST	0,15	-0,51	0,84	1,65	-1,19	-0,95	1,86	0,32	0,25	-1,27	-0,34	-0,81
CENPV	0,14	-0,90	1,23	0,21	-1,64	0,96	1,09	1,11	0,79	-1,02	-0,95	-1,02
PRPS1	-0,80	0,13	1,05	-0,31	-1,48	1,40	-1,14	-0,67	-0,93	0,31	1,62	0,81
UST	1,67	-0,58	-0,73	-1,11	1,01	-0,26	-0,56	-0,85	-1,12	1,14	1,55	-0,16
CDH24	1,90	-1,20	-0,34	-0,75	-0,13	0,52	-1,01	-1,40	-0,45	0,91	1,20	0,75
GPR87	-1,36	0,66	0,93	1,29	-0,72	-0,81	0,79	1,16	0,99	-0,85	-1,28	-0,82
LAMP3	0,77	-0,03	-0,51	-0,95	1,77	-1,05	-0,90	-1,05	-0,52	0,09	1,88	0,51
VMA21	-1,84	0,90	1,16	0,09	0,30	-0,60	1,23	1,00	0,48	-0,62	-0,46	-1,63
ZNF467	0,49	0,83	-1,15	-0,59	1,50	-1,08	-1,18	-0,46	-1,14	1,44	0,91	0,43
PBXIP1	0,75	0,03	-0,61	-0,97	1,78	-0,97	-1,05	-0,90	-1,03	0,90	1,17	0,92
PHLDA2	0,25	-0,27	0,18	-0,78	-1,27	1,90	-1,03	-1,44	-0,25	0,61	0,75	1,36
STRA6	1,56	-1,00	-0,47	-1,27	0,76	0,42	-0,96	-1,08	-0,86	0,67	0,78	1,46
TNFAIP3	2,02	-0,95	-0,99	0,01	0,12	-0,22	-1,02	-1,05	-0,52	0,32	0,47	1,80
TUBB2A	1,03	-0,47	-0,54	-0,61	-1,09	1,69	-1,15	-1,04	-0,37	0,92	0,03	1,62

	Cells						Exosomes					
gene	**WT1**	**WT2**	**WT3**	**CisR1**	**CisR2**	**CisR3**	**WT1**	**WT2**	**WT3**	**CisR1**	**CisR2**	**CisR3**
SDC4	1,70	-0,77	-0,94	-0,55	1,04	-0,48	-1,00	-1,13	-0,70	0,61	0,67	1,55
CDK6	1,84	-0,31	-1,54	-0,12	-0,16	0,30	1,30	0,68	0,95	-1,07	-0,75	-1,11
LINC00674	-1,74	0,83	0,89	-0,92	0,79	0,15	1,42	0,54	0,90	-0,73	-0,83	-1,29
GINS1	-1,79	0,35	1,34	0,77	-0,16	-0,51	1,03	0,93	1,03	-1,05	-0,90	-1,05
NFKBIA	1,80	-0,94	-1,01	-0,66	0,17	0,63	-1,03	-1,03	-0,80	0,65	0,66	1,54
PDE8A	1,87	-0,92	-1,11	-0,10	0,57	-0,32	1,10	0,77	1,07	-0,95	-0,69	-1,30
ICAM1	1,76	-0,86	-1,06	-0,25	0,88	-0,46	-0,96	-1,00	-0,85	0,73	0,49	1,60
AMMECR1	-0,17	-0,01	0,01	0,88	-1,93	1,22	1,61	0,52	0,58	-0,82	-1,36	-0,53
KIF4A	-1,23	1,46	-0,51	-0,55	-0,44	1,26	0,76	1,42	0,53	-1,30	-0,24	-1,17
HELZ2	1,42	-0,55	-1,22	-0,51	1,31	-0,45	-1,31	-0,65	-0,87	0,41	1,07	1,35
LDOC1	1,28	-1,42	-0,35	1,31	-0,15	-0,67	-0,43	-1,11	-0,85	0,12	1,93	0,33
APOBEC3B	1,67	-1,67	-0,54	0,04	0,30	0,21	-1,04	-1,08	-0,71	1,28	1,23	0,31
ZDHHC8	1,46	-0,36	-1,66	0,40	0,72	-0,56	-0,98	-1,14	-0,63	0,67	0,43	1,65
LIF	0,67	-1,05	-0,20	-1,03	1,82	-0,21	0,89	0,91	0,93	-1,74	-0,41	-0,57
SORT1	-1,07	0,02	0,27	-0,07	1,91	-1,06	-0,49	-1,27	-1,06	0,47	1,30	1,05
AMOTL2	1,41	-1,11	-1,15	-0,41	0,13	1,13	-1,23	-0,63	-0,97	0,84	1,49	0,49
ST3GAL1	1,52	-1,41	-0,96	0,68	-0,30	0,47	0,49	0,93	1,43	-0,64	-1,03	-1,18
PLK3	1,41	-1,07	-1,21	-0,07	-0,22	1,17	-1,09	-1,08	-0,75	0,59	1,16	1,18
IFIT1	-0,04	0,10	-0,98	-0,40	2,07	-0,75	-1,06	-1,06	-0,84	0,83	0,89	1,25
ABCD1	1,04	-1,16	-0,81	-0,97	0,64	1,26	-1,13	-0,92	-0,79	0,76	1,55	0,52
OASL	-0,55	0,57	-0,96	-0,49	1,98	-0,55	-1,03	-1,04	-0,82	0,64	0,79	1,46
IFIT2	-0,14	0,14	-0,96	-0,60	2,09	-0,53	-1,07	-1,00	-0,86	0,71	0,87	1,36
LPCAT1	1,43	-0,93	-1,50	0,19	-0,09	0,90	0,29	1,64	0,48	-0,56	-1,62	-0,23
MTMR1	-0,61	0,69	-1,11	1,83	-0,05	-0,76	1,29	1,20	0,31	-0,67	-1,26	-0,87
DECR1	-2,21	0,71	0,44	0,16	0,53	0,37	-0,88	-1,01	-0,56	1,15	-0,28	1,58
XIAP	-0,94	1,27	-1,47	-0,15	1,14	0,15	0,83	1,76	-0,03	-0,85	-0,72	-0,98
TXNRD1	-0,01	-1,23	0,09	0,37	-1,03	1,81	0,94	1,30	0,71	-0,95	-0,88	-1,12
MX1	-0,12	-0,32	-0,71	-0,43	2,19	-0,61	-0,98	-0,95	-0,79	0,41	0,56	1,75
ATF3	0,19	-0,42	-0,96	-0,36	2,11	-0,56	-1,00	-1,02	-0,64	0,38	0,52	1,77
DDX60	-0,21	0,00	-0,98	-0,27	2,12	-0,66	-1,04	-1,05	-0,81	0,63	0,82	1,45
ISG15	-0,23	-0,01	-1,00	-0,46	2,13	-0,43	-1,08	-1,08	-0,83	1,01	0,94	1,04
STK17A	-0,30	-0,10	-0,84	1,65	-1,30	0,89	-1,07	-0,66	-1,08	1,43	1,04	0,34
KIRREL	1,32	-0,87	-1,72	0,38	0,45	0,45	1,07	0,65	0,94	-0,49	-1,78	-0,39
LOXL2	1,31	-1,36	-1,23	0,01	0,43	0,85	-1,46	-1,24	0,17	0,64	1,20	0,68
IFIT3	-0,19	-0,19	-0,93	-0,33	2,16	-0,53	-1,06	-1,05	-0,83	0,76	0,80	1,37
ACADVL	0,96	-0,93	-1,34	0,43	1,40	-0,52	-0,86	-1,12	-0,68	0,40	0,50	1,77
GADD45A	1,25	-1,38	-1,25	0,07	0,42	0,89	-1,02	-1,17	-0,76	0,77	0,98	1,21
IGFL1	0,04	-0,67	-0,74	-0,45	2,16	-0,34	-1,14	-1,04	-0,72	1,40	0,86	0,63
TCEAL4	-1,80	0,59	-0,17	0,56	1,34	-0,52	-0,90	-1,36	-0,57	0,71	0,67	1,44
HLA-B	1,02	-0,89	-1,54	0,29	1,29	-0,18	-1,02	-1,01	-0,86	0,69	0,72	1,49

	Cells						Exosomes					
gene	**WT1**	**WT2**	**WT3**	**CisR1**	**CisR2**	**CisR3**	**WT1**	**WT2**	**WT3**	**CisR1**	**CisR2**	**CisR3**
OSMR	0,61	0,15	-2,17	0,30	0,85	0,27	-0,89	-1,29	-0,71	1,14	0,57	1,19
IRX3	1,18	-1,24	-1,45	0,24	0,40	0,87	-0,98	-1,04	-0,94	0,81	1,33	0,81
ABTB2	0,93	-0,81	-1,63	-0,23	0,52	1,22	-1,00	-1,01	-0,86	0,42	1,40	1,05
FGD4	-1,35	0,22	-0,39	-0,17	1,97	-0,27	0,72	1,13	1,06	-1,15	-0,53	-1,22
IFI44	-0,61	-0,04	-0,87	0,01	2,12	-0,61	-0,97	-1,03	-0,93	0,94	0,62	1,37
NEAT1	-0,39	-0,48	-0,67	0,15	2,14	-0,75	-0,98	-0,98	-0,95	0,57	0,92	1,42
IL1A	1,13	-1,27	-1,41	0,34	0,97	0,23	-1,12	-1,15	-0,64	0,84	1,31	0,76
ATP7A	0,24	-0,19	-1,61	-0,52	1,70	0,38	1,37	0,21	1,11	-0,37	-1,32	-0,99
OAS1	-0,24	-0,61	-0,81	-0,03	2,17	-0,47	-0,96	-0,95	-0,76	0,62	0,28	1,77
CA2	0,91	-1,24	-1,33	1,06	-0,22	0,82	-1,10	-0,42	-1,02	1,22	1,44	-0,12
ADIRF	-0,82	-0,70	-0,15	0,99	-1,00	1,68	-0,97	-1,14	-0,58	0,41	0,59	1,70
NFKB2	0,84	-1,05	-1,49	-0,09	0,50	1,30	-1,07	-0,96	-0,90	0,76	0,77	1,40
TCEAL8	-2,05	0,30	0,01	0,92	0,93	-0,12	-1,20	-1,06	-0,51	1,34	0,29	1,14
PCMTD1	-1,02	-0,10	-0,62	0,46	1,97	-0,69	1,20	1,54	-0,47	-0,51	-0,63	-1,14
SLFN5	0,71	-1,03	-1,47	-0,07	1,45	0,40	-0,98	-1,04	-0,87	0,47	1,29	1,14
MMP14	0,81	-1,01	-1,60	0,14	1,27	0,39	-0,88	-1,07	-0,98	1,15	0,58	1,21
CDH5	0,95	-1,25	-1,51	0,48	0,93	0,40	-1,09	-0,39	-0,48	-0,04	2,10	-0,10
RSPO4	0,14	-1,06	-0,93	0,96	1,60	-0,72	-0,75	-1,08	-0,84	0,21	1,72	0,75
ARHGEF9	-0,58	-0,41	-0,90	0,81	1,85	-0,77	0,64	1,42	0,86	-0,94	-0,98	-1,00
PLS3	-1,35	0,36	-0,91	0,95	-0,49	1,44	-0,89	-0,85	-0,84	0,46	1,87	0,25
HMOX1	-0,35	-0,77	-0,82	-0,22	0,03	2,14	-0,97	-1,04	-0,88	1,41	0,99	0,49
NUP62CL	-0,77	-0,14	-1,07	1,96	0,44	-0,42	0,51	1,56	0,76	-1,18	-0,80	-0,85
LRRC8A	0,26	-1,25	-1,06	0,43	-0,13	1,74	0,01	1,97	0,43	-0,84	-0,80	-0,78
KIF20B	-1,81	-0,10	-0,17	0,72	1,47	-0,11	-0,39	-0,72	-0,88	0,43	2,04	-0,48
CENPI	-0,52	-1,09	-0,52	-0,01	2,06	0,08	0,28	1,69	0,53	-0,85	-0,25	-1,41
TUBB3	-0,47	-0,76	-0,92	0,55	-0,38	1,98	-0,82	-1,05	-1,05	1,08	0,54	1,30
EGFL7	0,57	-1,42	-1,33	0,30	0,76	1,11	-1,03	-0,80	-0,99	1,62	0,57	0,62
METRNL	-0,31	-0,55	-1,36	-0,06	0,39	1,90	-1,12	-0,60	-1,14	0,89	0,57	1,41
ZNF337	-0,96	-0,47	-0,86	1,34	1,44	-0,49	0,76	1,62	0,41	-1,00	-0,98	-0,81
BRWD3	-0,06	-0,44	-1,80	0,22	1,47	0,60	0,76	1,08	1,14	-1,05	-0,92	-1,01
ATRX	-1,71	0,19	-0,80	0,58	1,41	0,32	0,97	1,11	0,82	-0,51	-1,39	-0,99
SEMA3C	0,03	-0,81	-1,55	0,34	1,65	0,34	-1,03	-0,91	-1,01	1,28	1,02	0,65
MED12	-0,23	-0,57	-1,54	0,00	1,67	0,68	-0,93	-0,90	-1,08	0,91	0,59	1,41
ISG20	-0,45	-0,73	-1,16	-0,19	1,85	0,68	-1,08	-1,06	-0,82	0,78	0,88	1,30
DLGAP5	-1,60	-0,06	-0,69	0,95	1,44	-0,03	-1,15	-1,16	-0,39	0,76	1,57	0,38
C2CD2	-0,37	-1,02	-0,99	0,82	-0,21	1,77	1,19	1,22	0,45	-0,61	-1,07	-1,18
MT2A	-0,10	-0,39	-1,90	1,27	0,55	0,57	-0,92	-1,32	-0,67	0,70	1,07	1,15
UPF3B	-1,81	-0,45	-0,13	1,40	0,33	0,66	-1,00	-1,15	-0,58	0,75	0,33	1,64
COL27A1	-0,51	-0,88	-1,00	1,39	1,37	-0,37	-0,60	-0,40	-1,12	0,23	-0,15	2,04
AQP3	-0,28	-0,99	-1,15	0,76	-0,08	1,75	-0,87	-1,02	-0,92	0,70	1,62	0,50

	Cells						Exosomes					
gene	**WT1**	**WT2**	**WT3**	**CisR1**	**CisR2**	**CisR3**	**WT1**	**WT2**	**WT3**	**CisR1**	**CisR2**	**CisR3**
KLK6	-1,00	-0,79	-0,64	0,94	-0,25	1,74	-1,17	-0,70	-0,90	1,39	0,22	1,16
L1CAM	-0,57	-0,96	-0,90	0,00	0,51	1,92	-1,10	-1,09	-0,74	0,76	0,86	1,31
ALDH16A1	0,17	-1,20	-1,41	0,84	0,28	1,32	-1,22	-0,40	-1,13	1,30	0,33	1,12
COBL	0,10	-1,14	-1,41	0,67	1,47	0,32	0,92	1,38	0,62	-0,99	-0,97	-0,97
IFI27	-0,78	-0,77	-0,91	1,07	1,66	-0,26	-1,05	-1,04	-0,68	0,85	0,32	1,60
TPM1	-0,31	-0,87	-1,29	0,15	0,54	1,78	-0,98	-0,92	-0,45	1,89	-0,18	0,62
SRPX2	-0,23	-0,98	-1,26	0,57	1,74	0,17	-0,98	-0,98	-0,98	0,95	1,32	0,68
COL17A1	-0,19	-1,03	-1,29	1,66	0,16	0,69	-1,18	-1,03	-0,69	0,55	1,10	1,24
DUSP1	-0,76	-0,92	-0,83	-0,10	0,81	1,80	-0,94	-1,03	-0,85	0,53	0,68	1,61
ARHGAP10	-0,05	-1,62	-0,85	0,57	1,45	0,49	0,77	0,70	1,44	-0,93	-1,03	-0,96
ATL3	-1,73	-0,43	-0,38	1,27	1,00	0,28	1,21	1,08	0,57	-0,62	-1,38	-0,87
TRIM38	-0,71	-0,40	-1,43	0,38	1,71	0,45	-0,98	-1,12	-0,75	0,97	0,46	1,44
FAM111A	-0,58	-0,81	-1,17	0,93	1,67	-0,03	-1,24	-1,23	-0,31	0,55	1,31	0,92
AKAP9	-1,70	-0,30	-0,57	0,67	1,42	0,47	0,55	1,84	0,06	-0,39	-1,20	-0,85
ASL	-0,63	-1,28	-0,67	0,98	-0,02	1,60	-1,11	-0,69	-0,68	-0,23	1,11	1,60
CEP350	-0,79	-0,31	-1,49	0,79	1,54	0,26	0,97	0,71	1,23	-1,23	-0,59	-1,09
HBEGF	-0,07	-1,31	-1,21	0,92	0,31	1,36	-0,97	-1,05	-0,70	0,58	0,41	1,72
PTGS1	-0,33	-0,75	-1,53	1,06	0,19	1,36	1,53	1,06	0,06	-0,57	-1,22	-0,86
CDKN1A	-0,38	-0,97	-1,26	0,03	1,27	1,31	-0,98	-1,02	-0,83	0,62	0,62	1,59
VAT1	-0,43	-1,01	-1,18	0,12	0,89	1,61	-0,99	-0,89	-0,91	1,13	1,44	0,23
SLC9A6	-0,73	-1,21	-0,69	1,68	0,84	0,11	0,98	0,36	1,42	-0,47	-1,31	-0,98
TLE1	-0,07	-1,08	-1,49	0,56	0,81	1,28	-1,19	-0,93	-0,69	0,32	1,35	1,14
LAMC2	-0,50	-1,00	-1,15	1,35	0,03	1,27	-1,19	-0,72	-0,61	0,57	0,12	1,83
IGFBP3	-0,82	-0,84	-1,00	1,00	1,62	0,04	-0,98	-1,00	-0,88	1,03	0,40	1,43
SERPINE2	-0,68	-0,86	-1,18	1,21	0,11	1,39	-1,01	-0,99	-0,83	0,32	1,43	1,09
ZNF292	-0,83	-0,71	-1,23	0,79	1,58	0,41	0,85	1,33	0,65	-0,94	-0,49	-1,40
WBP5	-1,24	-0,48	-1,10	1,05	1,31	0,45	-1,06	-1,20	-0,60	0,98	0,52	1,36
ZNF518A	-1,31	-0,78	-0,72	1,11	1,33	0,37	-0,80	-0,92	-1,06	0,97	1,54	0,27
CPVL	-1,12	-0,73	-0,96	0,93	1,51	0,38	-0,99	-0,84	-1,05	0,94	1,44	0,50
TGFB1	-0,84	-0,92	-1,07	0,49	0,76	1,58	-0,99	-0,95	-1,03	1,09	0,72	1,16
CD44	-0,76	-0,85	-1,21	1,52	0,47	0,84	-0,85	-1,09	-0,88	1,23	0,27	1,32
FSTL3	-0,42	-1,02	-1,39	1,29	0,75	0,78	-0,95	-1,06	-0,90	1,04	0,53	1,34
GOLGB1	-1,08	-0,62	-1,13	1,05	1,39	0,39	-1,09	-0,98	-0,87	1,32	0,64	0,98
PHLDA1	-0,35	-1,13	-1,36	1,13	0,82	0,89	-1,03	-0,84	-1,04	0,53	1,02	1,36
C1QTNF6	-0,52	-0,93	-1,39	0,60	1,25	1,00	-0,65	-1,36	-0,78	0,39	1,39	1,01
WARS	-0,70	-0,99	-1,16	0,42	1,12	1,32	-1,02	-1,09	-0,78	0,52	0,94	1,42
ANKRD12	-1,47	-0,53	-0,88	1,10	0,96	0,81	0,36	1,61	0,67	-1,10	-0,28	-1,25
CD55	-1,43	-0,65	-0,80	0,91	0,78	1,20	-0,95	-1,06	-0,93	0,89	0,70	1,35
FHL1	-0,74	-1,02	-1,14	0,77	0,73	1,40	-0,96	-1,05	-0,90	1,21	1,20	0,50
VPS13A	-0,82	-0,93	-1,16	0,92	1,38	0,61	1,26	1,07	0,60	-1,17	-0,81	-0,95

	Cells						Exosomes					
gene	**WT1**	**WT2**	**WT3**	**CisR1**	**CisR2**	**CisR3**	**WT1**	**WT2**	**WT3**	**CisR1**	**CisR2**	**CisR3**
DBN1	-0,74	-0,96	-1,23	0,63	1,15	1,14	-0,96	-0,94	-0,84	1,37	0,11	1,26
IGFBP6	-0,83	-0,96	-1,14	0,68	0,94	1,32	-1,02	-1,01	-0,93	0,70	1,00	1,26
AKAP12	-0,85	-1,05	-1,03	0,67	0,94	1,33	-1,13	-1,08	-0,75	1,17	0,75	1,04
F3	-0,85	-1,02	-1,09	0,97	0,73	1,25	-1,07	-1,19	-0,61	0,76	1,43	0,68
CHST11	-0,70	-1,15	-1,10	1,04	0,82	1,09	-0,93	-0,38	-1,12	-0,28	1,32	1,39
TSPAN6	-0,77	-1,19	-1,01	0,89	0,94	1,14	1,10	1,22	0,56	-0,70	-0,85	-1,34
CNN3	-1,14	-0,74	-1,10	0,93	1,02	1,02	-1,07	-0,99	-0,84	0,71	1,46	0,74
SLC4A7	-0,87	-0,93	-1,17	0,90	1,17	0,90	1,12	1,01	0,74	-0,43	-1,19	-1,26

6.2 ABBREVIATIONS

2D	Two-dimensional, on flat surface
3D	Three-dimensional
ABC	ATP binding casette
AKAP12	A-kinase anchor protein 12
BLMH	Bleomycin hydrolase
CDK8	Cyclin-dependent kinase 8
CFSE	Carboxyfluoresceinsuccinimidylester
circRNA	Circular RNA
CITED4	Cbp/P300 interacting transactivator with Glu/Asp rich Carboxy-terminal domain 4
CK	Cytokeratin
CSC	Cancer stem cell
CSV	Cell-surface vimentin
CTC	Circulating tumor cell
CTR1	Copper transporter receptor 1
DAPI	4,6-diamino-2-phenylindole
DLG3	Discs large MAGUK scaffold protein 3
DLS	Dynamic light scattering
DSB	DNA double-strand break
EC	Endothelial cell
ECr	Endogenous control
EGFR	Epithelial growth factor receptor
EMT	Epithelial-mesenchymal transition
ER	Endoplasmic reticulum
ERCC1	Excision repair cross-complementation group 1
ERCC3	Excision repair cross-complementation group 3
ESCRT	Endosomal sorting complex required for transport
EV	Extracellular vesicle
Exo^{CisR}	Exosomes from $FaDu^{CisR}$ cells
Exo^{WT}	Exosomes from $FaDu^{WT}$ cells
$FaDu^{CisR}$	Cisplatin-resistant FaDu sub-cell line generated from $FaDu^{WT}$ cells treated with sublethal cisplatin concentrations over 6 months
$FaDu^{WT}$	FaDu sub-cell line generated from single cell clone
FPKM	Fragments per kilobase
gDNA	Genomic DNA
GPI	Glycosylphosphatidylinositol
GSH	Glutathione
HNC	Head and neck cancer
HNSCC	Head and neck squamous cell carcinoma
HOMER2	Homer scaffolding protein 2
HOTAIR	Homeobox transcript antisense RNA
HPV	Human Papilloma Virus
HSP	Heat shock protein
IAP	Inhibitor of apoptosis
IFN	Interferon
IFRD1	Interferon-related developmental regulator 1
IGFBP6	Insulin like growth factor binding protein 6
ILV	Itraluminal vesicle

ITGB6	Integrin-β 6
lncRNA	Long non-coding RNA
LUV	Large unilammelar vesicle
MATE2	Multidrug and toxin extrusion 2
MDR	Multi drug resistance
MDRP	Multi drug resistance proteins
MET	Mesenchymal-epithelial transition
miRNA	Micro RNA
MMR	Mismatch repair
MSH2	MutS homolog 2
mtDNA	Mitochondrial DNA
MVB	Multivesicular body
MWCO	Molecular weight cutoff
ncRNA	Non-coding RNA
NER	Nucleotide excision repair
NK cell	Natural killer cell
NR	Nucleoplasmic reticulum
NTA	Nano-particle tracking analysis
OCT	Organic cation transporter
OCTN	Organic cation/carnitine transporter
OTUD1	OTU deubiquitinase 1
PAK	p21-activated kinase
PD-1	Programmed death 1
PEG	Polyethylene glycol
P-gp	P-glycoprotein
PMS2	Post-meiotic segregation 2
PRSS2	Serine protease 12
SEC	Size exclusion chromatography
SNP	Single nucleotide polymorphism
SOX2	Sex determining region Y box 2
SPAG9	Sperm-associated antigen 9
STAT	Signal transducer and activator of transcription
TCGA	The cancer genome atlas
TDE	Tumor derived exosome
TEM	Transmission electron microscopy
TGF	Tumor growth factor
TGFB1	Transforming growth factor beta 1
TIMP1	Tissue inhibitor of matrix metalloprotease 1
TME	Tumor microenvironment
TNC	Tenascin-C
TNF	Tumor necrosis factor
TNM-stage	Tumor, node, and metastasis stage
TP53	Tumor protein 53
TPT1	Translationally controlled tumor protein 1
TRAIL	Tumor necrosis factor related apoptosis inducing ligand
TRPS	Tunable resistive pulse sensing
UC	Ultracentrifugation
UF	Ultrafiltration
VRAC	Volume-regulated anion channel
WBC	White blood cell
ZBTB32	Zinc finger and BTB domain-containing protein 32

6.3 List of Figures

6.4 List of Tables

6.5 Additional Contributing Publications

Khamis, A.; Gül, D.; **Wandrey, M.**; Lu, Q.; Knauer, S. K.; Reinhardt, C.; Strieth, S.; Hagemann, J.; Stauber, R. H. (2022) *The Vitamin D Receptor-BIM Axis Overcomes Cisplatin Resistance in Head and Neck Cancer*. Cancers; 14 (20): 5131

Gribko, A.; Stiefel, J.; Liebetanz, L.; Nagel, S.M.; Künzel, J.; **Wandrey, M.**; Hagemann, J.; Stauber, R. H.; Freese, C.; Gül, D. (2021) *IsoMAG—An Automated System for the Immunomagnetic Isolation of Squamous Cell Carcinoma-Derived Circulating Tumor Cells*. Diagnostics; 11: 2040

6.8 Eidesstattliche Erklärung

Hiermit erkläre ich an Eides statt, dass ich diese Arbeit selbstständig und nur mit den angegebenen Hilfsmitteln verfasst habe. Alle aus fremden Quellen direkt oder indirekt übernommenen Gedanken sind als solche kenntlich gemacht.

Die Arbeit wurde keiner anderen Prüfungsbehörde vorgelegt und es wurde kein anderes Promotionsverfahren angestrengt.

Mainz, 09.07.2024

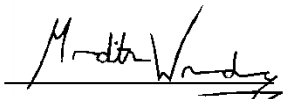

Madita Wandrey